A Systematic Methodology to Develop Scaling Laws for Thermal Features of Temperature Field Induced by a Moving Heat Source

by

Yi Lu

A thesis submitted in partial fulfillment of the requirements for the degree of

Doctor of Philosophy

in

Materials Engineering

Department of Chemical and Materials Engineering
University of Alberta

© Yi Lu, 2021

Abstract

A systematic methodology is developed to formulate scaling laws in closed-form for thermal features of moving line heat source and Gaussian heat source problems, with wide generality, high accuracy and practical simplicity, from fundamental principles. The expressions are written in form of a simple solution for the dominant factor and correction factors for secondary phenomena. In this thesis, the simple solutions are derived from asymptotic analysis of dimensionless models, and the correction factors are achieved with blending technique which is a standardized approach to generate a global approximation based on asymptotic solutions. The 1-D blending technique is modified to extend its scope of application and increase its accuracy. A systematic 2-D blending method is proposed to capture all possible cases of two independent variables.

This thesis presents explicit, predictive and simple expressions for vital thermal features of moving line heat source and Gaussian heat source, that are general to different materials, processes and operating parameters. Based on the Rosenthal's moving line heat source model, expressions for 13 thermal features are tabulated, including: isotherm half-width, location of the half-width, isotherm trailing length, centerline cooling rate, isotherm leading length, centerline heating rate, maximum temperature, gradients of maximum temperature, isotherm aspect ratio, melting efficiency, cooling time from 800 °C to 500 °C, solidification time, and thickness of the heat affected zone. All expressions are obtained with modified 1-D blending on one dimensionless group, Ro number that represents the intensity of heat source (except for maximum temperature), and are accurate to 8 % of the analytical solutions,

except heating rate at 16 %.

By employing the proposed 2-D blending method, correction factors of surface heat losses are established for isotherm half-width and its location, isotherm trailing length, and centerline cooling rate, resulting in errors within 12 %, with the introduction of the second dimensionless group h^*. For isotherms around the heat source, the energy distribution of the heat source affects the temperature field significantly. The correction factors of Gaussian heat source distribution are developed with the proposed 2-D blending method for isotherm half-width.

A comprehensive survey of published experiments and simulations is conducted to validate the proposed engineering expressions. The comparisons illustrate good agreements between predictions from the proposed expressions and collected data for a broad range of materials, processes, and parameters.

The engineering expressions for all thermal features of moving line heat source and Gaussian heat source are simple enough to be evaluated with a calculator or spreadsheet conveniently, and are useful for a broad range of diverse materials or processes. The expressions provide design guidelines for engineers and practitioners, bring physical intuitions and insights, and speed up designing cycles especially at conceptual stage in design and development of new technologies by inspiring creativity and filtering infeasible or inferior designing options by evaluating many optional parameters and processes. The blending method can be adopted in broader engineering problems since it captures the inherent essence of complex physical phenomena based on the governing equations.

Preface

This dissertation summarizes the author's research work and papers in CCWJ, Department of Chemical and Materials Engineering, University of Alberta, to pursue a Ph.D. degree under the supervision of Dr. Patricio Mendez.

Chapter 1 is the introduction of this dissertation. It is based on the author's candidacy report and the published paper "Mendez, P. F., Lu, Y., & Wang, Y. (2018). Scaling analysis of a moving point heat source in steady-state on a semi-infinite solid. Journal of Heat Transfer, 140(8)."

Chapter 2 is published as "Lu, Y., Wang, Y., & Mendez, P. F. (2020). Width of thermal features induced by a 2-D moving heat source. International Journal of Heat and Mass Transfer, 156, 119793." Ying Wang is the co-author of the paper. Her role was to collect published data to validate proposed formulae and contribute to the conceptualization and writing validation section. Dr. Patricio Mendez was the supervisory author, and he provided ideas and revised the paper before submission.

Chapter 3 is published as "Lu, Y., & Mendez, P. F. (2020). Characteristic values of the temperature field induced by a moving line heat source. International Journal of Heat and Mass Transfer, 120671." Dr. Patricio Mendez was the supervisory author, and he provided ideas and revised the paper before submission.

Chapter 4 is submitted to the Journal of Materials Processing Technology as "Lu, Y., & Mendez, P. F. (2021). Cooling rate in moving-heat-source manufacturing processes with intensive surface heat losses". Dr. Patricio Mendez was the supervisory author, and he provided ideas and revised the paper before submission.

Chapter 5 is under review to the International Journal of Heat and Mass Transfer

as "Lu, Y., Grams, M. R. & Mendez, P. F. (2021). Width of thermal features induced by a moving heat source on a thin plate with surface heat losses." Mitchell R. Grams is the co-author. He provided simulation data for validation and contributed to writing validation and discussion sections. Dr. Patricio Mendez was the supervisory author, and he provided ideas and revised the paper before submission.

Chapter 6 is a draft that will be submitted as "Isotherm half-width of Gaussian moving heat sources on a thick substrate". Ying Wang is the co-author of the paper. Her role was to collect published data to validate proposed formulae and contribute to the conceptualization and writing validation and introduction sections. Dr. Patricio Mendez was the supervisory author, and he provided ideas and revised the paper before submission.

Chapter 7 is the summary of the results, novelties of the papers and proposes recommendations for future work to continue the research.

The appendix chapters include the supplementary materials, such as supporting figures and Matlab codes, to achieve the equations in this thesis. The appendix also includes scaling laws and engineering expressions for catchment efficiencies of Gaussian distributed powder cloud under moving Gaussian heat source.

Dedicate this thesis to my partner for her love and support in my life.

Acknowledgements

These years at the University of Alberta have been a great and memorable time in my life. It could not happen without the ongoing help and support from many friends. At the final stage of my Ph.D. program, I want to convey my great gratitude to them in this thesis.

Firstly, I have to thank my supervisor Dr. Patricio Mendez. Thank you for your help in training my academic skills and systematic thinking, discussing new ideas and research directions, teaching writing skills and revising papers. Your passion and wisdom inspire me deeply. You also teach me about Canadian cultures and help me overcome the culture gap, and encourage me to make friends from different countries, join coffee breaks and parties. You also tried hard to learn Chinese cultures, reading Chinese characters and "The Analects". As an old Chinese saying goes, "Teacher is like a father." I am looking forward to keeping the friendship with you lifetime.

I would like to thank friends in the lab. Thank you, Goetz, for your help in lab activities and wise suggestions. Thank you, Mitch, for bouncing creative ideals, honing English writing skills, and engaging me in Canadian culture. Thank you, Dmytro, Alejandro, Syed, Daniel, and our alumni, Gentry, Nairn, Cory, Vivek, Matt, Steven. Your achievements, leadership and love for the CCWJ lab always motivate me. Thank you, Jason, Huan, Fan, Zhaoyang, Chaoqun. We have great fun celebrating Chinese festivals in Canada, making me feel at home.

I would like to acknowledge support from the Natural Sciences and EngineeringResearch Council of Canada (NSERC).

Thank you, my father and mother, for your consistent love and support. Most

importantly, I must thank my partner for your love and accompanying in these years. Thank you for your care and delicious food. You are an excellent cook now! Thank you for your encouragement and comfort when I am down. We went through many difficulties and challenges, joys and pleasures together in the past nine years. I hope we can go through all burdens and happiness for the rest of my life.

Table of Contents

List of Tables

List of Figures

Chapter 1

Introduction

1.1 Motivation

1.1.1 Background

This dissertation conducts a systematic research on important thermal features related to isotherms in temperature field of a moving line heat source or Gaussian distributed heat source model, where moving heat source model is referred to a heat source of constant intensity moving on a substrate at a constant speed, as illustrated in Figure 1.1. The research involves dimensional analysis to generalize the problem, asymptotic analysis in extreme regimes and blending to achieve global approximation. Many processes can be modelled as moving heat source problems in thermal analysis, such as welding [174, 175, 179], additive manufacturing [73, 85, 190], cladding [31, 219], surface treatment [86, 106, 124], cutting [66, 149], tribology [89, 94], grinding [25, 132], machining [51, 107], wheel and track contact [102, 103], bone surgery [121, 228] and many more.

An example is made to demonstrate the importance of studying thermal features of moving heat source problems for the welding process. Welding is one of the crucial fabrication technologies to form one component continuously from two by applying heat, some times with pressure, in which "rapprochement" is built by moving atoms close enough to share bonds. It is widely applied in many fields like chemical plants, oil and gas, mining, aerospace industry and many more. In the most common cir-

cumstance, the term welding is often referred to joining metals by applying heat. In fusion welding processes, a part of substrates is heated up by moving energy sources such as plasmas or laser beams, and a melt pool forms during heating where the base material mixes. Then, the molten materials solidify to form a continuous joint bead as heat source leaves and heat conducts away. The joint of fusion welds consists of a distinct fusion zone, heat-affected zones and unaffected base materials. For alloys, there is also a partially melted zone between the fusion zone and heat-affected zone.

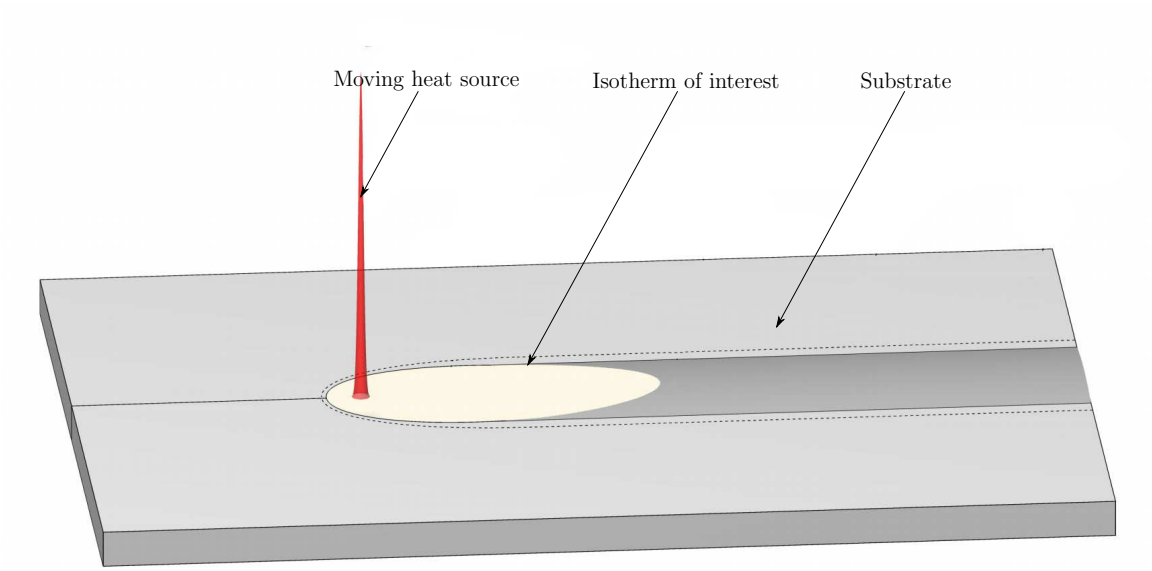

Figure 1.1: Schematic of moving heat source. The isotherm of interest can be temperatures such as melting temperature, phase transformation temperature, or thermal residual temperature, etc.

During this thermal cycle, some thermal features are crucial to reactions and properties of fusion welding processes, such as metallurgical phase transformation, mechanical properties, efficiencies, and reliabilities. For example, the isotherm width is a significant characteristic reflecting the shape of the weld pool, the region of phase transformation, and thermal residual stresses [76]; the cooling rate affects the phase transformation in solidification, martensitic transformation [87], and sensitivity to cold crack [99]; aspect ratio is a vital characteristic in in-situ monitoring [195]; melting efficiency is crucial to dilution in welding of dissimilar materials [49]; and many

more.

Similar to welding processes, investigations of thermal features related to isotherms of temperature field under moving heat sources are central to many other processes as addressed above, like additive manufacturing, cladding, surface treatment, cutting, tribology, grinding, machining, wheel and track contact, and bone surgery.

The research proposes a systematic approach to build explicit, general, convenient and practical formulae to describe relationships between operating parameters (like heat input, travel speed and plate thickness) and important thermal thermal features (like maximum temperature, cooling rate) for moving line heat source of two-dimensional problems or moving Gaussian heat source of three-dimensional problems. The practical formulae provide design guidelines for engineers and practitioners and bring insights into initial evaluations of the process mechanisms and parameters. The predictive formulae in closed form are suitable for transmission in textbooks and standards and general enough to be easily adapted to different materials and processes.

1.1.2 Knowledge gap

There is a significant lack of practical, reliable, and general engineering expressions for moving heat source processes to predict critical thermal features of interest to the practitioners, such as maximum temperature, cooling rate, size of the heat-affected zone, and melt pool size.

In the past thirty years, the rapidly evolving numerical simulations help understand and predict moving heat source processes such as laser cladding and additive manufacturing, building up more realistic and comprehensive models benefiting from explosively growing operator forces of computers. Simulation models are convenient when prototype is expensive, such as cars and airplanes. Sophisticated numerical simulations are usually difficult for practitioners without training or software, especially for highly interdisciplinary processes like welding. The experimental technologies are also developing rapidly for accurate control and measurements. Experiments can gen-

erate simple empirical models. Results of experiments and simulations are usually valid for given parameters with limit amount of generalities to specific materials and properties.

Despite the progress of simulation and experiment techniques, there is a lack of rigorous, general, explicit, convenient, accurate and physically meaningful engineering expressions for moving heat source problems, which are essential in conceptual designing at the first stage of engineering design [137]. At the conceptual designing stage, many concepts, optional processes, and parameters are proposed based on intuition and experience. The engineering expressions can filter infeasible or inferior designing options by evaluating a large amount of optional parameters and processes conveniently. With ample time and money, trial-and-error methods or numerical simulations could be utilized for accurate predictions and thorough explorations of the whole space of possible parameters and options. However, in practical applications, it is crucial to evaluate versatile considerations of technologies and materials with limited time or money, which prevents the usage of detailed analysis at beginning of designing. Moreover, the exact answer to particular materials, processes and operating parameters from perfect models or experiments is not enough as the possible parameter spaces of them also need to be explored at conceptual design stage. Basic design rules and engineering expressions are essential for the evaluation and creation of parameters and technologies at the conceptual stage. They deliver engineering understanding, inspire creativity and screens infeasible and inferior designing options. For the remaining designing options, further analysis in detail can the conducted with sophisticated numerical simulations or experiments to form the final design.

The success of engineering expressions have been implemented in a variety of engineering fields, such as stress concentration analysis in solid mechanics [165], drag coefficient in fluid dynamics [116], stress in gear teeth [187], and calculation of convection coefficient in heat transfer [92]. One concrete example of its implementation is the calculation of Nusselt number of external cross flows over a cylinder, which describes

the convective heat exchanging between the cylinder and flows, from the textbook "Fundamental of Heat and Mass Transfer" [92]. Correlation between average Nusselt number, Reynolds number and Prandtl number can be expressed as:

$$\overline{\mathrm{Nu_D}} = 0.3 + \frac{0.62\mathrm{Re_D}^{1/2}\mathrm{Pr}^{1/3}}{\left[1+(0.4/\mathrm{Pr})^{2/3}\right]^{1/4}}\left[1+\left(\frac{\mathrm{Re_D}}{282,000}\right)^{5/8}\right]^{4/5} \tag{1.1}$$

where $\mathrm{Nu_D}$ is defined as the ratio of convective heat transfer to conductive heat transfer, $\mathrm{Re_D}$ is the Reynolds number for the cylinder, and Pr number is the ratio of momentum diffusivity to thermal diffusivity of the cross flow. Equation 1.1 is comprehensive for calculating convection coefficients, covering a wide range of $\mathrm{Re_D}$ and Pr. Many engineering expressions in similar form in heat and mass transfer fields can not only provide an estimation of the heat transfer coefficient efficiently and economically but also bring engineering insights on the interplay between involved mechanisms and parameters. There are a bunch of correlations under different conditions, which do not provide an accurate solution to the Nusselt number but are significant and practical to the design of heat exchangers, bringing insightful and intuitive understandings of convective heat transfer. However, Equation 1.1 obtained with Churchill's blending methodology is recommended for $\mathrm{Re_D}\cdot\mathrm{Pr} \geq 0.2$ which can not cover all values of $\mathrm{Re_D}$ and Pr. There is lack of systematic approach to obtain blending depending on two dimensionless groups, which will be discussed later in this dissertation.

However, very few engineering expressions are developed for moving heat source problems, and some published correlations are not presented correctly. The engineering expressions are usually valid for a narrow range of materials and processes [137]. For example, in American Welding Society (AWS) standard D1.1 [9], standardized Charpy V-notch tests are required at the heat-affected zone. However, there are no predictive methods suitable for a standard to estimate the location of fusion and width of heat affected zone, namely bead width of melting isotherm and thickness of heat-affected zone, and only some rough values (1 mm and 5 mm) are attributed to thickness of heat-affected zone for different processes, which could vary significantly

with different operating parameters and base materials. Another example is the formula for cooling time from 800 °C to 500°C presented in British code [192], which is a crucial thermal feature associated with metallurgical transformations of steel, tightly related to mechanical properties of weld bead:

$$t_{8/5} = \frac{q^2}{4\pi k\rho c d^2 U^2} \times \left[\frac{1}{(500^{\circ}\mathrm{C} - T_0)^2} - \frac{1}{(800^{\circ}\mathrm{C} - T_0)^2}\right] \tag{1.2}$$

where $t_{8/5}$ represents the cooling time from 800 °C to 500 °C, q is the heat absorbed by the workpiece, k is the thermal conductivity of the base material, U is the speed, ρ is the density, c is the specific heat, d is the plate thickness, and T_0 is the initial or preheat temperature. Equation 1.2 provides some reasonable estimations when welding speed is fast enough. However, in many cases of practical welding parameters, travel speeds are not always large enough, and Equation 1.2 is not valid anymore, that was not addressed explicitly. There are a vast wealth of known expressions related to the heat flow and resulting thermal features; however, current knowledge is typically process-specific or material-specific. There is a lack of insightful, practical, convenient and general engineering expressions that are amenable to practitioners and engineers.

1.1.3 Scope

This dissertation is to propose a systematic approach to establish a set of practical, reliable and general engineering expressions for thermal features of moving heat source problems to deliver physical understanding, enhance engineering judgment and provide reasonable predictions. The engineering expressions are in the form of:

$$\begin{aligned}\text{Characteristic Value} = \ &\text{Ideal Solution} \times \text{Correction Factor} \times \\ &\text{Correction Factor} \times \ldots\end{aligned} \tag{1.3}$$

The ideal solution is an expression in closed-form with great simplicity for the ideal cases, typically obtained by considering only dominant phenomena. The dominant phenomena can be identified with analytical scaling analysis [138], experiments or

numerical simulations with extreme operating parameter values [61], or from practical engineering experience conceptually. Heat conduction or advection due to the motion of heat source is the dominant phenomenon for moving heat source problems depending on whether the isotherm of interest is close or far to the heat source. To ensure the generality of proposed engineering expressions to be independent of specific materials or processes, the ideal solutions in this dissertation are obtained by the asymptotic analysis of normalized analytical solutions based on the classic Rosenthal heat source model to capture the essence of heat flow under moving heat source.

Correction factors are developed to measure the departure of the ideal solutions for ideal cases from the "reality" to capture the secondary effects. The secondary phenomena can be surface heat loss to the environment, phase transformations, fluid dynamics, heat source distributions and many other more, which depend on practical processes and requirements. The "reality" can be analytical solutions, experiments, or numerical simulation results [141]. The correction factors can be formulated by statistic regression or blending technique. In this dissertation, the 1-D/2-D blending methodology is used to formulate correction factors for conduction or advection, effects of surface heat losses and size of Gaussian distributed heat source.

1.2 Literature review

Point heat source

The moving point heat source model, which was proposed and solved by Wilson [215] and popularized in welding engineering by Rosenthal [175], is the most classic moving heat source model. Rosenthal successfully applied the model to welding and cutting processes, and it presented reasonable estimations of the temperature field far away from the heat source. Comparisons have been made between experimental data and Rosenthal's prediction [160, 176]. Rosenthal and Schmerber [176] verified Rosenthal's thermal distribution theory on thin plates, measuring isotherms with thermocouples. It has been widely applied in many fields, including mass transfer [171], additive

manufacturing such as beam-based fabrication of thin-wall structures, [73, 85, 190] and metal cutting [66, 149], even general enough to be utilized to simulate the shell-forming by line heating [227]. It has also been adopted to speed up and verify numerical simulation procedures of heat flow due to its fundamental feature [52, 112, 163]. The experiments and theoretical equation are in satisfactory agreement on the thin plate, excepting the area close to the heat source and the edge regions.

The point heat source model is widely utilized in welding engineering due to its explicit analytical solution to the temperature field and capturing the essence of the moving heat source problems with much simplicity and reasonable accuracy. Heller et al. [84] characterized the radius of near field region, far-field region and transitional region of the temperature field based on point heat source models and achieved asymptotic expressions for the trailing length and maximum isotherm width. Goyal et al. [75] employed the point heat source model as an approximation of the heat input of droplets in modelling the thermal processes of PGMAW (Pulse Gas Metal Arc Welding). Yajun [205] integrated the two-dimensional and three-dimensional point heat source models and verified with measurements from EBM (Electron Beam Welding) experiments where good agreements were achieved between predicted and measured fusion line locations. Gajapathi et al. [64] reported simulation results of micro electron beam welding processes and compared the numerical temperature field against Rosenthal's point heat source solution in the far-field (out of $(-10\mu m, 1\mu m)$) in the centerline with good agreements.

Kou [112] developed a numerical model to simulate the steady-state, two-dimensional heat flow based on the finite difference method and adopted Rosenthal thin solution as the first guess to speed up the computation. Comparison between calculation given by this line heat model with his numerical results within the limits of listed assumptions showed that the numerical and analytical solutions are nearly identical for temperature below the melting temperature of the workpiece and thermal cycles are also nearly identical except at the location of heat source where the temperature

is infinity due to the point source assumption. Kazuya [154] tested the effect of latent heat on temperature field induced by a two-dimensional heat flow numerically and concluded that the latent heat might not be necessarily considered in the calculation for the cases of small heat input.

The model must be applied with an understanding of its limitations caused by its assumptions. The point heat source model is inferior in predicting temperature fields close to heat sources, but the model can provide fair estimations for points away from the heat source, where many critical regions locate such as the heat-affected zone. The moving point heat source is the critical model capturing the essence of moving heat source problems. Therefore, the moving point heat source model is utilized in the first step of current research and serves as the theoretical basis to establish preliminary engineering expressions. To capture the influence of sizes of heat source, Gaussian distributed heat source model, which are reviewed below, will be employed to develop engineering expressions for isotherm half-width associated with the vicinity of the heat source.

More sophisticated heat source models, for example, volumetric heat sources, as reviewed below, can improve the accuracy of temperature field prediction, particularly for the regions close to the heat source, with elaborate choices of parameters. However, here comes two problems. Firstly, the relevant parameters in the heat source models are challenging to measure or estimate. Secondly, it is nearly unachievable to control the parameters of volumetric heat sources in welding processes, making it impractical to involve the volumetric heat source parameters in designing rules.

Surface heat source

Surface heat source models, heat imposed on the flat surface of the base material, are utilized in many analytical and numerical methods because they provide a better temperature description around the heat source by taking the sizes of heat sources into account.

The most common surface heat source model is the moving Gaussian distributed heat source proposed by Eagar and Tsai [53]. Ghosh et al. [69] modelled the heat input of welding arc as a Gaussian distributed heat source. Akbari et al. [8] applied Gaussian distributed heat source model to simulations of laser beam welding of Ti6Al4V. Roberts et al. [170] and Nikam and Jain [151] employed Gaussian heat source model to simulate laser additive manufacturing processes.

There are some other types of surface heat sources other than the Gaussian distributed heat source. One typical model is the uniform distribution or top-hat heat source, and the top-hat models are widely used in laser beam processes [115, 161, 198]. Haghpanahi et al. [81] modelled a surface ring heat source to represent the heat generated by friction in the shear layers. To achieve a more realistic heat source model for simulations, Kubiak et al. [115] measured the energy distribution of Yd: YAG laser and built a mathematical model of the heat source by interpolation for more accuracy.

The surface heat source models introduce geometry parameters to capture the heat source's size and energy distribution, such as the distribution parameter σ for moving Gaussian distributed heat source models. Those parameters can be measured directly in experiments [115], or estimated based on the temperature fields [178].

Volumetric heat source

The heat input is not always imposed on a flat surface due to arc force and metal evaporation and so on, especially under high current or high energy density. Volumetric heat source models, or more accurately speaking, curved surface heat source models, are utilized, mostly in numerical simulations.

The double ellipsoidal heat source model proposed by Goldak et al. [74] is the most popular volumetric heat source model, which describes the heat distribution in front and rear parts as the of different sets of parameters. The size and shape of a double ellipsoidal heat source can be easily manipulated with seven parameters, which has the

advantage of versatility and flexibility to deal with different processes but also causes difficulty in setting appropriate geometry parameters. The double ellipsoidal heat source model is widely utilized in simulations of many moving heat source processes, such as electron beam welding [32], laser beam welding [16], plasma arc welding [125], and so on. Other than applications on simulations, the double ellipsoidal heat source is also utilized in analytical approaches. For example, Fachinotti et al. [56] analytically solved the temperature distribution of a double ellipsoidal heat source on a semi-infinite solid medium, reducing the computation cost to a large extent.

Some volumetric heat source models have been developed for specific processes or phenomena. Yadaiah and Bag [223] modified the double ellipsoidal heat source into an egg-shape configuration to capture the influence of molten metal. Parkitny and Winczek [158] built up a tilted Gaussian distributed volumetric heat source to describe the effect of the angle of laser. Piekarska and Kubiak [164] proposed a truncated cone-cylinder volumetric heat source model for lasers symmetric in x-y directions. Gajapathi et al. [64] presented an exponentially decaying Gaussian distribution heat source in the thickness direction for modelling of electron beams.

Hybrid models by integrations of well-established heat source models for different phenomena have been developed according to the superposition principle. Chowdhury et al. [32] reported a combination of Gaussian distribution model and conical heat source model to study the keyhole mode. Yajun et al. [205] merged moving point and line heat source model in the numerical simulation of the keyhole mode in electron beam welding. Goyal et al. [75] analytically described the temperature distribution of PGMAW as a combination of solutions to Rosenthal's point heat source model and double ellipsoidal model. Ghosh et al. [69] combined Gaussian heat density distribution and ellipsoidal heat source model to analyze the heat from the arc and molten metal separately. Winczek [216] solved the temperature field to heat sources with changeable directions by a straight segment method. Azar et al. [13] built a relationship between the point heat source model and ellipsoidal heat source by a

so-called "discretely distributed heat source model" where the temperature field of double ellipsoidal heat source was approximated by the summation of temperature field of point heat sources positioning in a fixed distance in horizontal and vertical directions.

Volumetric heat source models are usually more accurate with the careful selection of parameters. However, the parameters are difficult to be defined or evaluated before welding [14, 224]. The geometry parameters of volumetric heat sources, such as double ellipsoidal heat source, are nearly not possible directly obtained from measurements and are usually via trial and error methods from experiments [14, 224] or experience [10, 98]. Many efforts are made to achieve or reduce the unknown geometries parameters of volumetric heat source models. Jia et al. [98] achieved geometry parameters of double ellipsoidal heat source model from multiple regression and partial least-square regression analysis and verified the results from comparing width penetration and peak temperature. Yadaiah and Bag [224] established the relationship between the ratio of front and rear length and travel speed by least square regression of polynomial equation method.Bag et al. [14] developed an adaptive volumetric heat source model that does not need inputting of heat source parameters, relying on the heat source diameter and the real-time weld pool size, overcoming the disadvantage of the double ellipsoidal heat source model.

Because the geometry parameters of volumetric heat sources are usually unknown before experiments, and it is barely possible to control the geometry of volumetric heat inputs, the engineering expressions will not be established according to volumetric heat source models.

Experiments

Temperature distribution of the whole field or some of the points can be measured from thermocouples, camera, or estimation from microstructure.

Since the microstructure of weld bead is directly related to the thermal history,

specific temperatures can be estimated from microstructure distribution, such as the maximum temperature of the particle at fusion line is melting temperature, and the maximum temperature of the particle at heat affected zone line is phase transformation temperature [68, 75]. However, the transformation temperature is under uncertainty of chemical composition, heating rate and so on, bringing error in temperature estimation.

The temperature can be measured directly with thermocouples or thermal cameras. Thermocouple, a device based on thermoelectric effect, is widely utilized to measure the temperature at a certain point with time [8, 161], by attaching thermocouples on the workpiece. Thermal cameras, based on infrared radiation, are used to measure the radiation of the weld pool to show the temperature of a range of wavelengths. Chen and Gao[30] detected the size of molten pool on-the-fly with a high-speed near-infrared sensitive camera. Lammlein et al. [118] determined the temperature of shoulder edge temperature in friction stir welding (FSW). Heller et al. [84] measured the temperature distribution of laser keyhole welding from thermography images and verified his mathematical model of the combination of Rosenthal's two-dimensional and three-dimensional formula.

Analytical methods

The temperature distribution can be approached theoretically via solving the thermal diffusion equation, such as the solution to moving point heat source proposed by Rosenthal[175]. The analytical solutions are usually general, but limited to simple geometry [194] and constant physical properties [56, 161, 216, 217].

Green function method is popular to express the temperature field [56, 81, 101, 158, 161, 198, 216, 217, 223], and could be conventionally applied to various heat source configurations. Peng [161] presented a general solution for the transient temperature field by a moving laser heat source of uniform distribution and validated with experiments and FEM solutions. Van Elsen et al. [198] investigated the temperature

distribution of top-hat heat source or uniformly distributed heat source analytically and numerically. In analytical solutions, Green function is applied to integrate the instantaneous solution. Yadaiah et al. [223] analytically solved the temperature of his proposed egg-configuration heat source model for GTAW and validated it with experiments and simulations. Parkitny and Winczek [158] provided a solution to temperature distribution under a tilted Gaussian distributed heat source consider the angle of the heat source. Fachinotti et al. [56] analytically solved the temperature field of a double-elliptical heat sourced and compared it with FEM solution. Kidawa-Kukla [101] reported the solution to a moving heat source along an elliptical trajectory on a rectangle solid.

The analytical solution can be approached by the integration of established analytical solutions. Goyal et al. [75] combined the solutions to point heat source and distributed heat source to model PGMAW and validated with experiments. Ghosh et al. [69] predicted temperature distribution by modelling arc droplet and surface heat loss independently. Sundqvista et al. [188] superposed Gaussian distributed heat source to describe the temperature field of any heat source profiles. Heller et al. [84] analytically divided the workpiece plate into different regions according to their relative position to the heat source, and integrated Rosenthal's models for two-dimensional heat flow and three-dimensional heat flow to capture the temperature distribution of different region, and verified the integrated analytical model with laser beam keyhole weldings.

Both the simulation and analytical methods attempt to solve the same thermal diffusion equation in different approaches for the moving heat source problems. The numerical solutions are more visualized and intuitive, directly illustrating the temperature field, and can deal with complex material models, geometries and heat source models. However, it is more time and computational resource consuming and brings discretization error into the result. The analytical method can only deal with less complex models than numerical approaches, and analytical solutions are usually ob-

scure with complex integrals and summations. However, the analytical methods are accurate and general, independent of the specific values and easy to be transferred to different problems, and consume less time and computational resources.

Simulations

The temperature field can be approached by numerical simulations with fewer assumptions than analytical methods, bringing temperature-dependent variables into numerical models and considering secondary phenomena, but usually with more time or computational resource consumption.

To reduce the time and computational resource consumption of simulation, Ding et al. [45] reported modelling the moving heat source problem as a quasi-steady problem rather than a transient thermal problem and reduced the simulations time significantly from 51 hours 24 minutes down to 10 minutes, by 99%.

There are typically five methods to model melting and solidification in the moving heat source simulations: apparent heat capacity method, effective heat capacity method, heat integration method, source-based method, and enthalpy method, where the enthalpy method is the most popular one. Li et al. [125] utilized the enthalpy method, bringing enthalpy as a function of temperature into the governing equation, including the latent heat, and considered thermal conductivity, convection coefficient, and viscosity coefficient as piece-wise linear functions. Nisar et al. [152] carried out FEM analysis of laser enamelling processes considering the phase transformation latent heat employing enthalpy method. The latent heat of melting or solidification can also be treated as an energy source in the energy balance equation. Anca et al. [10], Bannour et al. [16] and Akbari et al. [8] treated latent heat as a term of heat source or sink located at fusion line. Piekarska and Kubiak [164] considered the latent heat of fusion into effective heat capacity based on the volumetric percentage of different phases. Van Elson et al. [198]study of temperature under moving top-hat heat source with FDM analysis, comparing different ways to accomplish latent heat; among the

five methods, the enthalpy method is the most stable, converges fast and incorporates the conservation of energy. Van Elsen investigated the influence of latent heat. For large thermal conductivity, the effect of latent heat is little, and for low thermal conductivity, the effect of latent heat causes sharping tail.

As addressed in the previous section, the physical properties are usually treated as constant in analytical methods. In simulations, more realistic models can be established for physical properties. Piece-wise linear functions are usually brought to model the temperature-dependent properties, such as heat capacity[8], thermal conductivity[8, 125]. Power-law functions are employed to describe the surface convection coefficient [8, 14, 224]. Akbari et al. [8] utilized the piece-wise linear function to describe the temperature-dependent heat capacity and heat conductivity, power-law function to describe the surface convection coefficient and constant value models to density and viscosity. Rouquette et al. [178] approximated the value of thermal properties of multiphase coexistence state with the law of mixture of different phases. Kubiak et al. [115] measured the realistic heat energy distribution of Yb: YAG laser and proposed an interpolated heat source model for exact heat input distribution, and compared different heat source models, Gaussian distributed heat source, top-hat heat source, super-Gaussian heat source model. Roberts et al. [170] simulated the transient temperature field in additive layer manufacturing processes (ALM), capturing the material deposition of multilayers with the element birth and death method (activation of new elements), where some thermal properties (enthalpy, density) are functions of temperature, while some properties (conductivity) are not only functions of temperature, but also depending on powder porosity. Chen et al. [28] assumed the physical properties are of different constants for gas, liquid and solid, established a set of transition rules for the transformation of the interface cells between three states. Komanduri and Ho reported that appropriate choice of the average value of thermal properties at intermediate temperature could compensate the assumption of constant thermal properties and yield reasonable results close to experimental observations as

long as room-temperature thermal properties are not taken [104, 106].

Bannour et al. [16] investigated the influence of thermal properties by comparing simulation results of temperature-dependent values and constant values. For density and enthalpy, the temperature field varies slightly between temperature-dependent values and constant values. For thermal conductivity and efficiency, the temperature field away from the heat source is underestimated, and at the high-temperature region around the heat source, a good estimation is performed.

The convective fluid flow in moving heat source processes enhances the heat transfer in the weld pool that could be captured by simulation but difficult to adequately describe. The surface tension force is the main drive force in molten metal flow and is usually considered as a boundary condition on the contact surface[8, 16, 125]. The buoyancy force is considered as a term in momentum balance in vertical direction [8, 16, 125, 172]. The electromagnetic force is considered a body force that is symmetric on the top surface, balancing the momentum in three equations, promoting fluid flow downward[125]. The convective molten fluid flow can be captured by modification on thermal properties or heat source model. Anca et al. [10] reported that molten metal flow in the welding pool could be treated as increasing conductivity. Nikam and Jain [151] treated the conductivity of molten liquid 2.5 times of solid to capture the Marangoni flow caused by surface tension. Yadaiah and Bag [223] established an egg configuration heat source for capturing the influence of convective molten metal.

The meshless simulation technique is employed to moving heat source problems. Pham [163] utilized the meshless element-free Galerkin method to approximate Rosenthal's two-dimensional quasi-steady temperature field for moving point heat source and Gaussian distributed heat source, and compared the temperature in centerline with FEM solutions.

Blending techniques

In many transfer processes, the asymptotic solutions for extremely large or small values of independent variables are known, while the solutions for non-asymptotic regions are typically not in closed form. For these intermediate regions, simple and accurate expressions can be obtained using the blending technique, which was first proposed by Acrivos [3, 4] for the rate of heat and mass transfer in several laminar boundary layer flows and was later extended and generalized by Churchill and Usagi [34, 38] named CUE (Churchill-Usagi equation):

$$Y = (1 + Z^n)^{1/n} \tag{1.4}$$

where Y and Z are expressions of asymptotic solutions of limiting values of the independent variable, and n is an empirical number that could be achieved numerically or experimentally. The proposed blending method is successfully applied to many problems, like heat transfer [35–37, 200], mass transfer [58], fluid dynamics [50]. The CUE provides a new paradigm to obtain a general solution over the whole domain in terms of simple, known, limiting solutions with a minimal degree of explicit empiricism, which is typically caused by the additional introduction of the blending exponent n.

Besides blending, there are also some other methodologies to obtain global approximation based on asymptotics for extreme values, such as asymptotic matching [159] by adding inner and outer asymptotics minus the matching term, which is usually used in perturbing differential equations.

1.3 Objectives

This work establishes predictive scaling expressions in the form of ideal solutions timing correction factors, for crucial and practical thermal features under a moving line heat source or Gaussian heat source. Some ideal solutions have been reported based on the moving line heat source model, such as cooling time [192] and isotherm width [190], and they are only valid for either “fast” or “slow” travel speed cases.

This work contributes ideal solutions to both "slow" and "fast" travel speed cases for thirteen thermal features of practical applications, if have not been reported. This work contributes modifications of blending to extend the scope of application to non-power-law, non-crossing asymptotics, and develops a systematic approach for two-dimensional blending. The proposed blending methods are practiced to establish correction factors for ideal solutions. This work contributes correction factors to ideal solutions to improve the usefulness to all cases covering "slow", "fast" and intermediate speeds. The work also contributes correction factors that depend on two dimensionless variables to account for secondary phenomena. They are correction factors for effects of surface heat losses for the isotherm width and its location, the trailing length and the cooling rate, and for effects of heat source distributions for the isotherm width on a thick plate.

The following objectives are fulfilled:

- Modify Churchill-Usagi 1-D blending equation systematic to extend its scope of application and improve accuracy at intermediate regimes to generate explicit scaling laws that predict characteristics of interest depending on one dimensionless group.

- Develop predictive engineering expressions for characteristics related to isotherms with an implement of the modified 1-D blending methodology proposed, including: maximum isotherm width $y_{\max}$ and its location $x_{\max}$, trailing length of isotherm x_{b}, leading length of isotherm x_{f}, centerline cooling rate $\dot{T}_{\mathrm{b}}$, centerline heating rate $\dot{T}_{\mathrm{f}}$, maximum temperature of a point in the cross-section $T_{\max}$ and transverse temperature gradient at the maximum isotherm width $\mathrm{d}T_{\max}/\mathrm{d}y$. Secondary thermal features are the aspect ratio $\mathcal{AR}$ of the chosen isotherm and melting efficiency η_{m} which is defined as the ratio of energy to melt the base material to that absorbed by the workpiece, solidification time t_{sl} which is important to the transformation of microstructures, cooling time from 800 °C to

500 °C, $t_{8/5}$, which is a key characteristic for steel processes, width of heat affected zone Δy_{HAZ}.

- Propose a systematic 2-D blending methodology that generates explicit scaling laws to predict characteristics of interest depending on two dimensionless groups.

- Develop correction factors of the effects of surface heat loss for isotherm trailing x_{b} and centerline cooling rate $\dot{T}_{\mathrm{b}}$ by implementing the proposed 2-D blending methodology.

- Develop correction factors of the effects of surface heat loss for isotherm width $y_{\max}$ by implementing the proposed 2-D blending methodology.

- Develop correction factors of the size of heat source for isotherm width $y^*_{\max}$ based on moving Gaussian heat source model by implementing the proposed 2-D blending methodology.

- Validate the proposed predictive formulae by comparing with data collected from published papers for a wide range of sources, materials, processes, and operating parameters.

1.4 Thesis outline

This dissertation includes chapters as follows:

- Chapter 2 proposes the modified 1-D blending methodology by introducing exponential modification term for non-crossing asymptotics. The implement of the modified 1-D blending methodology yields engineering expressions for isotherm half-width $y_{\max}$ under moving line heat source. A comprehensive survey of experimental results indicates a good agreement with the predictions resulting from the proposed expression.

- Chapter 3 proposes modified 1-D blending methodology by introducing a transitional term for better accuracy in the intermediate region. Based on the modified 1-D blending, the engineering expressions for thermal features of 12 magnitudes associated with a moving point heat source in a 2-D space are presented: location of maximum width, trailing length, centerline cooling rate, leading length, centerline heating rate, maximum temperature, the gradient of maximum temperature, aspect ratio, melting efficiency, cooling time from 800 °C to 500 °C, solidification time, the thickness of the heat-affected zone. The expressions for cooling rate, isotherm length ($x_{\mathrm{f}} - x_{\mathrm{b}}$), maximum temperature, heat-affected zone thickness, and isotherm aspect ratio are validated with data collected from published papers.

- Chapter 4 proposes a special case of 2-D blending and presents correction factor of trailing length and centerline cooling rate to account for the effects of surface heat losses based on the 2-D blending. The engineering expressions and correct factors proposed are validated with data collected from published data for welding, hard facing and additive manufacturing under water and air.

- Chapter 5 proposes a systematic approach to achieve 2-D blending and presents correction factor of isotherm width and its location to account for the effects of surface heat losses with the proposed 2-D blending approach. A comparison illustrates acceptable agreements between the predictive equations and collected data from published papers and welding simulation results for thermal residual stresses.

- Chapter 6 develops correction factors of size of heat source for isotherm half-width based on moving Gaussian heat source on thick plate, with the proposed 2-D blending approach. Comparisons of the proposed equations are conducted with measurements from literatures.

- Chapter 7 summarizes the results and novelties in this dissertation and proposes potential future work to continue this research.

- The appendix chapters list the supplementary materials to achieve the scaling laws in the papers, including figures supporting blending results and Matlab codes. The appendix chapters also proposed engineering expressions for catchment efficiencies of Gaussian distributed powder cloud.

References

[3] A. Acrivos, "On the solution of the convection equation in laminar boundary layer flows," *Chemical Engineering Science*, vol. 17, no. 6, pp. 457–465, 1962.

[4] A. Acrivos, "A rapid method for estimating the shear stress and the separation point in laminar incompressible boundary-layer flows," *Journal of the Aero/Space Sciences*, vol. 27, no. 4, pp. 314–315, 1960.

[8] M. Akbari, S. Saedodin, D. Toghraie, R. Shoja-Razavi, and F. Kowsari, "Experimental and numerical investigation of temperature distribution and melt pool geometry during pulsed laser welding of Ti6Al4V alloy," *Optics & Laser Technology*, vol. 59, pp. 52–59, 2014.

[9] American Welding Society (AWS) D1 Committee, *Structural welding code - steel*, American Welding Society (AWS) D1 Committee, 2015.

[10] A. Anca, A. Cardona, J. Risso, and V. D. Fachinotti, "Finite element modeling of welding processes," *Applied Mathematical Modelling*, vol. 35, no. 2, pp. 688–707, 2011.

[13] A. S. Azar, S. K. Ås, and O. M. Akselsen, "Determination of welding heat source parameters from actual bead shape," *Computational Materials Science*, vol. 54, pp. 176–182, 2012.

[14] S. Bag, A. Trivedi, and A. De, "Development of a finite element based heat transfer model for conduction mode laser spot welding process using an adaptive volumetric heat source," *International Journal of Thermal Sciences*, vol. 48, no. 10, pp. 1923–1931, 2009.

[16] S. Bannour, K. Abderrazak, H. Mhiri, and G. Le Palec, "Effects of temperature-dependent material properties and shielding gas on molten pool formation during continuous laser welding of AZ91 magnesium alloy," *Optics & Laser Technology*, vol. 44, no. 8, pp. 2459–2468, 2012.

[25] V. H. Bulsara, Y. Ahn, S. Chandrasekar, and T. N. Farris, "Polishing and lapping temperatures," *Journal of Tribology*, vol. 119, no. 1, pp. 163–170, 1997.

[28] S. Chen, G. Guillemot, and C.-A. Gandin, "Three-dimensional cellular automaton-finite element modeling of solidification grain structures for arc-welding processes," *Acta Materialia*, vol. 115, pp. 448–467, 2016.

[30] Z. Chen and X. Gao, "Detection of weld pool width using infrared imaging during high-power fiber laser welding of type 304 austenitic stainless steel," *The International Journal of Advanced Manufacturing Technology*, vol. 74, no. 9-12, pp. 1247–1254, 2014.

[31] J. Cheng and A. Kar, "Mathematical model for laser densification of ceramic coating," *Journal of materials science*, vol. 32, no. 23, pp. 6269–6278, 1997.

[32] S. Chowdhury, N. Yadaiah, S. M. Khan, R. Ozah, B. Das, and M. Muralidhar, "A perspective review on experimental investigation and numerical modeling of electron beam welding process," *Materials Today: Proceedings*, vol. 5, no. 2, pp. 4811–4817, 2018.

[34] S. W. Churchill and R. Usagi, "A general expression for the correlation of rates of transfer and other phenomena," *AIChE Journal*, vol. 18, no. 6, pp. 1121–1128, 1972.

[35] S. W. Churchill, "Comprehensive correlating equations for heat, mass and momentum transfer in fully developed flow in smooth tubes," *Industrial & Engineering Chemistry Fundamentals*, vol. 16, no. 1, pp. 109–116, 1977.

[36] S. W. Churchill, "Comprehensive, theoretically based, correlating equations for free convection from isothermal spheres," *Chemical Engineering Communications*, vol. 24, no. 4:6, pp. 339–352, 1983.

[37] S. W. Churchill and H. H. S. Chu, "Correlating equations for laminar and turbulent free convection from a horizontal cylinder," *International Journal of Heat and Mass Transfer*, vol. 18, no. 9, pp. 1049–1053, 1975.

[38] S. W. Churchill and R. Usagi, "A standardized procedure for the production of correlations in the form of a common empirical equation," *Industrial & Engineering Chemistry Fundamentals*, vol. 13, no. 1, pp. 39–44, 1974.

[45] J. Ding, P. Colegrove, J. Mehnen, S. Williams, F. Wang, and P. S. Almeida, "A computationally efficient finite element model of wire and arc additive manufacture," *The International Journal of Advanced Manufacturing Technology*, vol. 70, no. 1-4, pp. 227–236, 2014.

[49] J. DuPont, "Dilution in fusion welding," *ASM handbook*, vol. 6, pp. 115–121, 2011.

[50] F. Durst, S. Ray, B. Ünsal, and O. A. Bayoumi, "The development lengths of laminar pipe and channel flows," *Journal of Fluids Engineering*, vol. 127, no. 6, pp. 1154–1160, 2005.

[51] R. P. Dutt and R. C. Brewer, "On the theoretical determination of the temperature field in orthogonal machining," *International Journal of Production Research*, vol. 4, no. 2, pp. 91–114, 1965.

[52] D. Dye, O. Hunziker, and R. C. Reed, "Numerical analysis of the weldability of superalloys," *Acta Materialia*, vol. 49, no. 4, pp. 683–697, 2001.

[53] T. W. Eagar and N. S. Tsai, "Temperature fields produced by traveling distributed heat sources," *Welding Journal*, vol. 62, no. 12, pp. 346–355, 1983.

[56] V. D. Fachinotti, A. A. Anca, and A. Cardona, "Analytical solutions of the thermal field induced by moving double-ellipsoidal and double-elliptical heat sources in a semi-infinite body," *International Journal for Numerical Methods in Biomedical Engineerin*, vol. 27, pp. 595–607, 2011.

[58] P. S. Fedkiw and J. Newman, "Mass-transfer coefficients in packed beds at very low reynolds numbers," *International Journal of Heat and Mass Transfer*, vol. 25, no. 7, pp. 935–943, 1982.

[61] P. W. Fuerschbach and G. A. Knorovsky, "A study of melting efficiency in plasma arc and gas tungsten arc welding," *Welding Research Supplement*, vol. 70, no. 11, pp. 287–297, 1991.

[64] S. S. Gajapathi, S. K. Mitra, and P. F. Mendez, "Controlling heat transfer in micro electron beam welding using volumetric heating," *International Journal of Heat and Mass Transfer*, vol. 54, no. 25-26, pp. 5545–5553, 2011.

[66] E. Gariboldi and B. Previtali, "High tolerance plasma arc cutting of commercially pure titanium," *Journal of Materials Processing Technology*, vol. 160, no. 1, pp. 77–89, 2005.

[68] A. Ghosh and H. Chattopadhyay, "Mathematical modeling of moving heat source shape for submerged arc welding process," *The International Journal of Advanced Manufacturing Technology*, vol. 69, no. 9-12, pp. 2691–2701, 2013.

[69] A. Ghosh, A. Yadav, and A. Kumar, "Modelling and experimental validation of moving tilted volumetric heat source in gas metal arc welding process," *Journal of Materials Processing Technology*, vol. 239, pp. 52–65, 2017.

[73] J. Gockel, N. Klingbeil, and S. Bontha, "A closed-form solution for the effect of free edges on melt pool geometry and solidification microstructure in additive manufacturing of thin-wall geometries," *Metallurgical and Materials Transactions B*, vol. 47, no. 2, pp. 1400–1408, 2016.

[74] J. Goldak, A. Chakravarti, and M. Bibby, "A new finite element model for welding heat sources," *Metallurgical Transactions B*, vol. 15, no. 2, pp. 299–305, 1984.

[75] V. K. Goyal, P. K. Ghosh, and J. S. Saini, "Analytical studies on thermal behaviour and geometry of weld pool in pulsed current gas metal arc welding," *Journal of materials processing technology*, vol. 209, no. 3, pp. 1318–1336, 2009.

[76] M. R. Grams and P. F. Mendez, "Scaling analysis of the thermal stress field produced by a moving point heat source in a thin plate," *Journal of Applied Mechanics*, pp. 1–34, Sep. 2020.

[81] M. Haghpanahi, S. Salimi, P. Bahemmat, and S. Sima, "3-D transient analytical solution based on green's function to temperature field in friction stir welding," *Applied Mathematical Modelling*, vol. 37, no. 24, pp. 9865–9884, 2013.

[84] K. Heller, S. Kessler, F. Dorsch, P. Berger, and T. Graf, "Analytical description of the surface temperature for the characterization of laser welding processes," *International Journal of Heat and Mass Transfer*, vol. 106, pp. 958–969, 2017.

[85] H. Hemmer and Ø. Grong, "Prediction of penetration depths during electron beam welding," *Science and technology of welding and joining*, vol. 4, no. 4, pp. 219–225, 1999.

[86] J. W. Hill, M. J. Lee, and I. J. Spalding, "Surface treatments by laser," *Optics & Laser Technology*, vol. 6, no. 6, pp. 276–278, 1974.

[87] A. Hintze Cesaro and P. F. Mendez, "Models to predict hardness in the HAZ," *Weld Magazine*, pp. 42–55, 2019.

[89] Z. B. Hou and R. Komanduri, "General solutions for stationary/moving plane heat source problems in manufacturing and tribology," *International Journal of Heat and Mass Transfer*, vol. 43, no. 10, pp. 1679–1698, 2000.

[92] F. P. Incropera, D. P. DeWitt, T. L. Bergman, and A. S. Lavine, *Fundamentals of heat and mass transfer*. John Wiley & Sons, 2007.

[94] J. C. Jaeger, "Moving sources of heat and the temperature of sliding contacts," in *Proceedings of the royal society of New South Wales*, vol. 76, 1942, pp. 203–224.

[98] X. Jia, J. Xu, Z. Liu, S. Huang, Y. Fan, and Z. Sun, "A new method to estimate heat source parameters in gas metal arc welding simulation process," *Fusion Engineering and Design*, vol. 89, no. 1, pp. 40–48, 2014.

[99] T. Kasuya and N. Yurioka, "Prediction of welding thermal history by a comprehensive solution," *Welding Research Supplement*, vol. 72, no. 3, 107s–115s, 1993.

[101] J. Kidawa-Kukla, "Temperature distribution in a rectangular plate heated by a moving heat source," *International Journal of Heat and Mass Transfer*, vol. 51, pp. 865–872, 2008.

[102] K. Knothe and S. Liebelt, "Determination of temperatures for sliding contact with applications for wheel-rail systems," *Wear*, vol. 189, no. 1-2, pp. 91–99, 1995.

[103] F. Kolonits, "Analysis of the temperature of the rail/wheel contact surface using a half-space model and a moving heat source," *Proceedings of the Institution of Mechanical Engineers Part F: Journal of Rail and Rapid Transit*, vol. 230, no. 2, pp. 502–509, 2016.

[104] R. Komanduri and Z. B. Hou, "Thermal analysis of the arc welding process : Part I . general solutions," *Metallurgical and Materials Transactions B*, vol. 31B, no. 6, pp. 1353–1370, 2000.

[106] R. Komanduri and Z. B. Hou, "Thermal analysis of the laser surface transformation hardening process," *International Journal of Heat and Mass Transfer*, vol. 44, no. 15, pp. 2845–2862, 2001.

[107] R. Komanduri and Z. B. Hou, "Unified approach and interactive program for thermal analysis of various manufacturing processes with application to machining," *Machining Science and Technology*, vol. 13, no. 2, pp. 143–176, 2009.

[112] S. Kou, "Simulation of heat flow during the welding of thin plates," *Metallurgical Transactions A*, vol. 12, no. 12, pp. 2025–2030, 1981.

[115] M. Kubiak, W. Piekarska, and S. Stano, "Modelling of laser beam heat source based on experimental research of Yb : YAG laser power distribution," *International Journal of Heat and Mass Transfer*, vol. 83, pp. 679–689, 2015.

[116] P. K. Kundu, I. M. Cohen, and D. R. Dowling, *Fluid mechanics*, Fifth. Waltham, MA: Academic Press, 2012, ISBN: 978-0-12-382100-3.

[118] D. H. Lammlein, D. R. DeLapp, P. A. Fleming, A. M. Strauss, and G. E. Cook, "The application of shoulderless conical tools in friction stir welding: An experimental and theoretical study," *Materials & Design*, vol. 30, no. 10, pp. 4012–4022, 2009.

[121] J. Lee, O. B. Ozdoganlar, and Y. Rabin, "An experimental investigation on thermal exposure during bone drilling," *Medical Engineering & Physics*, vol. 34, no. 10, pp. 1510–1520, 2012.

[124] W.-B. Li, K. E. Easterling, and M. F. Ashby, "Laser transformation hardening of steel-II. hypereutectoid steels," *Acta Metallurgica*, vol. 34, no. 8, pp. 1533–1543, 1986.

[125] Y. Li, Y.-h. Feng, X.-x. Zhang, and C.-s. Wu, "An improved simulation of heat transfer and fluid flow in plasma arc welding with modified heat source model," *International Journal of Thermal Sciences*, vol. 64, pp. 93–104, 2013.

[132] S. Malkin, "Thermal aspects of grinding: Part 2 – surface temperatures and workpiece burn," *Journal of Engineering for Industry*, vol. 96, no. 4, pp. 1184–1191, 1974.

[137] P. F. Mendez, K. E. Tello, and S. S. Gajapathi, "Generalization and communication of welding simulations and experiments using scaling analysis design rules in welding design rules in engineering : Calibrated minimal representation approach," in *Trends in Welding Research, Proceedings of the 9th International Conference*, ASM International, 2012, pp. 249–258.

[138] P. F. Mendez, "Advanced scaling techniques for the modeling of materials processing," in *Industrial Practice*, vol. 7, ASME, 2006, pp. 393–404, ISBN: 978-0-7918-4358-1.

[141] P. F. Mendez, K. E. Tello, and T. J. Lienert, "Scaling of coupled heat transfer and plastic deformation around the pin in friction stir welding," *Acta Materialia*, vol. 58, no. 18, pp. 6012–6026, 2010.

[149] V. Nemchinsky, "Temperature created by a moving heat source that heats and melts the metal plate (plasma arc cutting)," *Journal of Heat Transfer*, vol. 138, no. 12, p. 122 301, 2016.

[151] S. H. Nikam and N. K. Jain, "Finite element simulation of pre-heating effect on melt pool size during micro-plasma transferred arc deposition process," in *IOP Conference Series: Materials Science and Engineering*, ser. IOP Conference Series: IOP Publishing, vol. 389, 2018, p. 012 006.

[152] A. Nisar, M. J. J. Schmidt, M. A. Sheikh, and L. Li, "Three-dimensional transient finite element analysis of the laser enamelling process and moving heat source and phase change considerations," *Proceedings of the Institution of Mechanical Engineers, Part B: Journal of Engineering Manufacture*, vol. 217, no. 6, pp. 753–764, 2003.

[154] K. Ogawa, "Analysis of temperature distribution around moving heat source in thin plate," *Journal of the Marine Engineering Society in Japan*, vol. 22, no. 4, pp. 257–262, 1987.

[158] R. Parkitny and J. Winczek, "Analytical solution of temporary temperature field in half-infinite body caused by moving tilted volumetric heat source," *International Journal of Heat and Mass Transfer*, vol. 60, pp. 469–479, 2013.

[159] W. Paulsen, *Asymptotic analysis and perturbation theory*. CRC Press, 2013.

[160] V. Pavelic, R. Tanbakuchi, O. A. Uyehara, and P. S. Myers, "Experimental and computed temperature histories in gas tungsten-arc welding of thin plates," *Welding Research Supplement*, vol. 48, pp. 295–305, 1969.

[161] Q. Peng, "An analytical solution for a transient temperature field during laser heating a finite slab," *Applied Mathematical Modelling*, vol. 40, no. 5-6, pp. 4129–4135, 2016.

[163] X.-T. Pham, "Two-dimensional Rosenthal moving heat source analysis using the meshless element free Galerkin method," *Numerical Heat Transfer, Part A: Applications*, vol. 63, no. 11, pp. 807–823, 2013.

[164] W. Piekarska and M. Kubiak, "Theoretical investigations into heat transfer in laser-welded steel sheets," *Journal of thermal analysis and calorimetry*, vol. 110, no. 1, pp. 159–166, 2012.

[165] W. D. Pilkey and D. F. Pilkey, *Peterson's stress concentration factors*. John Wiley & Sons, 2008.

[170] I. A. Roberts, C. J. Wang, R. Esterlein, M. Stanford, and D. J. Mynors, "A three-dimensional finite element analysis of the temperature field during laser melting of metal powders in additive layer manufacturing," *International Journal of Machine Tools and Manufacture*, vol. 49, no. 12-13, pp. 916–923, 2009.

[171] O. F. T. Roberts, "The theoretical scattering of smoke in a turbulent atmosphere," in *Proceedings of the Royal Society of London*, ser. Series A, Containing Papers of a Mathematical and Physical Character, vol. 104, Royal Society, 1923, pp. 640–654.

[172] M. Rohde, C. Markert, and W. Pfleging, "Laser micro-welding of aluminum alloys: Experimental studies and numerical modeling," *The International Journal of Advanced Manufacturing Technology*, vol. 50, no. 1-4, pp. 207–215, 2010.

[174] D. Rosenthal, "Etude théorique du régime thermique pendant la soudure à l'arc," *Congres National des Sciences Comptes Rendus Bruxelles*, vol. 2, pp. 1277–1292, 1935.

[175] D. Rosenthal, "The theory of moving sources of heat and its application to metal treatments," *Transactions of the A.S.M.E.*, vol. 68, pp. 849–866, 1946.

[176] D. Rosenthal and R. Schmerber, "Thermal study of arc welding," *Welding journal*, vol. 17, no. 4, pp. 2–8, 1938.

[178] S. Rouquette, J. Guo, and P. Le Masson, "Estimation of the parameters of a Gaussian heat source by the Levenberg–Marquardt method: Application to the electron beam welding," *International Journal of Thermal Sciences*, vol. 46, no. 2, pp. 128–138, 2007.

[179] N. N. Rykalin, *Calculation of heat flow in welding*. Mashgis, Moscow, Russia: Mashgis, 1951.

[187] Stock Drive Products / Sterling Instrument, *Handbook of METRIC drive components D805*. 2010.

[188] J. Sundqvist, A. F. H. Kaplan, L. Shachaf, and C. Kong, "Analytical heat conduction modelling for shaped laser beams," *Journal of Materials Processing Technology*, vol. 247, pp. 48–54, 2017.

[190] D. T. Swift-Hook and A. E. F. Gick, "Penetration welding with lasers," *Welding Research Supplement*, vol. 52, no. 11, 492s–499s, 1973.

[192] Technical Committee CEN/TC 121 Welding, *Welding - recommendations for welding of metallic materials - Part 2 : Arc welding of ferritic steels*, Technical Committee CEN/TC 121 Welding, 2001.

[194] K. Tello, U. Duman, and P. F. Mendez, "Scaling laws for the welding arc, weld penetration and friction stir welding," in *Trends in Welding Research, Proceedings of the 8th International Conference*, The Material Information Society, ASM International, 2009, pp. 172–181, ISBN: 9781615030026.

[195] R Trivedi, S. David, M. Eshelman, J. Vitek, S. Babu, T Hong, and T DebRoy, "In situ observations of weld pool solidification using transparent metal-analog systems," *Journal of applied physics*, vol. 93, no. 8, pp. 4885–4895, 2003.

[198] M. Van Elsen, M. Baelmans, P. Mercelis, and J.-P. Kruth, "Solutions for modelling moving heat sources in a semi-infinite medium and applications to laser material processing," *International Journal of Heat and Mass Transfer*, vol. 50, no. 23-24, pp. 4872–4882, 2007.

[200] C. S. W. and C. H. H.S., "Correlating equations for laminar and turbulent free convection from a vertical plate," *International Journal of Heat and Mass Transfer*, vol. 18, no. 11, 1975.

[205] Y. Wang, P. Fu, Y. Guan, Z. Lu, and Y. Wei, "Research on modeling of heat source for electron beam welding fusion-solidification zone," *Chinese Journal of Aeronautics*, vol. 26, no. 1, pp. 217–223, 2013.

[215] H. A. Wilson, "On convection of heat," in *Proceedings of the Cambridge Philosophical Society*, vol. 12, 1904, pp. 406–423.

[216] J. Winczek, "Analytical solution to transient temperature field in a half-infinite body caused by moving volumetric heat source," *International Journal of Heat and Mass Transfer*, vol. 53, no. 25-26, pp. 5774–5781, 2010.

[217] J. Winczek, A. Modrzycka, and E. Gawrońska, "Analytical description of the temperature field induced by laser heat source with any trajectory," *Procedia Engineering*, vol. 149, pp. 553–558, 2016.

[219] G. Wood and P. F. Mendez, "First order prediction of bead width and height in coaxial laser cladding," in *Proceedings of Numerical Analysis of Weldability*, Graz, Austria, 2015.

[223] N. Yadaiah and S. Bag, "Development of egg-configuration heat source model in numerical simulation of autogenous fusion welding process," *International Journal of Thermal Sciences*, vol. 86, pp. 125–138, 2014.

[224] N. Yadaiah and S. Bag, "Effect of heat source parameters in thermal and mechanical analysis of linear GTA welding process," *ISIJ international*, vol. 52, no. 11, pp. 2069–2075, 2012.

[227] G. Yu, R. J. Anderson, T. Maekawa, and N. M. Patrikalakis, "Efficient simulation of shell forming by line heating," *International Journal of Mechanical Sciences*, vol. 43, no. 10, pp. 2349–2370, 2001.

[228] L. Zhang, B. L. Tai, G. Wang, K. Zhang, S. Sullivan, and A. J. Shih, "Thermal model to investigate the temperature in bone grinding for skull base neurosurgery," *Medical Engineering & Physics*, vol. 35, no. 10, pp. 1391–1398, 2013.

Chapter 2

Width of thermal features induced by a 2-D moving heat source

2.1 Abstract

Novel expressions in explicit form are presented for the estimation of the width of the bead, location of heat affected zone, and the width of any chosen isotherm in materials processes such as welding, additive manufacturing, laser heat treatment, and cutting. These expressions are applicable when the substrate is relatively thin (as in most cases of welding and additive manufacturing of walls), or when the heat source penetrates deeply into the substrate (as in keyhole mode in laser or electron beam welding). The explicit expressions are based on the widely used Rosenthal 2-D solution, which yields results of the correct order of magnitude compared to experiments for a broad range of materials, processes, and parameters. Asymptotic analysis was applied and a new blending technique was developed to arrive to explicit expressions within 7% of the exact solution. The key dimensionless group in this case is the Rosenthal number Ro, which enables the blending of solutions corresponding to fast and slow heat sources. A comprehensive survey of experimental results indicates a good agreement with the predictions resulting from the proposed expression.

Table 2.1: Notation

Variables	Unit	Description
A_c	m^2	Cross sectional area of melt
c	$\mathrm{J\,kg^{-1}\,K^{-1}}$	Specific heat of the substrate
d	m	Thickness of the substrate
$d_{\mathrm{c,2D}}$	m	Maximum thickness to approximate as 2D
$d_{\mathrm{c,h}}$	m	Minimum thickness to ignore convection
h	$\mathrm{W\,m^{-2}\,K^{-1}}$	Convection coefficient on top surface
h'	$\mathrm{W\,m^{-2}\,K^{-1}}$	Convection coefficient on bottom surface
i_0	$\mathrm{J\,kg^{-1}}$	Enthalpy at the far temperature
i_l	$\mathrm{J\,kg^{-1}}$	Enthalpy at the liquidus temperature
i_sl	$\mathrm{J\,kg^{-1}}$	Latent heat of fusion
k	$\mathrm{W\,m^{-1}\,K^{-1}}$	Thermal conductivity of the substrate
q	W	Power absorbed by substrate
q'	$\mathrm{Wm^{-1}}$	Intensity of line heat source
r	m	Distance from the heat source
t	s	Time
T	K	Temperature
T_0	K	Far temperature or preheat
T_c	K	Temperature of interest
U	$\mathrm{m\,s^{-1}}$	Travel speed of the moving heat source
x, y	m	Cartesian coordinates
x_max	m	Location of maximum isotherm width
y_max	m	Isotherm half-width
Greek symbols		
α	$\mathrm{m^2\,s^{-1}}$	Thermal diffusivity of the substrate

Continued on next page

Table 2.1 – continued from previous page

Variables	Unit	Description
γ	1	Euler–Mascheroni constant
ρ	$\mathrm{kg\,m^{-3}}$	Density of the substrate
σ	m	Distribution parameter of the heat source
η_m	1	Melting efficiency
Dimensionless Groups		
Bi		Biot number
Pe		Peclet number
Ro		Rosenthal number
Ry		Rykalin number
St		Stefan number
Superscripts		
*		Dimensionless value
$\widehat{\ }$		Asymptotic behavior
$^+$		Correction for intermediate regions
Subscripts		
III		Regime III (large Ro, fast)
IV		Regime IV (small Ro, slow)
Acronyms		
AM		Additive manufacturing
EBW		Electron beam welding
FSW		Friction stir welding
GMAW		Gas metal arc welding
GTAW		Gas tungsten arc welding
HAZ		Heat affected zone

Continued on next page

Table 2.1 – continued from previous page

Variables	Unit	Description
LBW		Laser beam welding
SAW		Submerged arc welding
SMAW		Shielded metal arc welding

2.2 Introduction

In the thermal analysis of moving heat source problems, the estimation of the size and shape of isotherms is essential because it determines the extent of thermal alterations in the base metal and resulting properties. For example, in the field of welding, the size and shape of the melting isotherm determine critical features such as weld seam geometry and metallurgical dilution. For the case of steel, the maximum width of the isotherm of austenization temperature (A_{c1}) has a large influence in the reach of the heat affected zone (HAZ), which has a decisive effect on joint properties. Despite the importance of prediction of isotherm width and the numerous previous efforts to calculate it, there is no engineering expression to anticipate it in typical conditions, and in practice engineers typically resort to previous experience or trial and error when developing parameters for moving heat sources.

Previous efforts to predict the width of isotherms fall into three main categories: analytical approaches [53, 140, 179, 190, 213], measurements from experiments [54, 62, 71, 155, 176], and numerical simulations [12, 90, 146, 160, 163, 183].

Analytical approaches of isotherm width for extreme (asymptotic) cases have been investigated before; however, published expressions focus only on one extreme [145, 213], or both extremes [84, 88, 190], neglecting the intermediate regime. Paradoxically, most real-life applications are in the intermediate regime for which there is currently no available closed-form solution.

Case-by-case results of experiments with different processing parameters and par-

ent materials are insufficient to inform novel applications. Also, empirical equations in open literature [70, 96, 190, 213] are only valid for specific processes and limited to narrow ranges of operating parameters for which empirical parameters were fitted.

The practical application of numerical simulations is frequently restricted by the need of specialized software, demand of computational skills, and the need to consider parameters that are difficult to measure in real operating situations. Numerical simulations are seldom part of standards the way explicit expressions are, and are often difficult to implement into metamodels, while explicit expressions like those developed here can readily be assembled into larger models. The intuitive and pedagogical advantage of explicit expressions is often challenging to obtain with simulations.

The work presented here is part of a broader research program aimed at identifying moving heat source features and presenting practical and accurate predictive expressions useful to practitioners. The overall program is based on the understanding that many important aspects of complex problems such as welding and additive manufacturing can be treated using a minimal representation that captures only the dominant physics, with the secondary physics included as correction factors. This approach is often used in all engineering disciplines at an intuitive level, and a formal implementation is described in [134, 137, 140, 141, 218].

The predictive equations proposed in this investigation were developed within the framework of the broader program and also consist of closed-form asymptotic solutions and correction factors to account for intermediate cases. In this work, the asymptotic cases are based on Rosenthal's 2-D solution [176], also called the "thin plate" solution or "line heat source" solution. This solution is accurate enough to be used routinely used in practice for a wide range of materials and problems including arc welding [62, 160, 176, 213], laser and electron beam welding [73, 85, 190], metal cutting [66, 149], thermal forming of shells [227], and has even been adapted to mass transfer [171].

Due to its fundamental nature, the expressions developed in this work can be used for the estimation of heat source efficiency, optimization of processing parameters, or

determination of resulting material properties in a simple and economical manner in many applications, including welding with most techniques, additive manufacturing, laser heat treating, grinding, and machining. In addition, the effect of processing parameters and their interplay are displayed explicitly, bringing understanding and intuition for the physical phenomena involved.

2.3 Governing equation

The idealized model considered in this work consists of a point heat source of intensity q which moves with constant velocity along a straight path on an infinite 2-D domain of constant thermophysical properties. The 2-D domain represents in practice a substrate of thickness d which can be either very thin with a point heat source on the surface, or of any thickness with the heat source becoming a line of constant linear heat intensity $q' = q/d$ penetrating the full thickness, as represented in Figure 2.1. Surface heat losses by convection and radiation can be taken into account easily when the substrate is thin. It will be shown later that beyond certain thickness (typical of many processes such as welding) surface heat losses are negligible compared to conduction in the substrate.

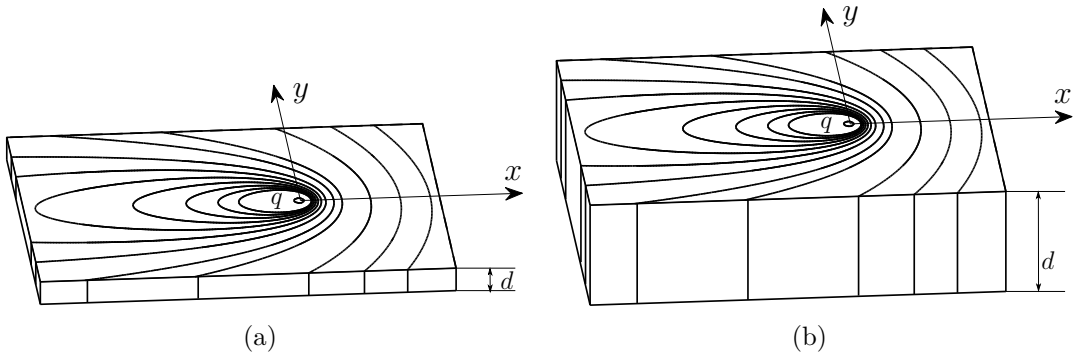

Figure 2.1: Isotherms for a 2-D point heat source of intensity q on a substrate of thickness d. The domain is $-\infty < x < \infty, -\infty < y < \infty$ and there are no gradients in z. The 2D behavior is approximated in thin plates (a) or thick plates with the heat input distributed uniformly along the thickness (b).

Except for the start and stop stages, the moving heat source is in a convenient

pseudo-steady state, captured with an Eulerian formulation with the heat source considered fixed and the substrate moving along the x-axis in the negative direction. The governing equation in this case is:

$$\frac{\partial^2 T}{\partial x^2} + \frac{\partial^2 T}{\partial y^2} = -\frac{U}{\alpha}\frac{\partial T}{\partial x} + \frac{h + h'}{kd}(T - T_0) \tag{2.1}$$

with the following boundary conditions:

$$\frac{\partial T}{\partial r} = -\frac{q}{2\pi r k d} \qquad \text{as } r \to 0 \tag{2.2}$$

$$T = T_0 \qquad \text{as } r \to \infty \tag{2.3}$$

where x, y are the coordinates defined in Figure 2.1, $r = \sqrt{x^2 + y^2}$, $T(x, y)$ is the temperature at each point, U is the relative velocity between the heat source and the substrate, h and h' are the effective convection coefficients on the top and bottom surface (they also account for radiation in an approximate way), α and k are the thermal diffusivity and thermal conductivity of the substrate, d is the substrate thickness, q is the rate of heat (W) absorbed by the substrate, which accounts for the thermal efficiency of the process, and T_0 is the uniform temperature of the substrate far from the heat source.

In Equation 2.1, the surface heat losses are be approximated as volumetric losses, in a way similar to the study of fins [19]. This is an accurate approximation for substrates thin enough as to have a small Biot number Bi= $(h+h')d/k$. This condition is common in practical processes such as arc welding; for example, a representative weld would have surface heat losses $h + h'$ of the order of 20 W/m^{2}K (natural convection in air) and a thermal conductivity of 50 W/mK (steel). In these conditions, a large substrate thickness such as 100 mm still would yield a small Biot number of 0.04.

This problem was first solved by Wilson in 1904 [215], and it was solved independently again by Rosenthal [175–177] in the 1940s, with a focus on welding. Comprehensive reviews of these solutions are in [27, 78, 145]. The solution to Equation 2.1 with the boundary conditions of Equation 2.2 and Equation 2.3 is:

$$T(x,y) = T_0 + \frac{q}{2\pi kd}\exp\left(-\frac{Ux}{2\alpha}\right) K_0\left[r\sqrt{\left(\frac{U}{2\alpha}\right)^2 + \frac{h+h'}{kd}}\right] \tag{2.4}$$

where K_0 is the modified Bessel function of second kind and zero order. This equation provides the temperature value for each point in the substrate. The singularity at the origin ($r = 0$) is a consequence of assuming the heat source is concentrated in an infinitesimal area.

2.4 Normalization and dimensional analysis

The analytical solution of Equation 2.4 can be expressed more concisely in dimensionless form as:

$$T^*(x^*, y^*) = \exp\left(-x^*\right) K_0\left(r^*\sqrt{1+h^*}\right) \tag{2.5}$$

where

$$T^* = \frac{2\pi kd\left(T - T_0\right)}{q} \tag{2.6}$$

$$h^* = \frac{4\alpha^2\left(h + h'\right)}{kdU^2} \tag{2.7}$$

$$x^* = \frac{Ux}{2\alpha} \tag{2.8}$$

$$y^* = \frac{Uy}{2\alpha} \tag{2.9}$$

$$r^* = \frac{Ur}{2\alpha} \tag{2.10}$$

In Equations 2.5-2.9, the * superscript indicates a dimensionless quantity, consistent with [43, 139, 140] and other modern literature. Equation 2.5 involves four dimensionless groups: two independent variables x^*, y^* (r^* is not independent), the dependent variable $T^*(x^*, y^*)$, and the parameter h^* associated with surface heat losses. Normalization of spatial variables x^* and y^* is similar to the definition of Peclet number in convection heat transfer, representing the ratio of the rate of advection to that of conduction mechanisms.

The number of dimensionless groups obtained is consistent with the number expected from applying dimensional analysis theory [24]. Equation 2.4 involves nine magnitudes with units: the two independent variables x, y, the dependent variable $T(x, y)$, and six problem parameters T_0, q/d,k,U, α, and $h + h'$. The groups q/d and $h + h'$ are considered together because they never appear separately in this analysis. There are four independent units for the magnitude with dimension (m, kg, s, °C) and the number of dimensionless groups is $9 - 4 - 1 = 4$ (the "-1" on the left hand side appears because no temperature must be measured in absolute terms [210]).

When considering the maximum width of isotherm $T^* = T_c^*$, the four dimensionless groups are constrained by Equation 2.5 and by the condition $y^*_{\max} = \max(y^*)$, leaving only two degrees of freedom. For practical reasons, and for consistency with previous literature, one of the degrees of freedom will be h^*, and the other the Rosenthal number (Ro), first proposed by Fuerschbach et al. [62], who used it to collapse onto a single curve several measurements with various welding methods and base materials. The expression of the Rosenthal number is:

$$\mathrm{Ro} = \frac{q}{2\pi k d\,(T_c - T_0)} = \frac{1}{T_c^*} \tag{2.11}$$

where the factor of $1/2\pi$ is included to simplify the final expressions detailed below. This definition is consistent with the dimensionless groups of [62, 85, 160, 186, 190].

Similarly to the Rykalin number (Ry) [140, 207], the Rosenthal number can also be interpreted as a Peclet number $\mathrm{Pe} = U\mathcal{L}/\alpha$ where the characteristic length $\mathcal{L} = Q"/\left(2\pi\rho c\Delta T\right)$ is related to the amount of heat deposited per unit length of travel and unit thickness of substrate $Q" = q/(Ud)$ and the heat absorbed by the substrate by heating the material next to the weld (within a distance $\mathcal{L}$ from the centerline) by an amount $\Delta T = T_c - T_0$. The Peclet number relates the effect of advection relative to conduction and therefore a high Ro value can be interpreted as a "fast heat source" where advection dominates over conduction, and a low Ro value can be interpreted as a "slow heat source" with heat transfer dominated by conduction. The dimensionless

groups Ro and Ry are related to each other as

$$\mathrm{Ro} = \frac{\mathrm{Ry}}{d^*} \tag{2.12}$$

where

$$d^* = \frac{Ud}{2\alpha} \tag{2.13}$$

2.5 Limitations of idealized model

The idealizations that result in Equation 2.4, enable for a much desired practical formula. Fortunately, the gains in practicality come at a relatively low cost in terms of accuracy. The most important simplifications have been addressed in previous research indicating that the idealizations are consistent with most practical problems. Four idealizations are reviewed here: the effect of a finite heat source, the effect of temperature on thermophysical properties, the effect of latent heat, and the effect of surface heat losses. The effects of more complex phenomena such as convective flows during melting involve multiple additional physics and new dimensionless groups, and deserve a special treatment such as [169].

2.5.1 Effect of finite heat source

Equation 2.4 considers that the heat source is concentrated in a point, contradicting the reality that all heat sources have a finite size. The effect of finite heat sources is noticeable when the heat source is larger than a critical value. A finite heat source can have many different distributions of surface heat intensity [144, 198] or volumetric heat intensity [64, 74]. Here, we consider a circular gaussian surface distribution which includes the additional parameter of distribution σ as the next step in complexity beyond a point heat source. It is reasonable to expect that heat sources other than gaussian, but of similar size will have comparable thresholds for separating point-like behavior from distributed behavior. Gaussian heat sources were studied for thick substrates in [39, 53] and intermediate thickness in [117, 133]. The expression of a

circular gaussian surface heat source is:

$$q"(x,y) = q"_{\max} \exp\left(-\frac{r^2}{2\sigma^2}\right) \tag{2.14}$$

where $q"_{\max} = q/(2\pi\sigma^2)$ and σ is the standard deviation of Gaussian distribution.

A preliminary numerical analysis using Matlab and COMSOL Multiphysics indicates that the maximum width assuming a point heat source is overestimated with an error smaller than 10% compared to a Gaussian heat source for 0.1<Ro<100:

$$\sigma^* = \frac{U\sigma}{2\alpha} < \sigma_c^* = 0.6\ \widehat{y}_{\max}^* < 0.6\ \frac{1+2\mathrm{Ro}}{1+\mathrm{Ro}}\ \widehat{y}_{\max}^* \tag{2.15}$$

where $y_{\max}^*$ is the dimensionless half-width of an isotherm, explained in detail later in this paper and expressed explicitly in Equation 2.25. The criteria $0.6(1+2\mathrm{Ro})/(1+\mathrm{Ro})\widehat{y}_{\max}^*$ agrees with the simulation results and could be simplified to $0.6y_{\max}^*$ as a conservative rule-of-thumb ($\sigma < 0.6y_{\max}$). The derivation of Equation 2.15 is included in Appendix 2.C. For the case of very fast moving heat sources (Ro$\gg$1), this criterion might be too conservative and is the subject of current research.

2.5.2 Effect of substrate thickness

When the heat source is a line of uniform intensity through the thickness of the substrate, if the intensity of the line heat source q' is constant through the thickness and surface heat losses are negligible, the substrate thickness is irrelevant. This condition also applies approximately for full penetration welds and for deep keyhole welds with partial penetration, in which the heat source is a segment; in this case the length of the line heat source is the keyhole penetration.

When the heat source is a point applied on the surface of a plate of finite thickness, 3D effects will exist near the heat source, but 2D conditions will exist further from the heat source. The 3D effects on maximum width of an isotherm are smaller for thinner substrates. A comparison of the 2D solution against the exact solution for plates of intermediate thickness was performed in [146]; following this work, the error

of in using the 2D for a point heat source on the surface of a finite plate is an underestimation smaller than 5% for $0.2 < \mathrm{Ro} < 100$ when

$$d^* < d^*_{\mathrm{c,2D}} \approx 1/4\ y^*_{\max} \tag{2.16}$$

2.5.3 Effect of temperature dependence on thermophysical properties

Equation 2.4 assumes that the thermophysical properties of the substrate are constant. Real materials have temperature-dependent properties, and this commonly use approximation must be assessed for practical cases. This assessment requires numerical methods and has been explored for the case of melt pool length in 304 stainless steels [20], showing that constant properties assessed at 1000 K result in errors within ±6.5%. For estimates of maximum width of weld pool in mild steel ($T_{\mathrm{melt}} \approx 1500°\mathrm{C}$) and heat affected zone width ($T_{\mathrm{HAZ}} \approx 727°\mathrm{C}$), the errors of assuming constant properties were approximately 5% and 2%, respectively, for all values of thermal properties in the temperature range of 400°C to 1300°C [106].

In this work, when effective thermophysical properties of the substrate needed to be calculated, they were obtained as detailed in Appendix 2.A.

2.5.4 Effect of melting

For the case of welding, where melting is involved, the assumption of constant thermophysical properties cannot account for the variations associated with the latent heat of phase change. Melting also introduces convective heat transfer in the melt.

The effect of convection has been studied extensively, for example [114, 156], and captured with scaling laws based on three dimensionless groups (Marangoni, Prandtl, and aspect ratio of cross section) [169]. These convective flows affect mostly the shape of the fusion line, often captured by width and depth. The effect of convective flows is less important in highly conductive materials (e.g. aluminum) and in small welds. Currently, it is known than in aluminum and steels with low sulfur or low oxygen

contents, weld are typically wider and shallower than predicted, while in steels with higher sulfur or oxygen welds are narrower and deeper. There is no general rule to assess when convective flows affect estimates of width and depth, and no attempt has been made on quantifying the magnitude of departure from the ideal case. A more comprehensive analysis is the focus of ongoing research. Other effects of melting also include the depression of the free surface [136], and impingement from metal transferred from the electrode [95].

The effect of latent heat on moving heat sources can be tackled with different numerical methods such as the apparent heat capacity method [40], the source based method [199], and the enthalpy approach [147]. The dimensionless group that accounts for latent heat is the Stefan number:

$$\mathrm{St} = c(T_m - T_0)/i_{\mathrm{sl}} \tag{2.17}$$

where i_{sl} is the latent heat of fusion. Larger Stefan numbers indicate a relatively smaller influence of the latent heat. Typical values for 304 stainless steel are St≈4.3 (properties from [57]), for mild steel St≈3.7 (properties from [55]), for Ti-6Al-4V, St≈3.2 (properties from [198]) and for aluminum St≈ 1.5 (properties from [54]). Ushio et al. [197] explored the influence of latent heat in mild steel and showed that the main effect on the temperature profile is to delay the point where isotherm width reaches a maximum (increasing the magnitude of x_{m} using the notation of [207], with y_{m} essentially unaffected. Numerical work on Ti-6Al-4V by Van Elsen et al. [198] also concluded that the influence of latent heat is small for Ti-6Al-4V, except for the case of a loose power bed.

2.5.5 Effect of surface heat losses

The surface of the substrate typically exchanges heat with the surroundings via convection and radiation. These surface heat losses act in parallel with the heat conduction through the bulk of the substrate. When the surface heat losses are low enough,

or when the substrate is thick enough, surface heat losses can be neglected. Asymptotic analysis indicates that the error in isotherm width when assuming an adiabatic surface is an overestimation below 10% when:

$$h^* < h_c^* = 0.2 \left[1 + \left(\frac{\pi}{2e}\mathrm{Ro}^2\right)^n\right]^{-1/n} \tag{2.18}$$

where h_c^* is the threshold ensuring an error below 10% in the estimation of isotherm width and $n = 0.9405$. Equation 2.18 is derived in Appendix 2.D. This criterion can be expressed in dimensional form in terms of plate thickness:

$$d > d_{c,h} = \frac{20\alpha^2 (h + h')}{kU^2} \left[1 + \left(\frac{\pi}{2e}\mathrm{Ro}^2\right)^n\right]^{1/n} \tag{2.19}$$

This condition is typically met in electron beam and laser beam welding in keyhole mode where the plate is usually relatively thick and velocities are large, arc welding of steel of plate thicker than about 0.2 mm and aluminum plate thicker than 0.7 mm (assuming U=10 mm/s and $h + h'$=100 W/m^{2}K), and most other practical cases with moderate convection coefficient. Surface heat losses become relevant in problems with enhanced heat transfer such as in-service weld repairs (e.g. "hot tapping"), and underwater wet welding in which liquid flow causes strong convective cooling, even in relatively thick material.

This paper focuses on the cases when surface heat losses can be neglected, where the solution to the governing equations (Equation 2.4) reduces to:

$$T = T_0 + \frac{q}{2\pi k d} \exp\left(-\frac{Ux}{2\alpha}\right) K_0\left(\frac{Ur}{2\alpha}\right) \tag{2.20}$$

2.6 Asymptotic analysis

When surface heat losses are neglected, the geometry of isotherms in dimensionless space depends only on the Rosenthal number, as illustrated in Figure 2.2. The value of Ro can vary between zero and infinity, defining two asymptotic regimes: Regime III, corresponding to large values of Ro, and Regime IV with small values of Ro,

representing the high-speed and low-speed limits of the problem. The naming of regimes is consistent with [140, 206, 207], where Regimes I and II are the 3D (thick substrate) equivalents of 2D Regimes III and IV.

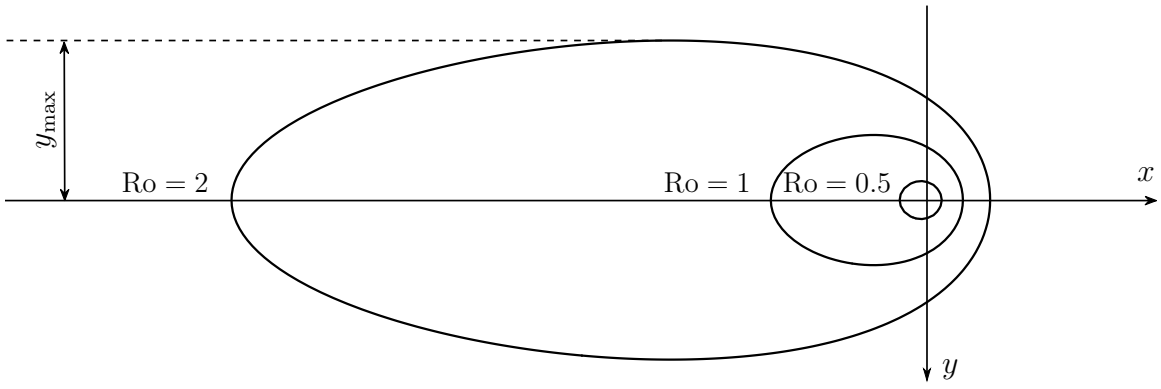

Figure 2.2: Isotherms corresponding to Ro = 0.5, 1, and 2. For large Ro (Regime III, fast) the isotherms are elongated, and for small Ro (Regime IV, slow), the isotherms are rounder and narrower.

The point of maximum width of the isotherm is located with two coordinates. In cartesian coordinates, the maximum width would occur at $(x^*_{\mathrm{m}}, y^*_{\mathrm{m}})$; however, for this analysis, it is convenient to consider a hybrid set of coordinates (x^*, r^*), where r^* is in polar coordinates, yielding the following coupled equations:

$$\frac{1}{\mathrm{Ro}} = \exp\left(-x^*_{\max}\right) K_0\left(r^*_{\max}\right) \tag{2.21}$$

$$\left.\frac{\partial T^*}{\partial x^*}\right|_{\substack{x^*=x^*_{\max}\\ y^*=y^*_{\max}}} = -\exp\left(-x^*_{\max}\right)\left[K_0\left(r^*_{\max}\right) + \frac{x^*_{\max}}{r^*_{\max}} K_1\left(r^*_{\max}\right)\right] = 0 \tag{2.22}$$

Equation 2.21 corresponds to the constraint given by Equation 2.20 at a selected isotherm $T = T_{\mathrm{c}}$, and Equation 2.22 corresponds to the zero-slope condition at a maximum width. The asymptotic analysis of these equations is detailed in Appendix 2.B, resulting in:

$$\widehat{y^*}_{\max_{\mathrm{III}}}(\mathrm{Ro}) = \sqrt{\frac{\pi}{2\mathrm{e}}}\mathrm{Ro} \qquad \text{for Regime III} \tag{2.23}$$

$$\widehat{y^*}_{\max_{\mathrm{IV}}}(\mathrm{Ro}) = 2\exp(-\gamma)\exp\left(-\mathrm{Ro}^{-1}\right) \qquad \text{for Regime IV} \tag{2.24}$$

where $\gamma = 0.5772\ldots$ is the Euler Mascheroni constant, and the symbol $\widehat{\ }$ indicates an asymptotic behavior. These asymptotic approximations are illustrated in Figure 2.3.

Equation 2.23 is consistent with similar asymptotic analysis in [84, 145, 179, 190] for fast moving heat sources, and Equation 2.24 is consistent with [84, 190] for slow moving heat sources. The asymptotic behavior of $y_{\max}$ is a power law in Regime III (fast) and an exponential dependence, not a power law, in Regime IV (slow).

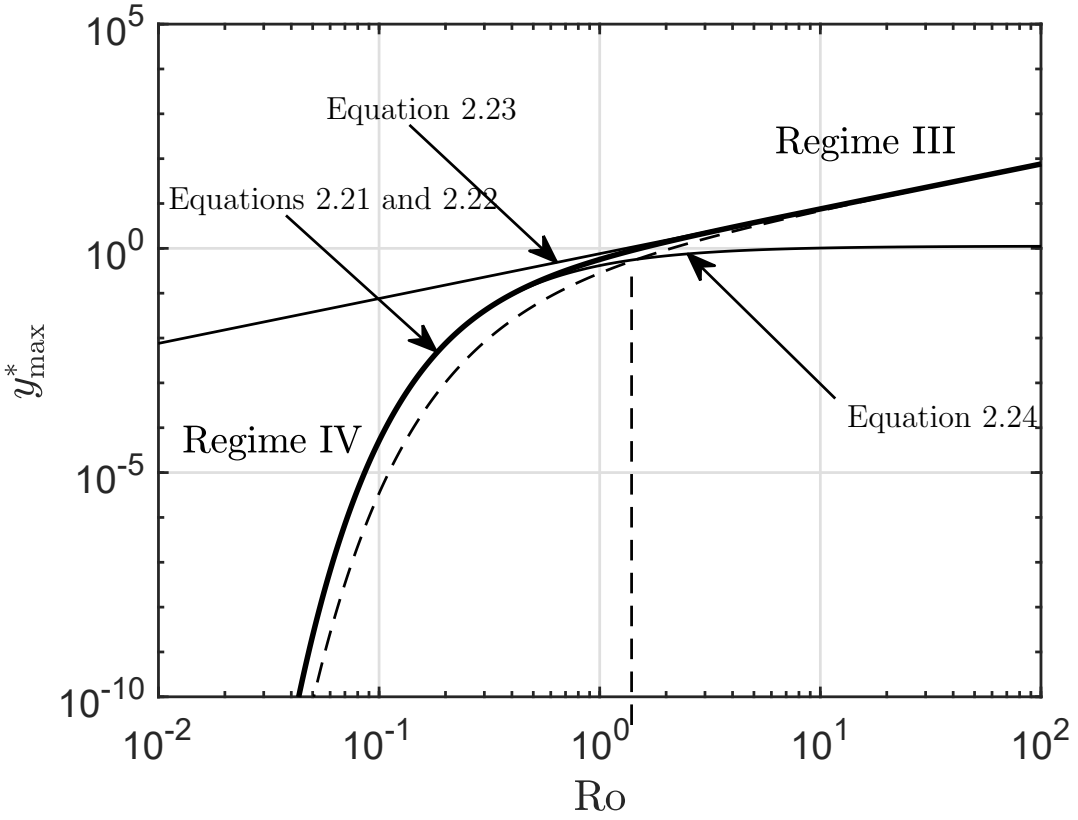

Figure 2.3: Dimensionless maximum isotherm half-width $y^*_{\max}$ as a function of Ro. Equation 2.23 and Equation 2.24 are asymptotic behaviors represented with thinner lines. The thicker solid line represents numerical calculations obtained by solving Equation 2.21 and Equation 2.22. The dashed line represents the modified asymptote in Regime III, which includes the modification factor $\exp\left(-\mathrm{Ro}^{-1}\right)$. The blended solution is undistinguishable from the numerical solution (thick solid line)

2.7 Blending of asymptotic solutions

The simple expressions obtained for each asymptotic regime are less accurate for intermediate values (Ro=O(1)). The powerful methodology of blending proposed in [34] and used in [140, 207] is not able to blend Equation 2.23 and Equation 2.24

because they do not cross, which is an essential requirement [34]. The extended blending technique proposed in [206] is used here. This extended technique is general, and useful for problems beyond maximum isothermal width, with non-crossing or non-power-law asymptotic behavior.

The extended blending technique consists of multiplying one of the non-crossing asymptotic functions by the factor $\exp(a\mathrm{Ro}^b)$ where a and b are constants (positive or negative), and then performing a standard blending technique. This approach forces the asymptotic functions to cross at an intermediate point without affecting their asymptotic behavior, thus enabling a standard blending approach. A similar approach was used in [58] to blend mass transfer limited Sherwood numbers for packed beds with the introduction of an exponential dependence on Reynolds number. This methodology is limited to asymptotic behaviors in which the asymptotic behavior is the same as or weaker than exponential.

In this work, the modification was applied to the asymptote for Regime III (represented graphically in dashed line in Figure 2.3) yielding the following blending expression:

$$\begin{aligned} y^*_{\max}(\mathrm{Ro}) &\approx \widehat{y^*}^{+}_{\max}(\mathrm{Ro}) = \\ &= \left\{ \left[\widehat{y^*}_{\max_{\mathrm{III}}}(\mathrm{Ro}) \exp\left(-\mathrm{Ro}^{-1}\right) \right]^n + \widehat{y^*}_{\max_{\mathrm{IV}}}(\mathrm{Ro})^n \right\}^{1/n} \end{aligned} \tag{2.25}$$

This choice of blending is convenient because by choosing $a = b = -1$, the exponential factor results in a common factor with Regime IV, helping simplify the resulting expression, and having only n as the adjustment variable in the optimization.

The optimal value of n is determined with the same optimization procedure detailed in [140], by minimizing the absolute maximum error of estimation compared to the value of $y_{\max}$ calculated by solving numerically the system of Equation 2.21 and Equation 2.22 over a wide range of Ro. The error has the same definition as in [137, 139, 140], and it is equivalent to the standard form of relative error when the error is

small:

$$\text{error} = \ln \frac{\widehat{y^*}^+_{\max}}{{y^*}_{\max}} \tag{2.26}$$

For the calculation of $y_{\max}$, the error depends only on Ro and n. Figure 2.4 illustrates the error as a function of Ro for different values of n. This figure also shows that the error tends to zero in the asymptotic extremes; this is not by coincidence, but an essential property of the blending methodology. Figure 2.5 illustrates the maximum absolute value of error (over all Ro) as a function of n. The sharp minimum is because the maximum error can be positive (for n below the optimum), or negative (for n above the optimum). For the optimum value n =1.407, the absolute value of the maximum error is below 6.8% over the whole domain of Ro ($0 < \text{Ro} < \infty$).

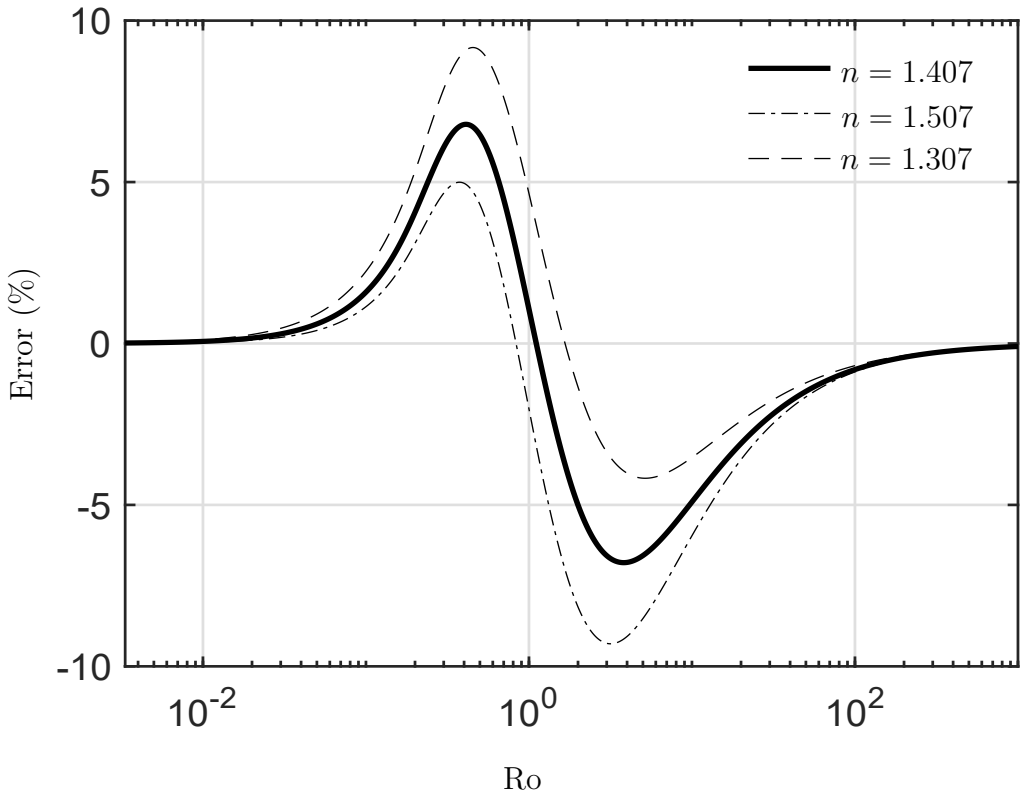

Figure 2.4: Blending error of dimensionless maximum isotherm half-width $y_{\max}$ as a function of Ro for the blending parameter n at or near the optimal value of 1.407.

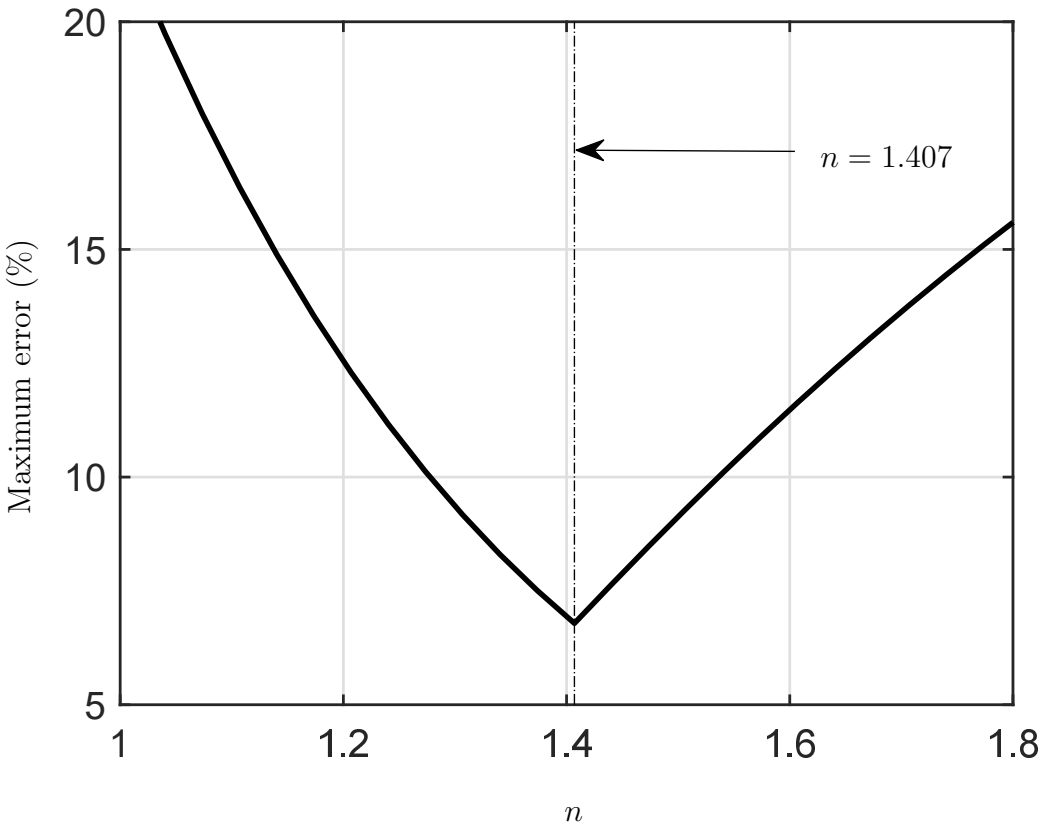

Figure 2.5: Maximum blending error as a function of the blending parameter n. The maximum error reaches its minimum, 6.8% at n =1.407.

2.7.1 Correction factors

Practical engineering expressions often have the form of a simple formula that provides a rough prediction accompanied by one or more correction factors. This is possible in this work too, and the correction factors addressing the effect of travel speed can be calculated explicitly. Correction factors addressing the simplifications beyond travel speed, addressed above, require further work, which is the focus of current research.

Because the formulation used in this work has two asymptotic extremes (high and low Ro), there are two simple formulae associated with each. The correction factors associated with the maximum isotherm half-width $y_{\max}$ can be derived directly by

rearranging Equation 2.25:

$$y_{\max} \approx \widehat{y}^{+}_{\max} = \widehat{y}_{\max_{\mathrm{III}}} \left\{ \left[\exp\left(-\mathrm{Ro}^{-1}\right) \right]^n + \left[\frac{\widehat{y^*}_{\max_{\mathrm{IV}}}(\mathrm{Ro})}{\widehat{y^*}_{\max_{\mathrm{III}}}(\mathrm{Ro})} \right]^n \right\}^{1/n} = \\ = \widehat{y}_{\max_{\mathrm{III}}} f_{y_{\max_{\mathrm{III}}}}(\mathrm{Ro}) \tag{2.27}$$

$$y_{\max} \approx \widehat{y}^{+}_{\max} = \widehat{y}_{\max_{\mathrm{IV}}} \left\{ 1 + \left[\frac{\widehat{y^*}_{\max_{\mathrm{III}}}(\mathrm{Ro}) \exp\left(-\mathrm{Ro}^{-1}\right)}{\widehat{y^*}_{\max_{\mathrm{IV}}}(\mathrm{Ro})} \right]^n \right\}^{1/n} = \\ = \widehat{y}_{\max_{\mathrm{IV}}} f_{y_{\max_{\mathrm{IV}}}}(\mathrm{Ro}) \tag{2.28}$$

where the optimal blending parameter $n = 1.407$ is the same for Equations 2.27 and 2.28.

Equations 2.27 and 2.28 are exactly equivalent and they are the same approximation to the exact solution, but based on the asymptotic solutions for Regime III and Regime IV, respectively. By substituting the asymptotic behavior in these equations, a practical closed-form for the correction factors can be obtained:

$$f_{y_{\max_{\mathrm{III}}}}(\mathrm{Ro}) = \exp(-\mathrm{Ro}^{-1}) \left\{ 1 + \left[\sqrt{\frac{8\mathrm{e}}{\pi}} \frac{\exp(-\gamma)}{\mathrm{Ro}} \right]^n \right\}^{1/n} \approx \\ \approx \exp(-\mathrm{Ro}^{-1}) \left[1 + \left(\frac{1.477}{\mathrm{Ro}} \right)^{1.407} \right]^{0.7107} \tag{2.29}$$

$$f_{y_{\max_{\mathrm{IV}}}}(\mathrm{Ro}) = \left\{ 1 + \left[\sqrt{\frac{8\mathrm{e}}{\pi}} \frac{\exp(-\gamma)}{\mathrm{Ro}} \right]^{-n} \right\}^{1/n} \approx \left[1 + \left(\frac{1.477}{\mathrm{Ro}} \right)^{-1.407} \right]^{0.7107} \tag{2.30}$$

These correction factors are illustrated in Figure 2.6. As Ro approaches infinity (Regime III), $f_{y_{\max_{\mathrm{III}}}}(\mathrm{Ro})$ tends to the exact value of 1 and when Ro tends to 0 (Regime IV), $f_{y_{\max_{\mathrm{IV}}}}(\mathrm{Ro})$ tends to 1 indicating that as the asymptotic regime is approximated, no correction is necessary. In traditional blending, a conventional limit between the two asymptotic regimes can be determined at the crossing point of the correction factors, where the error of ignoring both corrections would be the same. In this case in which modified blending is used, the correction factors in this case do not cross, and a new convention needs to be established to estimate a limit between the two regimes. The new convention proposed considers the value of Ro at which the *absolute*

value of the error is the same, resulting in a critical value $\mathrm{Ro_c}$ =0.9499. This value of O(1) is typical of the vast majority of limits between regimes.

The limits of 10% error (when the correction factor is 0.9 or 1.1) are useful to estimate when correction factors can be omitted. In Regime III, the error of omitting the correction factors is less than 10% when $\mathrm{Ro} > \mathrm{Ro_{III}} = 3.553$, and in Regime IV when $\mathrm{Ro} < \mathrm{Ro_{IV}} = 0.3856$.

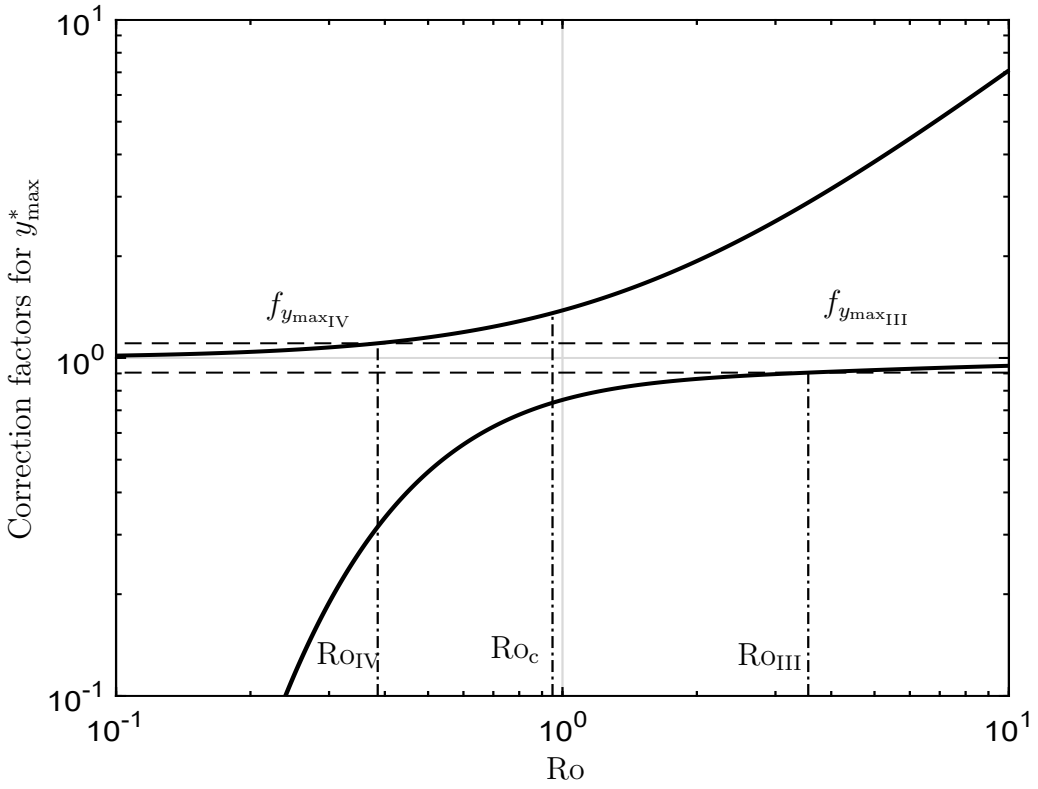

Figure 2.6: Correction factors for the maximum isotherm half-width $y_{\max}$ as functions of Ro. For $\mathrm{Ro} > 3.553$ or $\mathrm{Ro} < 0.3856$, neglecting correction factors yield an error in estimation smaller than 10% compared to blended solution of 2.25.

2.7.2 Expressions with units

In practical calculations it is convenient to count with explicit expressions using units. Conversion of Equations 2.27 and 2.28 into expressions with units is done by substi-

tuting Equation 2.9 and Equation 2.11 into Equation 2.25:

$$\widehat{y}^{+}_{\max} = \widehat{y}_{\max_{\mathrm{III}}} f_{y_{\max_{\mathrm{III}}}}(\mathrm{Ro}) = \frac{1}{\sqrt{2\pi \mathrm{e}}} \frac{q\alpha}{Ukd\,(T_c - T_0)} f_{y_{\max_{\mathrm{III}}}}(\mathrm{Ro}) \tag{2.31}$$

$$\widehat{y}^{+}_{\max} = \widehat{y}_{\max_{\mathrm{IV}}} f_{y_{\max_{\mathrm{IV}}}}(\mathrm{Ro}) = \frac{4\alpha}{U \exp(\gamma)} \exp\left(-\mathrm{Ro}^{-1}\right) f_{y_{\max_{\mathrm{IV}}}}(\mathrm{Ro}) \tag{2.32}$$

2.8 Validation

The focus of this paper is on the width of isotherms in general, not only the melting isotherm in welding. However, the high-quality data available in the literature is in its vast majority for the melt width, and it is the data that will be used for validation.

The validation of the proposed predictive expressions was made by comparison against published data and shown in Figures 2.7-2.9, spanning a range of Ro of two orders of magnitude from (0.1 to 10). Measurements were collected for arc welding processes including Gas Tungsten Arc Welding (GTAW), Shielded Metal Arc Welding (SMAW), Submerged Arc Welding (SAW), Gas Metal Arc Welding (GMAW); for concentrated heat sources including Laser Beam Welding (LBW), Electron Beam Welding (EBW); and for Additive Manufacturing (AM) for a wide range of materials including aluminum, titanium, carbon steel, stainless steel, and superalloys.

The published values were normalized using Equation 2.9 and Equation 2.11, and compared against the blended expression in Equation 2.25. Some of the experimental points were already in dimensionless form [62, 71, 160, 213]. In some cases, the isotherm width was not directly reported, but inferred from associated magnitudes such as cross sectional area [72] or melting efficiency [62, 213]. The characteristic temperature used in these calculations (T_{c}) corresponds to the melting temperature (T_{m}) in all cases, except some points in [142] which correspond to the edge of the HAZ (A_{c1}).

Assuming full penetration, 2D heat transfer, isotherm width and cross sectional area are related as follows:

$$y_{\max} \approx \frac{A_{\mathrm{c}}}{2d} \tag{2.33}$$

When melting efficiency is provided, the corresponding cross sectional area is:

$$A_{\mathrm{c}} = \frac{\eta_{\mathrm{m}} q}{\rho(i_{\mathrm{l}} - i_0)U} \tag{2.34}$$

where η_{m} is the melting efficiency, i_{l} is the enthalpy at liquidus temperature, and i_0 is the enthalpy at the far temperature T_0. For data corresponding to partial penetration keyhole welding [54], the plate thickness considered was that of the penetration, and the average width considered was half the width measured at the top surface.

The thermal properties, thermal efficiencies, and processing parameters used in the literature survey are listed in Table 2.2. When not listed in the original sources, the thermophysical properties were obtained from the literatures or software (JMat-Pro v11). Thermal efficiency was assessed from original sources or from the AWS handbook [96]. The far temperature T_0 was always assumed or given as 20°C except for [153], which measured 23°C. The data for GTAW in [62, 160] and EBW in [70] were published in dimensionless form. For assessment of surface heat losses in the references consulted, an approximate effective convection coefficient of 10 W/m^{2}K whose used to assess processes with low expected effective convection (EBW, SAW, and EB based AM), and a coefficient of 100 W/m^{2}K was used for processes with higher expected convective effects (GTAW, GMAW, SMAW, and LBW).

The validity of simplifying hypotheses discussed above was verified when data was available or could be inferred feasibly. In almost all cases the simplifying hypotheses are valid, except some points from [54] for which the heat source cannot be considered a point (Equation 2.15). Details about the verification of hypotheses are included as attached excel. The neglected secondary phenomena are a source of scatter in the comparisons. Other sources of scatter are uncertainties in the thermophysical properties used, uncertainties in thermal efficiency, which is especially broad for laser processes, and of course, experimental error. The criteria for negligible surface heat loss is fulfilled for all data collected.

Figure 2.7 compares Equation 2.25 with published data for width in four arc weld-

ing processes (GTAW, SMAW, SAW, GMAW). For these processes the agreement with experiments is good and unbiased, except with a slight overprediction of width at height Rosenthal numbers. Arc welding processes, unlike laser or electron beam processes, are not capable of keyhole penetration, and operate only as surface heat sources. In these cases, the face of the weld is much wider than the root (or waist in [153]), and incipient 3D effects might reduce the actual weld width at large values of Ro.

Figure 2.8 compares Equation 2.25 with published data for weld width in laser beam welding (LBW) and additive manufacturing (AM). The results are accurate and unbiased, except for a slight underprediction for the date from [153]. If the thermophysical properties and measurements are correct, the underprediction of width is typically due to the finite size of the heat source or to fluid flow effects in the weld pool. Given that the welds considered meet the criterion for "point heat source," the slight bias is likely to be due to fluid flow effects. The near-perfect agreement with [72] is not surprising, given that it corresponds to numerical simulations, not to experimental data. The excellent agreement also supports the applicability of Rosenthal's 2D solution and the small error caused by its simplifications.

Figure 2.9 compares Equation 2.25 with published data for electron beam welding (EBW) in a broad diversity of conditions. This figure includes points for which the "point heat source" simplification is invalid (indicated with different symbols). Predictably, Equation 2.25 underpredicts the width in those cases. The comparison with data from [190] shows a small systematic over prediction, while comparisons with [70] show a systematic underprediction. It is likely that these small and opposite systematic errors are associated with the materials and process properties used in the estimates. At low Ro, the underpredictions for [70] are larger; although no beam size is provided in this case, it is likely that the condition for point heat source is not met for those points. Another possible source of error for comparisons with [54] is that most of the welds considered are partial penetration keyhole welds, which have a 3D

effect at the bottom of the keyhole. For the comparisons, only welds with a depth to width ratio greater than 0.75 were considered.

Table 2.2: Operating conditions and average thermal properties utilized in calculation. The temperature of interest is the melting temperature in all cases except when marked. The blanks in the table correspond to data published only in normalized form.

Process	Material	Plate thickness (mm)	Power (kW)	Thermal Efficiency	Velocity (mm/s)	Conductivity (W/mK)	Diffusivity (m^2/s)	Tc (°C)	Ref.
GTAW	Kovar					75.2	1.1×10^{-5}	1490	[62]
	Hastelloy B2					50.6	7.2×10^{-6}	1431	[62]
	Aluminum 1100					237	6.0×10^{-6}	660	[62]
	Mild steel	1-4		0.75* [96]	0.4-12.7				[160]
	Stainless steel 304					38.4	6.3×10^{-6}	1454	[61, 62]
SMAW SAW	Mild steel	2-50		0.75			8.2×10^{-6}		[93, 213]
GMAW	Carbon steel	2	2.138-2.790	0.79-0.88	5.5-7	35 +	5.9×10^{-6}+	725×	[142]
	Carbon steel	2	2.138-2.790	0.79-0.88	5.5-7	43 +	8.4×10^{-6}+	1510	[142]
LBW	Inconel718	1.6	1.5-2.9	0.3 *[96]	11.85-38.94	20+	3.5×10^{-6}+	1375+	[153]
	Stainless steel 321	0.125-0.417	0.25	0.15	4.7-38	24	4.9×10^{-6}	1530	[190, 211]
	Stainless steel 302	0.125-0.250	0.25	0.15	4.2-21.1	24	4.9×10^{-6}	1530	[190, 211]
	17-7PH	0.125	0.25	0.15	47	27	5.9×10^{-6}	1530	[190, 211]
	Inconel	0.1-0.25	0.25	0.15	16.9-63.5	24	5×10^{-6}	1410	[190, 211]
	Nickel	0.125	0.25	0.15	14.8	67	1.3×10^{-5}	1450	[190, 211]
	Monel	0.25	0.25	0.15	6.4	35	7×10^{-5}	1340	[190, 211]
	Titanium	0.125-0.250	0.25	0.15	21.1-59	24	7.2×10^{-6}	1680	[190, 211]
	Stainless steel 304	6.4-8.9	8	0.5	12.5-16.7	24	4.9×10^{-6}	1530	[126, 190]
	Stainless steel 304	12.7-20.2	20	0.9	21.2-42.4	24	4.9×10^{-6}	1530	[126, 190]
	AA 6065T4	2.5	3	0.37/0.80	83.3-133	193-199+	$7.7\text{-}7.9 \times 10^{-5}$+	59-292	[1, 2]
AM	Ti-6Al-4V	12.7-20.2	1-5		0-42.3	17.6 [143]	5.6×10^{-6} [143]	1660	[72]
EBW	HY-130	3.3-0.04	1.5-22.5	0.9	4.16-41.6	35	7.3×10^{-6}	1530	[108, 190]
	EN58B	8.4	2.5	0.9	25	24	5.5×10^{-6}	1530	[79, 190]
	EN58J	8.8-12.5	3.6	0.9	5.7-25.9	24	5.3×10^{-6}	1530	[7, 190]
	EN58J	7.4-12	5.2	0.9	21.1-50.8	24	5.3×10^{-6}	1530	[6, 190]
	†								[70]
	Stainless steel 304	6.3	0.35-1.4	0.95	6.4-3200	25	4.5×10^{-6}	1433	[54]
	Aluminum 2024	6.3	0.3-1.2	0.95	6.4-3200	175	6.7×10^{-5}	595	[54]

* Estimated + Properties calculated by software JMatPro v11 × Ac1 † Aluminum 1100, 2024, 6061, carbon steel, and stainless steel 304 and 316

2.9 Example of application

Consider the LBW of 321 stainless steel of 0.005 in (0.127 mm) thickness performed by Webster [211]. The laser power was 250 W CO_2, with a spot diameter between 0.002 in (50 μm) and 0.005 in (127 μm), a travel speed of 90 in/min (38 mm/s),

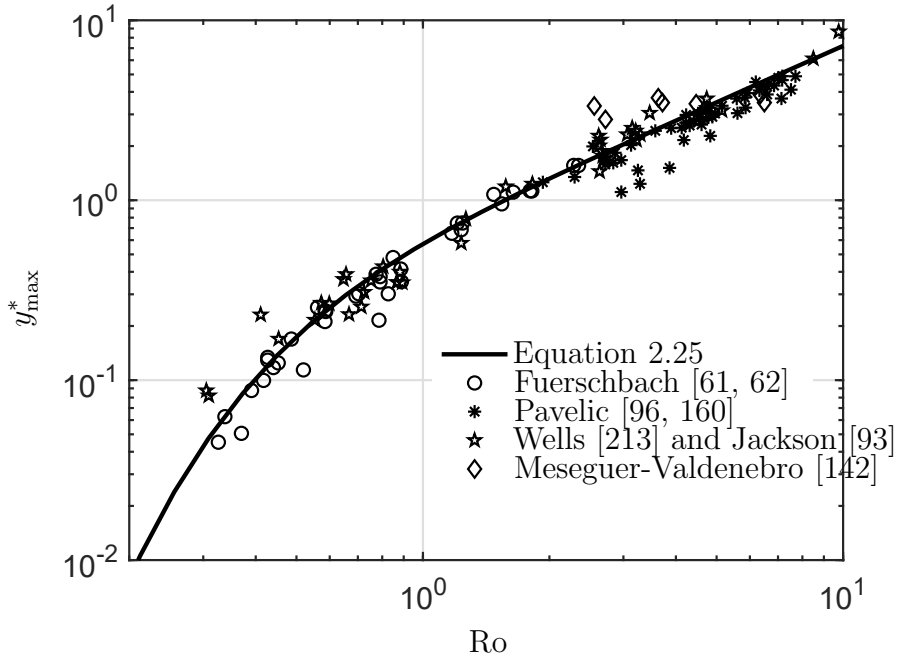

Figure 2.7: Comparison of explicit blending solution (Equation 2.25) with published data for weld width in arc welding (GTAW, SMAW, SAW, GMAW).

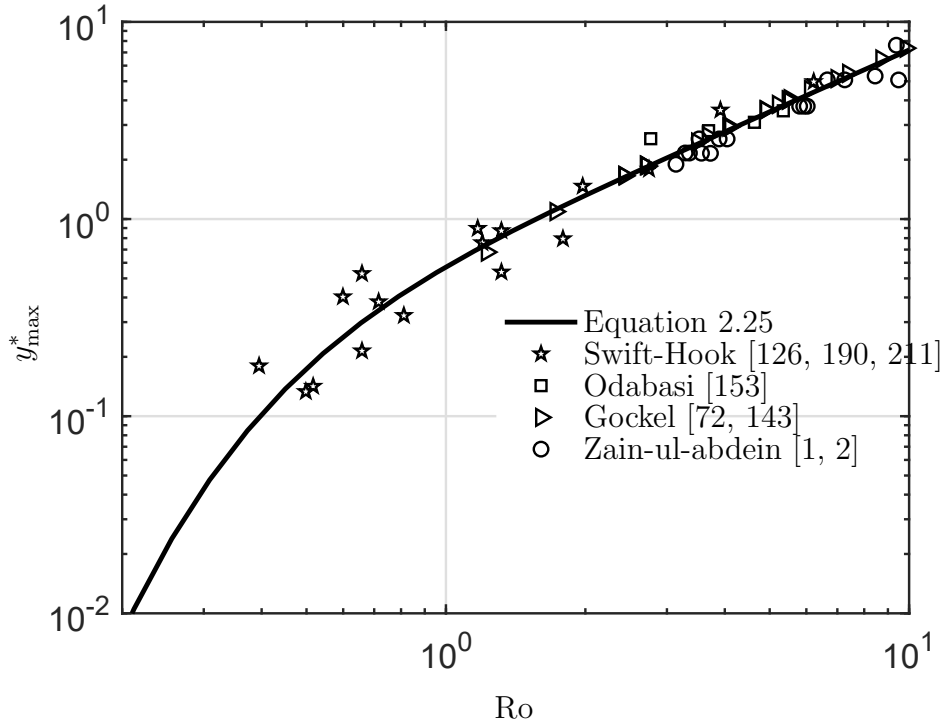

Figure 2.8: Comparison of explicit blending solution (Equation 2.25) with published data for isotherm width in laser processes (LBW, AM).

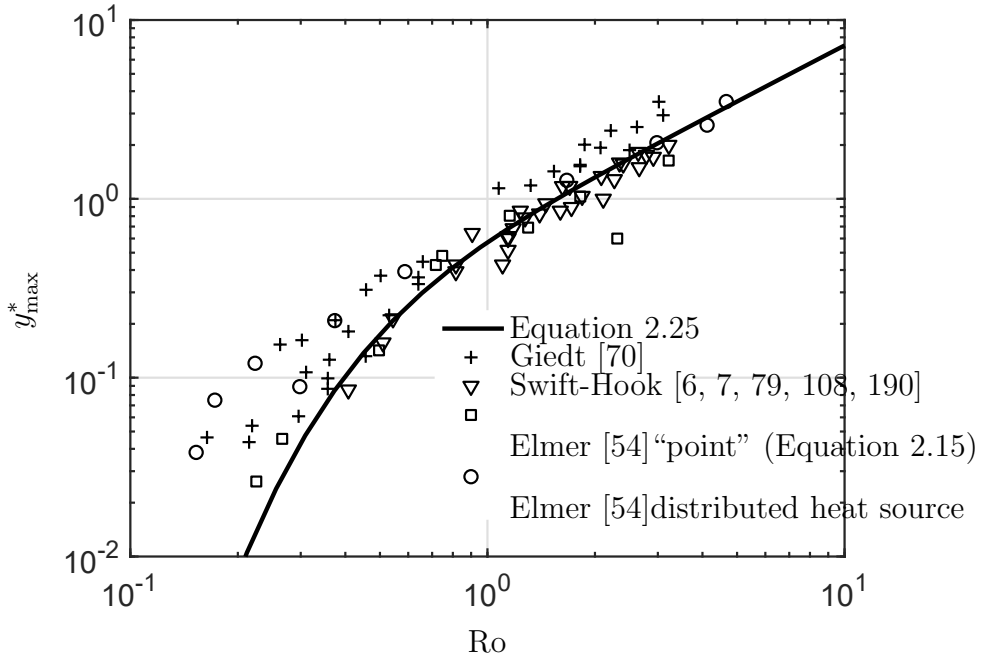

Figure 2.9: Comparison of explicit blending solution (Equation 2.25) with published data for weld width in EBW.

a thermal efficiency of 0.15 estimated based on analysis of [190]. Interpreting this spot size as a full width at half maximum (FWHM) in a gaussian distribution, the corresponding standard deviation σ ranges between 22 μm and 54 μm. Effective thermophysical properties and heat transfer efficiency are provided in [190] and listed in Table 2.2. The measured full width of bead was 0.018 in (457 μm).

For the weld considered, the Rosenthal number using weld penetration for d is Ro=1.3 (Equation 2.11), corresponding to Regime III (fast moving heat source). Equation 2.15 indicates that the heat source can be considered a point ($\sigma^* = 0.084$ to 0.21 <0.49), and Equation 2.19 indicates that the effect of surface heat losses are negligible (d= 0.005 in $> d_{\mathrm{c,h}}= 10^{-4}$ in, assuming $h + h'$=100 W/m^{2}K). A 2D model is appropriate in this case because this is a full penetration weld, and the criterion for thin substrate (Equation 2.16) is not relevant. For this example, the dimensionless plate thickness is larger than the critical thickness for 2D heat transfer for a point heat source on the surface (d^*=0.49> $d^*_{\mathrm{c,2D}}$=0.20), but this is not a problem. The

Stefan number for stainless is of the order of 4.3, indicating latent heat is not likely to affect the calculations significantly.

The prediction of weld width is made using the appropriate equation for Regime III (Equation 2.31), which yields $\widehat{y}_{\max_{\text{III}}} = 0.010$ in (254 μm), and $f_{y_{\max_{\text{III}}}}(\text{Ro}) = 0.81$ (Equation 2.27). The correction applied in this case is larger than 10%, consistently with the intermediate value of Ro. The predicted weld width is $2\widehat{y}^{+}_{\max}$ =0.016 in (406 μm), which is an underprediction with an error of 12% compared to the measured value of 0.018 in (457 μm).

2.10 Discussion

Consistently with the foundations established in [140], the analysis presented here dispels old misconceptions and brings new insights. Similarly as before, proper dimensional analysis of Equation 2.20 yields four, not five dimensionless groups as usually considered based on [33]. There is no variable-independent dimensionless group, as attempted unsuccessfully in [33], and the dimensionless group associated with temperature (Rosenthal number) is slightly different than in [140] (the Rykalin number), but carries the same physical meaning.

For fast welds (Regime III), the weld width is proportional to the heat input (q/U) making it an essential welding parameter; however, this relationship breaks down for slower welds (Regime IV). Codes and standards tend to omit the slow welding regime. This omission is seldom a problem since slow 2D welds are less frequent in practice; however, Regime IV is typical in friction stir welding (FSW) and full penetration gas tungsten arc welding (GTAW) of aluminum, among others process/material combinations. In Regime IV, two welds with the same heat input do not necessarily have similar width.

Similarly to [140], the work presented here brings new insight in the understanding of the origins of the Rosenthal number, and in agreement with [60], a single dimensionless group (in this case Ro) can be singled out as a key magnitude to characterize

the behavior of a moving heat source in 2D.

The extended blending technique used in this work overcomes the limitations of the Churchill-Usagi blending methodology, and can be used for problems beyond the one analyzed here. Although the factor introduced ($\exp(a\mathrm{Ro}^b)$) would involve a 3-parameter optimization (a, b, and n), a smart choice of a and b reduces the problem back to an optimization of a relatively simple expression with only n as the optimization variable. The error in the blending used here is always below 6.8%, for any value of Ro, and Figure 2.4 can be used together with Equation 2.26 to generate a local correction greatly reducing the error in a chosen range of interest. Just as in [140], the correction factors are accurate even far from the asymptotic regime.

The validation performed shows a relatively narrow and symmetric scatter, which is somewhat unexpected, considering the important approximations made in the model, the broad range of materials, processes, and authors, and also that the melting temperature isotherm is more affected by the "solid heat transfer" approximation than isotherms further into the solid substrate. It is not obvious at this stage how much of the scatter is due to the approximations of the model, how much is due to experimental error, and how much is due to error in the values used for thermophysical properties [134]. Although the errors observed suggest room for improvement (especially when the error is systematic), a validation of similar scope has never been performed between numerical results and experiments, at least for welding simulations. There is no evidence in the literature that a numerical simulation (without ad-hoc calibrations) would show less scatter when compared against the same dataset used in this work.

Possible sources for systematic underpredictions are the presence of outward thermocapillary flows. This possibility cannot be evaluated within the limitations of the formulation presented here. Other possible cause for underpredictions is that the heat source can sometimes bee too large to be considered a point. This is possible at the lowest Ro ranges, when the predicted isotherm width is unfeasibly small. Pre-

vious attempts to capture the low Ro regime assumed the dimensionless isotherm width to become zero at Ro<0.25, without proper physical justification or further considerations of the nature of different heat sources and their size. Possible causes for systematic overpredictions are 3D effects in partial penetration welds, or welds in which the root is much narrower than the face.

2.11 Conclusions

This work presents for the first time practical and rigorous expressions for calculating the width of an isotherm ($y_{\max}$, Equation 2.29 and Equation 2.30) in conditions of 2D heat transfer. The expressions proposed have the form of an asymptotic expression multiplied by a correction factor, and are based on theoretical analysis, not empirical fitting.

The dimensionless width depends only on the Rosenthal number, Ro, which is a metric of how fast or slow a heat source is in 2D conditions. The Rosenthal number divides all possible solutions in two regimes: Regime III corresponding to high Ro ("fast" 2D heat sources) and low Ro ("slow" 2D heat sources). Because Ro depends on a chosen temperature, moving 2D heat sources cannot be deemed as intrinsically fast or slow until a temperature of interest is selected.

The Churchill-Usagi blending equation has been extended to consider non-power-law, non-crossing asymptotic expressions (Equation 2.25). The modified blending technique approach is novel, and it overcomes a limitation of previous studies incapable of capturing properly the behavior of slow heat sources (e.g. [213]). These asymptotic expressions coincide with the exact solution in the extremes, and the blending expression for the intermediate regime, exhibits a discrepancy always within 7% of the exact solution.

The practical expressions presented here require much smaller computational effort than numerical methods, do not present convergence issues, and can be calculated using a handheld calculator or a basic spreadsheet; these expressions can also be used

to estimate, for example, the width of a weld, the size of zone affected by the heat source in a broad diversity of processes, or to validate numerical models.

The methodologies and results obtained are applicable to moving heat sources within the hypotheses of the problem formulation, and are valid beyond welding to additive manufacturing and many other manufacturing and broader engineering problems, since they capture the inherent essence of complex physical phenomena based on the governing equations.

Acknowledgments

The authors wish to acknowledge support from the Natural Sciences and Engineering Research Council of Canada (NSERC), and the China Scholarship Council (CSC). Student scholarships from the American Welding Society and the CWB Welding Foundation were also gratefully received.

References

[1] M. Zain-ul abdein, D. Nelias, J. F. Jullien, and D. Deloison, "Prediction of laser beam welding-induced distortions and residual stresses by numerical simulation for aeronautic application," *Journal of Materials Processing Technology*, vol. 209, no. 6, pp. 2907–2917, 2009.

[2] M. Zain-ul abdein, D. Nélias, J. F. Jullien, and D. Deloison, "Experimental investigation and finite element simulation of laser beam welding induced residual stresses and distortions in thin sheets of AA 6056-T4," *Materials Science and Engineering A*, vol. 527, no. 12, pp. 3025–3039, 2010.

[6] M. J. Adams, "High voltage electron-beam welding," *British Welding Journal*, vol. 15, pp. 451–467, 1968.

[7] M. J. Adams, "Low voltage electron-beam welding," *British Welding Journal*, vol. 15, pp. 134–142, 1968.

[12] H. J. Aval, A. Farzadi, S. Serajzadeh, and A. H. Kokabi, "Theoretical and experimental study of microstructures and weld pool geometry during GATW of 304 stainless steel," *International Journal of Advanced Manufacturing Technology*, vol. 42, no. 11-12, pp. 1043–1051, 2009.

[19] T. L. Bergman, F. P. Incropera, D. P. DeWitt, and A. S. Lavine, *Fundamentals of heat and mass transfer*. John Wiley & Sons, 2011.

[20] A. Birnbaum, P. Aggarangsi, and J. Beuth, "Process scaling and transient melt pool size control in laser-based additive manufacturing processes," in *Proceedings - Solid Freeform Fabrication Symposium*, University of Texas, 2003, pp. 328–339.

[21] I. N. Bronshtein, K. A. Semendyayev, G. Musiol, and H. Mühlig, *Handbook of mathematics*, Fifth. Berlin, Heidelberg: Springer-Verlag Berlin Heidelberg, 2007.

[24] E. Buckingham, "On physically similar systems; illustrations of the use of dimensional equations," *Physical Review*, vol. 4, no. 4, pp. 345–376, 1914.

[27] H. S. Carslaw and J. C. Jaeger, *Conduction of heat in solids*, Second. Oxford: Clarendon Press, 1959.

[33] N. Christensen, V. d. L. Davies, and K. Gjermundsen, "Distribution of temperatures in arc welding," *British Welding Journal*, vol. 12, no. 2, pp. 54–75, 1965.

[34] S. W. Churchill and R. Usagi, "A general expression for the correlation of rates of transfer and other phenomena," *AIChE Journal*, vol. 18, no. 6, pp. 1121–1128, 1972.

[39] H. E. Cline and T. R. Anthony, "Heat treating and melting material with a scanning laser or electron beam," *Journal of Applied Physics*, vol. 48, no. 9, pp. 3895–3900, 1977.

[40] G. Comini, S. Del Guidice, R. Lewis, and O. Zienkiewicz, "Finite element solution of non-linear heat conduction problems with special reference to phase change," *International Journal for Numerical Methods in Engineering*, vol. 8, no. 3, pp. 613–624, 1974.

[43] J. A. Dantzig and C. L. Tucker, *Modeling in materials processing*. Cambridge, England: Cambridge University Press, 2001.

[53] T. W. Eagar and N. S. Tsai, "Temperature fields produced by traveling distributed heat sources," *Welding Journal*, vol. 62, no. 12, pp. 346–355, 1983.

[54] J. W. Elmer, W. H. Giedt, and T. W. Eagar, "The transition from shallow to deep penetration during electron beam welding," *Welding Research Supplement*, vol. 69, no. 5, 167s–176s, 1990.

[55] G. V. Ermolaev, O. B. Kovalev, A. M. Orishich, and V. M. Fomin, "Mathematical modelling of striation formation in oxygen laser cutting of mild steel," *Journal of Physics D: Applied Physics*, vol. 39, no. 19, p. 4236, 2006.

[57] H. G. Fan, H.-L. Tsai, and S.-J. Na, "Heat transfer and fluid flow in a partially or fully penetrated weld pool in gas tungsten arc welding," *International Journal of heat and mass transfer*, vol. 44, no. 2, pp. 417–428, 2001.

[58] P. S. Fedkiw and J. Newman, "Mass-transfer coefficients in packed beds at very low reynolds numbers," *International Journal of Heat and Mass Transfer*, vol. 25, no. 7, pp. 935–943, 1982.

[60] P. W. Fuerschbach, "A dimensionless parameter model for arc welding processes," in *Trends in Welding Research, Proceedings of the 4th International Conference*, ASM International, 1994.

[61] P. W. Fuerschbach and G. A. Knorovsky, "A study of melting efficiency in plasma arc and gas tungsten arc welding," *Welding Research Supplement*, vol. 70, no. 11, pp. 287–297, 1991.

[62] P. W. Fuerschbach and G. R. Eisler, "Determination of material properties for welding models by means of arc weld experiments," in *Trends in Welding Research, Proceedings of the 6th International Conference*, Callaway Gardens Resort, Phoenix, Arizona: ASM International, 2002.

[64] S. S. Gajapathi, S. K. Mitra, and P. F. Mendez, "Controlling heat transfer in micro electron beam welding using volumetric heating," *International Journal of Heat and Mass Transfer*, vol. 54, no. 25-26, pp. 5545–5553, 2011.

[66] E. Gariboldi and B. Previtali, "High tolerance plasma arc cutting of commercially pure titanium," *Journal of Materials Processing Technology*, vol. 160, no. 1, pp. 77–89, 2005.

[70] W. H. Giedt and L. N. Tallerico, "Prediction of electron beam depth of penetration," *Welding Research Supplement*, vol. 67, no. 12, 299s–305s, 1988.

[71] W. H. Giedt, L. N. Tallerico, and P. W. Fuerschbach, "GTA welding efficiency : Calorimetric and temperature field measurements," *Welding Research Supplement*, vol. 68, no. 1, 28s–32s, 1989.

[72] J. Gockel, J. Fox, J. Beuth, and R. Hafley, "Integrated melt pool and microstructure control for Ti-6Al-4V thin wall additive manufacturing," *Materials Science and Technology*, vol. 31, no. 8, pp. 912–916, 2015.

[73] J. Gockel, N. Klingbeil, and S. Bontha, "A closed-form solution for the effect of free edges on melt pool geometry and solidification microstructure in additive manufacturing of thin-wall geometries," *Metallurgical and Materials Transactions B*, vol. 47, no. 2, pp. 1400–1408, 2016.

[74] J. Goldak, A. Chakravarti, and M. Bibby, "A new finite element model for welding heat sources," *Metallurgical Transactions B*, vol. 15, no. 2, pp. 299–305, 1984.

[78] Ø. Grong, *Metallurgical modelling of welding*, First. Cambridge, Great Britain: Institute of Materials, 1994.

[79] M. G. Gunn and E. G. King, "Electron-beam fusion zone penetration in 12 mm (1/2 in.) austenitic stainless steel," in *Advances in Welding Processes Conference*, Harrogate, 1970, pp. 183–186.

[84] K. Heller, S. Kessler, F. Dorsch, P. Berger, and T. Graf, "Analytical description of the surface temperature for the characterization of laser welding processes," *International Journal of Heat and Mass Transfer*, vol. 106, pp. 958–969, 2017.

[85] H. Hemmer and Ø. Grong, "Prediction of penetration depths during electron beam welding," *Science and technology of welding and joining*, vol. 4, no. 4, pp. 219–225, 1999.

[88] C. Y. Ho, "Asymptotic analysis for penetration depth during laser welding," *Procedia Engineering*, vol. 15, pp. 5212–5216, 2011.

[90] Y. F. Hsu and B. Rubinsky, "Two-dimensional heat transfer study on the keyhole plasma arc welding process," *International Journal of Heat and Mass Transfer*, vol. 31, no. 7, pp. 1409–1421, 1988.

[93] C. E. Jackson and A. E. Shrubsall, "Energy distribution in electric welding," *Welding Journal*, vol. 29, no. 5, 231s–241s, 1950.

[95] S. J. N. Jason Cheon Degala Venkata Kiran, "Cfd based visualization of the finger shaped evolution in the gas metal arc welding process," *International Journal of Heat and Mass Transfer*, 2016.

[96] C. L. Jenney and A. O'Brien, Eds., *Welding science and technology*, Ninth. American Welding Society (AWS), 2001, vol. 1, ISBN: 978-0-87171-657-6.

[106] R. Komanduri and Z. B. Hou, "Thermal analysis of the laser surface transformation hardening process," *International Journal of Heat and Mass Transfer*, vol. 44, no. 15, pp. 2845–2862, 2001.

[108] P. J. Konkol, P. M. Smith, C. F. Willibrand, and L. P. Connor, "Parameter study of electron-beam welding," *Welding Journal*, vol. 50, pp. 765–776, 1971.

[114] S. Kou and D. K. Sun, "Fluid Flow and Weld Penetration in Stationary Arc Welds," *Metallurgical Transactions A*, vol. 16, no. 2, pp. 203–213, 1985.

[117] Y. Kwon and D. C. Weckman, "Analytical thermal model of conduction mode double sided arc welding," *Science and Technology of Welding and Joining*, vol. 13, no. 6, pp. 539–549, 2008.

[126] E. V. Locke, E. D. Hoag, and R. A. Hella, "Deep penetration welding with high-power CO2 lasers," *IEEE Journal of Quantum Electronics*, vol. 8, no. 2, pp. 132–135, 1972.

[133] O. Manca, B. Morrone, and V. Naso, "Quasi-steady-state three-dimensional temperature distribution induced by a moving circular Gaussian heat source in a finite depth solid," *International Journal of Heat and Mass Transfer*, vol. 38, no. 7, pp. 1305–1315, 1995.

[134] P. F. Mendez, "Synthesis and generalisation of welding fundamentals to design new welding technologies: Status challenges and a promising approach," *Science and Technology of Welding and Joining*, vol. 16, no. 4, pp. 348–356, 2011.

[136] P. F. Mendez and T. W. Eagar, "Penetration and defect formation in high-current arc welding," *Welding Journal*, vol. 82, no. 10, 296S–306S, 2003.

[137] P. F. Mendez, K. E. Tello, and S. S. Gajapathi, "Generalization and communication of welding simulations and experiments using scaling analysis design rules in welding design rules in engineering : Calibrated minimal representation approach," in *Trends in Welding Research, Proceedings of the 9th International Conference*, ASM International, 2012, pp. 249–258.

[139] P. F. Mendez, "Characteristic values in the scaling of differential equations in engineering," *Journal of Applied Mechanics*, vol. 77, no. 6, p. 061 017, 2010.

[140] P. F. Mendez, Y. Lu, and Y. Wang, "Scaling analysis of a moving point heat source in steady- state on a semi-infinite solid," *Journal of Heat Transfer*, vol. 140, no. 8, p. 081 301, 2018.

[141] P. F. Mendez, K. E. Tello, and T. J. Lienert, "Scaling of coupled heat transfer and plastic deformation around the pin in friction stir welding," *Acta Materialia*, vol. 58, no. 18, pp. 6012–6026, 2010.

[142] J. L. Meseguer-Valdenebro, J. Serna, A. Portoles, M. Estrems, V. Miguel, and E. Martínez-Conesa, "Experimental validation of a numerical method that predicts the size of the heat affected zone. optimization of the welding parameters by the Taguchi's method," *Transactions of the Indian Institute of Metals*, vol. 69, no. 3, pp. 783–791, 2016.

[143] K. C. Mills, *Recommended values of thermophysical properties for selected commercial alloys*. Woodhead Publishing Limited, 2002.

[144] Y. S. Muzychka and M. M. Yovanovich, "Thermal resistance models for non-circular moving heat sources on a half space," *Journal of Heat Transfer*, vol. 123, no. 4, pp. 624–632, 2001.

[145] P. S. Myers, O. A. Uyehara, and G. L. Borman, "Fundamentals of heat flow in welding," *Welding Research Council Bulletin*, vol. 123, pp. 1–46, 1967.

[146] O. R. Myhr and Ø. Grong, "Dimensionless maps for heat flow analyses in fusion welding," *Acta Metallurgica et Materialia*, vol. 38, no. 3, pp. 449–460, 1990.

[147] A.-K. Nehad, "Enthalpy technique for solution of stefan problems: Application to the keyhole plasma arc welding process involving moving heat source," *International communications in heat and mass transfer*, vol. 22, no. 6, pp. 779–790, 1995.

[149] V. Nemchinsky, "Temperature created by a moving heat source that heats and melts the metal plate (plasma arc cutting)," *Journal of Heat Transfer*, vol. 138, no. 12, p. 122 301, 2016.

[153] A. Odabaşı, N. Ünlü, G. Göller, and M. N. Eruslu, "A Study on Laser Beam Welding (LBW) Technique: Effect of Heat Input on the Microstructural Evolution of Superalloy Inconel 718," *Metallurgical and Materials Transactions A*, vol. 41A, no. 9, pp. 2357–2365, 2010.

[155] N. Okui, D. Ketron, F. Bordelon, Y. Hirata, and G. Clark, "A methodology for prediction of fusion zone shape," *Welding Research Supplement*, vol. 86, no. 2, pp. 35–43, 2007.

[156] G. M. Oreper, T. W. Eagar, and J. Szekely, "Convection in arc weld pools," *Welding Journal*, vol. 62, no. 11, pp. 307–312, 1983.

[160] V. Pavelic, R. Tanbakuchi, O. A. Uyehara, and P. S. Myers, "Experimental and computed temperature histories in gas tungsten-arc welding of thin plates," *Welding Research Supplement*, vol. 48, pp. 295–305, 1969.

[163] X.-T. Pham, "Two-dimensional Rosenthal moving heat source analysis using the meshless element free Galerkin method," *Numerical Heat Transfer, Part A: Applications*, vol. 63, no. 11, pp. 807–823, 2013.

[169] D. Rivas and S. Ostrach, "Scaling of low-prandtl-number thermocapillary flows," *International Journal of Heat and Mass Transfer*, vol. 35, no. 6, pp. 1469–1479, 1992.

[171] O. F. T. Roberts, "The theoretical scattering of smoke in a turbulent atmosphere," in *Proceedings of the Royal Society of London*, ser. Series A, Containing Papers of a Mathematical and Physical Character, vol. 104, Royal Society, 1923, pp. 640–654.

[175] D. Rosenthal, "The theory of moving sources of heat and its application to metal treatments," *Transactions of the A.S.M.E.*, vol. 68, pp. 849–866, 1946.

[176] D. Rosenthal and R. Schmerber, "Thermal study of arc welding," *Welding journal*, vol. 17, no. 4, pp. 2–8, 1938.

[177] D. Rosenthal, "Mathematical theory of heat distribution during welding and cutting," *The Welding Journal*, vol. 20, no. 5, pp. 220–234, 1941.

[179] N. N. Rykalin, *Calculation of heat flow in welding*. Mashgis, Moscow, Russia: Mashgis, 1951.

[183] Y. Sharir, A. Grill, and J. Pelleg, "Computation of temperatures in thin tantalum sheet welding," *Metallurgical and Materials Transactions B*, vol. 11, no. 2, pp. 257–265, 1980.

[186] W. M. Steen and J. Mazumder, *Laser material processing*, Fourth. London: Springer, 2010.

[190] D. T. Swift-Hook and A. E. F. Gick, "Penetration welding with lasers," *Welding Research Supplement*, vol. 52, no. 11, 492s–499s, 1973.

[197] M. Ushio, T. Ishimura, F. Matsuda, and Y. Arata, "Theoretical calculation on shape of fusion boundary and temperature distribution around moving heat source (Report I)," *Transactions of JWRI*, vol. 6(1), no. 1, p1–p6, 1977.

[198] M. Van Elsen, M. Baelmans, P. Mercelis, and J.-P. Kruth, "Solutions for modelling moving heat sources in a semi-infinite medium and applications to laser material processing," *International Journal of Heat and Mass Transfer*, vol. 50, no. 23-24, pp. 4872–4882, 2007.

[199] V. R. Voller and C. R. Swaminathan, "General source-based method for solidification phase change," *Numerical Heat Transfer*, vol. 19, pp. 175–189, 1991.

[206] Y. Wang, Y. Lu, M. Grams, A. H. Cesaro, and P. F. Mendez, "Asymptotics and blending in the modeling of welding," in *Numerical Analysis of Weldability*, Graz, Austria, 2018.

[207] Y. Wang, Y. Lu, and P. F. Mendez, "Scaling expressions of characteristic values for a moving point heat source in steady state on a semi-infinite solid," *International Journal of Heat and Mass Transfer*, vol. 135, pp. 1118–1129, 2019.

[210] T. Washio and H. Motoda, "Extension of dimensional analysis for scale-types and its application to discovery of admissible models of complex processes," in *International Workshop on Similarity Method*, 1999, pp. 129–147.

[211] J. M. Webster, "Welding at high speed with the CO2 laser," *Metal Progress*, vol. 98, pp. 59–61, 1970.

[213] A. A. Wells, "Heat flow in welding," *Welding Research Supplement*, vol. 31, no. 5, 263s–267s, 1952.

[215] H. A. Wilson, "On convection of heat," in *Proceedings of the Cambridge Philosophical Society*, vol. 12, 1904, pp. 406–423.

[218] G. Wood, S. A. Islam, and P. F. Mendez, "Calibrated expressions for welding and their application to isotherm width in a thick plate," *Soldagem & Inspeção*, vol. 19, no. 3, pp. 212–220, 2014.

[227] G. Yu, R. J. Anderson, T. Maekawa, and N. M. Patrikalakis, "Efficient simulation of shell forming by line heating," *International Journal of Mechanical Sciences*, vol. 43, no. 10, pp. 2349–2370, 2001.

Appendix 2.A Estimation of effective thermophysical properties

2.A.1 Thermal diffusivity

Thermal diffusivity can ba calculated based on effective values of thermal conductivity and specific heat.

$$\alpha_{\text{eff}} = \frac{k_{\text{eff}}}{(\rho c)_{\text{eff}}} \tag{2.35}$$

2.A.2 Thermal conductivity

A reasonable approach to calculating an effective thermal conductivity k_{eff} is to consider the overall thermal resistance of a wall of thickness L in steady state.

$$\mathcal{R}'' = \frac{\Delta T}{q''} = \frac{L}{k_{\text{eff}}} \tag{2.36}$$

where $\mathcal{R}''$ is the thermal resistance associated with the absolute values of heat flux q'' (in the direction of coordinate ξ, perpendicular to the wall) and temperature difference ΔT through the thickness d of the wall. In steady state, the heat flux is constant because there can be no accumulation or depletion of heat at any point in the wall:

$$q'' = -k(T)\frac{\mathrm{d}T}{\mathrm{d}\xi} = \text{constant} \tag{2.37}$$

where $T = T(\xi)$ and $k = k(T)$. The temperature difference between the surfaces of the wall can be calculated by integration of Equation 2.37.

$$\Delta T = \int_L \frac{\mathrm{d}T}{\mathrm{d}\xi} d\xi = -\int_L \frac{q''}{k(T)} d\xi = -q'' \int_L \frac{d\xi}{k(T)} \tag{2.38}$$

Because $T = T(\xi)$, we can say

$$dT = \frac{\mathrm{d}T}{\mathrm{d}\xi} d\xi \tag{2.39}$$

Comparing Equations 2.36, 2.38, and 2.39 we obtain

$$k_{\text{eff}} = L \left[\int_{\Delta T} \frac{1}{\frac{\mathrm{d}T}{\mathrm{d}\xi}} \frac{dT}{k(T)} \right]^{-1} \tag{2.40}$$

which for the case when the temperature gradient is approximately constant can be approximated as

$$\frac{\mathrm{d}T}{\mathrm{d}\xi} \approx \frac{\Delta T}{L} = \text{constant} \tag{2.41}$$

resulting in

$$k_{\text{eff}} \approx \left[\frac{1}{\Delta T}\int_{\Delta T} k(T)^{-1} dT\right]^{-1} \tag{2.42}$$

where

$$\Delta T = T_{\text{c}} - T_0 \tag{2.43}$$

This definition of ΔT accounts for thermal conduction between the isotherm of interest T_{c} and the far regions of the substrate which are at the far temperature T_0.

2.A.3 Specific heat

The selection of an average value of c is potentially problematic. Phase changes cause peaks with significant amounts of enthalpy, but the peaks can be missed or underestimated in the resolution of thermodynamic calculations, and in the case of isothermal phase changes, the peak becomes a line at a given temperature. A better approach is to use the definition of specific heat:

$$c = \frac{\mathrm{d}i}{\mathrm{d}T} \tag{2.44}$$

Equation 2.44 requires a constant density, such that $c_p = c_v = c$, then it is possible to write, because density is considered constant in the governing equation,

$$\rho c = \frac{\mathrm{d}\rho i}{\mathrm{d}T} \tag{2.45}$$

$$(\rho c)_{\text{eff}} = \frac{\Delta(\rho i)}{\Delta T} \tag{2.46}$$

with the same definition of ΔT as before.

Appendix 2.B Asymptotics for maximum isotherm half-width

The maximum isotherm half-width y^*_{m} and its location x^*_{m} can be implicitly expressed as:

$$T^*_c = \exp\left(-x^*_{\max}\right) K_0\left(\sqrt{x^{*2}_{\mathrm{m}} + y^{*2}_{\mathrm{m}}}\right) \tag{2.47}$$

$$\left.\frac{\partial T^*}{\partial x^*}\right|_{x^*_{\mathrm{m}}, y^*_{\mathrm{m}}} = 0 \tag{2.48}$$

Based on the relationship between derivatives of Bessel function $K_n(\xi)$, $\dfrac{\mathrm{d}K_n(\xi)}{\mathrm{d}\xi} = -K_{n-1}(\xi) - \dfrac{n}{\xi}K_n(\xi)$[21], Equation 2.47 and Equation 2.48 can be represented by using the zeroth order (K_0) and first order (K_1) of the second kind of modified Bessel function to obtain:

$$1/\mathrm{Ro} = \exp\left(-x^*_{\max}\right) K_0\left(\sqrt{x^{*2}_{\mathrm{m}} + y^{*2}_{\mathrm{m}}}\right) \tag{2.49}$$

$$K_0\left(\sqrt{x^{*2}_{\mathrm{m}} + y^{*2}_{\mathrm{m}}}\right) + \frac{x^*_{\max} K_1\left(\sqrt{x^{*2}_{\mathrm{m}} + y^{*2}_{\mathrm{m}}}\right)}{\sqrt{x^{*2}_{\mathrm{m}} + y^{*2}_{\mathrm{m}}}} = 0 \tag{2.50}$$

Therefore, x^*_{m} and y^*_{m} can be written as a function of $r^*_{\mathrm{m}} = \sqrt{x^{*2}_{\mathrm{m}} + y^{*2}_{\mathrm{m}}}$:

$$x^*_{\max} = -r^*_{\max}\frac{K_0\left(r^*_{\max}\right)}{K_1\left(r^*_{\max}\right)} \tag{2.51}$$

$$y^*_{\mathrm{m}} = r^*_{\max}\sqrt{1 - \left[\frac{K_0\left(r^*_{\max}\right)}{K_1\left(r^*_{\max}\right)}\right]^2} \tag{2.52}$$

where r^*_{m} can be implicitly expressed as a function of Ro number by Equation 2.47:

$$1/\mathrm{Ro} = T^*_c\left(r^*_{\mathrm{m}}\right) = \exp\left[r^*_{\max}\frac{K_0\left(r^*_{\max}\right)}{K_1\left(r^*_{\max}\right)}\right] K_0\left(r^*_{\mathrm{m}}\right) \tag{2.53}$$

$T^*_c\left(r^*_{\mathrm{m}}\right)$ is continuous and has a strictly monotonic dependence on r^*_{m}, the inverse function of Equation 2.53($r^*_{\mathrm{m}}(\mathrm{Ro})$) exists and has an unique representation. Asymptotic analysis of Equation 2.53 yields two limiting solutions of $r^*_{\mathrm{m}}(\mathrm{Ro})$ in Regime III and IV, which would be substituted into Equation 2.52 to obtain asymptotes for maximum isotherm half-width $y^*_{\mathrm{m}}(\mathrm{Ro})$.

Regime III: $\mathrm{Ro} \to \infty$

In regime III where $\mathrm{Ro} \to \infty$ and $T_c^* \to 0$, the point locating at isotherm width is far from the heat source ($r^*_{\max_{\mathrm{III}}} \to \infty$). For large values of r^*_{m}, the asymptotic behavior of Ro number changing with r^*_{m} is achieved by asymptotic analysis of the right side of Equation 2.53:

$$1/\mathrm{Ro} = \sqrt{\frac{\pi}{2\mathrm{e}\ r^*_{\max_{\mathrm{III}}}}} + O\left(r^{*-3/2}_{\max_{\mathrm{III}}}\right) \tag{2.54}$$

To solve $r^*_{\max_{\mathrm{III}}}$, let $r^*_{\max_{\mathrm{III}}} = \frac{\pi}{2\mathrm{e}}\mathrm{Ro}^2\left[1+\epsilon\left(\mathrm{Ro}\right)\right]$, assuming $\epsilon\left(\mathrm{Ro}\right) \to 0$ which is equivalent to $\widehat{r}^*_{\max_{\mathrm{III}}} = \frac{\pi}{2\mathrm{e}}\mathrm{Ro}^2$. If $\epsilon\left(\mathrm{Ro}\right)$ can be solved and satisfies the assumption, the solution to $r^*_{\max_{\mathrm{III}}}$ for Equation 2.54 is determined and unique. Substituting the assumed expression of $r^*_{\max_{\mathrm{III}}}$ into Equation 2.54, Equation 2.54 turns into:

$$1/\mathrm{Ro} = \sqrt{\frac{1}{\mathrm{Ro}^2\left[1+\epsilon\left(\mathrm{Ro}\right)\right]}} + O\left\{\frac{\pi}{2\mathrm{e}}\mathrm{Ro}^2\left[1+\epsilon\left(\mathrm{Ro}\right)\right]\right\}^{-3/2} \tag{2.55}$$

According to the assumption $\epsilon\left(\mathrm{Ro}\right) \to 0$ in Regime III, ϵ is solved:

$$\epsilon\left(\mathrm{Ro}\right) = O\left(\mathrm{Ro}^{-2}\right) \tag{2.56}$$

The solution $O\left(\mathrm{Ro}^{-2}\right) \ll 1$ satisfies the assumption in Regime III where $\mathrm{Ro} \to \infty$. $r^*_{\max_{\mathrm{III}}}$ has a parabolic dependence on Ro in Regime III:

$$r^*_{\max_{\mathrm{III}}} = \frac{\pi}{2\mathrm{e}}\mathrm{Ro}^2\left[1+\epsilon\left(\mathrm{Ro}\right)\right] = \frac{\pi}{2\mathrm{e}}\mathrm{Ro}^2 + O(1) \tag{2.57}$$

Substituting Equation 2.57 into Equation 2.52 yields solution to half-width in Regime III:

$$y^*_{\max_{\mathrm{III}}} = r^*_{\max_{\mathrm{III}}}\sqrt{1-\left[\frac{K_0\left(r^*_{\max_{\mathrm{III}}}\right)}{K_1\left(r^*_{\max_{\mathrm{III}}}\right)}\right]^2} = \sqrt{\frac{\pi}{2\mathrm{e}}}\mathrm{Ro} + O\left(\frac{1}{\mathrm{Ro}}\right) \tag{2.58}$$

The asymptotic expression of half-width in Regime III is:

$$\widehat{y}^*_{\max_{\mathrm{III}}} = \sqrt{\frac{\pi}{2\mathrm{e}}}\mathrm{Ro} \tag{2.59}$$

Regime IV: $\mathrm{Ro} \to 0$

In Regime IV where $\mathrm{Ro} \to 0$ and $T_c^* \to \infty$, $r^*_{\max_{\mathrm{IV}}}$ is small as it decreases with T_c^*. The asymptotic analysis of the right side of Equation 2.53 for $r^*_{\max_{\mathrm{IV}}} \to 0$ in Regime IV produces:

$$1/\mathrm{Ro} = -\ln\left(r^*_{\max_{\mathrm{IV}}}\right) - \gamma + \ln(2) + O\left(r^{*2}_{\max_{\mathrm{IV}}}\right) \tag{2.60}$$

where $\gamma \approx 0.5772$ is Euler–Mascheroni constant. Performing exponential transformation on both sides yields:

$$\begin{aligned}\exp\left[-1/\mathrm{Ro} - \gamma + \ln(2)\right] &= r_{\max_{\mathrm{IV}}} \exp\left[O\left(r^{*2}_{\max_{\mathrm{IV}}}\right)\right] \\ &= r_{\max_{\mathrm{IV}}}\left\{1 + O\left[O\left(r^{*2}_{\max_{\mathrm{IV}}}\right)\right]\right\} = r_{\max_{\mathrm{IV}}}\left[1 + O\left(r^{*2}_{\max_{\mathrm{IV}}}\right)\right]\end{aligned} \tag{2.61}$$

As is the asymptotic analysis in Regime III Equation 2.55, writing the $r_{\max_{\mathrm{IV}}}$ as $r_{\max_{\mathrm{IV}}} = \exp\left[-1/\mathrm{Ro} - \gamma + \ln(2)\right]\left[1 + \epsilon\left(\mathrm{Ro}\right)\right]$ assuming $\epsilon\left(\mathrm{Ro}\right) \to 0$, into Equation 2.61:

$$\begin{aligned}1 &= \left[1 + \epsilon\left(\mathrm{Ro}\right)\right]\left\{1 + O\left\{\exp\left[-1/\mathrm{Ro} - \gamma + \ln(2)\right]^2\left[1 + \epsilon\left(\mathrm{Ro}\right)\right]^2\right\}\right\} \\ &= \left[1 + \epsilon\left(\mathrm{Ro}\right)\right]\left\{1 + O\left[\exp\left(-\frac{2}{\mathrm{Ro}}\right)\right]\right\}\end{aligned} \tag{2.62}$$

According to the assumption $\epsilon\left(\mathrm{Ro}\right) \to 0$, it is solved:

$$\epsilon\left(\mathrm{Ro}\right) = O\left[\exp\left(-\frac{2}{\mathrm{Ro}}\right)\right] \tag{2.63}$$

The solution $O\left[\exp\left(-\frac{2}{\mathrm{Ro}}\right)\right] \ll 1$ satisfies the assumption because $\mathrm{Ro} \to 0$ in Regime IV. Therefore, in Regime IV, the solution to Equation 2.53 is:

$$r^*_{\max_{\mathrm{IV}}} = 2\exp\left(-1/\mathrm{Ro} - \gamma\right) + O\left[\exp\left(-\frac{3}{\mathrm{Ro}}\right)\right] \tag{2.64}$$

The solution to half-width $y^*_{\max}$ in Regime IV can be obtained by substituting Equation 2.64 into Equation 2.52:

$$\begin{aligned}y_{\max_{\mathrm{IV}}} &= r^*_{\max_{\mathrm{IV}}}\sqrt{1 - \left[\frac{K_0\left(r^*_{\max_{\mathrm{IV}}}\right)}{K_1\left(r^*_{\max_{\mathrm{IV}}}\right)}\right]^2} \\ &= 2\exp\left(-\gamma - 1/\mathrm{Ro}\right) + O\left[\exp\left(-3/\mathrm{Ro}\right)\right]\end{aligned} \tag{2.65}$$

Therefore, the asymptotic expression to half-width of isotherm in regime IV when $\mathrm{Ro} \to 0$:

$$\widehat{y}^*_{\max_{\mathrm{IV}}} = 2\exp\left(-\gamma - 1/\mathrm{Ro}\right) \tag{2.66}$$

Appendix 2.C Criterion for point heat source

The criterion is established to ignore heat source size assuming under gaussian distribution. The temperature field is simulated with Comsol Multiphysics v5.4 setting thermal properties k, ρ, c_p, α as 1 for convenience of normalization. The simulations are under three groups of operating parameters:

$$q = 2\pi\mathrm{W}, U = 2\mathrm{m/s}, \sigma = 0.1:0.1:0.9, 1:1:55\mathrm{m} \tag{2.67}$$

$$q = 20\pi\mathrm{W}, U = 20\mathrm{m/s}, \sigma = 0.1:0.1:0.9, 1:1:55\mathrm{m} \tag{2.68}$$

$$q = 2\pi\mathrm{W}, U = 2\mathrm{m/s}, \sigma = 3:6\times10^{-4}, 3:6\times10^{-3}, 3:6\times10^{-2}\mathrm{m} \tag{2.69}$$

The result of simulation is illustrated in Figure 2.10. The criteria to neglect effect of heat source size for $0.1 < \mathrm{Ro} < 100$ is:

$$\sigma^*_{\mathrm{c}} \approx 0.6\widehat{y}^*_{\max} < 0.6\,\frac{1+2\mathrm{Ro}}{1+\mathrm{Ro}}\,\widehat{y}^*_{\max} \tag{2.70}$$

Appendix 2.D Criterion for insulated surface

Under mild convection for small values h^*, the isotherm width $y^*_{\max_{\mathrm{h}}}$ and its location $x^*_{\max_{\mathrm{h}}}$ can be written as:

$$x^*_{\max_{\mathrm{h}}} = x^*_{\max} + \delta^*_x \qquad y^*_{\max_{\mathrm{h}}} = y^*_{\max} + \delta^*_y$$

where $x^*_{\max}$ and $y^*_{\max}$ are isotherm width and its location for adiabatic surface cases that can be estimated with Equation 2.31 and Equation 2.32, and the variation $\delta^*_x \ll$

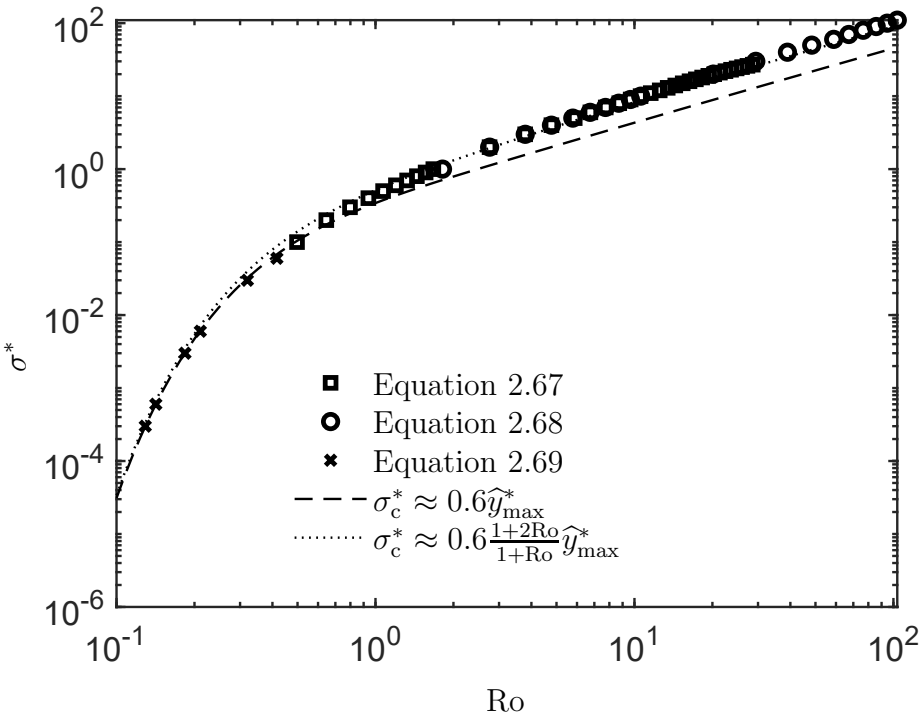

Figure 2.10: The simulation result and criteria proposed Equation 2.70 to neglect heat source size effect for isotherm width

$x^*_{\max}$, $\delta^*_y \ll y^*_{\max}$. The isotherm width can be expressed implicitly as:

$$\frac{1}{\mathrm{Ro}} = T^*\Big|_{x^*_{\max_h}, y^*_{\max_h}, h^*} \approx$$
$$\approx \frac{1}{2}\exp\left(-x^*_{\max}\right)\left[-\frac{K_1\left(r^*_{\max}\right)\left(2\delta^*_x x^*_{\max} + 2\delta^*_y y^*_{\max} + h^* r^{*2}_{\max}\right)}{r^*_{\max}} - 2(\delta^*_x - 1)K_0\left(r^*_{\max}\right)\right] \tag{2.71}$$

$$0 = \frac{\partial T^*}{\partial x^*}\Big|_{x^*_{\max_h}, y^*_{\max_h}, h^*} =$$
$$= \frac{1}{2}\exp\left(-x^*_{\max}\right)\left\{\frac{1}{r^{*2}_{\max}} x^*_{\max} K_2\left(r^*_{\max}\right)\left(2\delta^*_x x^*_{\max} + 2\delta^*_y y^*_{\max} + h^* r^{*2}_{\max}\right) + \right.$$
$$+ \frac{K_1\left(r^*_{\max}\right)\left[\delta^*_x(4x^*_{\max} - 2) + 2\delta^*_y y^*_{\max} + x^*_{\max} h^*(x^*_{\max} - 2) - 2x^*_{\max} + h^* y^{*2}_{\max}\right]}{r^*_{\max}} +$$
$$\left. +2(\delta^*_x - 1)K_0\left(r^*_{\max}\right)\right\} \tag{2.72}$$

According to the implicit expression of isotherm width and its location neglecting surface heat loss Equation 2.49 and Equation 2.50,

$$K_0\left(r^*_{\max}\right) = \frac{1}{\mathrm{Ro}} \exp\left(x^*_{\max}\right) \tag{2.73}$$

$$,K_1\left(r^*_{\max}\right) = -\frac{r^*_{\max} \exp\left(x^*_{\max}\right)}{x^*_{\max}\mathrm{Ro}}, \tag{2.74}$$

$$K_2\left(r^*_{\max}\right) = K_0\left(r^*_{\max}\right) + \frac{2}{r^*_{\max}} K_1\left(r^*_{\max}\right) \tag{2.75}$$

Bringing the relationships of equations 2.73 to 2.75 into Equation 2.71 and 2.72,

$$\delta^*_x \approx \frac{x^*_{\max}\left({x^*_{\max}}^2 + {y^*_{\max}}^2\right)}{{x^*_{\max}}^2 + (x^*_{\max} - 1){y^*_{\max}}^2} \cdot h^* \qquad \delta^*_y \approx -\frac{\left({x^*_{\max}}^2 + {y^*_{\max}}^2\right)}{2y^*_{\max}} \cdot h^* \tag{2.76}$$

For accepted relative error $\mathrm{E_A}\%$ for isotherm width,

$$\frac{\delta^*_y}{y^*_{\max}} = \frac{r^{*2}_{\max}}{2y^{*2}_{\max}} h^* \leq \mathrm{E_A}\% \tag{2.77}$$

The criteria to ignore surface convection under 10% accepted error is:

$$h^*_{\mathrm{c}} = 0.2\frac{y^{*2}_{\max}}{r^{*2}_{\max}} \approx 0.2\left[1 + \left(\frac{\pi}{2\mathrm{e}}\mathrm{Ro}^2\right)^n\right]^{-1/n} \tag{2.78}$$

$$d_{\mathrm{c,h}} = \frac{20\alpha^2\left(h + h'\right)}{kU^2}\left[1 + \left(\frac{\pi}{2\mathrm{e}}\mathrm{Ro}^2\right)^n\right]^{1/n} \tag{2.79}$$

where $n = 0.9405$ is the optimal blending parameter. The criterion of Equation 2.78 is compared to the numerical solution from Equation 2.5 in Figure 2.11.

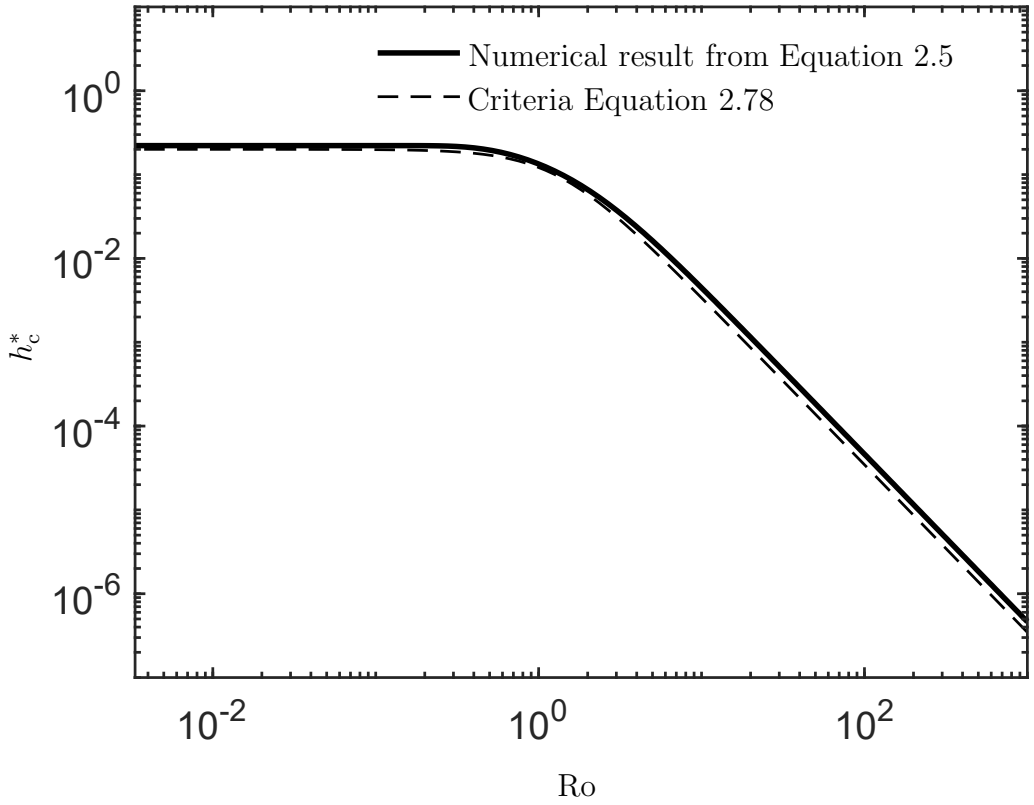

Figure 2.11: The numerical result and criteria proposed Equation 2.78 to neglect surface convection for isotherm width

Chapter 3

Characteristic values of a two-dimensional point moving heat source

3.1 Abstract

This paper presents engineering expressions for characteristic values of 12 magnitudes associated with a moving point heat source in a 2D space: location of maximum width, trailing length, centerline cooling rate, leading length, centerline heating rate, maximum temperature, gradient of maximum temperature, aspect ratio, melting efficiency, cooling time from 800 °C to 500 °C, solidification time, and thickness of the heat affected zone. A modification of the heat intensity enables the extension of predictions to dissimilar thicknesses and alternative joint configurations. All proposed expressions are obtained with a systematic approach and are accurate to within 8 % of the exact solutions, except heating rate at 16 %. The explicit expressions proposed depend on a single dimensionless group that captures all possible cases. This dimensionless number is the Rosenthal number (Ro) for all cases, except for the estimation of maximum temperature, for which a dimensionless width is used. The engineering equations obtained are simple enough to be evaluated with a calculator or spreadsheet, and are useful for a broad range of diverse applications such as welding, additive manufacturing, heat treating, sliding contact, and more.

Table 3.1: Notation.

Variables	**Unit**	**Description**
c	$\mathrm{J\,kg^{-1}\,K^{-1}}$	Specific heat
d	m	Thickness of substrate
f		Correction factor
i	$\mathrm{J\,kg^{-1}}$	Enthalpy
k	$\mathrm{W\,m^{-1}\,K^{-1}}$	Thermal conductivity
q	W	Power of heat source absorbed by substrate
r	m	Distance from the heat source
Ro	1	Rosenthal number
St	1	Stefan number
t	s	Time
$t_{8/5}$	s	Cooling time from 800 °C to 500 °C
T	K	Temperature
T_0	K	Initial temperature
$T_{\max}$	K	Maximum temperature
$\mathrm{d}T_{\max}/\mathrm{d}y$	$\mathrm{K\,m^{-1}}$	Gradient of maximum temperature
U	$\mathrm{m\,s^{-1}}$	Travel speed of moving heat source
W		Lambert function
x, y	m	Cartesian coordinates
Greek symbols		
α	$\mathrm{m^2\,s^{-1}}$	Thermal diffusivity
η_{m}	1	Melting efficiency
ϕ	°	Actual heat flow angle
γ	1	Euler-Mascheroni constant (0.5772...)
Superscripts		
*		Dimensionless value

Continued on next page

Table 3.1 – continued from previous page

Variables	Unit	Description
$\widehat{\ }$		Asymptotic behavior
$^+$		Correction for intermediate values
$\dot{}$		Time derivative
Subscripts		
500		500 °C
800		800 °C
b		Isotherm trailing point
c		Variable of interest
eff		Effective value
f		Isotherm leading point
HAZ		Heat affected zone
III		Regime III
IV		Regime IV
i		Intermediate value
m		Melting
max		Isotherm half-width
sl		Solidification
Others		
$\mathcal{AR}$	1	Aspect ratio of isotherm
Acronyms		
EBW		Electron Beam Welding
GMAW		Gas Metal Arc Welding
GTAW		Gas Tungsten Arc Welding
LBW		Laser Beam Welding
SAW		Submerged Arc Welding

Continued on next page

Table 3.1 – continued from previous page

Variables	Unit	Description
SMAW		Shielded Metal Arc Welding

3.2 Introduction

Moving heat sources are ubiquitous in heat transfer problems, with practical technological applications including welding [174, 175, 179], heat treatment [86, 106, 124], tribology [89, 94], grinding [25, 132], machining [51, 107], and railroad wheel and track contact [102, 103].

Despite the abundance of analytical solutions (e.g. [174, 175, 179, 212], also Green's function methods [157]), numerical solutions (e.g. [59, 74]), and empirical expressions (some of them compiled in [173, 181]), this knowledge is seldom used by practitioners. The main obstacle is that in practice, important temperatures are known, such as transformation temperatures, melting temperatures, and degradation temperatures, and what is desired is to know the extent of their reach into a substrate, the cooling or heating rate around transformation, or other process information associated with a particular temperature.

Analytic or numerical solutions calculate the temperature at a given location, which is the inverse of what is typically needed in practice; thus they do not readily provide an answer to many practical questions. Root finding and optimization algorithms can be used to obtain the desired answer, but at an increased level of involvement, which is often beyond the abilities or time availability of practitioners. The need to use numerical tools also makes the development of metamodels significantly more difficult.

Dimensional analysis indicates that idealized moving heat source problems can be much reduced in their number of degrees of freedom with mathematical exactness; for the cases studied in this paper, all magnitudes associated with a temperature depend

on a single dimensionless group, regardless the nature of the heat source and the base material. The theory of blending [34] enables the development of explicit expressions that approximate inverse functions with high accuracy.

This paper applies the methodologies of scaling analysis, asymptotic analysis, and blending techniques to the exact solutions originally developed by Rosenthal [174, 175] and verified experimentally in [176] for the study of temperature fields in welding. These exact solutions were independently developed also by Rykalin [179], Wilson [215] and Roberts [171] (for the case of mass transfer). Based on the exact solution, 12 novel characteristic values associated with the isotherm $T(x, y) = T_{\mathrm{c}}$ are calculated, represented in Figure 3.1. The approach used here is based on the Minimal Representation and Correction Factors methodology [135], and the details of its application to a moving point heat source on a thin plate are in [130], where only the maximum isotherm half-width ($y_{\max}$) was analyzed as demonstration of the methodology.

Closed-form, explicit expressions are presented for 7 new primary characteristic values (in addition to isotherm half-width $y_{\max}$ studied in [130]), and 5 associated secondary characteristic values. The new primary characteristic values are: the location of isotherm half-width $x_{\max}$, the trailing length of isotherm x_{b}, the centerline cooling rate $\dot{T}_{\mathrm{b}}$, the leading length of isotherm x_{f}, the centerline heating rate $\dot{T}_{\mathrm{f}}$, the maximum temperature $T_{\max}$ and the gradient of maximum temperature $\mathrm{d}T_{\max}/\mathrm{d}y$. The associated secondary characteristic values studied are the aspect ratio $\mathcal{AR}$ of isotherm, the melting efficiency η_{m} which is a rough approximation to estimate the dilution of filler metal in welding, especially important in corrosion resistant alloys such as stainless steels [48], centerline cooling time $t_{8/5}$ from 800 °C to 500 °C corresponding to the time it takes for the center line to cool from 800°Cto 500°C, and a key determinant of hardness in weldments [23, 87], solidification time t_{sl} which is a rough approximation of the time needed to dissipate the latent heat of fusion, and thickness of Heat Affected Zone Δy_{HAZ} which is the difference between isotherm half-widths.

The relevance of the characteristic values studied is detailed in [207].

The methodology used does not have problems of convergence, and the explicit expressions obtained can be implemented directly into higher order models, or spreadsheets for direct estimations. The effects of the parameters are directly visible in the expressions, and facilitate the intuitive understanding of the problem.

3.3 Mathematical model

The mathematical model employed here is the 2D solution for a moving point heat source in steady state in Eulerian coordinates presented in [171, 175, 215]:

$$T(x,y) = T_0 + \frac{q}{2\pi kd} \exp\left(-\frac{Ux}{2\alpha}\right) K_0\left(\frac{Ur}{2\alpha}\right) \tag{3.1}$$

where K_0 is modified Bessel function of the second kind and zeroth order, x and y are two independent variables illustrated in Figure 3.1, q is the heat input of the point heat source, d is the thickness of the substrate (in a 2D formulation, q and d always appear together as $q/d = q'$, where q' is the intensity per unit thickness in 2D model), k is the thermal conductivity of the substrate, T_0 is the temperature of the substrate far from the heat source, U is the velocity of the heat source relative to the substrate, and α is the thermal diffusivity of the substrate. The radial coordinate r is defined in relation to the independent variables as $r = \sqrt{x^2 + y^2}$. In the welding community, this solution is called the "thin-plate Rosenthal solution", although it is also applicable to thick substrates provided the heat source resembles a line through the thickness. In these cases, this same solution is often called the "moving line heat source solution"

The scope of this model and its range of validity is analyzed in detail in [130], including the effect of a finite heat source, substrate thickness, variable material properties, latent heat, and surface heat losses (convection and radiation). For the case of welding, these effects are shown to be secondary for most practical applications for temperatures below the melting point. The unrealistic asymptotic behavior at the

origin is an artifact of considering the heat source as a point and is not a problem in practice. Further validation against experimental and numerical data the authors found in the literature is also performed in this work.

Equation 3.1 can be rewritten in dimensionless form as:

$$T^* = \exp\left(-x^*\right) K_0\left(r^*\right) \tag{3.2}$$

where:

$$T^* = \frac{2\pi kd\left(T - T_0\right)}{q} \tag{3.3}$$

$$x^* = \frac{Ux}{2\alpha} \tag{3.4}$$

$$y^* = \frac{Uy}{2\alpha} \tag{3.5}$$

$$r^* = \frac{Ur}{2\alpha} \tag{3.6}$$

In Equations 3.3-3.6, the * superscript indicates a dimensionless quantity. Dimensional analysis suggests that dimensionless characteristic values for an isotherm T_c (except for maximum temperature) depend only on the Rosenthal number (Ro) [130]:

$$\mathrm{Ro} = \frac{q}{2\pi kd\left(T_\mathrm{c} - T_0\right)} \tag{3.7}$$

In this paper, expressions of characteristic values in asymptotic regimes are presented for the two regimes corresponding to high and low Ro. For consistency with previous work [130], these regimes are named Regime III (high Ro), and Regime IV (low Ro). Based on these regimes, correction factors are developed to provide explicit estimates at the intermediate Ro numbers regime with accuracy and simplicity. The correction factors are especially well suited for engineering applications.

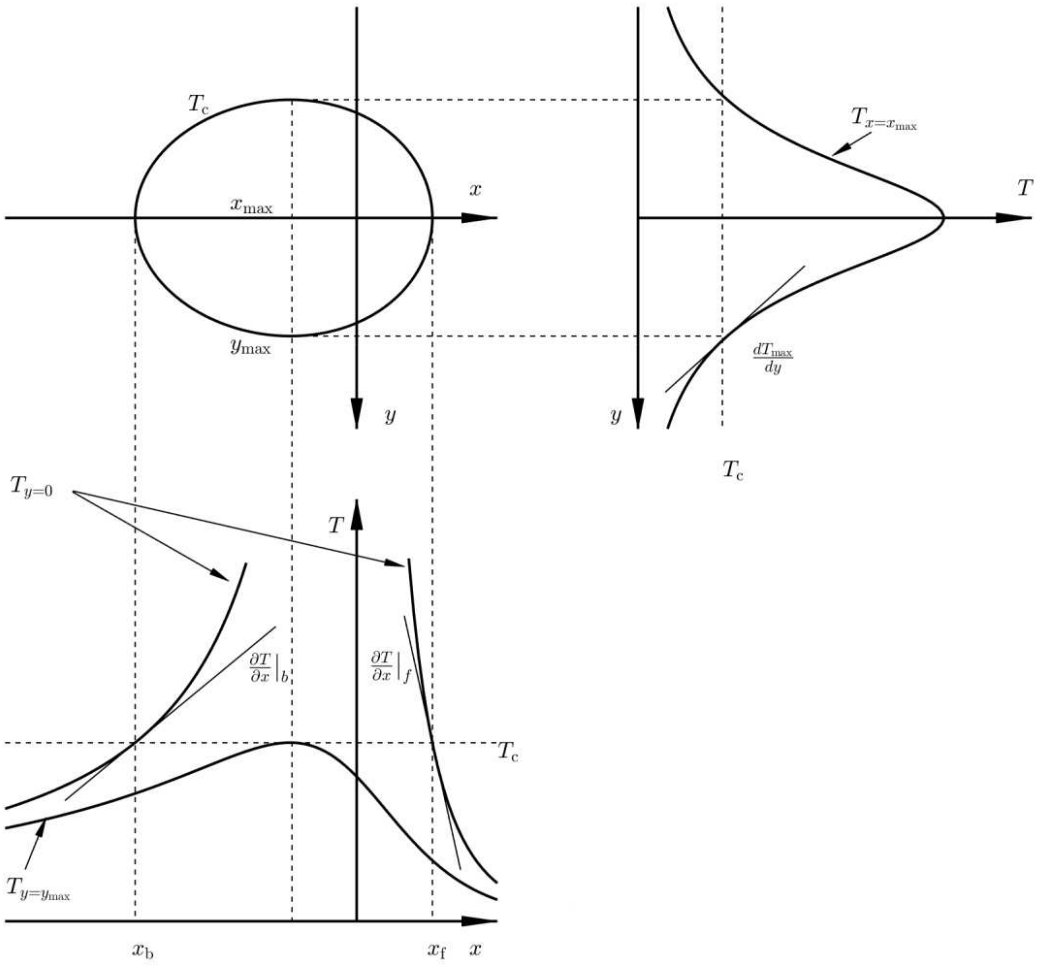

Figure 3.1: Characteristic values of isotherm $T = T_c$ for moving heat source problems [207].

3.4 Location of maximum isotherm half-width $x_{\max}$

For $x_{\max}$ the location of maximum isotherm half-width as illustrated in Figure 3.1, the dimensionless asymptotic behavior is:

$$\widehat{x}^{*}_{\max_{\mathrm{III}}}(\mathrm{Ro}) = -\frac{\pi}{2\mathrm{e}}\mathrm{Ro}^{2} \qquad \text{for Regime III} \tag{3.8}$$

$$\widehat{x}^{*}_{\max_{\mathrm{IV}}}(\mathrm{Ro}) = -\frac{4}{\mathrm{Ro}}\exp\left(-2\gamma - \frac{2}{\mathrm{Ro}}\right) \qquad \text{for Regime IV} \tag{3.9}$$

Equations 3.8 and 3.9 have an important asymmetry; the former is a power law, while the latter is an exponential. In this case, the advanced blending techniques explained in the Appendix yield a lower blending error than traditional blending techniques. The lowest blending error is obtained using the alternative methodology described in 3.A (Equation 3.113), resulting in:

$$\widehat{x}^{*+}_{\max}(\mathrm{Ro}) = -\exp\left(-\frac{2}{\mathrm{Ro}}\right)\left[\frac{\pi}{2\mathrm{e}}\mathrm{Ro}^{2} + \frac{4}{\exp(2\gamma)\,\mathrm{Ro}} + a\mathrm{Ro}^{b}\right] \tag{3.10}$$

where the optimal blending parameters are $a = 1.427, b = 1.077$, with a maximum error of 6.3%. The asymptotic behaviors cross at $\mathrm{Ro} = 0.6799$, and their error against the exact solution is less than 10 % for $\mathrm{Ro} > 1.650$ or $\mathrm{Ro} < 0.2999$. Traditional blending (Equation 3.104) would have resulted in a higher error (18% versus 6.3%).

Correction factors for asymptotic behaviors of equations 3.8 and 3.9 are obtained from Equation 3.10, yielding:

$$f_{x_{\max_{\mathrm{III}}}}(\mathrm{Ro}) = \exp\left(-\frac{2}{\mathrm{Ro}}\right)\left[1 + \frac{8}{\pi\exp(2\gamma-1)\,\mathrm{Ro}^{3}} + \frac{2a\mathrm{e}}{\pi}\mathrm{Ro}^{b-2}\right] \quad \text{for Regime III} \tag{3.11}$$

$$f_{x_{\max_{\mathrm{IV}}}}(\mathrm{Ro}) = \left[1 + \frac{\pi}{8}\exp(2\gamma-1)\mathrm{Ro}^{3} + \frac{a}{4}\exp(2\gamma)\,\mathrm{Ro}^{b+1}\right] \qquad \text{for Regime IV} \tag{3.12}$$

The engineering expressions with units are obtained for the location of isotherm half-

width as:

$$\widehat{x}^{+}_{\max} = \widehat{x}_{\max_{\mathrm{III}}} f_{x_{\max_{\mathrm{III}}}}(\mathrm{Ro}) = -\frac{\alpha q^2}{4\mathrm{e}\pi U d^2 k^2 \left(T_{\mathrm{c}} - T_0\right)^2} f_{x_{\max_{\mathrm{III}}}}(\mathrm{Ro}) \quad \text{for Regime III} \tag{3.13}$$

$$\widehat{x}^{+}_{\max} = \widehat{x}_{\max_{\mathrm{IV}}} f_{x_{\max_{\mathrm{IV}}}}(\mathrm{Ro}) = -\frac{16\pi\alpha d k \left(T_{\mathrm{c}} - T_0\right)}{U q \exp\left(2\gamma + 2/\mathrm{Ro}\right)} f_{x_{\max_{\mathrm{IV}}}}(\mathrm{Ro}) \quad \text{for Regime IV} \tag{3.14}$$

3.5 Trailing length of isotherm x_{b}

The trailing length, x_{b}, is the length of the hot area behind the heat source. The trailing length x^*_{b} is calculated by solving the negative root of Equation 3.2 ($T^* = T^*_{\mathrm{c}}$) at the centerline ($y^* = 0$) (the positive root is the leading length). Asymptotic analysis of Equation 3.2 yields:

$$\widehat{x}^{*}_{\mathrm{b}_{\mathrm{III}}}(\mathrm{Ro}) = -\frac{\pi}{2}\mathrm{Ro}^2 \quad \text{for Regime III} \tag{3.15}$$

$$\widehat{x}^{*}_{\mathrm{b}_{\mathrm{IV}}}(\mathrm{Ro}) = -2\exp\left(-\frac{1}{\mathrm{Ro}} - \gamma\right) \quad \text{for Regime IV} \tag{3.16}$$

The blending equation for trailing length x^*_{b} employing blending Equation 3.113 with a positive exponent is:

$$\widehat{x}^{*+}_{\mathrm{b}}(\mathrm{Ro}) = -\exp\left(-\frac{1}{\mathrm{Ro}}\right)\left[2\exp\left(-\gamma\right) + \frac{\pi}{2}\mathrm{Ro}^2 + a\mathrm{Ro}^b\right] \tag{3.17}$$

where the optimal blending parameters are $a = 0.7659, b = 1.541$, with a maximum error of 6.8%. The asymptotic behaviors cross at Ro = 0.5111, and have an error below 10 % against the exact solution when Ro > 1.700 or Ro < 0.1919. Similarly as before, the choice of blending technique was based on smallest error. If blending had been performed using Equation 3.104, the error would have been larger: 12% instead of 6.8% .

The blending Equation 3.17 generates the following correction factors for asymptotics Equation 3.15 and Equation 3.16:

$$f_{x_{\mathrm{b}_{\mathrm{III}}}}(\mathrm{Ro}) = \exp\left(-\frac{1}{\mathrm{Ro}}\right)\left[1 + \frac{4}{\pi\exp\left(\gamma\right)}\mathrm{Ro}^{-2} + \frac{2a}{\pi}\mathrm{Ro}^{b-2}\right] \quad \text{for Regime III} \tag{3.18}$$

$$f_{x_{\mathrm{b}_{\mathrm{IV}}}}(\mathrm{Ro}) = \left[1 + \frac{\pi}{4}\exp\left(\gamma\right)\mathrm{Ro}^2 + \frac{a}{2}\exp\left(\gamma\right)\mathrm{Ro}^b\right] \quad \text{for Regime IV} \tag{3.19}$$

The engineering expressions with units are obtained by substituting Equation 3.4 and 3.7 into Equation 3.15 and Equation 3.16:

$$\widehat{x}_{\mathrm{b}}^{+} = \widehat{x}_{\mathrm{b_{III}}}\, f_{x_{\mathrm{b_{III}}}}(\mathrm{Ro}) = -\frac{\alpha q^2}{4\pi U d^2 k^2 \left(T_{\mathrm{c}} - T_0\right)^2}\, f_{x_{\mathrm{b_{III}}}}(\mathrm{Ro}) \qquad \text{for Regime III} \tag{3.20}$$

$$\widehat{x}_{\mathrm{b}}^{+} = \widehat{x}_{\mathrm{b_{IV}}}\, f_{x_{\mathrm{b_{IV}}}}(\mathrm{Ro}) = -\frac{4\alpha}{U \exp\left(\gamma + \frac{1}{\mathrm{Ro}}\right)}\, f_{x_{\mathrm{b_{IV}}}}(\mathrm{Ro}) \qquad \text{for Regime IV} \tag{3.21}$$

3.6 Centerline cooling rate $\dot{T}_{\mathrm{b}}$

The centerline cooling rate is a crucial characteristic value to determine because of its dominant influence on the microstructure when phase transformations are present. Because of the Eulerian formulation of the problem, the cooling rate is defined using material derivatives:

$$\dot{T}_{\mathrm{b}} = \left.\frac{DT}{Dt}\right|_{x_{\mathrm{b}}} \tag{3.22}$$

Using the following definition of t^* [207]:

$$t^* = \frac{U^2 t}{2\alpha} \tag{3.23}$$

the cooling rate can be calculated using the following dimensionless expression:

$$\dot{T}_{\mathrm{b}}^* = \frac{4\pi k \alpha d}{q U^2} \left.\frac{DT}{Dt}\right|_{x_{\mathrm{b}}} = -\left.\frac{\partial T^*}{\partial x^*}\right|_{x_{\mathrm{b}}} \tag{3.24}$$

The derivative $\partial T^*/\partial x^*$ at the trailing point x_{b} is derived from Equation 3.2, resulting in:

$$\widehat{\dot{T}}^*_{\mathrm{b_{III}}}(\mathrm{Ro}) = -\frac{1}{\pi \mathrm{Ro}^3} \qquad \text{for Regime III} \tag{3.25}$$

$$\widehat{\dot{T}}^*_{\mathrm{b_{IV}}}(\mathrm{Ro}) = -\frac{1}{2}\exp\left(\frac{1}{\mathrm{Ro}} + \gamma\right) \qquad \text{for Regime IV} \tag{3.26}$$

The blending equation for cooling rate $\dot{T}_{\mathrm{b}}$ using blending Equation 3.113 with $n = -1$ is:

$$\widehat{\dot{T}}^{*+}_{\mathrm{b}}(\mathrm{Ro}) = -\frac{\exp\left(\frac{1}{\mathrm{Ro}}\right)}{\pi \mathrm{Ro}^3 + 2\exp\left(-\gamma\right) + a\mathrm{Ro}^{-b}} \tag{3.27}$$

where the optimal blending parameters are $a = 3.839, b = -2.108$ resulting in a maximum error of 5.8%. The asymptotic behaviors cross at $\mathrm{Ro} = 0.3338$ and have an error below 10 % for $\mathrm{Ro} > 0.7569$ or $\mathrm{Ro} < 0.1776$. The choice of blending technique was based on smallest error. If blending had been performed using Equation 3.104, the error would have been larger: 18% instead of 5.8%.

The blending Equation 3.27 generates the following correction factors for asymptotics Equation 3.25 and Equation 3.26:

$$f_{\dot{T}_{\mathrm{b_{III}}}}(\mathrm{Ro}) = \exp\left(\frac{1}{\mathrm{Ro}}\right)\left[1 + \frac{2}{\pi}\exp\left(-\gamma\right)\mathrm{Ro}^{-3} + a\mathrm{Ro}^{-b-3}\right]^{-1} \quad \text{for Regime III} \quad (3.28)$$

$$f_{\dot{T}_{\mathrm{b_{IV}}}}(\mathrm{Ro}) = \left[1 + \frac{1}{2}\pi\exp\left(\gamma\right)\mathrm{Ro}^{3} + \frac{1}{2}a\exp\left(\gamma\right)\mathrm{Ro}^{-b}\right]^{-1} \quad \text{for Regime IV} \quad (3.29)$$

The engineering expressions with units are obtained for cooling rate:

$$\widehat{\dot{T}}_{\mathrm{b}}^{+} = \widehat{\dot{T}}_{\mathrm{b_{III}}}\, f_{\dot{T}_{\mathrm{b_{III}}}}(\mathrm{Ro}) = -\frac{2\pi U^2 d^2 k^2 \left(T_{\mathrm{c}} - T_0\right)^3}{\alpha q^2}\, f_{\dot{T}_{\mathrm{b_{III}}}}(\mathrm{Ro}) \quad \text{for Regime III} \quad (3.30)$$

$$\widehat{\dot{T}}_{\mathrm{b}}^{+} = \widehat{\dot{T}}_{\mathrm{b_{IV}}}\, f_{\dot{T}_{\mathrm{b_{IV}}}}(\mathrm{Ro}) = -\frac{U^2 q}{8\pi\alpha d k}\exp\left(\gamma + \frac{1}{\mathrm{Ro}}\right)\, f_{\dot{T}_{\mathrm{b_{IV}}}}(\mathrm{Ro}) \quad \text{for Regime IV} \quad (3.31)$$

3.7 Leading length of isotherm x_{f}

The leading length of an isotherm, x_{f}, is a metric of heat conduction against advection ahead of the heat source. The magnitude x_{f}^* is the positive root of Equation 3.2 for $T = T_{\mathrm{c}}$ at the centerline. Asymptotic analysis of Equation 3.2 yields expressions for the leading length in Regime III and IV:

$$\widehat{x}_{\mathrm{f_{III}}}^*(\mathrm{Ro}) = \frac{1}{4}W\left(2\pi\mathrm{Ro}^2\right) \quad \text{for Regime III} \quad (3.32)$$

$$\widehat{x}_{\mathrm{f_{IV}}}^*(\mathrm{Ro}) = 2\exp\left(-\gamma - \frac{1}{\mathrm{Ro}}\right) \quad \text{for Regime IV} \quad (3.33)$$

where W is the Lambert W function [41], defined as the solution to $x = W\left(x\right)\exp\left[W\left(x\right)\right]$. The Lambert W function can be calculated numerically with existing code such as in Matlab, Scipy, and Mathematica. When a precoded function is not available, approximate functions using ubiquitous closed-form expressions can be used. The

approximation in [17] has a maximum error of 0.196 %, but it is tedious to input and prone to human input error. 3.B uses blending techniques to arrive to a much simpler expressions, albeit with a larger error of 5.9 %.

Blending in this case is performed using Equation 3.104 with $n = -1$ and applying the weight factor to the Regime IV asymptotics (neither of both asymptotics obeys power law), resulting in:

$$\widehat{x}_{\mathrm{f}}^{*}(\mathrm{Ro}) = \frac{1}{4W^{-1}(2\pi\mathrm{Ro}^2) + \frac{1}{2}\exp(\gamma + \frac{1}{\mathrm{Ro}} + a\mathrm{Ro}^b)} \tag{3.34}$$

where the optimal blending parameters are $a = 1.548, b = 1.389$, with a blending error smaller than 7.3%. The asymptotic behaviors cross at $\mathrm{Ro} = 0.6819$ and have an error below 10 % for $\mathrm{Ro} > 1.246$ or $\mathrm{Ro} < 0.2653$. If blending had been performed using Equation 3.104 with modification on asymptotic for Regime III, the error would have been larger: 30% instead of 7.3%.

The blending Equation 3.34 generates the following correction factors for asymptotics Equation 3.32 and Equation 3.33:

$$f_{x_{\mathrm{f_{III}}}}(\mathrm{Ro}) = \left[1 + \frac{1}{8}W\left(2\pi\mathrm{Ro}^2\right)\exp\left(\gamma + \frac{1}{\mathrm{Ro}} + a\mathrm{Ro}^b\right)\right]^{-1} \quad \text{for Regime III} \tag{3.35}$$

$$f_{x_{\mathrm{f_{IV}}}}(\mathrm{Ro}) = \left[\frac{8\exp\left(-\gamma - \frac{1}{\mathrm{Ro}}\right)}{W\left(2\pi\mathrm{Ro}^2\right)} + \exp\left(a\mathrm{Ro}^b\right)\right]^{-1} \quad \text{for Regime IV} \tag{3.36}$$

The corresponding engineering expressions with units are obtained by substituting Equation 3.4 into Equation 3.32 and Equation 3.33, resulting in:

$$\widehat{x}_{\mathrm{f}}^{+} = \widehat{x}_{\mathrm{f_{III}}}\, f_{x_{\mathrm{f_{III}}}}(\mathrm{Ro}) = \frac{\alpha}{2U}W\left(2\pi\mathrm{Ro}^2\right)\, f_{x_{\mathrm{f_{III}}}}(\mathrm{Ro}) \quad \text{for Regime III} \tag{3.37}$$

$$\widehat{x}_{\mathrm{f}}^{+} = \widehat{x}_{\mathrm{f_{IV}}}\, f_{x_{\mathrm{f_{IV}}}}(\mathrm{Ro}) = \frac{4\alpha}{U}\exp\left(-\gamma - \frac{1}{\mathrm{Ro}}\right)\, f_{x_{\mathrm{f_{IV}}}}(\mathrm{Ro}) \quad \text{for Regime IV} \tag{3.38}$$

3.8 Centerline heating rate $\dot{T}_{\mathrm{f}}$

The centerline heating rate, $\dot{T}_{\mathrm{f}}$, is relevant to understand phase transformations and phase changes in thermal processes. The derivations for $\dot{T}_{\mathrm{f}}$ follow the same path as

those for $\dot{T}_{\mathrm{b}}$, also involving Equation 3.24. Asymptotic analysis of Equation 3.2 yields:

$$\widehat{\dot{T}}^{*}_{\mathrm{f_{III}}}(\mathrm{Ro}) = \frac{2}{\mathrm{Ro}} \qquad \text{for Regime III} \tag{3.39}$$

$$\widehat{\dot{T}}^{*}_{\mathrm{f_{IV}}}(\mathrm{Ro}) = \frac{1}{2}\exp\left(\gamma + \frac{1}{\mathrm{Ro}}\right) \qquad \text{for Regime IV} \tag{3.40}$$

Blending for the heating rate $\dot{T}^{*}_{\mathrm{f}}$ is performed using Equation 3.113 with $n = -1$, resulting in:

$$\widehat{\dot{T}}^{*+}_{\mathrm{f}} = \frac{\exp\left(1/\mathrm{Ro}\right)}{\frac{1}{2}\mathrm{Ro} + 2\exp\left(-\gamma\right) + a\mathrm{Ro}^{b}} \tag{3.41}$$

where the optimal blending parameters are $a = -0.6618, b = 0.5055$, with a blending error smaller than 16%. The asymptotic behaviors cross at $\mathrm{Ro} = 3.440$ and have an error below 10 % for $\mathrm{Ro} > 175.6$ or $\mathrm{Ro} < 0.03730$. If blending had been performed using Equation 3.104, the error would have been larger: 36% instead of 16%. The blending Equation 3.41 generates the following correction factors for asymptotics Equation 3.39 and Equation 3.40:

$$f_{\dot{T}_{\mathrm{f_{III}}}}(\mathrm{Ro}) = \frac{\exp(1/\mathrm{Ro})}{1 + 4\mathrm{Ro}^{-1}\exp\left(-\gamma\right) + 2a\mathrm{Ro}^{b-1}} \qquad \text{for Regime III} \tag{3.42}$$

$$f_{\dot{T}_{\mathrm{f_{IV}}}}(\mathrm{Ro}) = \frac{1}{1 + \frac{1}{4}\exp\left(\gamma\right)\mathrm{Ro} + \frac{a}{2}\exp\left(\gamma\right)\mathrm{Ro}^{b}} \qquad \text{for Regime IV} \tag{3.43}$$

The corresponding engineering expressions with units are obtained by substituting Equation 3.3 into Equation 3.39 and Equation 3.40, resulting in:

$$\widehat{\dot{T}}^{+}_{\mathrm{f}} = \widehat{\dot{T}}_{\mathrm{f_{III}}}\, f_{x_{\mathrm{f_{III}}}}(\mathrm{Ro}) = \frac{U^2\left(T_{\mathrm{c}} - T_0\right)}{\alpha}\, f_{x_{\mathrm{f_{III}}}}(\mathrm{Ro}) \qquad \text{for Regime III} \tag{3.44}$$

$$\widehat{\dot{T}}^{+}_{\mathrm{f}} = \widehat{\dot{T}}_{\mathrm{f_{IV}}}\, f_{x_{\mathrm{f_{IV}}}}(\mathrm{Ro}) = \frac{U^2 q}{8\pi\alpha d k}\exp\left(\gamma + \frac{1}{\mathrm{Ro}}\right) f_{x_{\mathrm{f_{IV}}}}(\mathrm{Ro}) \qquad \text{for Regime IV} \tag{3.45}$$

3.9 Maximum temperature $T_{\mathbf{max}}$

The maximum temperature of a point at given y is an indication of possible thermal effects that are desired or should be avoided. In contrast with all previous characteristic values that depended on the Rosenthal number, in this case, dependence is on position and is the reverse of isotherm half-width $y^{*}_{\mathrm{max}}(\mathrm{Ro})$ studied in [130].

Asymptotic analysis of Equation 3.2 result in the asymptotic expressions of maximum temperature for Regime III and Regime IV:

$$\widehat{T}^*_{\max_{\mathrm{III}}}(y^*_{\mathrm{c}}) = \sqrt{\frac{\pi}{2\mathrm{e}}}\frac{1}{y^*_{\mathrm{c}}} \qquad \text{for Regime III} \tag{3.46}$$

$$\widehat{T}^*_{\max_{\mathrm{IV}}}(y^*_{\mathrm{c}}) = \ln\left(\frac{1}{y^*_{\mathrm{c}}}\right) \qquad \text{for Regime IV} \tag{3.47}$$

The asymptotic behavior of Equation 3.47 cannot be extended into Regime III to perform blending because it changes sign for $y^*_{\mathrm{c}} = 1$. 3.A describes the blending approach in this case, in which a modified function is proposed for the asymptotic of Regime IV:

$$\widehat{T}^{*\prime}_{\max_{\mathrm{IV}}}(y^*_{\mathrm{c}}) = \ln\left(\frac{1}{y^*_{\mathrm{c}}} + \frac{1}{a}\right) \qquad \text{modified for Regime IV} \tag{3.48}$$

which is valid for the whole domain when $a < 1$. The blending of Equation 3.46 and Equation 3.48 using equations 3.119 and 3.104 is:

$$\widehat{T^*}^{+}_{\max} = \left[\left(\sqrt{\frac{\pi}{2\mathrm{e}}}\frac{1}{y^*_{\mathrm{c}}}\right)^n + \ln\left(\frac{1}{y^*_{\mathrm{c}}} + \frac{1}{a}\right)^n\right]^{1/n} \tag{3.49}$$

where the optimal blending value is a =0.3350 and n =-2.013, with a blending error smaller than 2.1%. The asymptotic behaviors cross at Ro = 0.4645 and have an error below 10 % for Ro > 1.195 or Ro < 0.1632. The blending Equation 3.49 generates the following correction factors for asymptotics Equation 3.46 and Equation 3.47:

$$f_{T^*_{\max_{\mathrm{III}}}}(\mathrm{Ro}) = \left\{1 + \left[\sqrt{\frac{2\mathrm{e}}{\pi}}y^*_{\mathrm{c}}\ln\left(\frac{1}{y^*_{\mathrm{c}}} + \frac{1}{a}\right)\right]^n\right\}^{1/n} \qquad \text{for Regime III} \tag{3.50}$$

$$f_{T^*_{\max_{\mathrm{IV}}}}(\mathrm{Ro}) = \left\{1 + \left[\sqrt{\frac{\pi}{2\mathrm{e}}}\frac{1}{y^*_{\mathrm{c}}\ln\left(\frac{1}{y^*_{\mathrm{c}}} + \frac{1}{a}\right)}\right]^n\right\}^{1/n} \qquad \text{for Regime IV} \tag{3.51}$$

The corresponding dimensionless engineering expression for maximum temperature are generated by substituting Equation 3.3 and 3.5 into Equations 3.46 and 3.47,

resulting in:

$$\widehat{T}^{+}_{\max} = T_0 + \left(\widehat{T}_{\max_{\mathrm{III}}} - T_0\right) f_{T_{\max_{\mathrm{III}}}}(y^*_{\mathrm{c}}) = T_0 + \frac{\alpha q}{\sqrt{2\pi \mathrm{e}} U d k y_c} f_{T_{\max_{\mathrm{III}}}}(y^*_{\mathrm{c}}) \tag{3.52}$$

for Regime III

$$\widehat{T}^{+}_{\max} = T_0 + \left(\widehat{T}'_{\max_{\mathrm{IV}}} - T_0\right) f_{T_{\max_{\mathrm{IV}}}}(y^*_{\mathrm{c}}) = T_0 + \frac{q}{2\pi d k} \ln\left(\frac{2\alpha}{U y_c} + \frac{1}{a}\right) f_{T_{\max_{\mathrm{IV}}}}(y^*_{\mathrm{c}}) \tag{3.53}$$

for Regime IV

3.10 Gradient of maximum temperature $\mathrm{d}T_{\max}/\mathrm{d}y$

The maximum temperature experienced by each point in the plate depends on the distance to the center line y_{c}; therefore, there is a lateral gradient associated with the maximum temperature in the substrate. The gradient of maximum temperature is useful to build single-term predictions of thickness of areas affected by different temperatures such as the HAZ (heat affected zone) in welding. The dimensionless maximum temperature gradient can be calculated by the derivative of $T^*_{\max}(y^*) = T[x^*_{\max}(y^*), y^*]$, as shown in [207]:

$$\frac{\mathrm{d}T^*_{\max}}{\mathrm{d}y^*} = \left.\frac{\partial T^*}{\partial y^*}\right|_{x^*_{\max}, y^*_{\max}} \tag{3.54}$$

with the following asymptotics:

$$\left.\widehat{\frac{\mathrm{d}T^*_{\max}}{\mathrm{d}y^*}}\right|_{\mathrm{III}} (\mathrm{Ro}) = -\sqrt{\frac{2\mathrm{e}}{\pi}} \frac{1}{\mathrm{Ro}^2} \qquad \text{for Regime III} \tag{3.55}$$

$$\left.\widehat{\frac{\mathrm{d}T^*_{\max}}{\mathrm{d}y^*}}\right|_{\mathrm{IV}} (\mathrm{Ro}) = -\frac{1}{2} \exp\left(\gamma + \frac{1}{\mathrm{Ro}}\right) \qquad \text{for Regime IV} \tag{3.56}$$

Blending for the maximum temperature gradient $\mathrm{d}T^*_{\max}/\mathrm{d}y^*$ is performed using Equation 3.113 with $n = -1$, resulting in:

$$\widehat{\frac{\mathrm{d}T^*_{\max}}{\mathrm{d}y^*}}^{+} = -\frac{\exp(\frac{1}{\mathrm{Ro}})}{\sqrt{\frac{\pi}{2\mathrm{e}}}\mathrm{Ro}^2 + 2\exp(-\gamma) + a\mathrm{Ro}^b} \tag{3.57}$$

where the optimal blending parameters are $a = 0.2765, b = 1.629$, with a blending error smaller than 6.6%. The asymptotic behaviors cross at $\mathrm{Ro} = 0.3903$ and have an

error below 10 % for Ro > 0.4144 or Ro < 0.3158. If blending had been performed using Equation 3.104, the error would have been larger: 11% instead of 6.6%. The blending Equation 3.57 generates the following correction factors for asymptotics Equation 3.55 and Equation 3.56:

$$f_{\frac{\mathrm{d}T_{\max}}{\mathrm{d}y}|_{\mathrm{III}}}(\mathrm{Ro}) = \exp\left(\frac{1}{\mathrm{Ro}}\right)\left[1+\sqrt{\frac{8\mathrm{e}}{\pi}}\exp\left(-\gamma\right)\mathrm{Ro}^{-2}+a\sqrt{\frac{2\mathrm{e}}{\pi}}\mathrm{Ro}^{b-2}\right]^{-1} \qquad \text{for Regime III} \tag{3.58}$$

$$f_{\frac{\mathrm{d}T_{\max}}{\mathrm{d}y}|_{\mathrm{IV}}}(\mathrm{Ro}) = \left[1+\sqrt{\frac{\pi}{8\mathrm{e}}}\exp\left(\gamma\right)\mathrm{Ro}^{2}+\frac{1}{2}a\exp\left(\gamma\right)\mathrm{Ro}^{b}\right]^{-1} \qquad \text{for Regime IV} \tag{3.59}$$

The corresponding engineering expressions with units are:

$$\widehat{\frac{\mathrm{d}T_{\max}}{\mathrm{d}y}}^{+} = \left.\widehat{\frac{\mathrm{d}T_{\max}}{\mathrm{d}y}}\right|_{\mathrm{III}} f_{\frac{\mathrm{d}T_{\max}}{\mathrm{d}y}|_{\mathrm{III}}}(\mathrm{Ro}) = -\frac{\sqrt{2\pi\mathrm{e}}Udk\left(T_{\mathrm{c}}-T_0\right)^2}{\alpha q} f_{\frac{\mathrm{d}T_{\max}}{\mathrm{d}y}|_{\mathrm{III}}}(\mathrm{Ro}) \tag{3.60}$$

for Regime III

$$\widehat{\frac{\mathrm{d}T_{\max}}{\mathrm{d}y}}^{+} = \left.\widehat{\frac{\mathrm{d}T_{\max}}{\mathrm{d}y}}\right|_{\mathrm{IV}} f_{\frac{\mathrm{d}T_{\max}}{\mathrm{d}y}|_{\mathrm{IV}}}(\mathrm{Ro}) = -\frac{Uq}{8\pi\alpha dk}\exp\left(\gamma+\frac{1}{\mathrm{Ro}}\right) f_{\frac{\mathrm{d}T_{\max}}{\mathrm{d}y}|_{\mathrm{IV}}}(\mathrm{Ro}) \tag{3.61}$$

for Regime IV

3.11 Aspect ratio $\mathcal{AR}$

The aspect ratio of an isotherm is easily visualized in practice, and it is also a proxy for Ro because it depends only on Ro. The aspect ratio, $\mathcal{AR}$, is the ratio of length $(x_{\mathrm{f}}-x_{\mathrm{b}})$ to width $(2y_{\max})$ of an isotherm:

$$\mathcal{AR} = \frac{x_{\mathrm{f}}-x_{\mathrm{b}}}{2y_{\max}} = \frac{x_{\mathrm{f}}^*-x_{\mathrm{b}}^*}{2y_{\max}^*} \tag{3.62}$$

The asymptotic expressions for trailing length, leading length and isotherm half-width yield the following expressions for Regime III and Regime IV:

$$\widehat{\mathcal{AR}}_{\mathrm{III}}(\mathrm{Ro}) = \sqrt{\frac{\pi\mathrm{e}}{8}}\mathrm{Ro} \qquad \text{for Regime III} \tag{3.63}$$

$$\widehat{\mathcal{AR}}_{\mathrm{IV}}(\mathrm{Ro}) = 1 \qquad \text{for Regime IV} \tag{3.64}$$

The aspect ratio of 1 in Regime IV is consistent with the radical symmetry of the pure conduction problem. Blending in this case can be done using the traditional approach (Equation 3.99):

$$\widehat{\mathcal{R}}^{+} = \left[1 + \left(\sqrt{\frac{\pi \mathrm{e}}{8}}\mathrm{Ro}\right)^{n}\right]^{1/n} \tag{3.65}$$

with the optimal blending parameter $n = 1.972$ and an error always less than 3.3%. The crossover point for the asymptotes is $\mathrm{Ro} = 0.9679$. Asymptotic expressions result in an error less than 10 % for $\mathrm{Ro} > 2.095$ or $\mathrm{Ro} < 0.4471$. Equation 3.65 yields the following correction factors for Equation 3.63 and Equation 3.64:

$$f_{\mathcal{R}_{\mathrm{III}}}(\mathrm{Ro}) = \left[1 + \left(\sqrt{\frac{8}{\pi \mathrm{e}}}\frac{1}{\mathrm{Ro}}\right)^{n}\right]^{1/n} \qquad \text{for Regime III} \tag{3.66}$$

$$f_{\mathcal{R}_{\mathrm{IV}}}(\mathrm{Ro}) = \left[1 + \left(\sqrt{\frac{\pi \mathrm{e}}{8}}\mathrm{Ro}\right)^{n}\right]^{1/n} \qquad \text{for Regime IV} \tag{3.67}$$

The corresponding engineering expressions with units are obtained by substituting Equation 3.7 into Equations 3.63 and 3.64 to obtain:

$$\widehat{\mathcal{R}}^{+} = \widehat{\mathcal{R}}_{\mathrm{III}}\, f_{\mathcal{R}_{\mathrm{III}}}(\mathrm{Ro}) = \frac{\sqrt{2\mathrm{e}}q}{8\sqrt{\pi}dk\,(T_{\mathrm{c}} - T_0)}\, f_{\mathcal{R}_{\mathrm{III}}}(\mathrm{Ro}) \qquad \text{for Regime III} \tag{3.68}$$

$$\widehat{\mathcal{R}}^{+} = \widehat{\mathcal{R}}_{\mathrm{IV}}\, f_{\mathcal{R}_{\mathrm{IV}}}(\mathrm{Ro}) = 1 \cdot f_{\mathcal{R}_{\mathrm{IV}}}(\mathrm{Ro}) \qquad \text{for Regime IV} \tag{3.69}$$

3.12 Melting efficiency η_{m}

Melting efficiency, η_{m}, is a magnitude defined for fusion welding processes; despite the limitations of Rosenthal's equation, expressions for melting efficiency are qualitatively correct, and quantitatively not far from reality, as reviewed in [207].

The melting efficiency is the ratio of the energy used to reach liquidus temperature relative to the total energy deposited from the heat source. For 2D moving heat source problems, the energy per unit thickness needed to reach melting is $\rho c(T_{\mathrm{m}} - T_0)/d$, and the width of the fusion zone is $(2\, y_{\mathrm{max,m}})$, where subscript m indicates the isotherm of melting temperature. The melting efficiency can then be calculated as:

$$\eta_{\mathrm{m}} = \frac{\rho c U (T_{\mathrm{m}} - T_0)(2d\, y_{\mathrm{max,m}})}{q}$$

which can be rewritten using equations 3.5 and 3.7 as:

$$\eta_{\mathrm{m}} = \frac{2y^*_{\mathrm{max,m}}}{\pi \mathrm{Ro}_{\mathrm{m}}} \tag{3.70}$$

where Ro_{m} corresponds to melting temperature T_{m} (liquidus temperature). Replacing the asymptotic expressions for $\widehat{y}^*_{\mathrm{max}}$, Equation 3.70 yields the following dimensionless expressions:

$$\widehat{\eta}_{\mathrm{m_{III}}}(\mathrm{Ro}_{\mathrm{m}}) = \sqrt{\frac{2}{\pi \mathrm{e}}} \qquad \text{for Regime III} \tag{3.71}$$

$$\widehat{\eta}_{\mathrm{m_{IV}}}(\mathrm{Ro}_{\mathrm{m}}) = \frac{4}{\pi \mathrm{Ro}_{\mathrm{m}} \exp\left(\gamma + \frac{1}{\mathrm{Ro}_{\mathrm{m}}}\right)} \qquad \text{for Regime IV} \tag{3.72}$$

Because η_{m} is based on y^*_{max}, the correction factors for Regime III and Regime IV are the same as correction factors for y^*_{max}.

Equation 3.71 indicates that for 2D moving point heat source, the maximum of melting efficiency reaches 48.39 % for large Rosenthal numbers, but it never reaches 100 % because of the superheat inside the melt pool and the temperature gradients on substrate. Equation 3.72 indicates that for small Ro, heat conduction decreases the melting efficiency significantly.

Equations 3.71 and 3.72 suggest that the melting efficiency is always greater than zero, regardless of the power of the heat source; in practice, the finite size of the heat source implies that melting efficiency can be zero for diffuse heat sources [207].

The corresponding engineering expressions with units are obtained by substituting Equation 3.7 into Equations 3.71 and 3.72, obtaining:

$$\widehat{\eta}^+_{\mathrm{m}} = \widehat{\eta}_{\mathrm{m_{III}}}\, f_{\eta_{\mathrm{m_{III}}}}(\mathrm{Ro}_{\mathrm{m}}) = \sqrt{\frac{2}{\pi \mathrm{e}}}\, f_{y_{\mathrm{max_{III}}}}(\mathrm{Ro}_{\mathrm{m}}) \qquad \text{for Regime III} \tag{3.73}$$

$$\widehat{\eta}^+_{\mathrm{m}} = \widehat{\eta}_{\mathrm{m_{IV}}}\, f_{\eta_{\mathrm{m_{IV}}}}(\mathrm{Ro}_{\mathrm{m}}) = \frac{8dk\,(T_{\mathrm{c}} - T_0)}{q \exp\left(\gamma + \frac{1}{\mathrm{Ro}_{\mathrm{m}}}\right)}\, f_{y_{\mathrm{max_{IV}}}}(\mathrm{Ro}_{\mathrm{m}}) \qquad \text{for Regime IV} \tag{3.74}$$

where $f_{y_{\mathrm{max_{III}}}}(\mathrm{Ro})$ and $f_{y_{\mathrm{max_{IV}}}}(\mathrm{Ro})$ are the correction factors for isotherm half-width calculated from [130].

3.13 Cooling time $t_{8/5}$

The characteristic value $t_{8/5}$ is a metric of cooling rate for steels. $t_{8/5}$ is the time a point at centerline takes to cool down from 800 °C to 500 °C, which is equivalent to the time it takes for the heat source travelling the difference of the trailing length of two temperatures $x_{\mathrm{b},800}$ and $x_{\mathrm{b},500}$; thus:

$$t_{8/5} = \left| \frac{x_{\mathrm{b},800} - x_{\mathrm{b},500}}{U} \right| \tag{3.75}$$

where $x_{\mathrm{b},800}$ and $x_{\mathrm{b},500}$ are rear lengths for 800 °C and 500 °C. Substituting Equation 3.20 and Equation 3.21 into Equation 3.75 gives:

$$\widehat{t_{8/5}}^{+}_{\mathrm{III}} = \frac{\alpha q^2}{4\pi U^2 k^2 d^2} \left[\frac{f_{x_{\mathrm{b_{III}}}}(\mathrm{Ro}_{500})}{(T_{500} - T_0)^2} - \frac{f_{x_{\mathrm{b_{III}}}}(\mathrm{Ro}_{800})}{(T_{800} - T_0)^2} \right] \tag{3.76}$$

for Regime III

$$\widehat{t_{8/5}}^{+}_{\mathrm{IV}} = \frac{4\alpha}{U^2 \exp(\gamma)} \left[\exp\left(-\frac{1}{\mathrm{Ro}_{500}}\right) f_{x_{\mathrm{b_{IV}}}}(\mathrm{Ro}_{500}) - \exp\left(-\frac{1}{\mathrm{Ro}_{800}}\right) f_{x_{\mathrm{b_{IV}}}}(\mathrm{Ro}_{800}) \right] \tag{3.77}$$

for Regime IV

where Ro_{800} and Ro_{500} are the Rosenthal numbers for 800 °C and 500 °C, T_{800} and T_{500} represents 800 °C and 500 °C, $f_{x_{\mathrm{b_{III}}}}$ and $f_{x_{\mathrm{b_{IV}}}}$ are correction factors for trailing length of Regime III and IV. When $\mathrm{Ro}_{800} \gg 1$, in Equation 3.76, $f_{x_{\mathrm{b_{III}}}}(\mathrm{Ro}_{500}) = f_{x_{\mathrm{b_{III}}}}(\mathrm{Ro}_{800}) \approx 1$; when $\mathrm{Ro}_{500} \ll 1$, in Equation 3.77, $f_{x_{\mathrm{b_{IV}}}}(\mathrm{Ro}_{500}) = f_{x_{\mathrm{b_{IV}}}}(\mathrm{Ro}_{800}) \approx 1$.

The time $t_{8/5}$ can be approximated by using the cooling rate calculated above:

$$t_{8/5} \approx \frac{800°\mathrm{C} - 500°\mathrm{C}}{\left| \dot{T}_{\mathrm{b},\mathrm{i}} \right|} \tag{3.78}$$

where $\dot{T}_{\mathrm{b},\mathrm{i}}$ is the cooling rate of T_{i} between 500 °C and 800 °C. Replacing Equation 3.30 and Equation 3.31 into Equation 3.78 produces the following approximations:

$$\widehat{t_{8/5}}^{+}_{\mathrm{III}} \approx \frac{\alpha q^2 (T_{800} - T_{500})}{2\pi U^2 d^2 k^2 (T_{\mathrm{i}} - T_0)^3} f_{\dot{T}_{\mathrm{b_{III}}}}(\mathrm{Ro_i})^{-1} \qquad \text{for Regime III} \tag{3.79}$$

$$\widehat{t_{8/5}}^{+}_{\mathrm{IV}} \approx \frac{8\pi\alpha dk (T_{800} - T_{500})}{qU^2 \exp\left(\gamma + \frac{1}{\mathrm{Ro_i}}\right)} f_{\dot{T}_{\mathrm{b_{IV}}}}(\mathrm{Ro_i})^{-1} \qquad \text{for Regime IV} \tag{3.80}$$

where $\mathrm{Ro_i}$ is the Rosenthal number for intermediate temperature T_i, and $f_{\dot{T}_{\mathrm{b_{III}}}}(\mathrm{Ro_i})^{-1}$ and $f_{\dot{T}_{\mathrm{b_{IV}}}}(\mathrm{Ro_i})^{-1}$ are the reciprocal of correction factors for cooling rate.

There is an intermediate temperature T_i for which equations 3.76 and 3.77 are exactly the same as equations 3.79 and 3.80. The exact expression of that intermediate temperature is not practical, but following [207], it can be approximated as:

$$T_\mathrm{i} \approx T_0 + \sqrt{(T_{800} - T_0)\,(T_{500} - T_0)} \tag{3.81}$$

which for a 20 °C preheat corresponds to T_i ≈632°C.

3.14 Solidification time at centerline t_{sl}

The Rosenthal model can be extended to capture phase transformations when their presence causes second-order effects. At the trailing point x_b, the enthalpy loss rate can be estimated as:

$$\left.\frac{\mathrm{D}i}{\mathrm{D}t}\right|_{x_\mathrm{b}} = c\,\dot{T}_\mathrm{b} \tag{3.82}$$

where i is enthalpy per unit mass, and c is the effective specific heat assumed constant for all points in the domain, whether they are solid or liquid state.

When phase transformations have a small effect on the solution (as is the case of steels [197]), Rosenthal's formulation can be extended to estimate the phase transformation time by considering the rate of enthalpy loss. For solidification, the time t_sl could be calculated with the latent heat of solidification i_sl, which can be presented in dimensionless form:

$$\widehat{t}^{\,*}_{\mathrm{sl_{III}}} = \frac{\pi \mathrm{Ro_m^2}}{\mathrm{St}} \qquad \text{for Regime III} \tag{3.83}$$

$$\widehat{t}^{\,*}_{\mathrm{sl_{IV}}} = \frac{2}{\mathrm{Ro_m St}\exp\left(\gamma + \frac{1}{\mathrm{Ro_m}}\right)} \qquad \text{for Regime IV} \tag{3.84}$$

where $\mathrm{Ro_m}$ is Rosenthal number corresponding to melting temperature, t^*_sl is normal-

ized time and St is the Stefan number:

$$t^*_{\mathrm{sl}} = \frac{U^2 t_{\mathrm{sl}}}{2\alpha} \tag{3.85}$$

$$\mathrm{St} = \frac{c\,(T_{\mathrm{m}} - T_0)}{i_{\mathrm{sl}}} \tag{3.86}$$

where T_{m} ("melting temperature") is a temperature representative of the solidification, typically intermediate between liquidus and solidus.

The corresponding engineering expression with units can be expressed as:

$$\widehat{t}^{+}_{\mathrm{sl}_{\mathrm{III}}} = -\frac{i_{\mathrm{sl}}}{\mathrm{D}i/\mathrm{D}t|_{x_{\mathrm{b}}}} = \frac{\alpha q^2}{2\pi U^2 d^2 k^2 (T_{\mathrm{m}} - T_0)^3} \frac{i_{\mathrm{sl}}}{c}\, f_{\dot{T}_{\mathrm{b}_{\mathrm{III}}}}(\mathrm{Ro}_{\mathrm{m}})^{-1} \quad \text{for Regime III} \tag{3.87}$$

$$\widehat{t}^{+}_{\mathrm{sl}_{\mathrm{IV}}} = -\frac{i_{\mathrm{sl}}}{\mathrm{D}i/\mathrm{D}t|_{x_{\mathrm{b}}}} = \frac{8\pi\alpha d k}{qU^2 \exp\left(\gamma + \frac{1}{\mathrm{Ro}_{\mathrm{m}}}\right)} \frac{i_{\mathrm{sl}}}{c}\, f_{\dot{T}_{\mathrm{b}_{\mathrm{IV}}}}(\mathrm{Ro}_{\mathrm{m}})^{-1} \quad \text{for Regime IV} \tag{3.88}$$

where T_{m} ("melting temperature") is a temperature representative of the solidification, typically intermediate between liquidus and solidus, Ro_{m} is the corresponding Rosenthal number, $f_{\dot{T}_{\mathrm{b}_{\mathrm{III}}}}(\mathrm{Ro}_{\mathrm{m}})^{-1}$ and $f_{\dot{T}_{\mathrm{b}_{\mathrm{IV}}}}(\mathrm{Ro}_{\mathrm{m}})^{-1}$ are the reciprocal of correction factors for cooling rate. Note the similarity of equations 3.87 and 3.88 with equations 3.79 and 3.80, which are equivalent if the factor i_{sl}/c, which has units of temperature, is expressed as a temperature variation.

The extension of Rosenthal model can be applied to other phase transformations, for example austenite decomposition.

3.15 Thickness of the heat affected zone Δy_{HAZ}

The heat affected zone (HAZ) is a central concept in welding and thermal cutting of metals. It is defined as the amount of material that experiences temperatures between the melting temperature T_{m} (typically solidus) and a temperature specific to the metal T_{HAZ} (typically $A_{\mathrm{c},1}$ in the case of carbon steels. The thickness of the HAZ is then defined as:

$$\Delta y_{\mathrm{HAZ}} = y_{\mathrm{max,HAZ}} - y_{\mathrm{max,m}} \tag{3.89}$$

where $y_{\max,\mathrm{HAZ}}$ is the half-width of the isotherm T_{HAZ} and $y_{\max,\mathrm{m}}$ is the half-width of the melting isotherm T_{m}. Substituting T_{HAZ} and T_{m} into blending results of isotherm half-width $y_{\max}$ [130] results in the following predictions for thickness of the HAZ:

$$\widehat{\Delta y}^{+}_{\mathrm{HAZ}} = \frac{\alpha q}{\sqrt{2\pi \mathrm{e}} U dk}\left[\frac{f_{y\max_{\mathrm{III}}}(\mathrm{Ro}_{\mathrm{HAZ}})}{T_{\mathrm{HAZ}}-T_0} - \frac{f_{y\max_{\mathrm{III}}}(\mathrm{Ro}_{\mathrm{m}})}{T_{\mathrm{m}}-T_0}\right] \qquad \text{for Regime III} \tag{3.90}$$

$$\widehat{\Delta y}^{+}_{\mathrm{HAZ}} = \frac{4\alpha}{\exp(\gamma)\, U}\left[\frac{f_{y\max_{\mathrm{IV}}}(\mathrm{Ro}_{\mathrm{HAZ}})}{\exp(1/\mathrm{Ro}_{\mathrm{HAZ}})} - \frac{f_{y\max_{\mathrm{IV}}}(\mathrm{Ro}_{\mathrm{m}})}{\exp(1/\mathrm{Ro}_{\mathrm{m}})}\right] \qquad \text{for Regime IV} \tag{3.91}$$

For a relatively thin HAZ, its thickness can be approximated using the lateral temperature gradient:

$$\widehat{\Delta y}^{+}_{\mathrm{HAZ}} \approx \frac{T_{\mathrm{m}}-T_{\mathrm{HAZ}}}{|\mathrm{d}T_{\max}/\mathrm{d}y|_{\mathrm{i}}} = \frac{\alpha q (T_{\mathrm{m}}-T_{\mathrm{HAZ}})}{\sqrt{2\pi \mathrm{e}} U k d (T_{\mathrm{i}}-T_0)^2} f_{\frac{dT_{\max}}{dy}|_{\mathrm{III}}}(\mathrm{Ro}_{\mathrm{i}})^{-1} \quad \text{for Regime III} \tag{3.92}$$

$$\widehat{\Delta y}^{+}_{\mathrm{HAZ}} \approx \frac{T_{\mathrm{m}}-T_{\mathrm{HAZ}}}{|\mathrm{d}T_{\max}/\mathrm{d}y|_{\mathrm{i}}} = \frac{8\pi\alpha dk (T_{\mathrm{m}}-T_{\mathrm{HAZ}})}{qU \exp\left(\gamma + \frac{1}{\mathrm{Ro}_{\mathrm{i}}}\right)} f_{\frac{dT_{\max}}{dy}|_{\mathrm{IV}}}(\mathrm{Ro}_{\mathrm{i}})^{-1} \quad \text{for Regime IV} \tag{3.93}$$

where $\mathrm{d}T_{\max}/\mathrm{d}y|_{\mathrm{i}}$ is the gradient of maximum temperature in a cross section, evaluated at a temperature T_{i} intermediate between T_{HAZ} and T_{m}, Ro_{i} is the corresponding Rosenthal number, and $f_{\frac{dT_{\max}}{dy}|_{\mathrm{III}}}(\mathrm{Ro}_{\mathrm{i}})^{-1}$ and $f_{\frac{dT_{\max}}{dy}|_{\mathrm{IV}}}(\mathrm{Ro}_{\mathrm{i}})^{-1}$ are the reciprocal of correction factors of maximum temperature gradient as in Equation 3.58 and Equation 3.59. The dimensionless counterpart of equations 3.92 and 3.93 is expressed as:

$$\frac{\widehat{\Delta y^*}_{\mathrm{HAZ}}}{T^*_{\mathrm{m}}-T^*_{\mathrm{HAZ}}} = \left(\frac{\mathrm{d}T^*_{\max,\mathrm{m}}}{\mathrm{d}y^*}\right)^{-1} \tag{3.94}$$

where the right hand member depends only on Ro, and can be estimated using Equation 3.57.

A good choice for intermediate temperature is:

$$T_{\mathrm{i}} = T_0 + \sqrt{(T_{\mathrm{m}}-T_0)\,(T_{\mathrm{HAZ}}-T_0)} \tag{3.95}$$

which makes equations 3.90 and 3.92 and equations 3.93 and 3.92 nearly equivalent. For the asymptotics of Regime III, Equation 3.95 is exact.

3.16 Effect of joint configuration

The 2D moving point heat source model has two symmetrical heat flow paths, in the direction of $+y$ and $-y$ with a heat intensity per unit thickness $q/(2d)$ for each side. This configuration could be extended to multiple paths of heat flow in thin plates, such as those illustrated in Figure 3.2.

For a joint configuration involving m half-panels of thickness $d_1, d_2, \ldots, d_m$, there are m paths of heat flow with independent heat inputs $q_1, q_2, \ldots, q_m$ such that:

$$q = \sum_{i=1}^{m} q_i \tag{3.96}$$

and each panel experiences its own heat intensity per unit thickness $q'_j = q_j/d_j$. Considered individually, each panel behaves exactly as if it was a symmetric thin plate with a heat intensity per unit thickness of:

$$q'_{\text{eff}_j} = \frac{2q_j}{d_j} \tag{3.97}$$

All formulae developed above will be applicable to each individual heat path by replacing q/d by q'_{eff_j}. When the heat intensity per unit thickness is the same for all panels, this generalization is exact; when not, the asymmetry can cause heat transfer from one plate to another, which is not captured by the symmetric 2D formulation used here, and this generalization is only approximate.

An example of application of generalized joint configuration is the building of high thin walls in additive manufacturing, shown in Figure 3.2(c). In this case, the path of heat flow is only one (m =1), and all the predictions of characteristic values apply exactly when using an effective heat intensity per unit thickness of $2q/d$. This can be interpreted also as considering an effective heat intensity $q_{\text{eff}} = 2q$ and the nominal wall thickness, or a nominal heat intensity q and an effective wall thickness $d_{\text{eff}} = d/2$. Another example is the case of a T-joint of members of equal thickness (m =3, Figure 3.2(e)), assuming the heat intensity q is divided equally in all three directions, the effective heat intensity per unit thickness in each direction would be

$(2/3)q/d$. This can be interpreted also as considering an effective heat intensity $q_{\text{eff}} = (2/3)q$ and the nominal thickness, or a nominal heat intensity q and an effective wall thickness $d_{\text{eff}} = (3/2)d$. These joints configurations are contemplated already in standards such as [192].

Typically, the same characteristic values (such as cooling rate) are desirable for all members of the joint. In this case, the generalization to m paths of heat flow is exact, and the heat intensity applied to each path of heat flow is proportional to the thickness of the path:

$$\frac{q_j}{q} = \frac{d_j}{\sum_{i=1}^{m} q_i} \tag{3.98}$$

where $j = 1, 2 \ldots m$ identifies each heat path. For example, for the dissimilar thickness butt joint of Figure 3.2(b), $d_2 = 1.5d_1$, resulting in $q_1 = qd_1/(d_1 + 1.5d_1) = 0.4q$ and $q_2 = q1.5d_1/(d_1 + 1.5d_1) = 0.6q$. In this case, the partition of heat for welding should be 40 % on the thinner side, and 60 % on the thicker side. The same approach can be applied to other joint configuration examples Figure 3.2(c) to 3.2(e). The practical implementation of partition of heat in welding is discussed in detail in [207].

3.17 Validation

The proposed predictive expressions are validated against available published data for cooling rate $\dot{T}_{\text{b}}$, weld pool length $(x_{\text{f}} - x_{\text{b}})$, maximum temperature ($T_{\max}$, away from the centerline), HAZ thickness (Δy_{HAZ}), and isotherm aspect ratio $\mathcal{R}$, shown in figures 3.3 to 3.7.

Experimental values were collected for various welding processes including surface hardening, Gas Tungsten Arc Welding (GTAW), Shielded Metal Arc Welding (SMAW), Submerged Arc Welding (SAW), Gas Metal Arc Welding (GMAW), under water wet welding, Laser Beam Welding (LBW) and Electron Beam Welding (EBW) for a wide range of materials including aluminum, titanium, carbon steel, stainless steel, ultra-high-strength steel and superalloys.

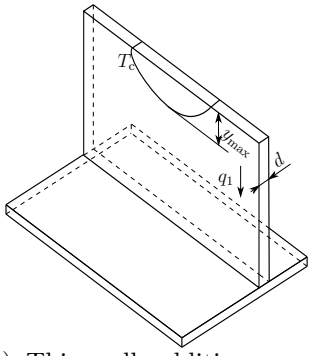

(a) Thin-wall additive manufacturing $q'_{\text{eff}} = \frac{2q}{d_1}$.

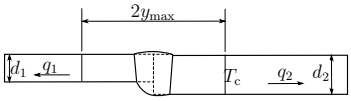

(b) Joining of different thickness plates $q'_{\text{eff}} = \frac{2q}{d_1+d_2}$.

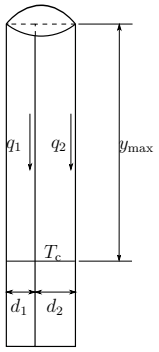

(c) Edge joint $q'_{\text{eff}} = \frac{2q}{d_1+d_2}$.

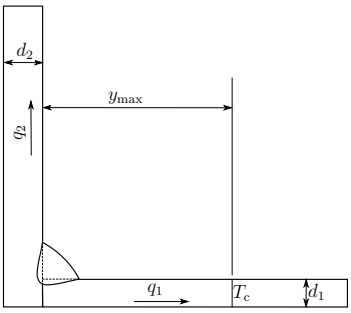

(d) Corner joint $q'_{\text{eff}} = \frac{2q}{d_1+d_2}$.

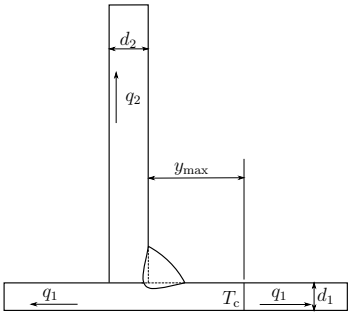

(e) Tee joint $q'_{\text{eff}} = \frac{2q}{2d_1+d_2}$.

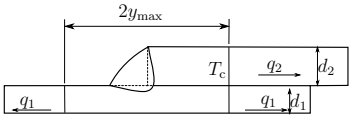

(f) Lap joint $q'_{\text{eff}} = \frac{2q}{2d_1+d_2}$.

Figure 3.2: Equivalent power source intensity (q'_{eff}) and energy distribution (q_i) for typical welding joint.

The thermal properties used for the calculation of predictive expressions were obtained from the original sources, other literature, or software (JMatPro v11). When temperature-dependent properties were available, effective values were obtained using the methodology introduced in [130]. Thermal efficiency, when not listed in the original sources, was assessed from the American Welding Society handbook [96]. The far temperature T_0 was either reported [99, 120, 142, 166, 184, 189] or assumed to be 20 °C. The raw data from literature and all values used to calculate the points are listed in the supporting online material.

Figure 3.3 compares the cooling rate predictions of Equation 3.27 with data for nine published sources. In the comparison, the thermal efficiency is estimated 0.8 for GMAW [63]. When cooling time $t_{8/5}$ was provided instead of cooling rate [12, 99, 120, 166, 182, 184, 189], the cooling rate at 632 °C was estimated as $300°\mathrm{C}/t_{8/5}$, with effective thermal properties calculated between 500 °C and 800 °C. The agreement of the predictions with eight sources shows a relatively narrow scatter and a slight underprediction (in absolute value) for large Ro numbers and a slight overprediction in absolute value for small Ro numbers. The ninth source ([63]) shows cooling rates much faster in absolute value than predicted. This discrepancy is because the data considered corresponds to underwater wet welding, where the very intense convection invalidates the hypothesis of negligible surface heat losses. Surface heat losses might also be the main source of the small systematic error observed. This effect is considered in current work to be published separately.

Figure 3.4 compares the weld pool length ($\widehat{x}^*_{\mathrm{f}} - \widehat{x}^*_{\mathrm{b}}$) predicted using Equation 3.17, against measurements for two different welding processes (GTAW in [109, 160], and LBW in [46]). The thermal efficiency for [160] is assumed as 0.5. The comparison shows a relatively narrow scatter and a no obvious bias.

Figure 3.5 compares maximum temperature away from the centerline predicted using Equation 3.49 against experiments from five sources from the literature. In this comparison, the thermal efficiency for EBW is estimated as 0.95, for LBW in

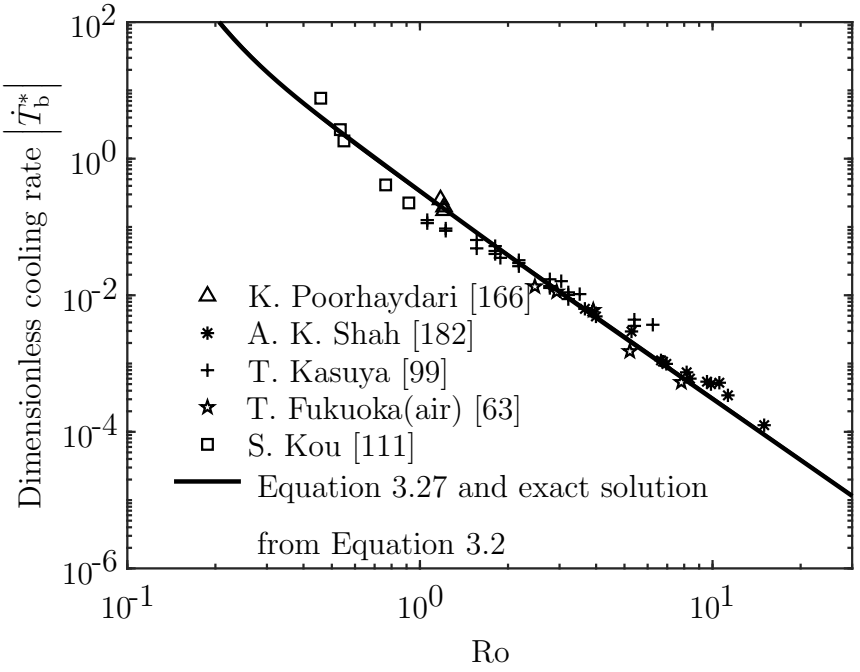

Figure 3.3: Validation of predictions for cooling rate using Equation 3.27. The curve corresponding to the exact solution (Equation 3.2) is undistinguishable within the thickness of the line.

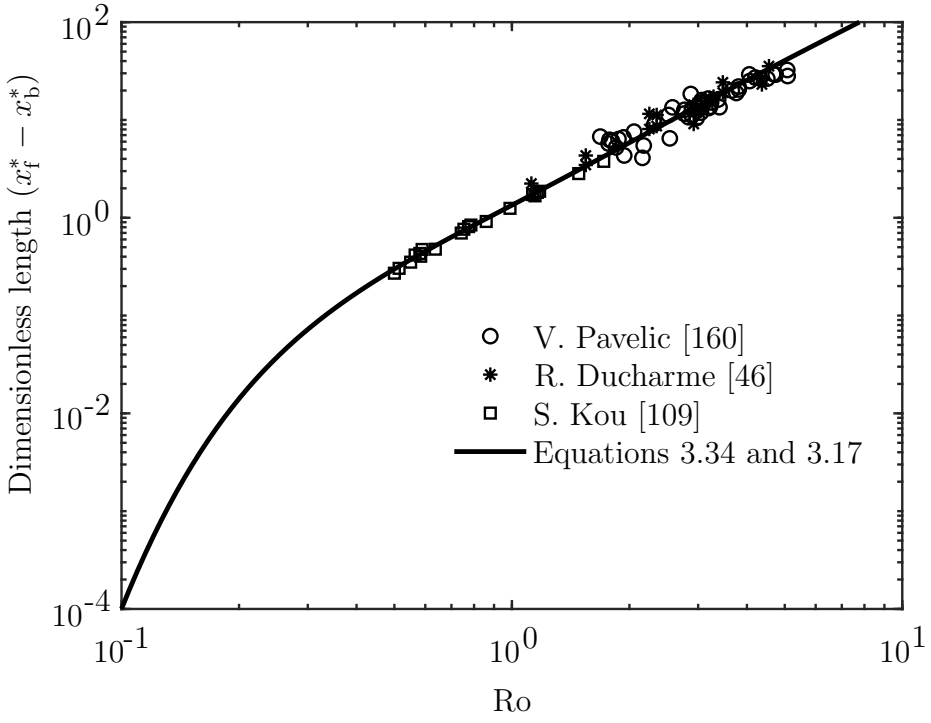

Figure 3.4: Validation of predictions of isotherm length $\widehat{l}^* = \widehat{x}_\mathrm{f}^* - \widehat{x}_\mathrm{b}^*$ using equations 3.34 and 3.17.

conduction mode as 0.15, for LBW keyhole mode as 0.9 [190]. The comparison shows a relatively narrow scatter and a consistent slight overprediction against most authors.

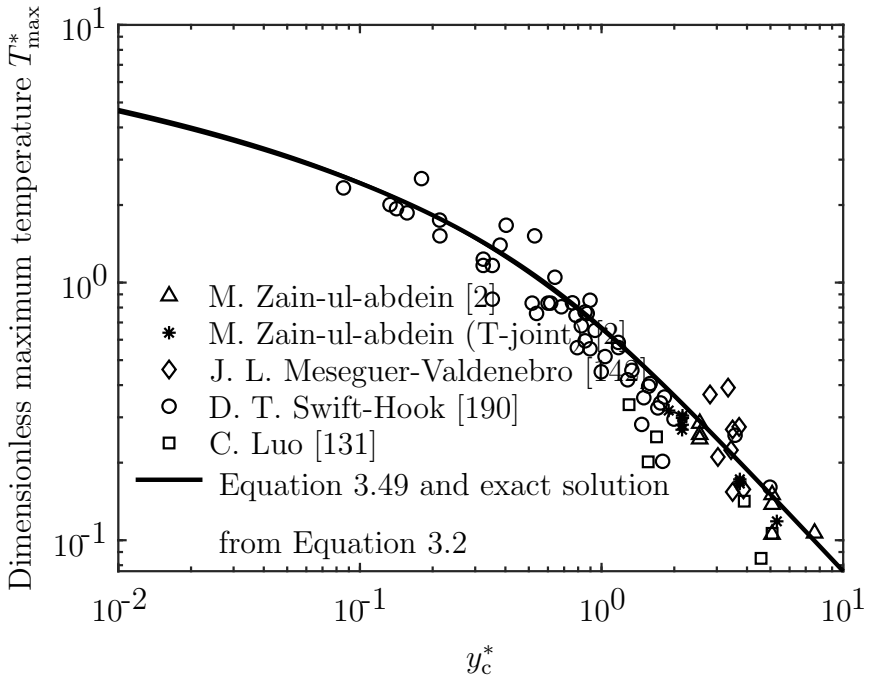

Figure 3.5: Validation of predictions of maximum temperature using Equation 3.49. The curve corresponding to the exact solution (Equation 3.2) is undistinguishable within the thickness of the line.

Figure 3.6 compares the thickness of heat affected zone predicted using Equation 3.92 against experiments from three sources from the literature. The thermal efficiency is estimated as 0.9 for LBW on ultra-high-strength steel [131] and 0.7 for LBW on Ti-6Al-4V [185]. The effective thermal properties are calculated between melting temperature T_{m} and heat affected zone temperature T_{HAZ}. T_{HAZ} for Ti-6Al-4V is listed as 995°C [143], and for ultra-high-strength steel, it is stated that it is below A_{c1} [131] , and is assumed as 500°C, which is when martensite tempering accelerates greatly [42].

Figure 3.7 compares the weld pool aspect ratio predicted using Equation 3.65 against three sources from the literature. The shape of weld pool was measured from

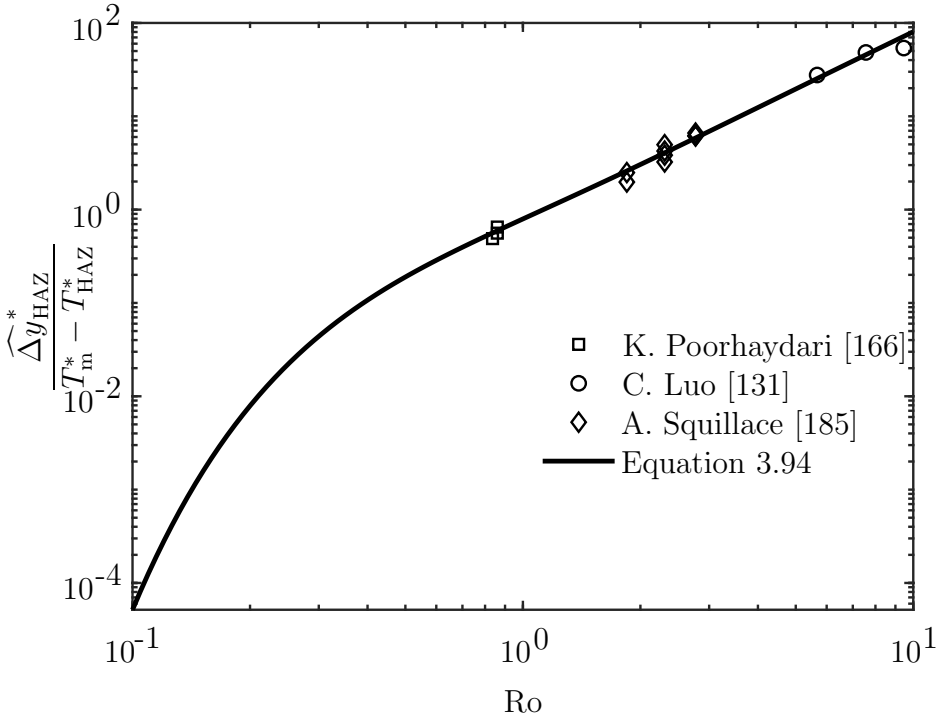

Figure 3.6: Validation of predictions of heat affected zone half-width using Equation 3.94.

optical images for [46, 204] and from simulations for [109]. The comparison shows a relatively narrow scatter and slight systematic error of underprediction.

3.18 Discussion

The formulae in closed form for a 2D moving heat source are novel. They are different from previous research in that the intermediate regime can now be calculated with explicit expressions. A single dimensionless group is identified that determines all characteristic values. This dimensionless group is defined as the Rosenthal number for most of the characteristic value except for maximum temperature (y_c^*) that is proposed by Fuerschbach and Knorovsky [61] based on experiments, but had not been widely adopted by the heat transfer or welding communities. This approach is also consistent with [207], in which the Rykalin number is used to generalize 3D moving heat sources. The characteristic values can be calculated with the proposed

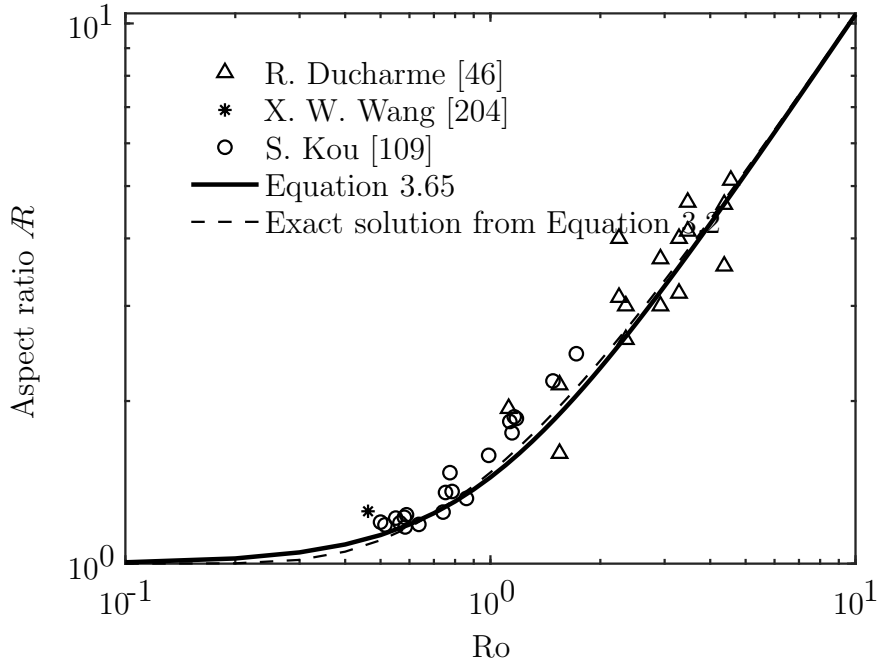

Figure 3.7: Validation of predictions of isotherm aspect ratio using Equation 3.65.

formulae using ubiquitous means such as calculators or spreadsheets.

The engineering expressions are based on the equation of heat diffusion, are simple to use and general to a wide range of processes and materials, and are within 8 % of the exact analytical solutions with the only exception of heating rate (16 % maximum error against exact solution). Comparisons of the expressions proposed against experiments or simulations show relatively low scatter and systematic error comparable with the experimental error in welding experiments (random error in GTAW experiments were assessed to be of the order of ± 15 % [47]).

Aside from heating rate, for values of Ro larger than 10 or smaller than 0.1, the correction factors account for less than 10 % and can be omitted in most applications; the final expressions are very simple and practical. Many industrial applications, such as laser and electron beams operate at Rosenthal values consistently much larger than 10.

The accuracy of proposed expressions cannot exceed that of the original exact solu-

tion, which includes many simplifications to the physics and mathematics of moving heat source problem. Some of those limitations can be overcome in practical ways. The limitation of constant thermophysical properties can be addressed in a practical way by using effective values, such as those proposed in [130]. The limitation of a point heat source can be addressed with the consideration of distributed heat sources, which would add precision and physical meaning with a single extra parameter (dimensionless size of the heat source). For heating rate, the errors in the blending expressions are secondary to the errors incurred by neglecting the finite size of the heat source, this is because the front of the isotherm is very close to the origin. The limitation of considering only conduction can be addressed by accounting for the effect of fluid flow as in [169], which would add two dimensionless groups (Prandtl number and Marangoni number). The challenge to considering secondary phenomena is that blending must be extended to two or more dimensionless groups, which is beyond the capabilities of the techniques described in 3.A and is the focus of current research [135].

The asymptotic formulae and correction factors proposed also serve as accurate predictors of actual processes and their metallurgical implications, in a way similar, but more general and based on fundamentals than the predictions of [91] used in [181]. In these references, the correction factors to asymptotic solutions are developed empirically.

The engineering expressions developed also enhance engineering intuition and reflect quantitative effects of process parameters and their implications for the thermal history of the material involved. Although most validations were carried out for welding and additive manufacturing cases, the methodology (asymptotic analysis, blending and correction factors) and engineering expressions obtained can be applied to a number of processes and materials in different disciplines, since they capture the essence of the thermal problem based on fundamental equations, not ad-hoc treatment.

3.19 Conclusions

This work presents novel engineering expressions for 12 characteristic values of technological relevance in welding, additive manufacturing, and other processes involving a moving heat source. The characteristic values analyzed are: location of isotherm half-width, trailing length of an isotherm, cooling rate at a given temperature in the center line, leading length of an isotherm, heating rate at a given temperature in the center line, maximum temperature at a point away from the center line, lateral gradient of maximum temperature, aspect ratio of an isotherm, melting efficiency, cooling time from 800 °C to 500 °C, solidification time and heat affected zone thickness. The expressions associated with these characteristic values are listed in Table 3.2.

The findings of Table 3.2 can be extended to alternative joint configurations by replacing the intensity of the heat source $q' = q/d$ by q'_{eff} according to Equation 3.97.

As a general rule of thumb, for Ro < 0.1 or Ro > 10 except for heating rate, the asymptotic solutions alone yield an error below 8 % against analytical results for listed characteristic values.

The engineering expressions were validated against published data when it was available in the literature: length of isotherm (Figure 3.4), centerline cooling rate (Figure 3.3), maximum temperature (Figure 3.5), thickness of heat affected zone (Figure 3.6), and isotherm aspect ratio (Figure 3.7).

Acknowledgment

The authors wish to acknowledge funding support from the Natural Sciences and Engineering Research Council of Canada (NSERC). Student scholarships from the American Welding Society and the Canadian Welding Association Foundation were gratefully received.

References

[2] M. Zain-ul abdein, D. Nélias, J. F. Jullien, and D. Deloison, "Experimental investigation and finite element simulation of laser beam welding induced residual stresses and distortions in thin sheets of AA 6056-T4," *Materials Science and Engineering A*, vol. 527, no. 12, pp. 3025–3039, 2010.

[3] A. Acrivos, "On the solution of the convection equation in laminar boundary layer flows," *Chemical Engineering Science*, vol. 17, no. 6, pp. 457–465, 1962.

[4] A. Acrivos, "A rapid method for estimating the shear stress and the separation point in laminar incompressible boundary-layer flows," *Journal of the Aero/Space Sciences*, vol. 27, no. 4, pp. 314–315, 1960.

[12] H. J. Aval, A. Farzadi, S. Serajzadeh, and A. H. Kokabi, "Theoretical and experimental study of microstructures and weld pool geometry during GATW of 304 stainless steel," *International Journal of Advanced Manufacturing Technology*, vol. 42, no. 11-12, pp. 1043–1051, 2009.

[17] D. A. Barry, J. Parlange, L. Li, H. Prommer, C. J. Cunningham, and F. Stagnitti, "Analytical approximations for real values of the Lambert W function," *Mathematics and Computers in Simulation*, vol. 53, pp. 95–103, 2000.

[23] B. Buchmayr and J. S. Kirkaldy, "Modeling of the temperature field, transformation behavior, hardness and mechanical response of low alloy steels during cooling from the austenite region," *Journal of heat treating*, vol. 8, no. 2, pp. 127–136, 1990.

[25] V. H. Bulsara, Y. Ahn, S. Chandrasekar, and T. N. Farris, "Polishing and lapping temperatures," *Journal of Tribology*, vol. 119, no. 1, pp. 163–170, 1997.

[34] S. W. Churchill and R. Usagi, "A general expression for the correlation of rates of transfer and other phenomena," *AIChE Journal*, vol. 18, no. 6, pp. 1121–1128, 1972.

[38] S. W. Churchill and R. Usagi, "A standardized procedure for the production of correlations in the form of a common empirical equation," *Industrial & Engineering Chemistry Fundamentals*, vol. 13, no. 1, pp. 39–44, 1974.

[41] R. M. Corless, G. H. Gonnet, D. E. G. Hare, D. J. Jeffrey, and D. E. Knuth, "On the Lambert W function," *Advances in Computational Mathematics*, vol. 5, no. 1, pp. 329–359, 1996.

[42] L. Cretteur, "Welding and joining of advanced high strength steels (AHSS)," in, ser. Woodhead publishing series in welding and other joining technologies 85. Elsevier, 2015, ch. High-power beam welding of advanced high-strength steels (AHSS), pp. 93–119, ISBN: 978-0-85709-858-0.

[46] R. Ducharme, K. Williams, P. Kapadia, J. Dowden, B. Steen, and M. Glowacki, "The laser welding of thin metal sheets: An integrated keyhole and weld pool model with supporting experiments," *Journal of Physics D: Appllied Physics*, vol. 27, pp. 1619–1627, 1994.

[47] U. Duman, "Modeling of weld penetration in high productivity GTAW," Ph.D. Colorado School of Mines, 2009.

[48] J. N. DuPont and A. R. Marder, "Thermal efficiency of arc welding processes," *Welding Research Supplement*, vol. 74, no. 12, 406s–416s, 1995.

[51] R. P. Dutt and R. C. Brewer, "On the theoretical determination of the temperature field in orthogonal machining," *International Journal of Production Research*, vol. 4, no. 2, pp. 91–114, 1965.

[59] E. Friedman, "Thermomechanical analysis of the welding process using the finite element method," *Journal of Pressure Vessel Technology*, vol. 97, no. 3, pp. 206–213, 1975.

[61] P. W. Fuerschbach and G. A. Knorovsky, "A study of melting efficiency in plasma arc and gas tungsten arc welding," *Welding Research Supplement*, vol. 70, no. 11, pp. 287–297, 1991.

[63] T. Fukuoka and S. Fuku, "Analysis for cooling process of underwater welding–comparison with welding in air," *Bulletin of Marine Engineering Society in Japan*, vol. 22, no. 2, pp. 86–92, 1994.

[74] J. Goldak, A. Chakravarti, and M. Bibby, "A new finite element model for welding heat sources," *Metallurgical Transactions B*, vol. 15, no. 2, pp. 299–305, 1984.

[86] J. W. Hill, M. J. Lee, and I. J. Spalding, "Surface treatments by laser," *Optics & Laser Technology*, vol. 6, no. 6, pp. 276–278, 1974.

[87] A. Hintze Cesaro and P. F. Mendez, "Models to predict hardness in the HAZ," *Weld Magazine*, pp. 42–55, 2019.

[89] Z. B. Hou and R. Komanduri, "General solutions for stationary/moving plane heat source problems in manufacturing and tribology," *International Journal of Heat and Mass Transfer*, vol. 43, no. 10, pp. 1679–1698, 2000.

[91] M. Inagaki, H. Nakamura, and A. Okada, "Studies of cooling processes in the cases of welding with coated electrode and submerged arc welding," *Journal of the Japan Welding Society*, vol. 34, no. 10, pp. 1064–1075, 1965.

[94] J. C. Jaeger, "Moving sources of heat and the temperature of sliding contacts," in *Proceedings of the royal society of New South Wales*, vol. 76, 1942, pp. 203–224.

[96] C. L. Jenney and A. O'Brien, Eds., *Welding science and technology*, Ninth. American Welding Society (AWS), 2001, vol. 1, ISBN: 978-0-87171-657-6.

[99] T. Kasuya and N. Yurioka, "Prediction of welding thermal history by a comprehensive solution," *Welding Research Supplement*, vol. 72, no. 3, 107s–115s, 1993.

[102] K. Knothe and S. Liebelt, "Determination of temperatures for sliding contact with applications for wheel-rail systems," *Wear*, vol. 189, no. 1-2, pp. 91–99, 1995.

[103] F. Kolonits, "Analysis of the temperature of the rail/wheel contact surface using a half-space model and a moving heat source," *Proceedings of the Institution of Mechanical Engineers Part F: Journal of Rail and Rapid Transit*, vol. 230, no. 2, pp. 502–509, 2016.

[106] R. Komanduri and Z. B. Hou, "Thermal analysis of the laser surface transformation hardening process," *International Journal of Heat and Mass Transfer*, vol. 44, no. 15, pp. 2845–2862, 2001.

[107] R. Komanduri and Z. B. Hou, "Unified approach and interactive program for thermal analysis of various manufacturing processes with application to machining," *Machining Science and Technology*, vol. 13, no. 2, pp. 143–176, 2009.

[109] S. Kou, T. Kanevsky, and S. Fyfitch, "Welding thin plates of aluminum alloys–a quantitative heat-flow analysis," *Welding Research Supplement*, vol. 61, no. 6, 175s–181s, 1982.

[111] S. Kou and Y. Le, "Welding parameters and the grain structure of weld metal – A thermodynamic consideration," *Metallurgical Transactions A*, vol. 19, no. 4, pp. 1075–1082, 1988.

[120] V. N. Lazić, A. S. Sedmak, M. M. Živković, S. M. Aleksandrović, R. D. Čukić, R. D. Jovičić, and I. B. Ivanović, "Theoretical-experimental determining of cooling time ($t_8/5$) in hard facing of steels for forging dies," *Thermal Science*, vol. 14, no. 1, pp. 235–246, 2010.

[124] W.-B. Li, K. E. Easterling, and M. F. Ashby, "Laser transformation hardening of steel-II. hypereutectoid steels," *Acta Metallurgica*, vol. 34, no. 8, pp. 1533–1543, 1986.

[130] Y. Lu, Y. Wang, and P. F. Mendez, "Width of thermal features induced by a 2-D moving heat source," *International Journal of Heat and Mass Transfer*, vol. 156, p. 119 793, 2020.

[131] C. Luo, Y. Cao, Y. Zhao, L. Zhao, and J. Shan, "Fiber laser welding of 1700-MPa, ultrahigh-strength," *Welding Journal*, vol. 97, 214s–228s, 2018.

[132] S. Malkin, "Thermal aspects of grinding: Part 2 – surface temperatures and workpiece burn," *Journal of Engineering for Industry*, vol. 96, no. 4, pp. 1184–1191, 1974.

[135] P. F. Mendez, "Reduced order models for welding and solidification processes," in *Proceedings of the 15th Modelling of Casting, Welding and Advanced Solidification Processes Conference (MCWASP XV)*, IOP Conference series: Materials Science and Engineering, 2020.

[142] J. L. Meseguer-Valdenebro, J. Serna, A. Portoles, M. Estrems, V. Miguel, and E. Martínez-Conesa, "Experimental validation of a numerical method that predicts the size of the heat affected zone. optimization of the welding parameters by the Taguchi's method," *Transactions of the Indian Institute of Metals*, vol. 69, no. 3, pp. 783–791, 2016.

[143] K. C. Mills, *Recommended values of thermophysical properties for selected commercial alloys*. Woodhead Publishing Limited, 2002.

[157] M. N. Özisik, *Heat conduction*, Second. New York;Toronto: A Wiley-Interscience Publication, 1993.

[160] V. Pavelic, R. Tanbakuchi, O. A. Uyehara, and P. S. Myers, "Experimental and computed temperature histories in gas tungsten-arc welding of thin plates," *Welding Research Supplement*, vol. 48, pp. 295–305, 1969.

[166] K. Poorhaydari, B. M. Patchett, and D. G. Ivey, "Estimation of cooling rate in the welding of plates with intermediate thickness," *Welding Journal*, vol. 84, no. 10, 149s–155s, 2005.

[169] D. Rivas and S. Ostrach, "Scaling of low-prandtl-number thermocapillary flows," *International Journal of Heat and Mass Transfer*, vol. 35, no. 6, pp. 1469–1479, 1992.

[171] O. F. T. Roberts, "The theoretical scattering of smoke in a turbulent atmosphere," in *Proceedings of the Royal Society of London*, ser. Series A, Containing Papers of a Mathematical and Physical Character, vol. 104, Royal Society, 1923, pp. 640–654.

[173] W. M. Rohsenow, J. P. Hartnett, Y. I. Cho, *et al.*, *Handbook of heat transfer*, Third, W. M. Rohsenow, J. P. Hartnett, and Y. I. Cho, Eds., ser. McGraw-Hill handbooks. New York: McGraw-Hill, 1998.

[174] D. Rosenthal, "Etude théorique du régime thermique pendant la soudure à l'arc," *Congres National des Sciences Comptes Rendus Bruxelles*, vol. 2, pp. 1277–1292, 1935.

[175] D. Rosenthal, "The theory of moving sources of heat and its application to metal treatments," *Transactions of the A.S.M.E.*, vol. 68, pp. 849–866, 1946.

[176] D. Rosenthal and R. Schmerber, "Thermal study of arc welding," *Welding journal*, vol. 17, no. 4, pp. 2–8, 1938.

[179] N. N. Rykalin, *Calculation of heat flow in welding*. Mashgis, Moscow, Russia: Mashgis, 1951.

[181] P. Seyffarth, B. Meyer, and A. Scharff, *Grosser atlas schweiss-ztu-schaubilder*, ser. Fachbuchreihe Schweisstechnik. Düsseldorf: Deutscher Verlag für Schweisstechnik, 1992, ISBN: 9783871551277.

[182] A. K. Shah, S. D. Kulkarni, V. Gopinathan, and R. Krishnan, "Weld heat-affected zone in Ti-6AI-4V alloy Part l–computer simulation of the effect of weld variables on the thermal cycles in the HAZ," *Welding Research Supplement*, vol. 74, no. 9, pp. 297–304, 1995.

[184] S. Shen, I. N. A. Oguocha, and S. Yannacopoulos, "Effect of heat input on weld bead geometry of submerged arc welded ASTM A709 Grade 50 steel joints," *Journal of Materials Processing Technology*, vol. 212, no. 1, pp. 286–294, 2012.

[185] A. Squillace, U. Prisco, S. Ciliberto, and A. Astarita, "Effect of welding parameters on morphology and mechanical properties of Ti-6Al-4V laser beam welded butt joints," *Journal of Materials Processing Technology*, vol. 212, no. 2, pp. 427–436, 2012.

[189] L. E. Svensson, B. Gretoft, and H. K. D. H. Bhadeshia, "An analysis of cooling curves from the fusion zone of steel weld deposits," *Scandinavian Journal of Metallurgy*, vol. 15, pp. 97–103, 1986.

[190] D. T. Swift-Hook and A. E. F. Gick, "Penetration welding with lasers," *Welding Research Supplement*, vol. 52, no. 11, 492s–499s, 1973.

[192] Technical Committee CEN/TC 121 Welding, *Welding - recommendations for welding of metallic materials - Part 2 : Arc welding of ferritic steels*, Technical Committee CEN/TC 121 Welding, 2001.

[197] M. Ushio, T. Ishimura, F. Matsuda, and Y. Arata, "Theoretical calculation on shape of fusion boundary and temperature distribution around moving heat source (Report I)," *Transactions of JWRI*, vol. 6(1), no. 1, p1–p6, 1977.

[204] X. Wang and R. Li, "Intelligent modelling of back-side weld bead geometry using weld pool surface characteristic parameters," *Journal of Intelligent Manufacturing*, vol. 25, no. 6, pp. 1301–1313, Jan. 2014.

[207] Y. Wang, Y. Lu, and P. F. Mendez, "Scaling expressions of characteristic values for a moving point heat source in steady state on a semi-infinite solid," *International Journal of Heat and Mass Transfer*, vol. 135, pp. 1118–1129, 2019.

[212] P. S. Wei and W. H. Giedt, "Surface tension gradient-driven flow around an electron beam welding cavity," *Welding Journal*, vol. 64, no. 9, 251s–259s, 1985.

[215] H. A. Wilson, "On convection of heat," in *Proceedings of the Cambridge Philosophical Society*, vol. 12, 1904, pp. 406–423.

Table 3.2: Summary of characteristic values and correction factors.

Variable	Regime	Asymptotic	Correction factor	Parameter	Error(%)	Eq.
$y_{\max}$	III	$\frac{\alpha q}{\sqrt{2\pi \mathrm{e}} U dk(T_\mathrm{c}-T_0)}$	$\exp\left(-\frac{1}{\mathrm{Ro}}\right)\left\{1+\left[2\sqrt{\frac{2\mathrm{e}}{\pi}}\frac{1}{\exp(\gamma)\mathrm{Ro}}\right]^n\right\}^{1/n}$	$n=1.407$	6.8%	[130]
	IV	$\frac{4\alpha}{U}\exp\left(-\gamma-\frac{1}{\mathrm{Ro}}\right)$	$\left\{1+\left[\sqrt{\frac{\pi}{8\mathrm{e}}}\exp(\gamma)\,\mathrm{Ro}\right]^n\right\}^{1/n}$			[130]
$x_{\max}$	III	$-\frac{\alpha q^2}{4\mathrm{e}\pi U d^2 k^2 (T_\mathrm{c}-T_0)^2}$	$\exp\left(-\frac{2}{\mathrm{Ro}}\right)\left[1+\frac{8}{\pi\exp(2\gamma-1)\mathrm{Ro}^3}+\frac{2a\mathrm{e}}{\pi}\mathrm{Ro}^{b-2}\right]$	$a=1.427$	6.3%	3.13
	IV	$-\frac{16\pi\alpha dk(T_\mathrm{c}-T_0)}{Uq\exp(2\gamma+2/\mathrm{Ro})}$	$\left[1+\frac{\pi}{8}\exp(2\gamma-1)\mathrm{Ro}^3+\frac{a}{4}\exp(2\gamma)\,\mathrm{Ro}^{b+1}\right]$	$b=1.077$		3.14
x_b	III	$-\frac{\alpha q^2}{4\pi U d^2 k^2 (T_\mathrm{c}-T_0)^2}$	$\exp\left(-\frac{1}{\mathrm{Ro}}\right)\left[1+\frac{4}{\pi\exp(\gamma)}\mathrm{Ro}^{-2}+\frac{2a}{\pi}\mathrm{Ro}^{b-2}\right]$	$a=0.7659$	6.8%	3.20
	IV	$-\frac{4\alpha}{U\exp\left(\gamma+\frac{1}{\mathrm{Ro}}\right)}$	$\left[1+\frac{\pi}{4}\exp(\gamma)\,\mathrm{Ro}^2+\frac{a}{2}\exp(\gamma)\,\mathrm{Ro}^b\right]$	$b=1.541$		3.21
$\dot{T}_\mathrm{b}$	III	$-\frac{2\pi U^2 d^2 k^2 (T_\mathrm{c}-T_0)^3}{\alpha q^2}$	$\exp\left(\frac{1}{\mathrm{Ro}}\right)\left[1+\frac{2}{\pi}\exp(-\gamma)\,\mathrm{Ro}^{-3}+a\mathrm{Ro}^{-b-3}\right]^{-1}$	$a=3.839$	5.8%	3.30
	IV	$-\frac{U^2 q}{8\pi\alpha dk}\exp\left(\gamma+\frac{1}{\mathrm{Ro}}\right)$	$\left[1+\frac{1}{2}\pi\exp(\gamma)\,\mathrm{Ro}^3+\frac{1}{2}a\exp(\gamma)\,\mathrm{Ro}^{-b}\right]^{-1}$	$b=-2.108$		3.31
x_f	III	$\frac{\alpha}{2U}W\left(2\pi\mathrm{Ro}^2\right)$	$\left[1+\frac{1}{8}W\left(2\pi\mathrm{Ro}^2\right)\exp\left(\gamma+\frac{1}{\mathrm{Ro}}+a\mathrm{Ro}^b\right)\right]^{-1}$	$a=1.548$	7.3%	3.37
	IV	$\frac{4\alpha}{U}\exp\left(-\gamma-\frac{1}{\mathrm{Ro}}\right)$	$\left[\frac{8\exp\left(-\gamma-\frac{1}{\mathrm{Ro}}\right)}{W\left(2\pi\mathrm{Ro}^2\right)}+\exp\left(a\mathrm{Ro}^b\right)\right]^{-1}$	$b=1.389$		3.38
$\dot{T}_\mathrm{f}$	III	$\frac{U^2(T_\mathrm{c}-T_0)}{\alpha}$	$\frac{\exp(1/\mathrm{Ro})}{1+4\mathrm{Ro}^{-1}\exp(-\gamma)+2a\mathrm{Ro}^{b-1}}$	$a=-0.6618$	16%	3.44
	IV	$\frac{U^2 q}{8\pi\alpha dk}\exp\left(\gamma+\frac{1}{\mathrm{Ro}}\right)$	$\frac{1}{1+\frac{1}{4}\exp(\gamma)\mathrm{Ro}+\frac{a}{2}\exp(\gamma)\mathrm{Ro}^b}$	$b=0.5055$		3.45
$T_{\max}-T_0$	III	$\frac{\alpha q}{\sqrt{2\pi \mathrm{e}} U dk y_\mathrm{c}}$	$\left\{1+\left[\sqrt{\frac{2\mathrm{e}}{\pi}}y_\mathrm{c}^*\ln\left(\frac{1}{y_\mathrm{c}^*}+\frac{1}{a}\right)\right]^n\right\}^{1/n}$	$a=0.3350$	2.1%	3.52
	IV	$\frac{q}{2\pi dk}\ln\left(\frac{2\alpha}{Uy_\mathrm{c}}+\frac{1}{a}\right)$	$\left\{1+\left[\sqrt{\frac{\pi}{2\mathrm{e}}}\frac{1}{y_\mathrm{c}^*\ln\left(\frac{1}{y_\mathrm{c}^*}+\frac{1}{a}\right)}\right]^n\right\}^{1/n}$	$n=-2.013$		3.53
$dT_{\max}/dy$	III	$-\frac{\sqrt{2\pi \mathrm{e}} U dk(T_\mathrm{c}-T_0)^2}{\alpha q}$	$\exp\left(\frac{1}{\mathrm{Ro}}\right)\left[1+\sqrt{\frac{8\mathrm{e}}{\pi}}\exp(-\gamma)\mathrm{Ro}^{-2}+a\sqrt{\frac{2\mathrm{e}}{\pi}}\mathrm{Ro}^{b-2}\right]^{-1}$	$a=0.2765$	6.6%	3.60
	IV	$-\frac{Uq}{8\pi\alpha dk}\exp\left(\gamma+\frac{1}{\mathrm{Ro}}\right)$	$\left[1+\sqrt{\frac{\pi}{8\mathrm{e}}}\exp(\gamma)\,\mathrm{Ro}^2+\frac{1}{2}a\exp(\gamma)\,\mathrm{Ro}^b\right]^{-1}$	$b=1.629$		3.61
$\mathcal{R}$	III	$\frac{\sqrt{2\mathrm{e}}q}{8\sqrt{\pi}dk(T_\mathrm{c}-T_0)}$	$\left[1+\left(\sqrt{\frac{8}{\pi\mathrm{e}}}\frac{1}{\mathrm{Ro}}\right)^n\right]^{1/n}$	$n=1.972$	3.3%	3.68
	IV	1	$\left[1+\left(\sqrt{\frac{\pi\mathrm{e}}{8}}\mathrm{Ro}\right)^n\right]^{1/n}$			3.69
η_m	III	$\sqrt{\frac{2}{\pi\mathrm{e}}}$	$\exp\left(-\frac{1}{\mathrm{Ro_m}}\right)\left\{1+\left[2\sqrt{\frac{2\mathrm{e}}{\pi}}\frac{1}{\exp(\gamma)\mathrm{Ro_m}}\right]^n\right\}^{1/n}$	$n=1.407$	6.8%	3.73
	IV	$\frac{8dk(T_\mathrm{c}-T_0)}{q\exp\left(\gamma+\frac{1}{\mathrm{Ro_m}}\right)}$	$\left\{1+\left[\sqrt{\frac{\pi}{8\mathrm{e}}}\exp(\gamma)\,\mathrm{Ro_m}\right]^n\right\}^{1/n}$			3.74
t_sl	III	$\frac{\alpha q^2}{2\pi U^2 d^2 k^2 (T_\mathrm{m}-T_0)^3}\frac{i_\mathrm{sl}}{c}$	$\exp\left(-\frac{1}{\mathrm{Ro_m}}\right)\left[1+\frac{2}{\pi}\exp(-\gamma)\,{\mathrm{Ro_m}}^{-3}+a{\mathrm{Ro_m}}^{b-3}\right]$	$a=3.839$		3.87
	IV	$\frac{8\pi\alpha dk}{qU^2\exp\left(\gamma+\frac{1}{\mathrm{Ro_m}}\right)}\frac{i_\mathrm{sl}}{c}$	$\left[1+\frac{1}{2}\pi\exp(\gamma)\,{\mathrm{Ro_m}}^3+\frac{1}{2}a\exp(\gamma)\,{\mathrm{Ro_m}}^b\right]$	$b=-2.108$		3.88
$t_{8/5}$	III	$\frac{\alpha q^2}{4\pi U^2 k^2 d^2}\left[\frac{f_{x_{\mathrm{b_{III}}}}(\mathrm{Ro}_{500})}{(T_{500}-T_0)^2}-\frac{f_{x_{\mathrm{b_{III}}}}(\mathrm{Ro}_{800})}{(T_{800}-T_0)^2}\right]$				3.76
	IV	$\frac{4\alpha}{U^2\exp(\gamma)}\left[\exp\left(-\frac{1}{\mathrm{Ro}_{500}}\right)f_{x_{\mathrm{b_{IV}}}}(\mathrm{Ro}_{500})-\exp\left(-\frac{1}{\mathrm{Ro}_{800}}\right)f_{x_{\mathrm{b_{IV}}}}(\mathrm{Ro}_{800})\right]$				3.77
	III	$\frac{\alpha q^2(T_{800}-T_{500})}{2\pi U^2 d^2 k^2 (T_\mathrm{i}-T_0)^3}$	$\exp\left(-\frac{1}{\mathrm{Ro_i}}\right)\left[1+\frac{2}{\pi}\exp(-\gamma)\,{\mathrm{Ro_i}}^{-3}+a{\mathrm{Ro_i}}^{b-3}\right]$	$a=3.839$		3.79
	IV	$\frac{8\pi\alpha dk(T_{800}-T_{500})}{qU^2\exp\left(\gamma+\frac{1}{\mathrm{Ro_i}}\right)}$	$\left[1+\frac{1}{2}\pi\exp(\gamma)\,{\mathrm{Ro_i}}^3+\frac{1}{2}a\exp(\gamma)\,{\mathrm{Ro_i}}^b\right]$	$b=-2.108$		3.80
Δy_HAZ	III	$\frac{\alpha q}{\sqrt{2\pi \mathrm{e}} U dk}\left[\frac{f_{y_{\max_{\mathrm{III}}}}(\mathrm{Ro_{HAZ}})}{T_\mathrm{HAZ}-T_0}-\frac{f_{y_{\max_{\mathrm{III}}}}(\mathrm{Ro_m})}{T_\mathrm{m}-T_0}\right]$				3.90
	IV	$\frac{4\alpha}{\exp(\gamma)U}\left[\frac{f_{y_{\max_{\mathrm{IV}}}}(\mathrm{Ro_{HAZ}})}{\exp(1/\mathrm{Ro_{HAZ}})}-\frac{f_{y_{\max_{\mathrm{IV}}}}(\mathrm{Ro_m})}{\exp(1/\mathrm{Ro_m})}\right]$				3.91
	III	$\frac{\alpha q(T_\mathrm{m}-T_\mathrm{HAZ})}{\sqrt{2\pi \mathrm{e}} U kd(T_\mathrm{i}-T_0)^2}$	$\exp\left(-\frac{1}{\mathrm{Ro_i}}\right)\left[1+\sqrt{\frac{8\mathrm{e}}{\pi}}\exp(-\gamma){\mathrm{Ro_i}}^{-2}+a\sqrt{\frac{2\mathrm{e}}{\pi}}{\mathrm{Ro_i}}^{b-2}\right]$	$a=0.2765$		3.92
	IV	$\frac{8\pi\alpha dk(T_\mathrm{m}-T_\mathrm{HAZ})}{qU\exp\left(\gamma+\frac{1}{\mathrm{Ro_i}}\right)}$	$\left[1+\sqrt{\frac{\pi}{8\mathrm{e}}}\exp(\gamma)\,{\mathrm{Ro_i}}^2+\frac{1}{2}a\exp(\gamma)\,{\mathrm{Ro_i}}^b\right]$	$b=1.629$		3.93

Appendix 3.A Blending of asymptotic solutions

Blending is a methodology to achieve simple expressions for all conditions, based on the expressions for asymptotic regimes. It is based on the observation that almost always intermediate cases yield results that are based on combinations of asymptotic cases, for example. Blending has been explored in [3, 4] and generalized in [34, 38] for simpler cases. As an example of traditional blending, consider the two asymptotic behaviors of the dimensionless characteristic value $u_c^*(\Pi)$: $\widehat{u_{ci}^*}(\Pi)$, when $\Pi \to 0$, and $\widehat{u_{cj}^*}(\Pi)$, when $\Pi \to \infty$. When these asymptotic behaviors are monotonous in Π and cross only once, traditional blending yields:

$$\widehat{u_c^{*+}}(\Pi) = \left[\widehat{u_{ci}^*}^n(\Pi) + \widehat{u_{cj}^*}^n(\Pi)\right]^{1/n} \tag{3.99}$$

where $\widehat{u_c^{*+}}(\Pi)$ is the blending approximation of $u_c^*(\Pi)$ and is illustrated schematically in Figure 3.8(a) for the case of blending two power laws. In this methodology and all that follow, the general expressions used have the following corresponding concepts in the blending derivations of this paper when they are based on Ro:

$$\Pi = \text{Ro} \tag{3.100}$$

$$\text{Regime } i = \text{Regime IV} \tag{3.101}$$

$$\text{Regime } j = \text{Regime III} \tag{3.102}$$

Many asymptotic behaviors studied in this paper cannot be blended with the traditional approach described above, or yield larger errors than the novel alternatives developed here. In these paper, three extensions of traditional blending techniques were developed: for the case of monotonic functions that do not cross or are not power laws, for functions in which the error in traditional blending is too high, and for functions that change sign or are not defined over the whole domain.

Blending of monotonic functions that do not cross or are not power laws

Consider a modification of the previous example in which $\widehat{u^*_{\mathrm{c}i}}(\Pi)$ is not a power law, and it is possible that it does not cross $\widehat{u^*_{\mathrm{c}j}}(\Pi)$; in this case, it can be expressed as:

$$\widehat{u^*_{\mathrm{c}i}}(\Pi) = v_i^*(\Pi) p_i^*(\Pi) \tag{3.103}$$

where $p_i^*(\Pi)$ is a power law and $v_i^*(\Pi)$ is not, but $v_i^*(\Pi)$ is chosen such that $v_i^*(\Pi) \to 1$ in Regime j. In this case, the power law $\widehat{u^*_{\mathrm{c}j}}(\Pi)$ can be replaced by $v_i^*(\Pi)\widehat{u^*_{\mathrm{c}j}}(\Pi)$, with the same asymptotic behavior, and after taking v_i^* as a common factor, the blending involves two power laws that typically cross, and can be blended, for example, using the traditional approach:

$$\widehat{u_{\mathrm{c}}^{*+}}(\Pi) = v_i^*(\Pi) \left[{p_i^*}^n(\Pi) + \widehat{u^*_{\mathrm{c}j}}^n(\Pi) \right]^{1/n} \tag{3.104}$$

and the resulting correction factors are:

$$f_i(\Pi) = \left(1 + \frac{\widehat{u^*_{\mathrm{c}j}}(\Pi)}{p_i^*(\Pi)} \right) \tag{3.105}$$

$$f_j(\Pi) = v_i^*(\Pi) \left(1 + \frac{p_i^*(\Pi)}{\widehat{u^*_{\mathrm{c}j}}(\Pi)} \right) \tag{3.106}$$

This blending methodology is illustrated in Figure 3.8(b), and is applied, for example to the calculation of maximum isotherm half-width $y_{\max}$. The asymptotic behavior for $\widehat{{y^*}_{\max_{\mathrm{III}}}}(\mathrm{Ro})$ is a power law, while $\widehat{{y^*}_{\max_{\mathrm{IV}}}}(\mathrm{Ro})$ is not [130]. In this case:

$$\widehat{u^*_{\mathrm{c}i}}(\Pi) = 2\exp\left(\gamma - \mathrm{Ro}^{-1}\right) \tag{3.107}$$

$$\widehat{u^*_{\mathrm{c}j}}(\Pi) = \sqrt{\frac{\pi}{2\mathrm{e}}\mathrm{Ro}} \tag{3.108}$$

$$v_i^*(\Pi) = \exp\left(-\mathrm{Ro}^{-1}\right) \tag{3.109}$$

$$p_i^*(\Pi) = 2\exp(\gamma) \tag{3.110}$$

The blending of these two equations based on Equation 3.104 is:

$$\widehat{{y^*}^+_{\max}}(\mathrm{Ro}) = \exp\left(-\mathrm{Ro}^{-1}\right) \left\{ \left[2\exp\left(-\gamma\right)\right]^n + \left(\sqrt{\frac{\pi}{2\mathrm{e}}}\mathrm{Ro}\right)^n \right\}^{1/n} \tag{3.111}$$

from which the correction factors $f_{y_{\max_{\mathrm{III}}}}(\mathrm{Ro})$ and $f_{y_{\max_{\mathrm{IV}}}}(\mathrm{Ro})$ are derived.

Alternative blending of monotonic functions that cross

An effective novel approach can yield blending errors smaller than Equation 3.99, often when one or both asymptotic behaviors are not power laws:

$$\widehat{u_{\mathrm{c}}^*}^{+}(\Pi) = \left[\widehat{u_{\mathrm{c}i}^*}^{\pm 1}(\Pi) + \widehat{u_{\mathrm{c}j}^*}^{\pm 1}(\Pi) + a\Pi^{\pm b}\right]^{\pm 1} \tag{3.112}$$

where $a > 0$ and b are determined by optimization minimizing the maximum error over all values of Π. The value of 1 in the exponents could also be replaced by a third adjusting parameter c and $1/c$; however, fixing it to 1 reduces the complexity of the expression, and experience has shown that the two adjusting parameters a and b are enough to give acceptable errors. This approach requires the asymptotic behaviors to be monotonic and to cross one each other. When $\widehat{u_{\mathrm{c}i}^*}(\Pi)$ and $\widehat{u_{\mathrm{c}j}^*}(\Pi)$ are power laws (illustrated in Figure 3.8(c)), the exponent b in Equation 3.112 is intermediate between the exponent of the two power laws.

If the functions that do not cross or are not power laws, instead of the blending of Equation 3.104, this alternative approach would yield:

$$\widehat{u_{\mathrm{c}}^*}^{+}(\Pi) = v_i^*(\Pi)\left[\widehat{p^*}_i^{\pm 1}(\Pi) + \widehat{u_{\mathrm{c}j}^*}^{\pm 1}(\Pi) + a\Pi^{\pm b}\right]^{\pm 1} \tag{3.113}$$

This blending methodology is applied, for example, to the calculation of centerline cooling rate $\dot{T}_{\mathrm{b}}^*(\mathrm{Ro})$. The asymptotic behavior $\widehat{\dot{T}^*}_{\mathrm{b_{III}}}(\mathrm{Ro})$ is a power law (Equation 3.25), while $\widehat{\dot{T}^*}_{\mathrm{b_{IV}}}(\mathrm{Ro})$ is not (Equation 3.26). These two asymptotic behaviors do not cross; in this case:

$$\widehat{u_{\mathrm{c}i}^*}(\Pi) = \frac{1}{2}\exp\left(\gamma + \mathrm{Ro}^{-1}\right) \tag{3.114}$$

$$\widehat{u_{\mathrm{c}j}^*}(\Pi) = \frac{1}{\pi}\mathrm{Ro}^{-3} \tag{3.115}$$

$$v_i^*(\Pi) = \exp\left(\mathrm{Ro}^{-1}\right) \tag{3.116}$$

$$p_i^*(\Pi) = \frac{1}{2}\exp(\gamma) \tag{3.117}$$

$$\tag{3.118}$$

and Equation 3.112 with negative exponents yields a lower error than Equation 3.112, resulting in the blended expression of Equation 3.27.

Blending of functions that change sign or are not defined over the whole domain

Consider the case in which $\widehat{u^*_{\mathrm{c}i}}(\Pi)$ is not defined or changes sign for values of Π below or above a certain critical value Π_c, and $\widehat{u^*_{\mathrm{c}j}}(\Pi)$ is a power law. A new function $\widehat{v^*_{\mathrm{c}i}}(\Pi)$ can be defined as:

$$\widehat{v^*_{\mathrm{c}i}}(\Pi) = \widehat{u^*_{\mathrm{c}i}}\left[\left(\Pi^{\pm 1} + a^{\pm 1}\right)^{\pm 1}\right] \tag{3.119}$$

with values of a always positive, and in the range in which the domain is defined, and positive exponents when the problems with the domain are at small values of Π and negative exponents when they are at large values of Π. The value of a is adjusted by optimization; the value of 1 in the exponents was chosen for simplicity similarly to the previous blending extension discussed. For all values of a, the asymptotic behavior of $\widehat{v^*_{\mathrm{c}i}}(\Pi)$ is the same as $\widehat{u^*_{\mathrm{c}i}}(\Pi)$ in Regime i, and function $\widehat{v^*_{\mathrm{c}i}}(\Pi)$ can replace $\widehat{u^*_{\mathrm{c}i}}(\Pi)$ in any of the blending techniques described above. The correction factor is applied to $\widehat{v^*_{\mathrm{c}i}}(\Pi)$, not $\widehat{u^*_{\mathrm{c}i}}(\Pi)$.

This blending methodology is illustrated in Figure 3.8(d), and is applied, for example to the calculation of maximum temperature at a distance y_c from the centerline. The asymptotic behavior for $\widehat{T^*}_{\max_{\mathrm{III}}}(y^*_\mathrm{c})$ is a power law (Equation 3.46), while $\widehat{T^*}_{\max_{\mathrm{IV}}}(y^*_\mathrm{c})$ (Equation 3.47) involves a change in sign above $y^*_\mathrm{c} = 1$. In this case, the equivalent asymptotic behavior is obtained using the negative sign, resulting in:

$$\Pi = y^*_\mathrm{c} \tag{3.120}$$

$$\text{Regime } i = y^*_\mathrm{c} \to 0 \qquad \text{(Regime IV)} \tag{3.121}$$

$$\text{Regime } j = y^*_\mathrm{c} \to \infty \qquad \text{(Regime III)} \tag{3.122}$$

$$\widehat{u^*_{\mathrm{c}i}}(y^*_\mathrm{c}) = \ln\left(y^{*-1}_\mathrm{c}\right) \tag{3.123}$$

$$v^*_i(y^*_\mathrm{c}) = \ln\left(y^{*-1}_\mathrm{c} + a^{-1}\right) \tag{3.124}$$

which is blended with $\widehat{T^*}_{\max_{\text{III}}}(y_c^*)$ using Equation 3.99, resulting in the blended expression of Equation 3.49.

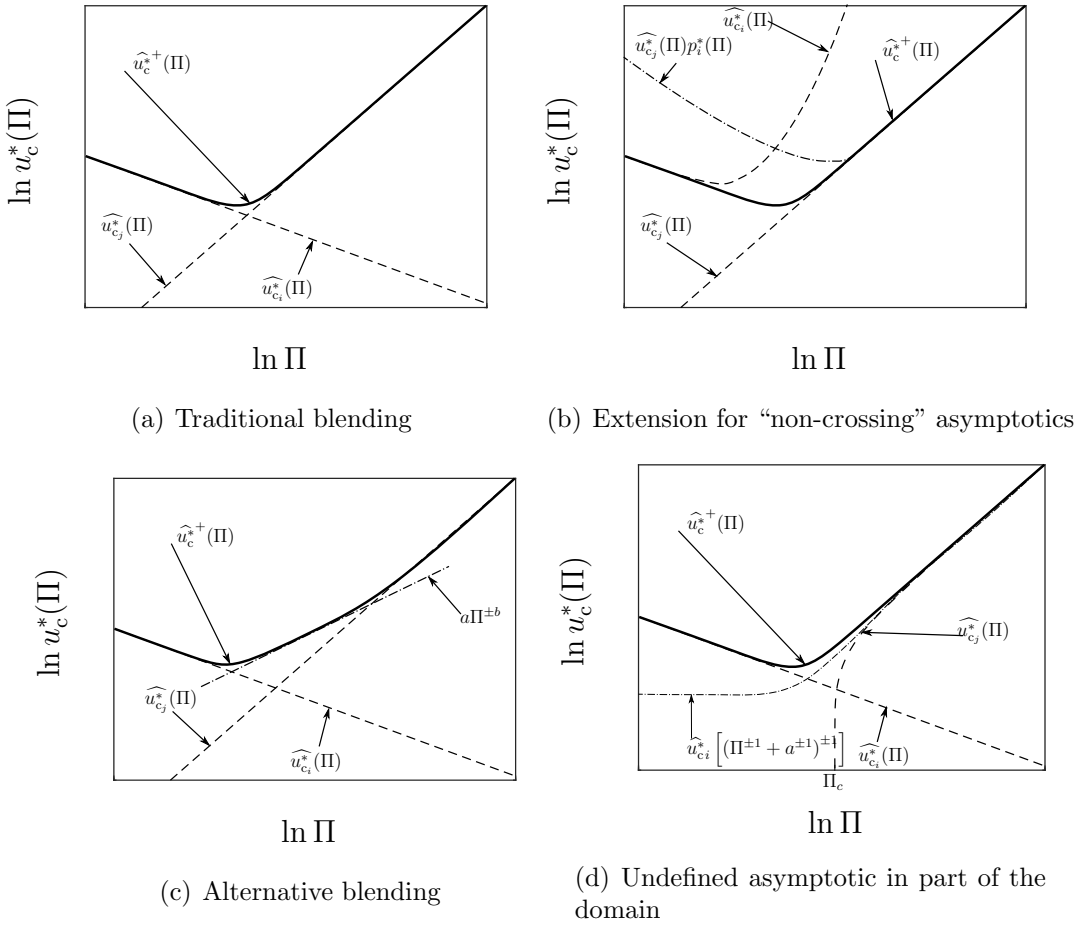

(a) Traditional blending

(b) Extension for "non-crossing" asymptotics

(c) Alternative blending

(d) Undefined asymptotic in part of the domain

Figure 3.8: Traditional blending and three extended methodologies.

Appendix 3.B Blending of Lambert W function

The Lambert W function $W(x)$ is the solution to:

$$W(x)\exp[W(x)] = x \tag{3.125}$$

The asymptotic expressions to Lambert W function, according to Equation 3.125, for large and small x are:

$$\widehat{W}_{\text{I}}(x) = \ln(x) \qquad \text{for large } x \tag{3.126}$$

$$\widehat{W}_{\text{II}}(x) = x \qquad \text{for small } x \tag{3.127}$$

Using equations 3.112 and 3.119 from the blending methods introduced above, the positive branch of the Lambert W function could be calculated approximately with:

$$\widehat{W}^{+}(x) = \left[x^{-1} + \ln(x+c)^{-1} + a\,x^{-b}\right]^{-1} \tag{3.128}$$

where $a = 0.08568$, $b = 0.1028$, $c = 2.586$, and the relative error is smaller than 5.9 % for the positive branch and all $x > 0$.

Chapter 4

Cooling rate in moving-heat-source manufacturing processes with intensive surface heat losses

4.1 Abstract

Closed-form engineering expressions for trailing length and cooling rate at a given temperature are developed based on a two dimensional moving point heat source model which also accounts for surface heat losses. Cooling rate is a dominant factor in determining material properties, and trailing length determines the needed reach of gas shielding in moving heat source problems such as welding and additive manufacturing. The consideration of surface heat losses enables the extension of the moving heat source analysis to complex, but technologically relevant problems such as underwater wet welding, in-service welding, additive manufacturing of thin walls, and combinations of thickness and low target temperatures where natural convection in air becomes relevant (e.g. analysis of residual stresses) for which closed-form predictive expressions do not exist. The novel expressions presented are generalized using two dimensionless numbers: the Rosenthal number, which captures the balance of conduction and advection, and a dimensionless surface heat loss coefficient which takes into account the effect of surface heat loss. These expressions consist of asymptotic expressions with rigorous correction factors for the intermediate cases. The

correction factors are developed for all possible combinations of Rosenthal number and dimensionless surface heat loss coefficient, yielding predictions with a maximum relative error less than 8 % compared to the exact analytical solution. The engineering expressions proposed are validated with data collected from published data for welding, hard facing and additive manufacturing on steel under water and air. These expressions are also applicable to moving heat sources in biological tissue that can be represented with the bioheat equation.

Table 4.1: Variables used in the paper with the units and description.

Variables	**Unit**	**Description**
c	$\mathrm{J\,kg^{-1}\,K^{-1}}$	Specific heat of the substrate
d	m	Thickness of the substrate
f, g	-	Correction factors
h	$\mathrm{W\,m^{-2}\,K^{-1}}$	Surface heat loss coefficient on top surface
h'	$\mathrm{W\,m^{-2}\,K^{-1}}$	Surface heat loss coefficient on bottom surface
k	$\mathrm{W\,m^{-1}\,K^{-1}}$	Thermal conductivity of the substrate
q	W	Power absorbed by substrate
r	m	Distance from the heat source
Ro	1	Rosenthal number
t	s	Time
$t_{8/5}$	s	Cooling time from 800°C to 500°C
T	K	Temperature
T_0	K	Initial temperature or preheat
T_c	K	Temperature of interest
$\dot{T}_\mathrm{b}$	K/s	Cooling rate
U	$\mathrm{m\,s^{-1}}$	Travel speed of the moving heat source
W_0	-	Principal branch Lambert W function

Continued on next page

Table 4.1 – continued from previous page

Variables	Unit	Description
x, y	m	Cartesian coordinates
Greek symbols		
α	$\mathrm{m^2\,s^{-1}}$	Thermal diffusivity of the substrate
γ	1	Euler–Mascheroni constant
ρ	$\mathrm{kg\,m^{-3}}$	Density of the substrate
ω	$\mathrm{m^3\,s^{-1}}$	Perfusion rate
ϵ	1	Emissivity
ϵ_A	1	Acceptable relative error
σ	$\mathrm{Wm^{-2}\,K^{-4}}$	Stefan–Boltzmann constant
Superscripts		
*		Dimensionless value
$\widehat{\ }$		Asymptotic behavior
$^+$		Improvement or modification over asymptotic
$\cdot$		Time derivative
Subscripts		
b		Trailing point of isotherm
c		Critical value
i		Intermediate value
III		Regime III
IV		Regime IV
IIIa		Regime IIIa
IVa		Regime IVa

4.2 Introduction

In thermal analysis of moving heat source problems, trailing length and cooling rate (represented in Figure 4.1) determine key properties such as microstructure, mechanical properties, and need for shielding gas in welding and additive manufacturing. For example, for a given steel composition, the microstructures resulting from the decomposition of austenite, which are crucial to the properties of fabrications and laser or wire-arc additive manufacturing (WAAM), are often predicted by the cooling time between 800 °C and 500 °C, which can be calculated by trailing length or approximated by an average cooling rate.

Previous investigations have proposed predictive scaling laws for trailing length, and cooling rate without considering the effect of surface heat loss in thick plates [140, 207] and thin plates [128, 130]. The resulting scaling expressions neglecting heat losses match well with available data for processes under mild convection conditions. However, these expressions are unable to capture technological relevant processes such as underwater wet welding, in-service weld repairs, and water cooling in additive manufacturing. This work aims to close this gap.

The validity of ignoring surface heat loss is discussed in [130]. For the case of isotherm width, the criterion to ignore surface heat loss within 10 % of relative error is proposed as:

$$d > \frac{20\alpha^2 \left(h + h'\right)}{kU^2} \left[1 + \left(\frac{\pi}{2\mathrm{e}}\mathrm{Ro}^2\right)^n\right]^{1/n} \tag{4.1}$$

where d is the thickness of substrate, h and h' are surface heat loss coefficient on top and bottom surface, k is the thermal conductivity, U is the traveling speed of heat source, Ro is a dimensionless number representing isotherm which is defined as Equation 4.9 consistently with [128, 130].

Equation 4.1 indicates that the relevance of surface heat loss depends not only on surface heat transfer coefficient, but also on parameters such as plate thicknesses, velocities, and the temperature of interest.

Empirical or semi-empirical correction factors of the effect of surface heat loss have to been implemented for processes with intense surface heat loss such as underwater wet welding [63] or in-service welding [22, 29], thin-wall additive manufacturing [15, 203], thin-plate welding [111], and problems concerning low temperatures far away from heat source (residual stress zone [76], hydrogen cracking [99]). Correction factors are typically based on a single parameter (1D blending techniques). 1D blending is studied in detail in [128, 130, 140, 207]. The consideration of the two parameters in this paper (surface heat losses and Rosenthal number) required the novel extension of blending techniques to two parameters (2D blending).

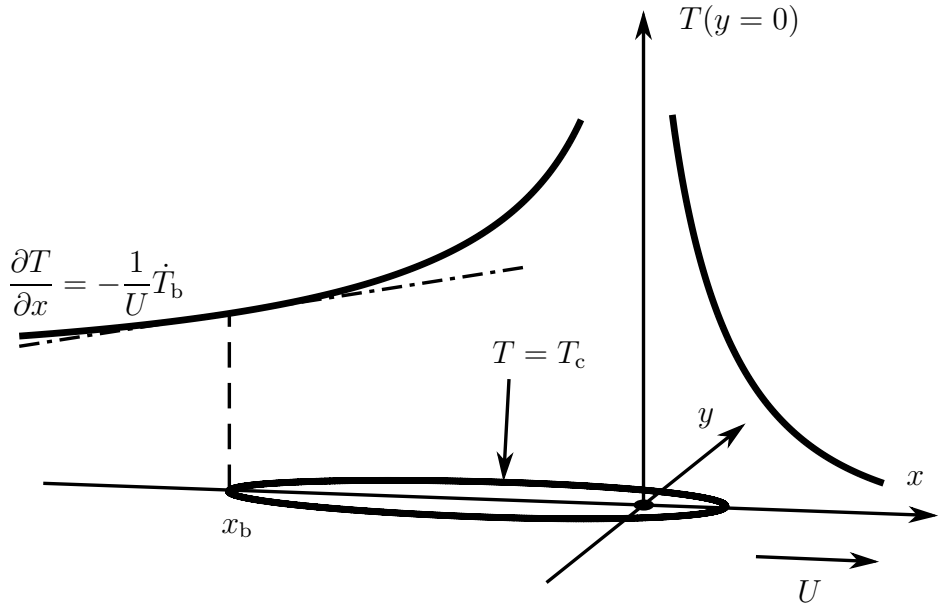

Figure 4.1: Schematic of trailing length x_b and cooling rate $\dot{T}_\mathrm{b} = -U\ \partial T/\partial x$ associated with isotherm $T = T_\mathrm{c}$ induced by a point heat source at the origin moving at velocity U.

This paper aims to establish practical and accurate engineering expressions for characteristic values of moving heat source problems. The engineering expressions close up the gap in textbooks and standards, synthesize the essence of simultaneous conduction and advection, and deliver understanding of process scaling. The scaling law formulae have clear physical relevance, and provide a means for accurate and insightful predictions for engineering practitioners.

4.3 Moving heat source model

The two dimensional moving point heat source model, which is also often termed as 'moving line heat source model', describes a point heat source traveling on a 2D panel that is large enough to ignore edge effects, as illustrated in Figure 4.1.

The assumptions, limitations, validity, and scope of this model have been discussed in detail in [128, 130]. In this approach, the substrate is assumed to have constant thermophysical properties, the heat flow is essentially 2D in a substrate which is infinite in the x and y directions, the heat source is very small in the x and y dimensions, and is moving in a straight line with constant velocity. These hypotheses prevent the model from being applied to small workpieces due to edge effects and from capturing melting and fluid flow effects accurately. The effect of surface heat losses, however intense, are accounted for, which is an important new consideration that has not been made before for explicit predictive expressions.

In this model, the temperature field is pseudo-steady in the coordinate system of the moving heat source, which establishes quickly after the start of heat deposition, typically on the order of seconds [105]. The 2D temperature field is proposed as [27, 175, 215]:

$$T = T_0 + \frac{q}{2\pi kd} \mathrm{e}^{-\frac{Ux}{2\alpha}} K_0 \left[r \sqrt{\left(\frac{U}{2\alpha}\right)^2 + \frac{h+h'}{kd}} \right] \tag{4.2}$$

where K_0 is the modified Bessel function of the second kind and zero order, T_0 is the ambient temperature or preheat temperature of substrate, x, y are spatial location, $r = \sqrt{x^2 + y^2}$ is distance to the heat source, q is amount of heat applied on the base material, and other parameters are the same as introduced in Equation 4.1. Equation 4.2 implies the following heat transfer mechanisms: conduction in the solid workpiece, advection due to relative motion, and surface heat loss. In Equation 4.2, the assumption of point heat source exerts a singularity at the origin $r = 0$. The heat input per unit thickness, $q' = q/d$, can be defined to represent heat input intensity and extend the Equation 4.2 to configurations in addition to a 2D panel, which has

been discussed in [130].

Equation 4.2 can be normalized as follows:

$$T^* = \exp\left(-x^*\right) K_0\left(r^*\sqrt{1+h^*}\right) \tag{4.3}$$

where the dimensionless groups are defined as:

$$T^* = \frac{2\pi kd\left(T-T_0\right)}{q} \tag{4.4}$$

$$x^* = \frac{Ux}{2\alpha} \tag{4.5}$$

$$y^* = \frac{Uy}{2\alpha} \tag{4.6}$$

$$r^* = \frac{Ur}{2\alpha} \tag{4.7}$$

$$h^* = \frac{4\alpha^2(h+h')}{kU^2d} \tag{4.8}$$

The dimensionless groups (equations 4.4 to 4.8) are consistent with normalization in previous work [128, 130]. The dimensionless variables x^* and y^* are essentially Peclet numbers that that capture the relative relevance of advection to conduction [144], and the dimensionless heat loss factor h^* has been interpreted as Biot number [109], although the physical meaning of its effective length is not obvious.

Following [130], the dimensional analysis of Equation 4.2 suggests four dimensionless groups, consistently with Buckingham Pi theorem [24], and corresponding to equations 4.4 to 4.8 ($r^* = \sqrt{x^{*2}+y^{*2}}$ is not an independent variable).

Typically, a particular temperature $T^* = T_\mathrm{c}^*$ is of interest, which leads to, defining the Rosenthal number as:

$$\mathrm{Ro} = \frac{q}{2\pi kd(T_\mathrm{c}-T_0)} = \frac{1}{T_\mathrm{c}^*} \tag{4.9}$$

The Rosenthal number has shown to be useful to synthesize and data of 2D heat flow for diverse processes and materials [26, 62, 128, 130].

4.4 Scaling Considerations

4.4.1 Asymptotic Regimes

In the calculations of trailing length and cooling rate, two constraints are implied: a temperature of interest $T = T_c$, which defines an isotherm, and location at the centerline $y = 0$. These two constraints reduce the number of independent dimensionless groups (degrees of freedom) from four to two, which are chosen as the Rosenthal number (Equation 4.9) and the normalized surface heat loss coefficient h^* (Equation 4.8).

The Rosenthal number Ro has been discussed in previous work [128, 130]; it characterizes 2D moving heat source problems and is always larger than zero. Large Ro typically indicates fast speed, low-temperature region or high-intensity heat sources. The dimensionless heat loss coefficient h^* is greater than or equal to zero, with $h^* = 0$ indicating adiabatic surfaces; large h^* typically indicates intense surface heat loss such as in underwater wet welding, in-service welding, or welding of thin plates.

With the definition of Ro and h^*, four asymptotic regimes are identified:

- Regime III ($\mathrm{Ro} \to \infty,\ h^* \to 0$), corresponding to fast heat sources with negligible heat losses
- Regime IV ($\mathrm{Ro} \to 0,\ h^* \to 0$), corresponding to slow heat sources with negligible heat losses
- Regime IIIa ($\mathrm{Ro} \to \infty,\ h^* \to \infty$), corresponding to fast heat sources dominated by heat losses
- Regime IVa ($\mathrm{Ro} \to 0,\ h^* \to \infty$), corresponding to slow heat sources dominated by heat losses

The choice of names for the regimes is consistent with [128, 130]. The four asymptotic regimes for trailing length and cooling rate are illustrated in figures 4.2 and 4.4. The transition between regimes is not sharp, but gradual. Different criteria can be used to divide regimes.

A useful criterion to bound the regimes, is to determine the boundary at which the error (defined as in [140]) between the asymptotic behavior and the exact solution reaches a small arbitrary number. In figures 4.2 and 4.4, the dashed lines correspond to the application of this criterion with an error of 10 %.

When the asymptotic expressions between contiguous regimes intersect, the line of intersection is a reasonable heuristic for the division between regimes. This is the criterion used to draw the continuous lines between regimes IV and IVa, IIIa and IVa in Figure 4.2 and regimes IV and IVa in Figure 4.4.

When the asymptotic expressions between contiguous regimes do not intersect, the line of division between regimes can be determined as the points where the absolute relative error of each asymptotic regime (relative to the exact solution) is the same. This is the criterion used to draw the continuous lines between regimes III and IV, III and IIIa in Figures 4.2 and regimes III and IV, III and IIIa, IIIa and IVa in Figures 4.4.

Some of the solid lines near the center of the figures have been excluded because of their complex geometry in that region, which betrays the intuitive purpose of placing a line to identify a smooth transition.

4.4.2 2D Blending

Blending is a rigorous approach to achieve approximate, but accurate engineering expressions in closed-form when the exact expression is expressed in implicit form, or when asymptotic behavior at the extremes is known form experiments or simulations. From blending expressions, correction factors can be developed to extend the range of validity of an asymptotic expression. Often, the correction factors extend the validity of an asymptotic formula into its opposite asymptotic extreme [135]. Blending techniques are typically simple and practical approximations with accuracy better than 10 %; occasionally, blending results in exact expressions.

When blending depends only on one dimensionless group (1D blending) the method-

ology is well understood [3, 4, 34]. 1D blending has been used successfully used to develop engineering expressions for moving heat sources on a thick substrate [140, 207] (with the Rykalin number as blending parameter) and on thin substrates [128, 130] (with the Rosenthal number as blending parameter).

This investigation in this paper faces and important challenge, in which the dimensionless exact solution depends on two, not one parameter (2D blending). The two dimensionless parameters are Ro and h^*. The increase in complexity is enormous, comparable to the increase in complexity from single variable calculus to multivariate calculus, and there is no generalized approach for 2D blending. Some fundamental concepts are lay down here to help solve the concrete problem of interest, and also to pave the way for future progress in 2D (and higher order) blending.

Fully asymptotic regimes correspond to situations in which all blending parameters are at an asymptotic extreme, and will be identified with just one label (e.g. Regime III). Not all 2D blending problems have 4 fully asymptotic regimes, for example in [82], the 2D parameter domain is divided into five fully asymptotic regimes. For trailing length and cooling rate in this research, the two dimensionless groups define four fully asymptotic regimes. All asymptotic expressions are indicated with a $\widehat{}$symbol.

In addition to the four fully asymptotic regimes (Regimes III, IV, IIIa, and IVa) and the blending over the full domain (full blending), there is blending over subdomains ("partial blending"). Partial blending has two forms: "side blending" and "corner blending," corresponding to "side regimes" and "corner regimes". All blending expressions are based on asymptotic expressions and carry the $\widehat{}$symbol. Blending expressions are distinguished from fully asymptotic regimes with a $^+$ superscript.

Side regimes are problem configurations in which all but one of the blending parameters are at an asymptotic extreme. Side blending consists of 1D blending of two contiguous regimes across one of the blending parameters, while all other blending parameters are at an asymptotic extreme. Side regimes will be identified with two labels (e.g. Regime III-IIIa). There are four side regimes in this research: Regime

III-IIIa (yielding exact blending), and side regimes IV – IVa, IIIa – IVa, and III – IV, yielding approximate 1D blending.

Corner regimes are problem configurations around a fully asymptotic regime, and its contiguous regimes. In these configurations, at least one of the blending parameters corresponds to the reference fully asymptotic regime. Corner blending consists of an asymptotic expression corresponding to a regime, with its range of validity extended into the two adjacent regimes using correction factors. In 2D blending, corner regimes will be identified with three labels, with the first label corresponding to the central fully asymptotic regime. The corner regime of relevance in this work is Regime III-IIIa-IV, developed around Regime III.

Full blending (or overall blending) consists of an approximate expression that approximates the target magnitude over the whole blending domain. When full blending is based on a particular fully asymptotic regime, the corresponding expressions indicate this regime. If no regime is indicated, the expression corresponds to full blending without a particular fully asymptotic regime as center.

The methodology employed here to obtain 2D blending expressions for trailing length and cooling rate over the whole domain has three steps: First, expressions for all four fully asymptotic regimes are obtained. Second, partial blending is defined on asymptotic side and corner regimes. Third, 2D blending for the full domain is obtained by combining partial blending results.

In this paper, the 2D blended expressions trailing length and cooling rate have the form of an asymptotic expression for Regime III multiplied by correction factors that account for motion of the heat source and heat losses extend the validity of calculations to fast and slow heat sources with negligible or dominant heat losses.

4.5 Trailing length x_{b}

Trailing length x_{b} is the location of the rear point of the isotherm $T = T_{\mathrm{c}}$. At large Rosenthal numbers, x_{b} is also a good estimate of the length of an isotherm.

4.5.1 Asymptotic analysis of trailing length

To perform 2D blending of the trailing length, four asymptotic expressions are obtained for each of the four asymptotic regimes: III, IV, IIIa and IVa.

In regimes III and IV, where $h^* \to 0$, the surface heat loss is negligible. The asymptotic expressions for trailing length are derived from Equation 4.3 with $h^* = 0$ and $y^* = 0$, and were obtained in previous work [128]:

$$\widehat{x}^*_{\mathrm{b_{III}}} = -\frac{\pi}{2}\mathrm{Ro}^2 \tag{4.10}$$

$$\widehat{x}^*_{\mathrm{b_{IV}}} = -2\exp\left(-\frac{1}{\mathrm{Ro}} - \gamma\right) \tag{4.11}$$

In Regime IIIa, where $\mathrm{Ro} \to \infty$ and $h^* \to \infty$, isotherms of low temperatures away from the heat source are studied under intense surface heat loss conditions. The asymptotic behavior of trailing length in Regime IIIa is derived in 4.A, resulting in:

$$\widehat{x}^*_{\mathrm{b_{IIIa}}} = -\frac{1}{2\sqrt{h^*}} W_0\left(\pi\mathrm{Ro}^2\right) \tag{4.12}$$

where $W_0(x)$ is the principal branch of the Lambert W function, which is the solution to $x = W_0(x)\exp\left[W_0(x)\right]$ [41]. The Lambert W function is built-in in Matlab, Mathematica and other common scientific software. It can also be approximated by explicit functions such as [17]. A practical simple approximation using 1D blending is proposed in [128]:

$$\widehat{W}_0^+(x) = \left[x^{-1} + \ln(x+c)^{-1} + a\,x^b\right]^{-1} \tag{4.13}$$

where x and $\ln(x)$ are asymptotic expressions for small and large values of x. The optimal blending parameters are $a = 0.08568$, $b = -0.1028$, $c = 2.586$. The maximum relative error Equation 4.13 for all $x > 0$ is 5.9 %.

In Regime IVa, where $\mathrm{Ro} \to 0$ and $h^* \to \infty$, the isotherms of interest are in the high-temperature zone closed to the heat source. The asymptotic behavior of trailing length in Regime IVa is derived in 4.B, resulting in:

$$\widehat{x}^*_{\mathrm{b_{IVa}}} = -\frac{2}{\sqrt{h^*}}\exp\left(-\frac{1}{\mathrm{Ro}} - \gamma\right) \tag{4.14}$$

4.5.2 Partial blending of trailing length

The asymptotics expressions, equations 4.10 to 4.12 and 4.14, are accurate at each asymptotic regime but less accurate at intermediate regimes, as shown in Figure 4.2. Along four asymptotic side regimes: III – IV ($h^* \to 0$), III – IIIa ($\mathrm{Ro} \to \infty$), IV – IVa ($\mathrm{Ro} \to 0$) and IIIa – IVa ($h^* \to \infty$), side blending expressions are obtained to provide accurate estimations at intermediate regimes between adjacent asymptotic regimes.

In side Regime III – IV, where h^* tends to zero (negligible surface heat loss), the behavior of trailing length changes only with Ro. Side partial blending in this case reduces to 1D blending of equations 4.12 and 4.14, obtained in [128]:

$$\widehat{x}^{*+}_{\mathrm{b_{III-IV}}} = -\mathrm{e}^{-\frac{1}{\mathrm{Ro}}}\left[2\exp\left(-\gamma\right) + \frac{\pi}{2}\mathrm{Ro}^2 + a\mathrm{Ro}^b\right] \tag{4.15}$$

where the optimal blending parameters are $a = 0.7659$, $b = 1.541$. The maximum error is 6.8 % [128].

In side Regime IIIa – IVa, where h^* tends to infinity (surface heat loss is dominant), the behavior of trailing length changes only with Ro. Side partial blending in this case reduces to 1D blending of equations 4.12 and 4.14:

$$\widehat{x}^{*+}_{\mathrm{b_{IIIa-IVa}}} = -\frac{\mathrm{e}^{-\frac{1}{\mathrm{Ro}}}}{2\sqrt{h^*}}\left\{\left[W_0\left(\pi\mathrm{Ro}^2\right)\right]^n + \left[4\mathrm{e}^{-\gamma}\right]^n\right\}^{1/n} \tag{4.16}$$

where the blending parameter $n = 2.205$ and the maximum error 2.4%.

In side Regime III – IIIa, where Ro tends to infinity (fast heat source), considering isotherms away from the heat source, the behavior of trailing length changes with both Ro and h^* according to equations 4.10 and 4.12; therefore, the 1D blending on one variable cannot be applied directly. The scaling law for trailing length along asymptotic side III – IIIa is obtained by asymptotic analysis of large Ro according to 4.A:

$$\widehat{x}^{*}_{\mathrm{b_{III\text{-}IIIa}}} = -\frac{1}{2\sqrt{1+h^*}-2}W_0\left[\pi\left(1-\frac{1}{\sqrt{1+h^*}}\right)\mathrm{Ro}^2\right] \tag{4.17}$$

which is an exact asymptotic expression for trailing length for $\mathrm{Ro} \to \infty$ with no blending parameters involved.

In side Regime IV – IVa, where Ro tends to zero (low heat source), considering isotherms close to the heat source, the behavior of trailing length changes only with h^*. Side partial blending in this case reduces to 1D blending of equations 4.11 and 4.14:

$$\widehat{x}^*_{\mathrm{b_{IV\text{-}IVa}}} = -2\exp\left(-\frac{1}{\mathrm{Ro}} - \gamma\right)\left[1 + \left(\frac{1}{\sqrt{h^*}}\right)^n\right]^{1/n} \tag{4.18}$$

where $n = -2$. In this case, the 1D blending is also the exact expression, derived from asymptotic analysis for small Ro in 4.B.

4.5.3 Full blending of trailing length

The expressions developed above provide accurate estimations for four fully asymptotic regimes (III, IV, IIIa, IVa) and four side regimes (III – IV, III – IIIa, IV – IVa, IIIa – IVa). Full blending over the 2D domain is carried out by a combination of partial blending results and fully asymptotic expressions. In addition, the parameters of partial blending are improved by simultaneous optimization of the full blending expression over the whole domain.

With the expressions for fully asymptotic regimes (equations 4.10 to 4.12 and 4.14) and side blending expressions (equations 4.15 to 4.18), 2D blending of trailing length over the full domain can be developed around Regime III as:

$$\widehat{x}^{*+}_{\mathrm{b}}\left(\mathrm{Ro}, h^*\right) = -\frac{\pi}{2}\mathrm{Ro}^2 \cdot f(\mathrm{Ro}) \cdot g\left(\mathrm{Ro}, h^*\right) \tag{4.19}$$

where $f(\mathrm{Ro})$ is a correction factor between regimes III and IV according to Equation 4.15:

$$f(\mathrm{Ro}) = \mathrm{e}^{-\frac{1}{\mathrm{Ro}}}\left[1 + \frac{4}{\pi \mathrm{e}^{\gamma}}\mathrm{Ro}^{-2} + \frac{2a_1}{\pi}\mathrm{Ro}^{b_1-2}\right] \tag{4.20}$$

where the blending parameter $a_1 = 0.7659$, $b_1 = 1.541$. The correction factor $f(\mathrm{Ro})$ are from [128].

$g(\mathrm{Ro}, h^*)$ is a correction factor for the effect of surface heat loss according to Equa-

tion 4.17, depending on both Ro and h^*:

$$g\left(\mathrm{Ro}, h^*\right) = \frac{W_0\left[\pi\left(1-\frac{1}{\sqrt{h^*+1}}\right)\mathrm{Ro}^2\right]}{\pi\left(\sqrt{1+h^*}-1\right)\mathrm{Ro}^2} \tag{4.21}$$

$$\approx \frac{\left[\Pi^{-1}+\ln\left(\Pi+c_2\right)^{-1}+a_2\,\Pi^{b_2}\right]^{-1}}{\pi\left(\sqrt{1+h^*}-1\right)\mathrm{Ro}^2} \tag{4.22}$$

where Π is denoted as $\Pi = \pi\left(1-\frac{1}{\sqrt{h^*+1}}\right)\mathrm{Ro}^2$, $a_2 = 0.08568$, $b_2 = -0.1028$, $c_2 = 2.586$ adhering to the approximation of Lambert W function (Equation 4.13). The maximum relative error over the full domain is 13 %. The 2D blending for trailing length, equations 4.19 to 4.22, satisfies all of the asymptotic expressions in extreme regimes and sides and provides estimation over all values of Ro and h^*.

The blending parameters are optimal for partial blendings along asymptotic sides, but not optimal over the full domain. With the adjustment of blending parameters, the maximum relative error over the full domain is reduced to 7.1 % when $a_1 = 0.7806$, $b_1 = 1.517$, $a_2 = 0.1260$, $b_2 = -0.1273$, $c_2 = 3.815$. The relative error of trailing length over the full domain of Ro and h^* is illustrated in Figure 4.2. Figure 4.3 relates the blending result of trailing length $\widehat{x}_{\mathrm{b}}^{*+}$ and surface heat loss h^* for Ro =0.1, 1 and 10 from Equation 4.19 to 4.22.

The engineering expressions with units for trailing length x_{b} is:

$$\widehat{x}_{\mathrm{b}}^{+} = -\frac{\alpha q^2}{4\pi U d^2 k^2 (T_{\mathrm{c}}-T_0)^2}\cdot f(\mathrm{Ro})\cdot g\left(\mathrm{Ro}, h^*\right) \tag{4.23}$$

where $f(\mathrm{Ro})$ is proposed as Equation 4.20 and $g(\mathrm{Ro}, h^*)$ is proposed as Equation 4.22.

4.6 Centerline cooling rate $\dot{T}_{\mathrm{b}}$

Cooling rate is a crucial magnitude to assess phase transformations associated with engineered moving heat sources such as welding, laser heat treating, or accidental heat sources such as sliding contact in railroad wheels.

The cooling rate at the centerline is often representative of the whole area experiencing phase transformations. For example, the cooling rate in the heat affected zone in welding is just 5 % to 10 % lower than in the centerline [97, 166].

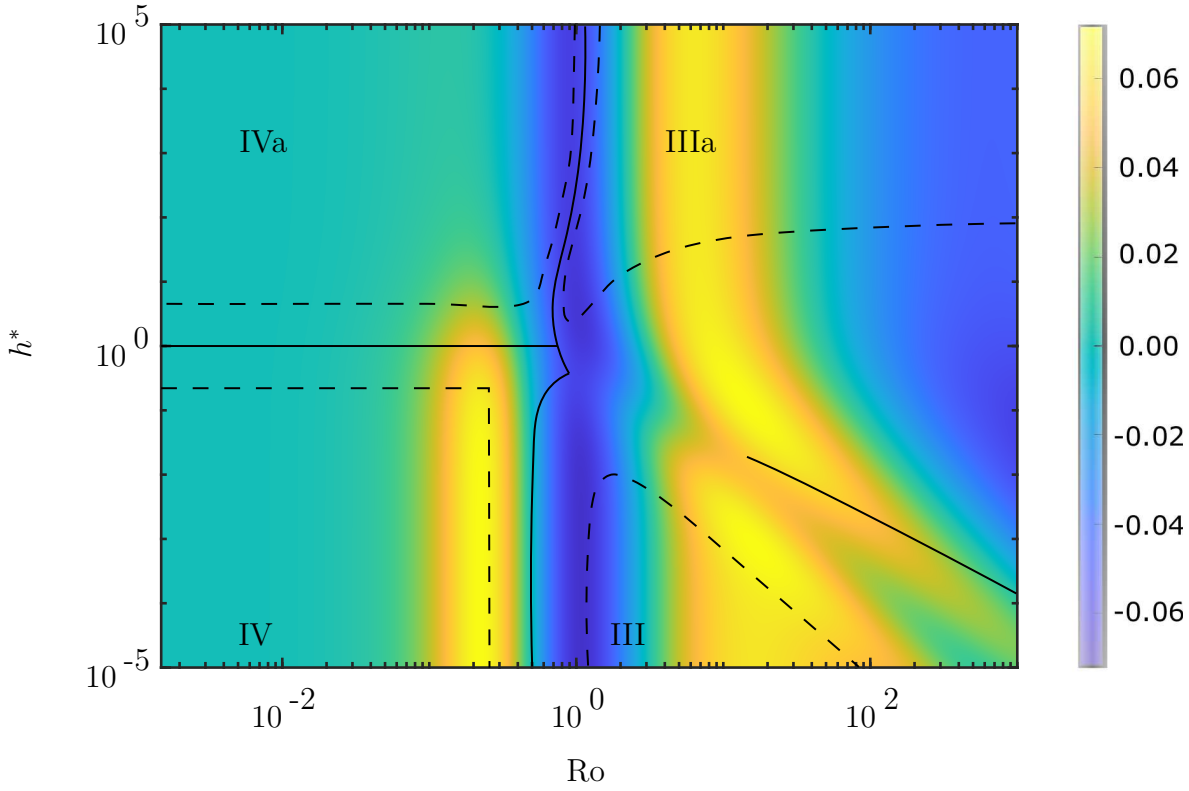

Figure 4.2: Error map of blending of trailing length (Equations 4.19 to 4.22) for the optimal blending parameters $a_1 = 0.7806$, $b_1 = 1.517$, $a_2 = 0.1260$, $b_2 = -0.1273$, $c_2 = 3.815$. The maximum relative error is 7.1 %.

Centerline cooling rate can be derived from the temperature gradient $\partial T/\partial x$ by the material derivative as introduced in [128]:

$$\dot{T}_\mathrm{b} \equiv \left.\frac{DT}{Dt}\right|_{x_\mathrm{b}} = -\,U \left.\frac{\partial T}{\partial x}\right|_{x_\mathrm{b}} \tag{4.24}$$

In dimensionless form, the centerline cooling rate can be calculated with:

$$\dot{T}^*_\mathrm{b} = \frac{4\pi k \alpha d}{qU^2}\,\frac{DT}{Dt} = -\left.\frac{\partial T^*}{\partial x^*}\right|_{x^*_\mathrm{b}} \tag{4.25}$$

which is consistent with [128]. According to equations 4.3 and 4.25, $\dot{T}^*_\mathrm{b}$ can be explicitly expressed in terms of Ro, h^* and x^*_b:

$$\dot{T}^*_\mathrm{b} = \frac{1}{\mathrm{Ro}}\left[1 - \frac{\sqrt{h^*+1}K_1\left(-x^*_\mathrm{b}\sqrt{h^*+1}\right)}{K_0\left(-x^*_\mathrm{b}\sqrt{h^*+1}\right)}\right] \tag{4.26}$$

where x^*_b is a function of Ro and h^* that can be estimated by Equations 4.19 to 4.22.

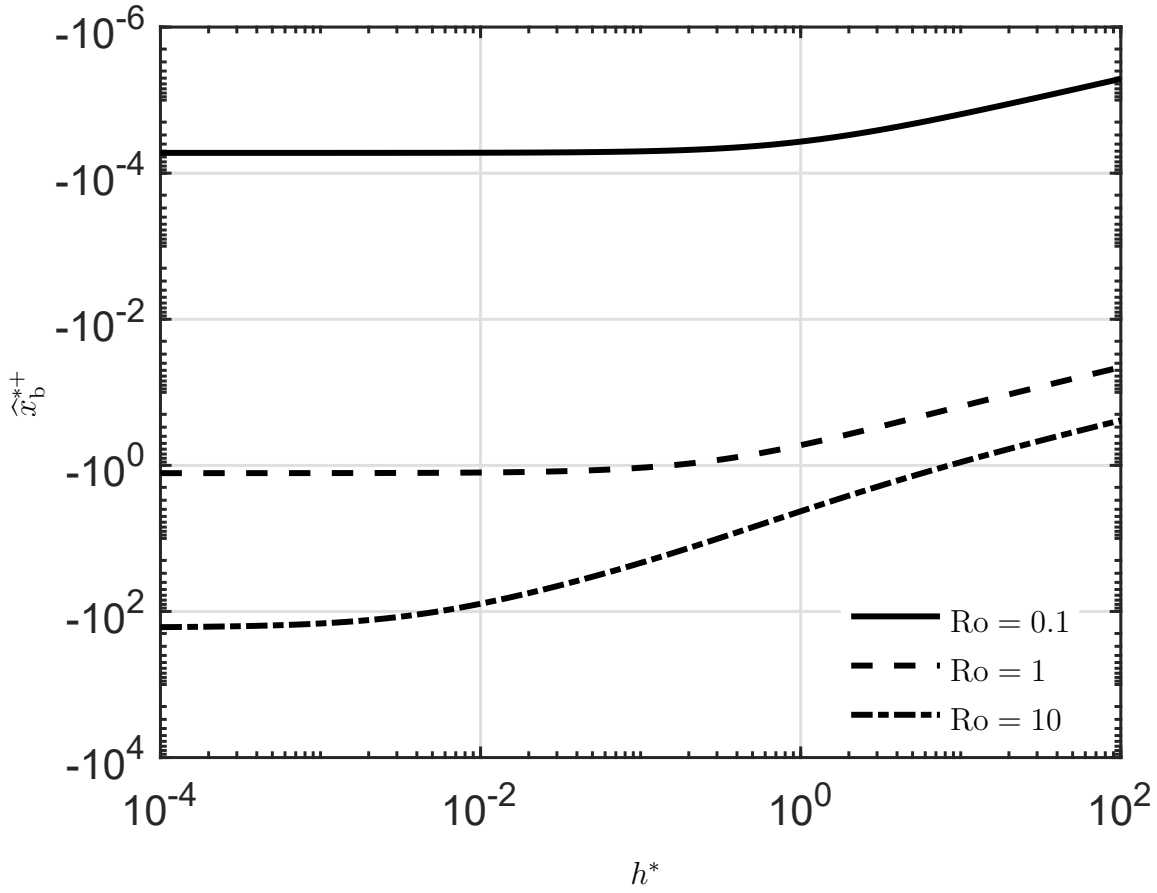

Figure 4.3: The $\widehat{x}_{\mathrm{b}}^{*+}$, calculated from the blending result Equation 4.19 to 4.22, changes with h^* for Ro = 0.1, 1, 10.

4.6.1 Asymptotic analysis of cooling rate

Asymptotic expressions for cooling rate are obtained by combining the asymptotic expressions for trailing length (equations 4.10 and 4.11) into Equation 4.26 as studied in previous work [128]. In regimes III and IV, h^* tends to zero with negligible surface heat loss, resulting in

$$\widehat{T}_{\mathrm{b_{III}}}^{*} = -\frac{1}{\pi \mathrm{Ro}^3} \tag{4.27}$$

$$\widehat{T}_{\mathrm{b_{IV}}}^{*} = -\frac{1}{2}\exp\left(\frac{1}{\mathrm{Ro}} + \gamma\right) \tag{4.28}$$

In Regime IIIa, where $\mathrm{Ro} \to \infty$ and $h^* \to \infty$, low-temperature isotherms experience intense surface heat loss. According to Equation 4.74 derived in Appendix, the

asymptotic behavior of cooling rates in Regime IIIa is:

$$\widehat{\dot{T}}^{*}_{\mathrm{b_{IIIa}}} = -\frac{\sqrt{h^*}}{\mathrm{Ro}} \tag{4.29}$$

In Regime IVa, where $\mathrm{Ro} \to 0$ and $h^* \to \infty$, the asymptotic behavior of cooling rate is derived in the Appendix (Equation 4.79), resulting in

$$\widehat{\dot{T}}^{*}_{\mathrm{b_{IVa}}} = -\frac{1}{2}\sqrt{h^*}\exp\left(\frac{1}{\mathrm{Ro}} + \gamma\right) \tag{4.30}$$

4.6.2 Partial blending of cooling rate

Similar to trailing length, partial blending of cooling rate are obtained along four asymptotic sides with 1D blending between adjacent asymptotic regimes (III – IV, IV – IVa, IIIa – IVa) and asymptotic analysis in III – IIIa where the asymptotic behavior changes with both Ro and h^* and 1D blending is not applicable.

In side Regime III – IV, where $h^* \to 0$ with negligible surface heat loss, the behavior of cooling rate changes only with Ro. The side blending of cooling rate has been presented in previous work by 1D blending of equation 4.27 and 4.28 [128]:

$$\widehat{\dot{T}}^{*+}_{\mathrm{b_{III-IV}}} = -\frac{\exp\left(\frac{1}{\mathrm{Ro}}\right)}{\pi\mathrm{Ro}^3 + 2\exp\left(-\gamma\right) + a\mathrm{Ro}^b} \tag{4.31}$$

where the optimal blending parameters are $a = 3.839, b = 2.108$ and the maximum error is 5.8% [128].

In side Regime IIIa – IVa, where $h^* \to \infty$ with intense surface heat loss, the behavior of cooling rate changes only with Ro. The side blending of cooling rate is obtained by 1D blending of equations 4.29 and 4.30:

$$\widehat{\dot{T}}^{*+}_{\mathrm{b_{IIIa-IVa}}} = -\frac{\sqrt{h^*}\exp\left(\frac{1}{\mathrm{Ro}}\right)}{2\exp\left(-\gamma\right) + \mathrm{Ro} + a\mathrm{Ro}^b} \tag{4.32}$$

where the optimal blending parameters are $a = -0.6004, b = 0.6014$ and the maximum error reaches 4.7%.

In side Regime III – IIIa, where $\mathrm{Ro} \to \infty$ considering isotherms away from the heat source, the asymptotic behavior of trailing length changes with both Ro and h^*

according to equations 4.27 and 4.29. Similar to $x^*_{\mathrm{b_{III\text{-}IIIa}}}$, the scaling law for cooling rate in the asymptotic side III – IIIa is obtained by asymptotic analysis of large Ro number according to Equation 4.73 derived in Appendix:

$$\widehat{\dot{T}}^{*+}_{\mathrm{b_{III-IIIa}}} = -\frac{\sqrt{h^*+1}-1}{\mathrm{Ro}}\left\{1+\frac{1}{W_0\left[\pi\left(1-\frac{1}{\sqrt{h^*+1}}\right)\mathrm{Ro}^2\right]}\right\} \tag{4.33}$$

In side Regime IV – IVa, where $\mathrm{Ro}\to 0$ considering heat transfer around the heat source, the behavior of cooling rate changes only with h^*. The side blending of cooling rate is obtained by 1D blending of equations 4.28 and 4.30:

$$\widehat{\dot{T}}^{*+}_{\mathrm{b_{IV-IVa}}} = -\frac{1}{2}\exp\left(\frac{1}{\mathrm{Ro}}+\gamma\right)\left[1+\left(\sqrt{h^*}\right)^n\right]^{\frac{1}{n}} \tag{4.34}$$

where $n = 2$. Akin to Equation 4.18, the value of n is derived from asymmetric analysis according ton Appendix 4.78, rather than from blending processes.

4.6.3 Full blending of cooling rate

Similar to 2D blending of trailing length (equations 4.19 to 4.22), 2D blending of cooling rate over the full domain is carried out by combination of asymptotic expressions (equations 4.27 to 4.30) and partial blending results (equations 4.31 to 4.34). 2D blending of cooling length for all Ro and h^* can be expressed based on asymptotic of Regime III together with two correction factors:

$$\widehat{\dot{T}}^{*+}_{\mathrm{b}}\left(\mathrm{Ro}, h^*\right) = -\frac{1}{\pi\mathrm{Ro}^3}\cdot f\left(\mathrm{Ro}\right)\cdot g\left(\mathrm{Ro}, h^*\right) \tag{4.35}$$

$f\left(\mathrm{Ro}\right)$ is a correction factor between regimes III and IV according to Equation 4.31:

$$f(\mathrm{Ro}) = \mathrm{e}^{\frac{1}{\mathrm{Ro}}}\left[1+\frac{2}{\pi\mathrm{e}^{\gamma}}\mathrm{Ro}^{-3}+\frac{a_1}{\pi}\mathrm{Ro}^{b_1-3}\right]^{-1} \tag{4.36}$$

where the blending parameter $a_1 = 3.652$, $b_1 = 1.971$. The correction factor is consistent [128].

$g\left(\mathrm{Ro}, h^*\right)$ is a correction factor for the effect of surface heat loss depending on both

Ro and h^* according to Equation 4.33:

$$g(\mathrm{Ro}, h^*) = \pi\left(\sqrt{1+h^*}-1\right)\mathrm{Ro}^2 \cdot \quad \left\{1+\frac{1}{W_0\left[\pi\left(1-\frac{1}{\sqrt{1+h^*}}\mathrm{Ro}^2\right)\right]}\right\}$$
$$\approx \sqrt{1+h^*}\left[1+\Pi+\frac{\Pi}{\ln(\Pi+c_2)}+a_2\,\Pi^{b_2+1}\right] \quad (4.37)$$

where $\Pi = \pi\left(1-\frac{1}{\sqrt{h^*+1}}\right)\mathrm{Ro}^2$, $a_2 = 0.08568$, $b_2 = -0.1028$, $c_2 = 2.586$ when using the approximation of lambert function of Equation 4.13, yielding a maximum error of 20 %. The 2D blending for cooling rate, equations 4.35 to 4.37, satisfies asymptotic expressions in all regimes and sides. If the parameters of Equation 4.13 are reassessed in a global optimization together with blending, the blending parameters are adjusted to $a_2 = 0.06407$, $b_2 = -0.1004$, $c_2 = 6.252$, the maximum error is reduced to 7.6 %. The maximum absolute error of 2D blending of cooling rate, equation 4.35 to 4.37 is much lower (20 %), as is illustrated in Figure 4.4. Figure 4.5 relates the blending result of cooling rate $\widehat{\dot{T}}_{\mathrm{b}}^{*+}$ and surface heat loss h^* for Ro =0.1, 1 and 10 from Equation 4.35 to 4.37.

The engineering expressions with units for cooling rate $\dot{T}_{\mathrm{b}}$ is:

$$\widehat{\dot{T}}_{\mathrm{b}}^{+} = -\frac{2\pi U^2 d^2 k^2 (T_c - T_0)^3}{\alpha q^2} \cdot f(\mathrm{Ro}) \cdot g\left(\mathrm{Ro}, h^*\right) \quad (4.38)$$

where $f\left(\mathrm{Ro}\right)$ corresponds to Equation 4.36, and $g\left(\mathrm{Ro}, h^*\right)$ corresponds to Equation 4.37 that expresses the effect of surface heat loss.

4.7 Criterion to neglect surface heat loss

When the surface heat loss is mild, the trailing length and cooling rates could be calculated directly with equations 4.15 and 4.31, without the correction factors for surface heat loss $g(\mathrm{Ro}, h^*)$, equation 4.22 and 4.37. For a certain acceptable relative error of ϵ_{A}, the critical heat loss coefficients in dimensionless form to neglect surface dissipation in the prediction of trailing length are obtained by comparing equation 4.19 and 4.15 with equations 4.35 and 4.31.

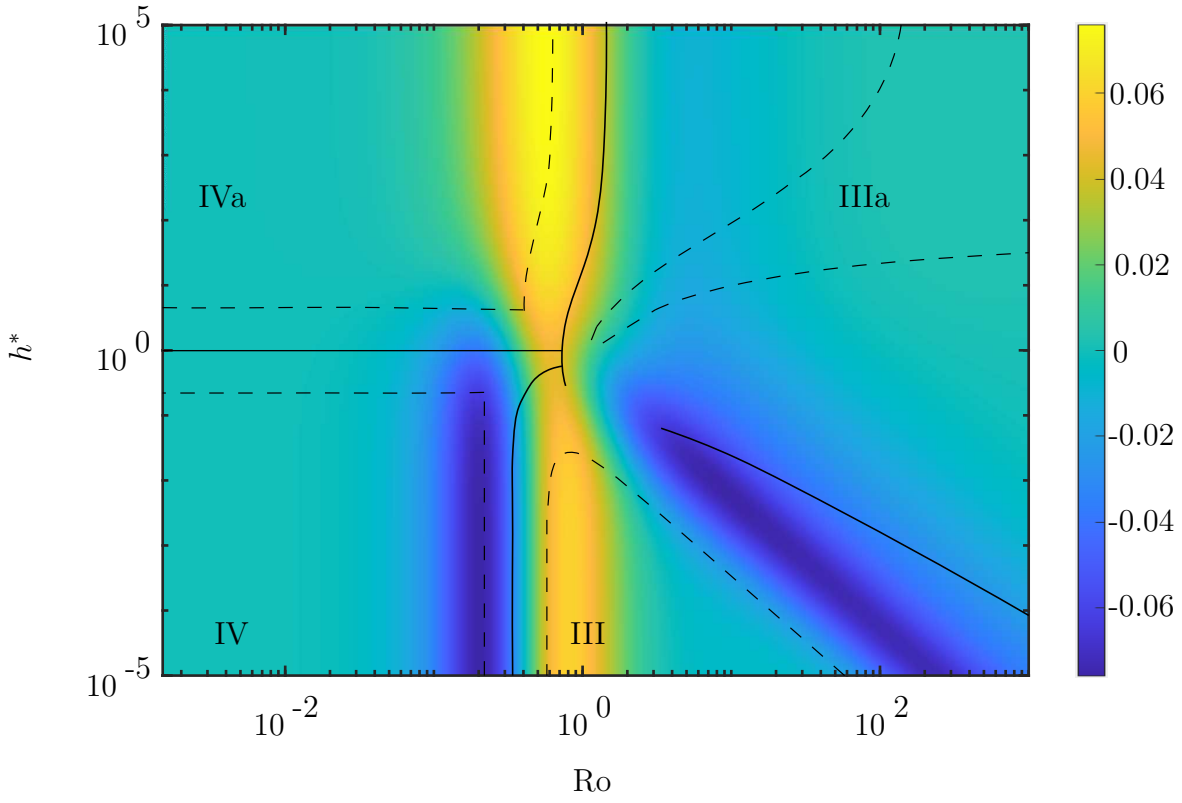

Figure 4.4: Error map of blending of cooling rate (Equations 4.35 to 4.37) for the optimal blending parameters $a_1 = 3.652$, $b_1 = 1.971$, $a_2 = 0.06407$, $b_2 = -0.1004$, $c_2 = 6.252$. The maximum relative error is 7.6 %.

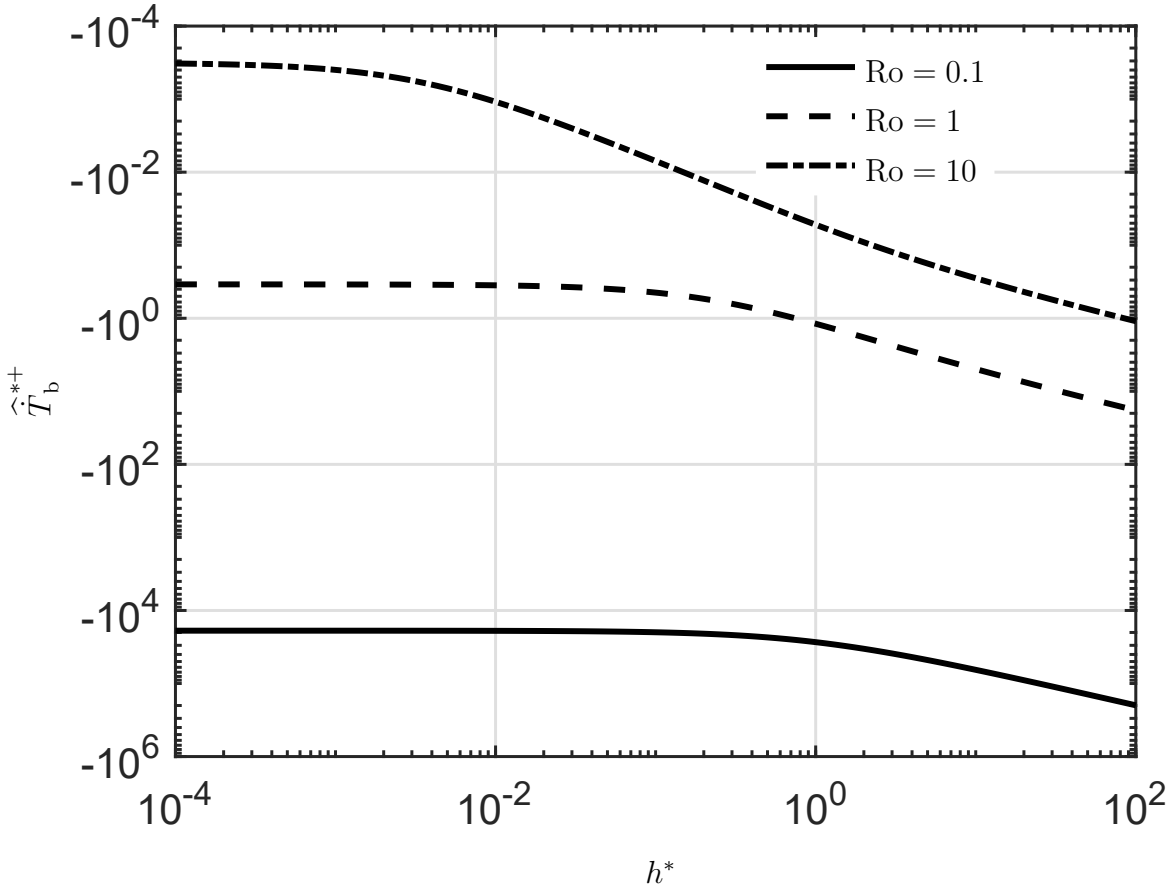

Figure 4.5: The $\hat{\dot{T}}_{\mathrm{b}}^{*+}$, calculated from the blending result Equation 4.35 to 4.37, changes with h^* for Ro = 0.1, 1, 10.

For trailing length, following the derivation in the Appendix (Equation 4.83), the critical value for h^* is:

$$\widehat{h}^*_{\mathrm{c},x^*_{\mathrm{b}}} = 2\epsilon_{\mathrm{A}} \left[1 - \frac{K_0\left(-\widehat{x}^*_{\mathrm{b_{III\text{-}IV}}}\right)}{K_1\left(-\widehat{x}^*_{\mathrm{b_{III\text{-}IV}}}\right)} \right] \tag{4.39}$$

while for cooling rate, according to 4.87 in the Appendix, the critical value for h^* is:

$$\widehat{h}^*_{\mathrm{c},\dot{T}^*_{\mathrm{b}}} = \Big| 2\epsilon_{\mathrm{A}} \left[K_0\left(-\widehat{x}^*_{\mathrm{b_{III\text{-}IV}}}\right) - K_1\left(-\widehat{x}^*_{\mathrm{b_{III\text{-}IV}}}\right) \right]^2 \cdot \left[\left(\widehat{x}^*_{\mathrm{b_{III\text{-}IV}}} + 1\right) K_1\left(-\widehat{x}^*_{\mathrm{b_{III\text{-}IV}}}\right)^2 - \widehat{x}^*_{\mathrm{b_{III\text{-}IV}}} K_0\left(-\widehat{x}^*_{\mathrm{b_{III\text{-}IV}}}\right)^2 \right]^{-1} \Big| \tag{4.40}$$

In Regime III, according to equations 4.88 and 4.84 derived in Appendix, the

critical values of surface heat loss coefficient to neglect surface heat loss are:

$$\widehat{h}^*_{\mathrm{c},x^*_{\mathrm{b}},\mathrm{III}} \approx \frac{2\epsilon_{\mathrm{A}}}{\pi \mathrm{Ro}^2} \tag{4.41}$$

$$\widehat{h}^*_{\mathrm{c},\dot{T}^*_{\mathrm{b}},\mathrm{III}} \approx \frac{\epsilon_{\mathrm{A}}}{\pi \mathrm{Ro}^2} \tag{4.42}$$

In Regime IV, according to equations 4.89 and 4.85 derived in Appendix, the critical values of surface heat loss coefficient to neglect surface heat loss are:

$$\widehat{h}^*_{\mathrm{c},x^*_{\mathrm{b}},\mathrm{IV}} \approx \widehat{h}^*_{\mathrm{c},\dot{T}^*_{\mathrm{b}},\mathrm{IV}} \approx 2\epsilon_{\mathrm{A}} \tag{4.43}$$

The critical values of h^* (Equations 4.39 and 4.40) and their approximations (Equations 4.39 and 4.40) are illustrated in Figure 4.6.

For fast moving heat sources, substituting equations 4.8 and 4.9 into Equation 4.42 to obtain the critical heat transfer coefficient with units within 10 % error in Regimes III for cooling rate:

$$h + h' \leq \frac{\pi (T_{\mathrm{c}} - T_0)^2 k^3 d^3}{10 \alpha^2 (q/U)^2} \tag{4.44}$$

The power law on each parameter in Equation 4.44 is the same as the condition proposed by Jhaveri [97]. Equation 4.44 implies that surface heat loss may become important for large convection coefficients, such as in underwater wet welding and in-service welding, large heat input q/U such as in thick welding passes, materials having low thermal conductivity such as titanium, thin sheets, and isotherms of low temperature such as the yield temperatures associated with plasticity in welding. Correction factors for surface heat losses are necessary when they exceed the threshold given by Equation 4.44.

As an example, consider the case of welding of steel under typical conditions, assuming thermal conductivity is $k \approx 50$ W/mK, thermal diffusivity of $\alpha \approx 10^{-5}$ m^2/s and an absorbed power of 2000 W supplied at a speed of 10 mm/s with a total heat loss coefficient 200 $\mathrm{W/m^2K}$, typical of cooling in a gentle current of air. For the isotherm of 632 °C which is an effective intermediate temperature representing the cooling rate between 800 °C and 500 °C [207], the effect of surface heat loss is negligible

for steel plates thicker than 4 mm (Ro = 2.6). For steel of 1 mm (Ro = 2.9×10^{-4}), the critical value to neglect surface heat loss is 3.7 W/m^{2}K, which is below typical values of natural convection, and would require surface insulation. For the case of additive manufacturing, local surface heat losses are relevant for walls thinner than 6 mm or interpass temperatures above 1244 °C. Surface heat losses affecting the overall (not just local) accumulation of heat and interpass temperatures involve different calculations outside the scope of this work.

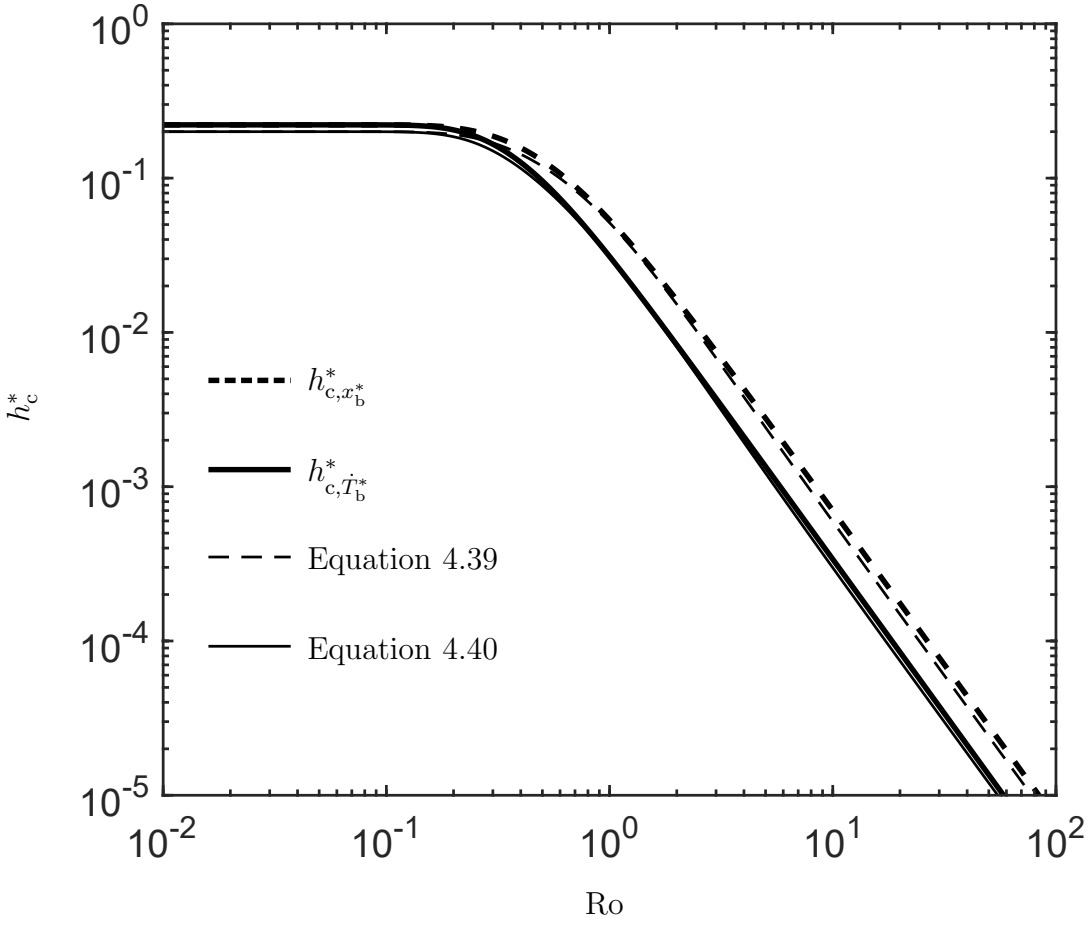

Figure 4.6: Critical values of h^* to neglect the effect of surface heat loss results in a relative errors within 10 % between side blending at side Regime III – IV and exact numerical results. The thick lines h^*_{c,x_b^*} and $h^*_{c,\dot{T}_b^*}$ are critical values for trailing length and cooling rate. The thin lines equations 4.39 and 4.40 are estimation of the critical values h_c^*.

4.8 Validation

The engineering expressions proposed for cooling rate, equations 4.35 to 4.37, are validated with data collected from published research, as illustrated in Figure 4.7 Measurements were collected for processes including: Gas Tungsten Arc Welding (GTAW), Submerged Arc Welding (SAW), Gas Metal Arc Welding (GMAW), hard facing, additive manufacturing and underwater wet welding.

The published cooling rates are normalized with Equation 4.25. Some cooling rates are reported directly at a given temperature [63, 111]. In other measurements, cooling rates are not reported directly, but calculated by cooling time, such as cooling time from 800 °C to 500 °C ($t_{8/5}$) [120, 166]. An intermediate temperature is estimated by Equation 4.53. For the case of room temperature at 20 °C, the intermediate temperature for $t_{8/5}$ calculations is 632 °C.

Thermal properties, like conductivity and diffusivity, are either listed in original sources or obtained from software (JMatPro v11). An estimate of effective thermal conductivity is in the Appendix, and estimates for other effective properties are in [130]. Thermal efficiency, the ratio of amount of heat deposited on the substrate to the heat generated, is assumed 0.8 for underwater arc welding [63, 122].

For underwater processes, surface heat loss coefficients are assumed 4000 W/m^{2}K for underwater flux-cored arc welding conducted by Li et al. [122] and 10000 W/m^{2}K for underwater wet welding conducted by Fukuoka [63], which are in the range of surface heat loss coefficients involving boiling [19]. For processes in atmosphere, the surface heat loss coefficient is assumed 100 W/m^{2}K for GTAW by Poorhaydari et al. [166] and GMAW by Fukuoka et al. [63] and 300 W/m^{2}K for hard facing by Lazic et al. [120] and additive manufacturing by Wang et al. [202].

Figure 4.7(a) compares the published data with predictions calculated with equations 4.35 and 4.36, without taking into account the correction factor for the effect of surface heat loss $g\,(\mathrm{Ro}, h^*)$. Figure 4.7(b) compares the published data with predic-

tions calculated with equations 4.35 and 4.36. In general, the predictions lacking the correction factor of surface heat loss can underestimate cooling rates severely, while the predictions with correction factors (Equation 4.37) agree with experiments and show no obvious bias.

4.9 Extensions of Results

4.9.1 Extension to different geometries

When the effects of surface heat losses are secondary, satisfying the criteria of Equation 4.40 for the case of cooling rate, the obtained engineering expressions can be extended to other geometries in addition to a flat plate, including plates of different thicknesses, thin-wall additive manufacturing, and Tee-joints [128]. Those configurations are treated as combination of half-panels. For example, a flat plate can be treated as two half-panels of the same thickness, while additive manufacturing of thin walls corresponds to a single half-panel.

All formulae developed above will be applicable to each individual half-panel by replacing q/d by q'_{eff_j}.

$$q'_{\text{eff}_j} = \frac{2q_j}{d_j} \tag{4.45}$$

When the heat intensity per unit thickness q'_{eff_j} is the same for all panels, and when the h_j^* is the same for all panels, this generalization is exact; when not, the asymmetry can cause heat transfer from one plate to another, which is not captured by the symmetric 2D formulation used here, and this generalization is only approximate. Additive manufacturing of thin walls and welding of plates of same thickness with similar heat loss conditions approximate closely the conditions for exact predictions.

4.9.2 Consideration of the bioheat equation

The "fin" treatment of heat losses, in which they are equivalent to a volumetric heat loss in a thin plate, opens the door to applying the results obtained to systems with

actual volumetric heat losses, such as energy exchange between blood and tissue in human body captured by the bioheat equation.

The bioheat equation was first introduced in [162], with generalizations to beyond 1D [44] and moving heat sources [191] and can be written in 2D as

$$\frac{\partial^2 T}{\partial x^2} + \frac{\partial^2 T}{\partial y^2} + \frac{\dot{q}_m}{k} + \frac{\omega \rho_b c_b}{k}(T_a - T) = 0 \tag{4.46}$$

where $T(x, y, z)$ is the local tissue temperature, $\dot{q}_m$ is metabolic heat generation, ω is the perfusion rate, ρ_b and c_b are blood density and specific heat, k is the thermal conductivity of tissue, and T_a is the arterial temperature entering capillaries.

With a change to Eulerian coordinates x', y' fixed to a heat source moving with constant velocity U in the x' direction and a variable substitution

$$T'(x', y') = T(x, y) - \dot{q}_m / \omega \rho_b c_b \tag{4.47}$$

Equation 4.46 can then be rewritten as

$$\frac{\partial^2 T'}{\partial x'^2} + \frac{\partial^2 T'}{\partial y'^2} = -\frac{U}{\alpha}\frac{\partial T'}{\partial x'} + \frac{\omega \rho_b c_b}{k}(T_a - T') = 0 \tag{4.48}$$

which is the exact equivalent of Equation 1 in [130] and is the governing equation for moving heat sources in 2D, of which Equation 4.2 is the solution. In this equivalency, the heat transfer by blood perfusion is captured by the surface heat loss term when

$$\frac{h + h'}{d} = \omega \rho_b c_b \tag{4.49}$$

$$T_0 = T_a \tag{4.50}$$

The expressions derived in this work are thus applicable to 2D moving heat sources in biological systems that obey the bioheat equation.

4.10 Discussion

The Ro is a key number of characterizing isotherms of 2D moving heat source problems, that has been analyzed in [128, 130]. The h^* is a dimensionless number reflecting

the significance of surface heat loss. According to the definition Equation 4.8, the value of h^* depends not only on the surface heat loss conditions h and h' on each side, but also on material properties, travel speed, plate thickness. The definition of normalized surface heat loss coefficient is consistent with the dimensionless number proposed by Kou et al. [109] and Heller et al. [84] except by a factor of 4, where h^* was interpreted as a Biot number [109] with characteristic length $\mathcal{L} = \alpha^2/kU^2$.

The value of heat loss coefficients h and h' can be measured [83] or calculated based on theoretical or semi-empirical correlations [19, 214]. The surface heat loss mechanisms usually involve convection and radiation, or thermal contact.

The natural convection coefficient h_{conv} is a magnitude of the order of 2 W/m^{2}K to 25 W/m^{2}K in gases, while forced convection involving externally imposed flows is of the order of magnitude of 25 W/m^{2}K to 250 W/m^{2}K for gases such as air or shielding gas, and of the order of magnitude of 100 W/m^{2}K to 20,000 W/m^{2}K for liquids, such as in in-service welding. The presence of bubbling in underwater wet welding is comparable to boiling heat transfer with convection coefficients of the order of 2500 W/m^{2}K to 100,000 W/m^{2}K [19]. Natural convection during welding was determined also in [15, 83].

In general, surface convection is mild and negligible for processes in air when the isotherms of melting temperature are studied. Surface heat loss for welding in air is reported less than 1 % of the heat input for aluminum alloys by Kou and Le [110], and less than 5 % for carbon steels by Tekriwal and Mazumder [193]. When study the isotherms in low temperature zones, surface heat loss is usually crucial, even for small values of h^*, because the critical value to ignore surface heat loss decreases considerably for large values of Ro, as illustrated in Figure 4.6.

The effect of surface convection is central to many processes such as welding on thin plates, underwater wet welding, in-service welding, or when considering the low-temperatures away from the heat source, as in the case of calculation of residual stresses. For thin plates, resistance to conduction in the substrate is larger than that

for thick plates, and the heat loss plays a more significant role on characteristic values.

For underwater wet welding processes, the surface heat loss coefficient could increase considerably of orders of magnitude. Habchi reported a Leidenfrost temperature (the critical temperature for film boiling) for water on stainless steel at 1 atm to be around 280 °C [80], which is below the typical temperatures of interest for processes like welding.

Besides convection, radiation and thermal contact resistance can also be taken into account with equivalent coefficients. One practical equivalent coefficient to account radiation within the formulation of this work is [19]:

$$h_{\text{rad}} = \epsilon\sigma(T_i^2 + T_0^2)(T_i + T_0) \tag{4.51}$$

where ϵ is emissivity, σ is Stefan-Boltzmann constant, and T_i is an intermediate temperature between the temperature of interest. This coefficient assumes that radiation is towards an environment at T_0. All temperatures in Equation 4.51 are in absolute scale.

The heat transfer between the workpiece and backing plate can be captured with a coefficient $h_{\text{cont}}$of the order of magnitude of 10^4 W/m^{2}K under the contact pressure in the order of $0.1 - 10$ MPa as reported by Yovanovich [226].

The total surface heat loss coefficient, h_{tot}, is the summation of the three surface heat loss coefficients.

The trailing length and cooling rate magnitudes yield much information related to the cooling time from 800 °C to 500 °C ($t_{8/5}$), which has a decisive effect on phase transformations in steel, the cooling time from solidification temperature to 100 °C which is in relevance with evolution of hydrogen and cold cracking [99], and the cooling time from 400 °C to 290 °C which affects the tensile strengths for high quench sensitivity aluminum alloy [148]. With the engineering expressions for trailing

length and cooling rate, cooling time from T_1 to T_2 can be calculated as

$$\widehat{\Delta t}\Big|_{T_1}^{T_2} = \frac{1}{U}\left(\widehat{x}_{\mathrm{b,T_2}} - \widehat{x}_{\mathrm{b,T_1}}\right) \approx \frac{T_1 - T_2}{\widehat{\dot{T}}_{\mathrm{b,T_i}}} \tag{4.52}$$

where T_i is an intermediate temperature between T_1 and T_2. Consistently with [128, 207], the intermediate temperature can be approximated by geometric mean:

$$T_{\mathrm{i}} = T_0 + \sqrt{(T_1 - T_0)(T_2 - T_0)} \tag{4.53}$$

4.11 Conclusions

Practical engineering expressions derived from fundamental analysis are presented for the trailing length (equations 4.19 to 4.22) and cooling rate (equations 4.35 to 4.37) of an isotherm for the case of 2D heat sources subject to surface heat losses. The engineering expressions depends on two dimensionless groups, Ro and h^*, and the blending technique is extended to consider two parameters. The engineering expressions developed are not empirical, and are valid for all materials (metallic or otherwise), heat sources, and surface heat losses that match the framework of the problem. Their closed-form is amenable to practical calculations, for example with spreadsheets. The predicted cooling rates are validated against experimental work from the literature (Figure 4.7(b)).

The engineering expressions coincide with the exact solution in four asymptotic regimes, and exhibit a discrepancy within 8 % of the exact solution in the intermediate regimes. A critical value of dimensionless heat transfer coefficient is proposed (equations 4.39 and 4.40); for larger values, the correction factors for surface heat losses enable predictions within acceptable errors (for Ro = $O(1)$, the critical value of h^* is around 0.01). The expressions obtained are also applicable to moving heat sources in biological tissue that can be represented with the bioheat equation.

Acknowledgment

The authors wish to acknowledge support from the Natural Sciences and Engineering Research Council of Canada (NSERC RGPIN-2019-05981). Student scholarships from the AWS and the CWB-A Foundation were also gratefully received.

References

[3] A. Acrivos, "On the solution of the convection equation in laminar boundary layer flows," *Chemical Engineering Science*, vol. 17, no. 6, pp. 457–465, 1962.

[4] A. Acrivos, "A rapid method for estimating the shear stress and the separation point in laminar incompressible boundary-layer flows," *Journal of the Aero/Space Sciences*, vol. 27, no. 4, pp. 314–315, 1960.

[15] X. Bai, H. Zhang, and G. Wang, "Improving prediction accuracy of thermal analysis for weld-based additive manufacturing by calibrating input parameters using IR imaging," *The International Journal of Advanced Manufacturing Technology*, vol. 69, no. 5-8, pp. 1087–1095, 2013.

[17] D. A. Barry, J. Parlange, L. Li, H. Prommer, C. J. Cunningham, and F. Stagnitti, "Analytical approximations for real values of the Lambert W function," *Mathematics and Computers in Simulation*, vol. 53, pp. 95–103, 2000.

[19] T. L. Bergman, F. P. Incropera, D. P. DeWitt, and A. S. Lavine, *Fundamentals of heat and mass transfer*. John Wiley & Sons, 2011.

[22] W. A. Bruce and M. A. Boring, "Comparison of methods for predicting safe parameters for welding onto in-service pipelines," in *2006 International Pipeline Conference*, American Society of Mechanical Engineers Digital Collection, 2006, pp. 283–296.

[24] E. Buckingham, "On physically similar systems; illustrations of the use of dimensional equations," *Physical Review*, vol. 4, no. 4, pp. 345–376, 1914.

[26] P. Burgardt and C. R. Heiple, "Weld penetration sensitivity to welding variables when near full joint penetration," *Welding journal*, vol. 72, no. 9, pp. 341–347, 1992.

[27] H. S. Carslaw and J. C. Jaeger, *Conduction of heat in solids*, Second. Oxford: Clarendon Press, 1959.

[29] Y. H. Chen, Y. Wang, and Z. F. Wang, "Numerical simulation of thermal cycle of in-service welding on X70 steel gas pipeline," in *Multi-Functional Materials and Structures II*, ser. Advanced Materials Research, vol. 79, Trans Tech Publications Ltd, Nov. 2009, pp. 1169–1172.

[34] S. W. Churchill and R. Usagi, "A general expression for the correlation of rates of transfer and other phenomena," *AIChE Journal*, vol. 18, no. 6, pp. 1121–1128, 1972.

[41] R. M. Corless, G. H. Gonnet, D. E. G. Hare, D. J. Jeffrey, and D. E. Knuth, "On the Lambert W function," *Advances in Computational Mathematics*, vol. 5, no. 1, pp. 329–359, 1996.

[44] Z.-S. Deng and J. Liu, "Analytical solutions to 3-D bioheat transfer problems with or without phase change," *Heat Transfer Phenomena and Applications*, p. 205, 2012.

[62] P. W. Fuerschbach and G. R. Eisler, "Determination of material properties for welding models by means of arc weld experiments," in *Trends in Welding Research, Proceedings of the 6th International Conference*, Callaway Gardens Resort, Phoenix, Arizona: ASM International, 2002.

[63] T. Fukuoka and S. Fuku, "Analysis for cooling process of underwater welding–comparison with welding in air," *Bulletin of Marine Engineering Society in Japan*, vol. 22, no. 2, pp. 86–92, 1994.

[76] M. R. Grams and P. F. Mendez, "Scaling analysis of the thermal stress field produced by a moving point heat source in a thin plate," *Journal of Applied Mechanics*, pp. 1–34, Sep. 2020.

[80] C. Habchi, "New correlations for Leidenfrost and Nukiyama temperatures with gas pressure-application to liquid film boiling simulation," in *ILASS Europe*, 2010.

[82] D. Havrylov, "Hydrodynamic regimes in autogenous fusion welding," PhD thesis, University of Alberta, 2020.

[83] J. C. Heigel, P. Michaleris, and E. W. Reutzel, "Thermo-mechanical model development and validation of directed energy deposition additive manufacturing of Ti–6Al–4V," *Additive manufacturing*, vol. 5, pp. 9–19, 2015.

[84] K. Heller, S. Kessler, F. Dorsch, P. Berger, and T. Graf, "Analytical description of the surface temperature for the characterization of laser welding processes," *International Journal of Heat and Mass Transfer*, vol. 106, pp. 958–969, 2017.

[97] P. Jhaveri, W. G. Moffatt, and C. M. Adams, "The effect of plate thickness and radiation on heat flow in welding and cutting," *Welding Research Supplement*, vol. 41, no. 1, 12s–16s, 1962.

[99] T. Kasuya and N. Yurioka, "Prediction of welding thermal history by a comprehensive solution," *Welding Research Supplement*, vol. 72, no. 3, 107s–115s, 1993.

[105] R. Komanduri and Z. B. Hou, "Thermal analysis of the arc welding process. Part II: Effect of variation of thermophysical properties with temperature.," *Metallurgical and Materials Transactions B*, vol. 32, no. 3, 2001.

[109] S. Kou, T. Kanevsky, and S. Fyfitch, "Welding thin plates of aluminum alloys–a quantitative heat-flow analysis," *Welding Research Supplement*, vol. 61, no. 6, 175s–181s, 1982.

[110] S. Kou and Y. Le, "Three-dimensional heat flow and solidification during the autogeneous GTA welding of aluminum plates," *Metallurgical Transactions A*, vol. 14, no. 11, pp. 2245–2253, 1983.

[111] S. Kou and Y. Le, "Welding parameters and the grain structure of weld metal – A thermodynamic consideration," *Metallurgical Transactions A*, vol. 19, no. 4, pp. 1075–1082, 1988.

[120] V. N. Lazić, A. S. Sedmak, M. M. Živković, S. M. Aleksandrović, R. D. Čukić, R. D. Jovičić, and I. B. Ivanović, "Theoretical-experimental determining of cooling time ($t_8/5$) in hard facing of steels for forging dies," *Thermal Science*, vol. 14, no. 1, pp. 235–246, 2010.

[122] H. Li, D. Liu, Y. Yan, N. Guo, Y. Liu, and J. Feng, "Effects of heat input on arc stability and weld quality in underwater wet flux-cored arc welding of E40 steel," *Journal of Manufacturing Processes*, vol. 31, pp. 833–843, 2018.

[128] Y. Lu and P. F. Mendez, "Characteristic values of the temperature field induced by a moving line heat source," *International Journal of Heat and Mass Transfer*, p. 120 671, 2020.

[130] Y. Lu, Y. Wang, and P. F. Mendez, "Width of thermal features induced by a 2-D moving heat source," *International Journal of Heat and Mass Transfer*, vol. 156, p. 119 793, 2020.

[135] P. F. Mendez, "Reduced order models for welding and solidification processes," in *Proceedings of the 15th Modelling of Casting, Welding and Advanced Solidification Processes Conference (MCWASP XV)*, IOP Conference series: Materials Science and Engineering, 2020.

[140] P. F. Mendez, Y. Lu, and Y. Wang, "Scaling analysis of a moving point heat source in steady- state on a semi-infinite solid," *Journal of Heat Transfer*, vol. 140, no. 8, p. 081 301, 2018.

[144] Y. S. Muzychka and M. M. Yovanovich, "Thermal resistance models for non-circular moving heat sources on a half space," *Journal of Heat Transfer*, vol. 123, no. 4, pp. 624–632, 2001.

[148] T. W. Nelson, R. J. Steel, and W. J. Arbegast, "In situthermal studies and post-weld mechanical properties of friction stir welds in age hardenable aluminium alloys," *Science and Technology of Welding and Joining*, vol. 8, no. 4, pp. 283–288, Aug. 2003.

[162] H. H. Pennes, "Analysis of tissue and arterial blood temperatures in the resting human forearm," *Journal of applied physiology*, vol. 1, no. 2, pp. 93–122, 1948.

[166] K. Poorhaydari, B. M. Patchett, and D. G. Ivey, "Estimation of cooling rate in the welding of plates with intermediate thickness," *Welding Journal*, vol. 84, no. 10, 149s–155s, 2005.

[175] D. Rosenthal, "The theory of moving sources of heat and its application to metal treatments," *Transactions of the A.S.M.E.*, vol. 68, pp. 849–866, 1946.

[191] M. R. Talaee and A. Kabiri, "Exact analytical solution of bioheat equation subjected to intensive moving heat source," *Journal of Mechanics in Medicine and Biology*, vol. 17, no. 05, p. 1 750 081, 2017.

[193] P. Tekriwal and J. Mazumder, "Finite element analysis of three-dimensional transient heat transfer in GMA welding," *Welding Research Supplement*, vol. 67, 150s–156s, 1988.

[202] L. Wang, S. Felicelli, Y. Gooroochurn, P. T. Wang, and M. F. Horstemeyer, "Optimization of the LENS® process for steady molten pool size," *Materials Science and Engineering: A*, vol. 474, no. 1-2, pp. 148–156, 2008.

[203] L. Wang and S. Felicelli, "Analysis of thermal phenomena in LENS^{TM} deposition," *Materials Science and Engineering: A*, vol. 435, pp. 625–631, 2006.

[207] Y. Wang, Y. Lu, and P. F. Mendez, "Scaling expressions of characteristic values for a moving point heat source in steady state on a semi-infinite solid," *International Journal of Heat and Mass Transfer*, vol. 135, pp. 1118–1129, 2019.

[214] J. B. Will, N. P. Kruyt, and C. H. Venner, "An experimental study of forced convective heat transfer from smooth, solid spheres," *International Journal of Heat and Mass Transfer*, vol. 109, pp. 1059–1067, 2017.

[215] H. A. Wilson, "On convection of heat," in *Proceedings of the Cambridge Philosophical Society*, vol. 12, 1904, pp. 406–423.

[226] M. M. Yovanovich, "Four decades of research on thermal contact, gap, and joint resistance in microelectronics," *IEEE transactions on components and packaging technologies*, vol. 28, no. 2, pp. 182–206, 2005.

Appendix 4.A Asymptotics of x_{b}^* in the asymptotic side Regime III – IIIa

In the asymptotic side Regime III – IIIa, where $\mathrm{Ro} \to \infty$ and $T_c^* \to 0$, $-x_{\mathrm{b_{III\text{-}IIIa}}}^* \sqrt{h^*+1}$ tends to infinity since $\exp(-x_{\mathrm{b_{III\text{-}IIIa}}}^*) > 1$ for $x_{\mathrm{b_{III\text{-}IIIa}}}^* < 0$. Therefore, centerline temperature distribution in Regimes III – IIIa is:

$$T_{\mathrm{c}}^* = \exp\left[x_{\mathrm{b_{III\text{-}IIIa}}}^* \left(\sqrt{1+h^*}-1\right)\right] \cdot \left[\sqrt{\frac{\pi}{-2\sqrt{1+h^*}x_{\mathrm{b_{III\text{-}IIIa}}}^*}} + O\left(\sqrt{1+h^*}x_{\mathrm{b_{III\text{-}IIIa}}}^*\right)^{-\frac{3}{2}}\right] \tag{4.54}$$

For simplicity, the denotation $w = W\left[\pi\left(1-\frac{1}{\sqrt{1+h^*}}\right)\mathrm{Ro}^2\right]$ is utilized in the current section. Let $x_{\mathrm{b_{III\text{-}IIIa}}}^* = -\frac{w}{2\left(\sqrt{1+h^*}-1\right)}(1+\epsilon)$, and to find the solution to trailing length is equivalent to finding ϵ. Because there is one root to ϵ corresponding to each Ro, if ϵ is solved based on assumption $\epsilon \ll 1$, the asymptotic is achieved. The right side of temperature distribution, Equation 4.54, can be rewritten asymptotically,

$$T_{\mathrm{c}}^* \quad = \quad \exp\left[-\frac{w\left(\epsilon+1\right)}{2}\right]\sqrt{\frac{\pi\left(\sqrt{1+h^*}-1\right)}{w\left(\epsilon+1\right)\sqrt{1+h^*}}} \cdot \left[1+O\left(\frac{\sqrt{1+h^*}-1}{w\sqrt{1+h^*}}\right)\right] \tag{4.55}$$

The root of ϵ is found:

$$\epsilon = \frac{W\left\{\pi\left(1-\frac{1}{\sqrt{1+h^*}}\right)\mathrm{Ro}^2\left[1+O\left(\frac{\sqrt{1+h^*}-1}{w\sqrt{1+h^*}}\right)\right]\right\}}{W\left[\pi\left(1-\frac{1}{\sqrt{1+h^*}}\right)\mathrm{Ro}^2\right]} - 1 \tag{4.56}$$

Because $\frac{W[\chi(\upsilon+1)]}{W(\chi)} = 1 + \frac{\upsilon}{W(\chi)+1} + O\left(\upsilon^2\right) = 1 + O\left(\upsilon\right)$ when $\upsilon \to 0$, the ϵ is:

$$\epsilon = O\left\{\frac{1-\frac{1}{\sqrt{1+h^*}}}{W\left[\pi\left(1-\frac{1}{\sqrt{1+h^*}}\right)\mathrm{Ro}^2\right]}\right\} \tag{4.57}$$

Because

$$\frac{d}{dh^*}\frac{1-\frac{1}{\sqrt{1+h^*}}}{W\left[\pi\left(1-\frac{1}{\sqrt{1+h^*}}\right)\mathrm{Ro}^2\right]} = \frac{1/2\left(h^*+1\right)^{-\frac{3}{2}}}{1+W\left[\pi\left(1-\frac{1}{\sqrt{1+h^*}}\right)\mathrm{Ro}^2\right]} > 0$$

,

$$\epsilon = O\left\{\lim_{h^*\to\infty}\frac{1-\frac{1}{\sqrt{1+h^*}}}{W\left[\pi\left(1-\frac{1}{\sqrt{1+h^*}}\right)\mathrm{Ro}^2\right]}\right\} = O\left[\frac{1}{W\left(\pi\mathrm{Ro}^2\right)}\right] \ll 1 \qquad \text{as} \quad \mathrm{Ro} \quad \to \infty \tag{4.58}$$

As the solution to ϵ is found and much smaller than one, the solution to trailing length is

$$x^*_{\text{b}_{\text{III-IIIa}}} = -\frac{W\left[\pi\left(1-\frac{1}{\sqrt{1+h^*}}\right)\text{Ro}^2\right]}{2\left(\sqrt{1+h^*}-1\right)} \cdot \left\{1+O\left[\frac{1}{W\left(\pi\text{Ro}^2\right)}\right]\right\} \quad (4.59)$$

The asymptotic expression for the dimensionless trailing length when $\text{Ro}\to\infty$ (the asymptotic side III – IIIa) is:

$$\widehat{x}^*_{\text{b}_{\text{III-IIIa}}} = -\frac{W\left[\pi\left(1-\frac{1}{\sqrt{1+h^*}}\right)\text{Ro}^2\right]}{2\left(\sqrt{1+h^*}-1\right)} \quad (4.60)$$

In Regime III when $h^*\to 0$, $\pi\left(1-\frac{1}{\sqrt{1+h^*}}\right)\text{Ro}^2$ tends to zero, and the Equation 4.60 can thus be simplified to asymptotic expression of trailing length in Regime III:

$$\widehat{x}^*_{\text{b}_{\text{III}}} = -\frac{\pi\text{Ro}^2}{2} \quad (4.61)$$

In regime IIIa when $h^*\to\infty$, the asymptotic expression can be derived from Equation 4.60 as:

$$\widehat{x}^*_{\text{b}_{\text{IIIa}}} = -\frac{W\left(\pi\text{Ro}^2\right)}{2\sqrt{h^*}} \quad (4.62)$$

Appendix 4.B Asymptotics of x^*_{b} in the asymptotic side Regime IV − IVa

In the asymptotic side Regime IV – IVa when $\text{Ro}\to 0$, $x^*_{\text{b}_{\text{IV-IVa}}}\to 0$ $x^*_{\text{b}_{\text{IV-IVa}}}\sqrt{h^*+1}\to 0$, and temperature distribution at centerline can thus be written as:

$$T^* = \left[1+O\left(x^*_{\text{b}_{\text{IV-IVa}}}\right)\right]\cdot\left[\ln\left(\frac{2}{-x^*_{\text{b}_{\text{IV-IVa}}}\sqrt{h^*+1}}\right)-\gamma+O\left(x^*_{\text{b}_{\text{IV-IVa}}}\sqrt{h^*+1}\right)\right] \quad (4.63)$$

Let $x^*_{\text{b}_{\text{IV-IVa}}} = -\frac{2}{\sqrt{h^*+1}}\exp\left(-\frac{1}{\text{Ro}}-\gamma\right)(1+\epsilon)$, assuming $\epsilon\ll 1$, resulting in the following temperature field at trailing length:

$$T^* = \left[1+O\left(\text{e}^{-\frac{1}{\text{Ro}}}\right)\right]\left\{\ln\left[(1+\epsilon)\,\text{e}^{\frac{1}{\text{Ro}}}\right]+O\left(\text{e}^{-\frac{1}{\text{Ro}}}\right)\right\} \quad (4.64)$$

The ϵ is solved:

$$\epsilon = \mathrm{e}^{\frac{O\left(\mathrm{e}^{-\frac{1}{\mathrm{Ro}}}\right)-\gamma}{O\left(\mathrm{e}^{-\frac{1}{\mathrm{Ro}}}\right)+1}-\frac{1}{\mathrm{Ro}\left[O\left(1+\mathrm{e}^{-\frac{1}{\mathrm{Ro}}}\right)\right]}+\frac{1}{\mathrm{Ro}}+\gamma} - 1 = \quad O\left(\tfrac{1}{\mathrm{Ro}}\mathrm{e}^{-\frac{1}{\mathrm{Ro}}}\right) \ll 1 \qquad \text{as} \quad \mathrm{Ro} \to 0 \tag{4.65}$$

Therefore, the solution to trailing length for $\mathrm{Ro} \to 0$ is:

$$x^*_{\mathrm{b_{IV\text{-}IVa}}} = -\frac{2\mathrm{e}^{-\frac{1}{\mathrm{Ro}}-\gamma}}{\sqrt{h^*+1}}\left[1+O\left(\tfrac{1}{\mathrm{Ro}}\mathrm{e}^{-\frac{1}{\mathrm{Ro}}}\right)\right] \tag{4.66}$$

and the asymptotic for x^*_{b} in the asymptotic side Regime IV – IVa is:

$$\widehat{x}^*_{\mathrm{b_{IV\text{-}IVa}}} = -\frac{2}{\sqrt{h^*+1}}\exp\left(-\tfrac{1}{\mathrm{Ro}}-\gamma\right) \tag{4.67}$$

In Regime IV when $h^* \to 0$, the Equation 4.67 can be simplified to asymptotic expression of trailing length in Regime IV:

$$\widehat{x}^*_{\mathrm{b_{IV}}} = -2\exp\left(-\tfrac{1}{\mathrm{Ro}}-\gamma\right) \tag{4.68}$$

In Regime IVa when $h^* \to \infty$, the Equation 4.67 can be simplified to asymptotic expression of trailing length in Regime IVa:

$$\widehat{x}^*_{\mathrm{b_{IVa}}} = -\frac{2}{\sqrt{h^*}}\exp\left(-\tfrac{1}{\mathrm{Ro}}-\gamma\right) \tag{4.69}$$

Appendix 4.C Asymptotics of $\dot{T}^*_{\mathrm{b}}$ in the asymptotic side Regime III – IIIa

In the asymptotic side Regime III – IIIa, $-x^*_{\mathrm{b}}\sqrt{h^*+1} \to \infty$, the right side of Equation 4.26 could be expressed asymptotically:

$$\dot{T}^*_{\mathrm{b}} = \frac{1}{\mathrm{Ro}}\left[1-\sqrt{h^*+1}+\frac{1}{2x^*_{\mathrm{b_{III\text{-}IIIa}}}}+O\left(\frac{1}{\sqrt{h^*+1}x^*_{\mathrm{b_{III\text{-}IIIa}}}}\right)^2\right] \tag{4.70}$$

$$= \frac{1}{\mathrm{Ro}}\left\{1-\sqrt{h^*+1}+\frac{1}{2x^*_{\mathrm{b_{III\text{-}IIIa}}}\left\{O\left[\frac{1}{W\left(\pi\mathrm{Ro}^2\right)}\right]+1\right\}}+O\left(\frac{1}{\sqrt{h^*+1}x^*_{\mathrm{b_{III\text{-}IIIa}}}}\right)^2\right\} \tag{4.71}$$

$$= \frac{1}{\mathrm{Ro}}\left\{1-\sqrt{h^*+1}+\frac{1}{2x^*_{\mathrm{b_{III\text{-}IIIa}}}}+O\left[\frac{1}{x^*_{\mathrm{b_{III\text{-}IIIa}}}W\left(\pi\mathrm{Ro}^2\right)}\right]+O\left(\frac{1}{\sqrt{h^*+1}x^*_{\mathrm{b_{III\text{-}IIIa}}}}\right)^2\right\} \tag{4.72}$$

Because $O\left[\frac{1}{x^*_{\mathrm{b_{III\text{-}IIIa}}} W\left(\pi \mathrm{Ro}^2\right)}\right] \ll \left|\frac{1}{2x^*_{\mathrm{b_{III\text{-}IIIa}}}}\right|$ and $O\left(\frac{1}{\sqrt{h^*+1}x^*_{\mathrm{b_{III\text{-}IIIa}}}}\right)^2 \ll \left|\frac{1}{2x^*_{\mathrm{b_{III\text{-}IIIa}}}}\right|$ for large Ro number and $\left|x^*_{\mathrm{b}}\sqrt{h^*+1}\right|$, the asymptotic cooling rate is derived by substitution Equation 4.59:

$$\widehat{\dot{T}}^*_{\mathrm{b_{III\text{-}IIIa}}} = -\frac{\sqrt{h^*+1}-1}{\mathrm{Ro}} \left\{ 1 + \frac{1}{W\left[\pi\left(1-\frac{1}{\sqrt{h^*+1}}\right)\mathrm{Ro}^2\right]} \right\} \tag{4.73}$$

In Regime IIIa, h^* tends to infinity, the asymptotic cooling rate is:

$$\widehat{\dot{T}}^*_{\mathrm{b_{IIIa}}} = -\frac{\sqrt{h^*}}{\mathrm{Ro}} \tag{4.74}$$

In Regime III, h^* tends to zero, the asymptotic cooling rate is:

$$\widehat{\dot{T}}^*_{\mathrm{b_{III}}} = -\frac{1}{\pi \mathrm{Ro}^3} \tag{4.75}$$

Appendix 4.D Asymptotics of $\dot{T}^*_{\mathrm{b}}$ in the asymptotic side Regime IV – IVa

In the asymptotic side Regime IV – IVa, $-x^*_{\mathrm{b}}\sqrt{h^*+1} \to 0$, the right side of Equation 4.26 could be expressed asymptotically:

$$\widehat{\dot{T}}^*_{\mathrm{b_{IV\text{-}IVa}}} \quad = \quad -\frac{1}{-x^*_{\mathrm{b}}\mathrm{Ro}\left[\ln\left(-\frac{1}{2}\sqrt{h+1}x^*_{\mathrm{b}}\right)+\gamma\right]} \quad + \quad O\left(\frac{1}{\mathrm{Ro}}\right) \tag{4.76}$$

Bringing the solution to trailing length Equation 4.67 into Equation 4.76, the cooling rate is:

$$\begin{aligned}\widehat{\dot{T}}^*_{\mathrm{b}} &= -\frac{\sqrt{h^*+1}\,\mathrm{e}^{\frac{1}{\mathrm{Ro}}+\gamma}}{2\left[1+O\left(\frac{1}{\mathrm{Ro}}\mathrm{e}^{-\frac{1}{\mathrm{Ro}}}\right)\right]\left[1+O\left(\mathrm{e}^{-\frac{1}{\mathrm{Ro}}}\right)\right]} + O\left(\frac{1}{\mathrm{Ro}}\right) \\ &= -\frac{1}{2}\sqrt{h^*+1}\,\mathrm{e}^{\frac{1}{\mathrm{Ro}}+\gamma} + O\left(\frac{\sqrt{h^*+1}}{\mathrm{Ro}}\right)\end{aligned} \tag{4.77}$$

Because $O\left(\frac{\sqrt{h+1}}{\mathrm{Ro}}\right) \ll \left|-\frac{1}{2}\sqrt{h^*+1}\,\mathrm{e}^{\frac{1}{\mathrm{Ro}}+\gamma}\right|$ for small Ro number, the asymptotic cooling rate in the asymptotic side Regime IV – IVa is:

$$\widehat{\dot{T}}^*_{\mathrm{b_{IV\text{-}IVa}}} = -\frac{1}{2}\sqrt{h^*+1}\,\mathrm{e}^{\frac{1}{\mathrm{Ro}}+\gamma} \tag{4.78}$$

In Regime IVa, h^* tends to infinity, the asymptotic cooling rate is:

$$\widehat{\dot{T}}^*_{\mathrm{b_{IVa}}} = -\frac{\sqrt{h^*}}{2}\,\mathrm{e}^{\frac{1}{\mathrm{Ro}}+\gamma} \tag{4.79}$$

In Regime IV, h^* tends to zero, the asymptotic cooling rate is:

$$\widehat{\dot{T}}^*_{\mathrm{b_{IV}}} = -\frac{1}{2}\,\mathrm{e}^{\frac{1}{\mathrm{Ro}}+\gamma} \tag{4.80}$$

Appendix 4.E Critical surface heat loss

For small h^*, trailing length is expressed as perturbation $x^*_{\mathrm{b}} = x^*_{\mathrm{b_{III\text{-}IV}}} + \delta_x$, where $\delta_x \ll x^*_{\mathrm{b_{III\text{-}IV}}}$. Substitution of $x^*_{\mathrm{b}} = x^*_{\mathrm{b_{III\text{-}IV}}} + \delta_x$ into Equation 4.3 yields the following temperature distribution at the trailing length:

$$\begin{aligned} T^*_{\mathrm{c}} &= \mathrm{e}^{-x^*_{\mathrm{b_{III\text{-}IV}}}-\delta_x} K_0\left[-\left(x^*_{\mathrm{b_{III\text{-}IV}}}+\delta_x\right)\sqrt{h^*+1}\right] \\ &\approx T^*_{\mathrm{c}} - T^*_{\mathrm{c}}\left[\delta_x - \left(\delta_x + \tfrac{h^* x^*_{\mathrm{b_{III\text{-}IV}}}}{2}\right)\frac{K_1\left(-x^*_{\mathrm{b_{III\text{-}IV}}}\right)}{K_0\left(-x^*_{\mathrm{b_{III\text{-}IV}}}\right)}\right] \end{aligned} \tag{4.81}$$

Thus, the solution to δ_x is:

$$\delta_x \approx \frac{h^* x^*_{\mathrm{b_{III\text{-}IV}}} K_1\left(-x^*_{\mathrm{b_{III\text{-}IV}}}\right)}{2\left[K_0\left(-x^*_{\mathrm{b_{III\text{-}IV}}}\right) - K_1\left(-x^*_{\mathrm{b_{III\text{-}IV}}}\right)\right]} \tag{4.82}$$

Considering certain percent error $\epsilon_{\mathrm{A}} = \left|\frac{\delta_x}{x^*_{\mathrm{b_{III\text{-}IV}}}}\right|$, the critical value of h^*_c to neglect surface heat loss for trailing length can be obtained:

$$h^*_{\mathrm{c},x^*_{\mathrm{b}}} \approx 2\epsilon_{\mathrm{A}}\left[1 - \frac{K_0\left(-\widehat{x}^*_{\mathrm{b_{III\text{-}IV}}}\right)}{K_1\left(-\widehat{x}^*_{\mathrm{b_{III\text{-}IV}}}\right)}\right] \tag{4.83}$$

In Regimes III, when $\mathrm{Ro} \to \infty$, Equation 4.83 is simplified as:

$$h^*_{\mathrm{c},x^*_{\mathrm{b}}} \approx \frac{2\epsilon_{\mathrm{A}}}{\pi \mathrm{Ro}^2} \tag{4.84}$$

In Regimes IV, when $\mathrm{Ro} \to 0$, Equation 4.83 is simplified as:

$$h^*_{\mathrm{c},x^*_{\mathrm{b}}} \approx 2\epsilon_{\mathrm{A}} \tag{4.85}$$

For small values of h^*, according to Equation 4.82 and 4.26, the cooling rate can be written as:

$$\dot{T}_{\mathrm{b}}^* = \frac{1}{\mathrm{Ro}}\left\{1 - \frac{\sqrt{h^*+1}K_1\left[-\sqrt{h^*+1}\left(x^*_{\mathrm{b_{III\text{-}IV}}}+\delta_x\right)\right]}{K_0\left[-\sqrt{h^*+1}\left(x^*_{\mathrm{b_{III\text{-}IV}}}+\delta_x\right)\right]}\right\}$$
$$\approx \dot{T}^*_{\mathrm{b_{III\text{-}IV}}}\left\{1+\frac{h^*}{2}\left[\left(x^*_{\mathrm{b_{III\text{-}IV}}}+1\right)K_1\left(-x^*_{\mathrm{b_{III\text{-}IV}}}\right)^2 - x^*_{\mathrm{b_{III\text{-}IV}}}K_0\left(-x^*_{\mathrm{b_{III\text{-}IV}}}\right)^2\right]\left[K_0\left(-x^*_{\mathrm{b_{III\text{-}IV}}}\right)-K_1\left(-x^*_{\mathrm{b_{III\text{-}IV}}}\right)\right]^{-2}\right\} \quad (4.86)$$

Considering certain relative error $\epsilon_{\mathrm{A}} = \left|\dot{T}^*_{\mathrm{b_{III\text{-}IV}}}/\dot{T}^*_{\mathrm{b}} - 1\right|$, the critical value of h^*_c to neglect surface heat loss for cooling rate can be obtained:

$$h^*_{\mathrm{c},\dot{T}^*_{\mathrm{b}}} = \left|2\epsilon_{\mathrm{A}}\left[K_0\left(-x^*_{\mathrm{b_{III\text{-}IV}}}\right)-K_1\left(-x^*_{\mathrm{b_{III\text{-}IV}}}\right)\right]^2\cdot \left[\left(x^*_{\mathrm{b_{III\text{-}IV}}}+1\right)K_1\left(-x^*_{\mathrm{b_{III\text{-}IV}}}\right)^2 - x^*_{\mathrm{b_{III\text{-}IV}}}K_0\left(-x^*_{\mathrm{b_{III\text{-}IV}}}\right)^2\right]^{-1}\right| \quad (4.87)$$

In Regime III, when $\mathrm{Ro}\to\infty$, Equation 4.83 is simplified as:

$$h^*_{\mathrm{c},\dot{T}^*_{\mathrm{b}}} \approx \frac{\epsilon_{\mathrm{A}}}{\pi \mathrm{Ro}^2} \quad (4.88)$$

In Regime IV, when $\mathrm{Ro}\to 0$, Equation 4.83 is simplified as:

$$h^*_{\mathrm{c},\dot{T}^*_{\mathrm{b}}} \approx 2\epsilon_{\mathrm{A}} \quad (4.89)$$

Appendix 4.F Estimation of effective thermal conductivity

An effective thermal conductivity k_{eff} can be approximated as the constant conductivity yielding the same thermal resistance in a wall of thickness L in steady state.

$$\mathcal{R}'' = -\frac{\Delta T}{q''} = \frac{L}{k_{\mathrm{eff}}} \quad (4.90)$$

where $\mathcal{R}''$ is the thermal resistance associated with the absolute values of heat flux q'' in the direction of coordinate ξ, perpendicular to the wall, and temperature difference ΔT through the thickness d of the wall. In steady state, without accumulation or depletion of heat:

$$q'' = -k(T)\frac{\mathrm{d}T}{\mathrm{d}\xi} = \text{constant} \quad (4.91)$$

Integrating Equation 4.91 along the thickness of the wall results in

$$\int_0^L -k(T)\frac{\mathrm{d}T}{\mathrm{d}\xi}\mathrm{d}\xi = \int_{T_1}^{T_2} -k(T)dT = q''L \tag{4.92}$$

Combining equations 4.92 and 4.90 results in

$$k_{\text{eff}} = \frac{1}{\Delta T}\int_0^L k(T)dT \tag{4.93}$$

indicating that a good approximation to the effective value of thermal conductivity is the average value between two temperatures. For problems involving just one temperature of interest, the average is suggested between T_0 and the temperature of interest T_{c}. For problems involving a temperature range, the suggested average is within that range, for example, between 800 °C and 500 °C for $t_{8/5}$.

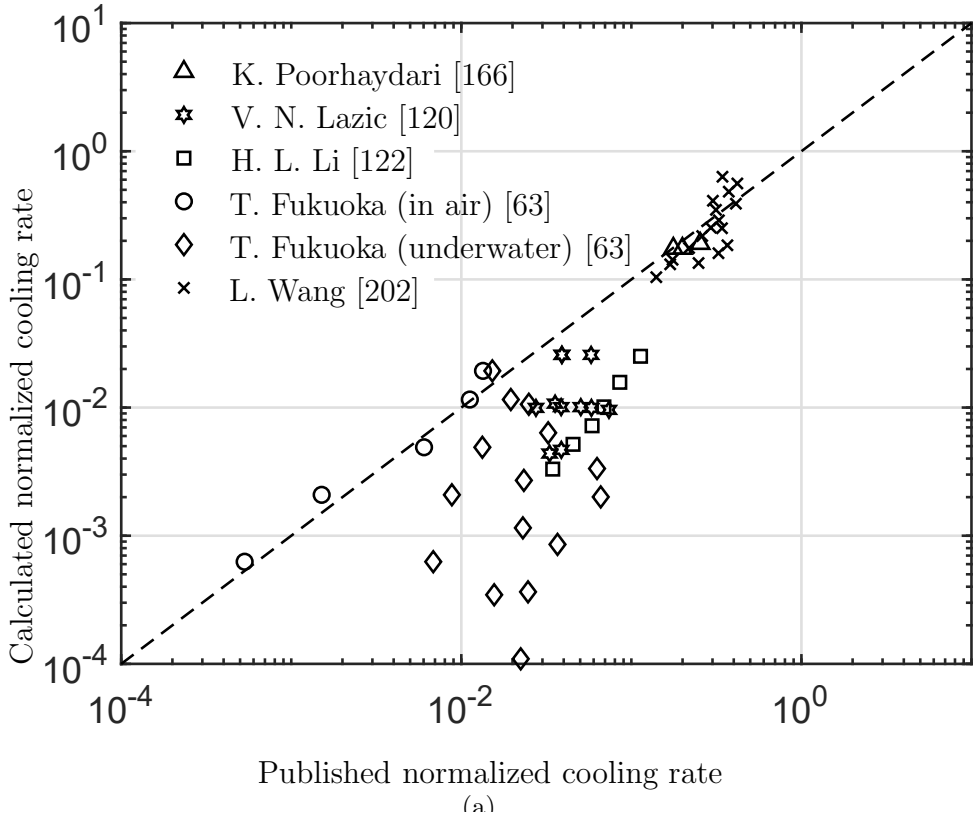

(a)

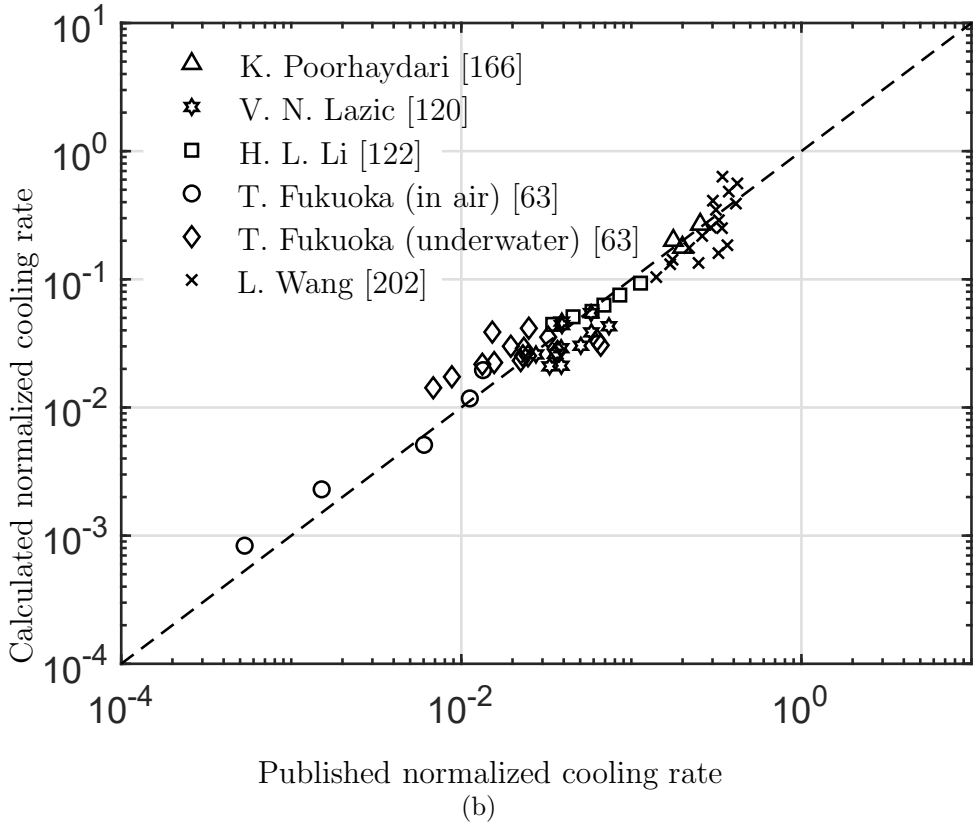

(b)

Figure 4.7: Comparisons of predictions of cooling rate. 4.7(a): Equation 4.35 without corrections for surface heat loss. 4.7(b): Equation 4.37 with correction factors for surface heat loss.

Chapter 5

Width of thermal features induced by a moving heat source on a thin plate with surface heat losses

5.1 Abstract

This paper proposes explicit expressions to estimate isotherm half-width and its location of moving heat source on a thin plate with correction factors for the effect of surface heat losses. The expressions depend on two dimensionless groups: the Rosenthal number relative to the intensity of the heat source and h^* representing the effects of surface heat losses. A systematic approach is proposed to establish 2-D blending with the two dimensionless groups, which yields predictive equations in closed-form within 9.6 % and 12 % of the exact solution for isotherm width and location. Validation against published experimental results and simulations shows a close agreement with the predictive equations.

Table 5.1: Notation

Variables	**Unit**	**Description**
d	m	Thickness of the substrate
h	$\mathrm{W\,m^{-2}\,K^{-1}}$	Convection coefficient on top surface
h'	$\mathrm{W\,m^{-2}\,K^{-1}}$	Convection coefficient on bottom surface

Continued on next page

Table 5.1 – continued from previous page

Variables	Unit	Description
k	$\mathrm{W\,m^{-1}\,K^{-1}}$	Thermal conductivity of the substrate
K_0		Modified Bessel function of the second kind, zero order
q	W	Power absorbed by substrate
r	m	Distance from the heat source
T	K	Temperature
T_0	K	Far temperature or preheat
u_c		Dependent variable for 2-D blending
U	$\mathrm{m\,s^{-1}}$	Travel speed of the moving heat source
W		Lambert function
x, y	m	Cartesian coordinates
Greek symbols		
α	$\mathrm{m^2\,s^{-1}}$	Thermal diffusivity of the substrate
γ		Euler–Mascheroni constant
η	1	Thermal efficiency
Π		Independent variables for 2-D blending
Superscripts		
*		Dimensionless value
$\widehat{\ }$		Asymptotic behavior
$^+$		Correction for intermediate regions
Subscripts		
c		Critical values
max		Related to maximum isotherm half-width
III		Regime III
IV		Regime IV
IIIa		Regime IIIa

Continued on next page

Table 5.1 – continued from previous page

Variables	Unit	Description
IVa		Regime IVa

5.2 Introduction

The estimation of the half-width of an isotherm is one of the central questions in analyzing moving heat sources. For example, in laser cladding, the half-width of the melting isotherm determines the half-width of the bead [219]; in the analysis of thermal distortions in welding or additive manufacturing, the amount of material experiencing plasticity is determined by the isotherm of yield temperature [76].

While numerical simulations can often make an accurate prediction, in practice, engineers typically resort to previous experience or trial and error when developing parameters for moving heat sources. Engineering expressions and empirical formulae have been explored to predict the half-width of an isotherm induced by a moving heat source in a very large substrate [140] and a 2-D situation such as thin plates [70, 84, 88, 96, 130, 145, 190, 213]. For neither of these cases, the effect of surface heat losses was considered.

While for moving heat sources on a thick substrate, the effect of surface heat losses is negligible in almost all practical conditions. The effects of surface heat losses on a thin substrate are relevant in two common families of problems. The first type of problems includes systems experiencing intense convection, such as in-service welding where the weld is made on a pipe carrying a moving fluid [22], or underwater wet welding [67], in which the plate is exposed to the convective cooling of water. The second type of problems includes the calculation of residual stresses during welding, in which the yield temperature is low (of the order of 100 °C), compared to other temperatures of interest such as melting (around 1500 °C for steels) or transformations (around 700 °C in steels).

The aim of this work is not to obtain predictions for particular cases, for which numerical simulations are already very advanced [222]; or to solve particular problems, which are routinely solved by trial and error in practice. Instead, this work aims to provide predictions of great generality, simplicity, and accurate enough for practical applications. The results presented here are valid for any material and any type of heat source within the basic hypotheses.

The work presented here is part of a broader research program aimed at identifying moving heat source features and presenting practical and accurate predictive expressions useful to practitioners. The overall program is based on the understanding that many important aspects of complex problems such as welding and additive manufacturing can be treated using a minimal representation that captures only the dominant physics, with the secondary physics included as correction factors. This approach is often used in all engineering disciplines at an intuitive level, and a formal implementation is described in [134, 137, 140, 141, 144, 167, 218].

The proposed predictive equations consist of closed-form asymptotic solutions and correction factors to account for intermediate cases. In this work, the asymptotic cases are based on Rosenthal's 2-D solution [176], also called the "thin plate" solution or "line heat source" solution. This solution is accurate enough to be used routinely used in practice for a wide range of materials and problems including arc welding [62, 160, 176, 213], laser and electron beam welding [73, 85, 190], metal cutting [66, 149], thermal forming of shells [227], and has even been adapted to mass transfer [171].

5.3 Governing equation

The model considered in this work consists of a point heat source of intensity q moving with constant velocity along a straight path on a thin plate of thickness d, infinite length and width, and constant thermophysical properties, as illustrated in Figure 5.1.

The formulation of this problem is discussed in detail in [130]. The governing

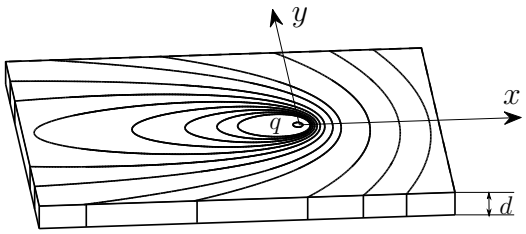

Figure 5.1: Isotherms for a point heat source of intensity q on a thin substrate of thickness d. The domain is $-\infty < x < \infty, -\infty < y < \infty$ and gradients in z are negligible [130].

equation is:

$$\frac{\partial^2 T}{\partial x^2} + \frac{\partial^2 T}{\partial y^2} = -\frac{U}{\alpha}\frac{\partial T}{\partial x} + \frac{h + h'}{kd}(T - T_0) \tag{5.1}$$

with the following boundary conditions:

$$\frac{\partial T}{\partial r} = -\frac{q}{2\pi r k d} \qquad \text{as } r \to 0 \tag{5.2}$$

$$T = T_0 \qquad \text{as } r \to \infty \tag{5.3}$$

where x, y are the coordinates defined in Figure 5.1, $r = \sqrt{x^2 + y^2}$ is the distance to the heat source, T is the temperature field, q and U are the rate of heat and velocity of the heat source, h and h' are surface heat loss coefficients on the top and bottom surfaces combining the effects of convection, radiation and contact resistance, α, k, d and T_0 are the thermal diffusivity, conductivity, thickness and initial temperature of the substrate.

This equation approximates the surface heat losses as volumetric losses, as it is common in the study of fins, which is accurate for substrates with a small Biot number Bi$= (h + h')d/k$. Equation 5.1 can also capture the transient behavior of a fin under the condition of an instant amount of heat deposited at the root. This problem is of much relevance for the calculation of residual stresses in manufacturing processes involving moving heat sources such as additive manufacturing of walls or welding of relatively thin plates [77].

The solution of Equation 5.1 with boundary conditions of equations 5.2-5.3 and

accounting for surface heat losses was first obtained by [176]:

$$T(x,y) = T_0 + \frac{q}{2\pi kd} \exp\left(-\frac{Ux}{2\alpha}\right) K_0 \left[r\sqrt{\left(\frac{U}{2\alpha}\right)^2 + \frac{h+h'}{kd}} \right] \tag{5.4}$$

where K_0 is the modified Bessel function of second kind and zero order. This equation provides the temperature value for each point in the substrate.

The idealizations used to obtain Equation 5.4 have relatively little impact on the predictive accuracy and were reviewed in detail in [130]. The fin approximation is accurate for most welding conditions; for example, a representative underwater wet weld would have surface heat losses $h + h'$ of the order of 50 – 1000 W/m^{2}K (natural convection in water) and thermal conductivity of 50 W/mK (steel). In these conditions, a large substrate thickness such as 25 mm still would yield a small Biot number of 0.5.

5.4 Normalization and asymptotics

The normalization of Equation 5.4 is discussed in detail in [130], resulting in:

$$T^*(x^*, y^*) = \exp\left(-x^*\right) K_0 \left(r^* \sqrt{1 + h^*} \right) \tag{5.5}$$

where the * superscript indicates a dimensionless quantity:

$$T^* = \frac{2\pi kd\,(T - T_0)}{q} \tag{5.6}$$

$$h^* = \frac{4\alpha^2\,(h + h')}{kdU^2} \tag{5.7}$$

$$x^* = \frac{Ux}{2\alpha} \tag{5.8}$$

$$y^* = \frac{Uy}{2\alpha} \tag{5.9}$$

$$r^* = \frac{Ur}{2\alpha} \tag{5.10}$$

where $r^* = \sqrt{x^{*2} + y^{*2}}$. Equation 5.5 involves four dimensionless groups: two independent variables x^*, y^* (r^* is not independent), the dependent variable $T^*(x^*, y^*)$, and the parameter h^* associated with surface heat losses.

When considering the maximum half-width of isotherm $T^* = T_c^*$, the four dimensionless groups are constrained by Equation 5.5 and by the condition $y^*_{\max} = \max(y^*)$, leaving only two degrees of freedom: h^*, and the Rosenthal number (Ro) [62, 130]:

$$\mathrm{Ro} = \frac{q}{2\pi k d\,(T_c - T_0)} = \frac{1}{T_c^*} \tag{5.11}$$

When surface heat losses are considered, the geometry of isotherms in dimensionless space depends on Ro and h^*, as illustrated in Figure 5.2. The values of Ro and h^* can vary between zero and infinity, defining four asymptotic regimes in this paper, illustrated in Figure 5.4. For small values of h^*, Regimes III (for large Ro) and Regime IV (for low Ro) were introduced in [130]. When surface heat losses are important, two new regimes appear: Regime IIIa for high values of h^* and high values of Ro, and Regime IVa, for high values of h^* and low values of Ro. Regime I and Regime II correspond to a moving heat source in 3D conditions and were defined in [140].

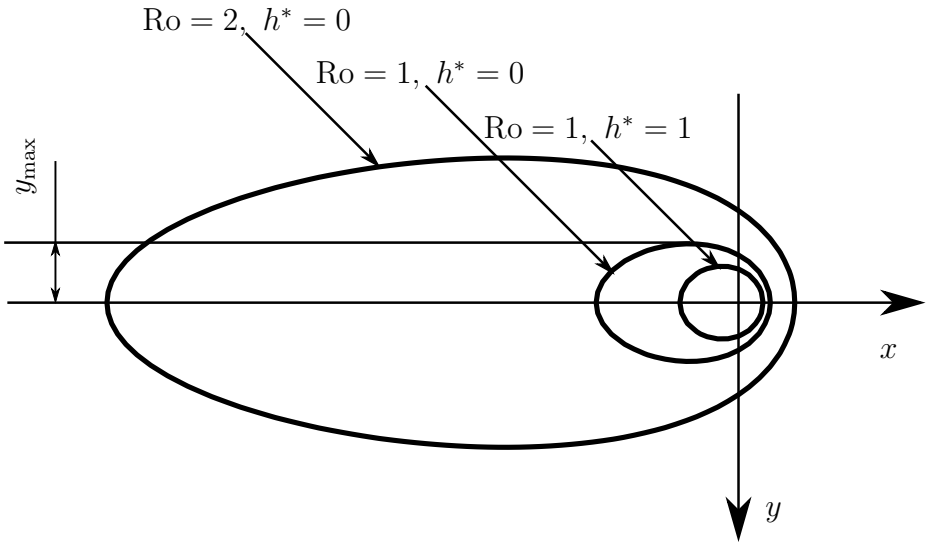

Figure 5.2: Isotherms corresponding to Ro = 1 and 2, and h^*=0 and 1. The surface heat losses have a significant effect on the half-width of the isotherm.

5.5 Two-dimensional blending

Blending is a methodology that produces explicit prediction on the full domain for all values of dependent variables. The full domain can be divided into asymptotic

regimes where variables tend to extreme values, like zero or infinity, and intermediate transitional regimes. At asymptotic regimes, simple expressions can be obtained with asymptotic analysis or regression on experimental data; by combining two or more asymptotic expressions, blending yields closed-form approximate expressions that cover not only asymptotic regimes but also intermediate regimes.

For a characteristic value u_c^* depending on one variable Π, two asymptotic regimes are: $\widehat{u}_{c_i}^*(\Pi)$ at Regime i (R_i) where $\Pi \to 0$ and $\widehat{u}_{c_j}^*(\Pi)$ at Regime j (R_j) where $\Pi \to \infty$, where the superscript $\widehat{\ }$ indicates asymptotic behavior. 1-D blending results in an approximation over the full domain $\widehat{u^*}^+(\Pi)$ where the superscript + indicates results of blending, as discussed at [4, 34, 38, 140, 207] and modified to extend its scope of applicability as discussed at [128, 130].

For a characteristic value u_c^* that depends on two variables Π_1 and Π_2, the general approach to two-dimensional blending has not yet been established systematically. Previous attempts achieve the partial 1-D blending on a subdomain that works only for a limited range of variables [214]. A general and systematic approach is proposed to achieve 2-D blending of $u_c^*(\Pi_1, \Pi_2)$ as follows.

For extreme values of Π_1 and Π_2, the full domain of (Π_1, Π_2) is divided into four asymptotic regimes: $\widehat{u}_{c_i}^*(\Pi_1, \Pi_2)$ at Regime i (R_i) where $\Pi_1 \to 0$ and $\Pi_2 \to 0$, $\widehat{u}_{c_j}^*(\Pi_1, \Pi_2)$ at Regime j (R_j) where $\Pi_1 \to \infty$ and $\Pi_2 \to 0$, $\widehat{u}_{c_k}^*(\Pi_1, \Pi_2)$ at Regime k (R_k) where $\Pi_1 \to 0$ and $\Pi_2 \to \infty$, $\widehat{u}_{c_l}^*(\Pi_1, \Pi_2)$ at Regime l (R_l) where $\Pi_1 \to \infty$ and $\Pi_2 \to \infty$, as illustrated in Figure 5.3. In this paper, the general expressions used

have the following corresponding concepts in the blending derivations:

$$u_{\mathrm{c}}^* = y_{\max}^* \quad \text{or} \quad x_{\max}^* \tag{5.12}$$

$$\Pi_1 = \mathrm{Ro} \tag{5.13}$$

$$\Pi_2 = h^* \tag{5.14}$$

$$\text{Regime} \quad i = \mathrm{R}_i = \text{Regime} \quad \text{IV} \tag{5.15}$$

$$\text{Regime} \quad j = \mathrm{R}_j = \text{Regime} \quad \text{III} \tag{5.16}$$

$$\text{Regime} \quad k = \mathrm{R}_k = \text{Regime} \quad \text{IVa} \tag{5.17}$$

$$\text{Regime} \quad l = \mathrm{R}_l = \text{Regime} \quad \text{IIIa} \tag{5.18}$$

The subscripts III and IV indicated the previously identified regimes for the case of negligible surface losses [130]. The subscripts IIIa and IVa refer to the corresponding regimes with intense surface loss.

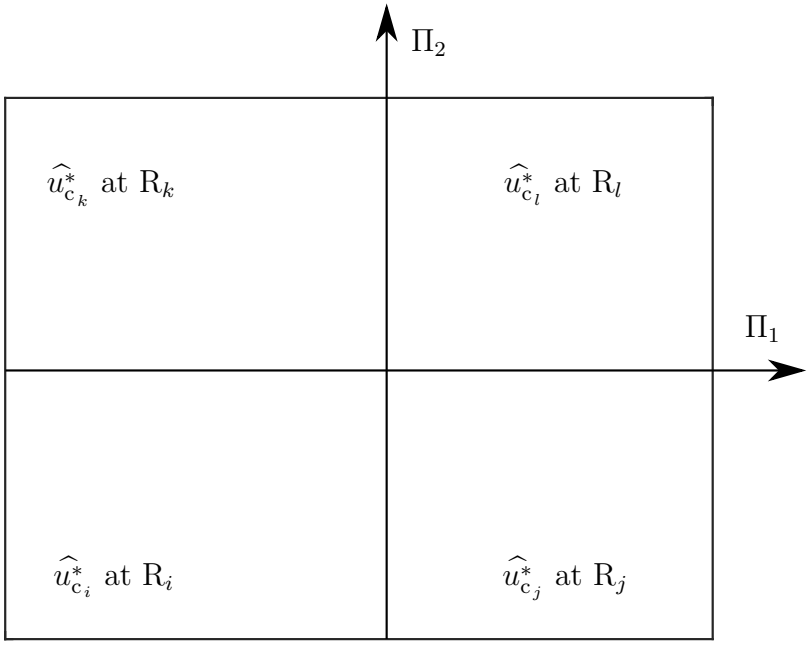

Figure 5.3: Schematic of process map u_{c}^* depending on Π_1 and Π_2. Four asymptotic regimes are defined for extreme values of Π_1 and Π_2.

Along asymptotic 'sides' of the full domain, partial blending results are achieved for

the following combined regimes: side Regime $i-j$ (R_{i-j}) when $\Pi_2 \to 0$, side Regime $k-l$ (R_{k-l}) when $\Pi_2 \to \infty$, side Regime $i-k$ (R_{i-k}) when $\Pi_1 \to 0$, side Regime $j-l$ (R_{j-l}) when $\Pi_1 \to \infty$. Side partial blending, for example $\widehat{u^*_{\mathrm{c}_{i-j}}}(\Pi_1, \Pi_2)$ along the asymptotic side R_{i-j}, can be obtained with 1-D blending when side asymptotic behaviours change with one variable (Π_1 for side R_{i-j} and R_{k-l}, Π_2 for side R_{i-k} and R_{j-l}). When side asymptotic behaviours change with both Π_1 and Π_2, 1-D blending cannot be applied directly and side partial blending must be derived using asymptotic analysis.

After obtaining side partial blending results, correction factors (f) can be developed for each of the asymptotic formulae. For instance, the correction factor can be obtained for side R_{i-j} based on the asymptotic formula for R_i is:

$$f_{i-j}(\Pi_1, \Pi_2) = \frac{\widehat{u^*_{\mathrm{c}_{i-j}}}^{+}(\Pi_1, \Pi_2)}{\widehat{u^*_{\mathrm{c}_i}}(\Pi_1, \Pi_2)} \tag{5.19}$$

At asymptotic 'corners' of the full domain, partial blending results are defined on the subdomain consisting of two asymptotic sides sharing the same base asymptotic regime, for example the asymptotic corner R_{i-j-k} based on R_i containing side R_{i-j} and side R_{i-k}. Corner partial blending combines asymptotic expressions at the base regime and correction factors along both sides, for example at corner R_{i-j-k} based on R_i:

$$\widehat{u^*_{\mathrm{c}_{i-j-k}}}^{+}(\Pi_1, \Pi_2) = \widehat{u^*_{\mathrm{c}_i}} \cdot f_{i-k} \cdot f_{i-j} \tag{5.20}$$

where $f_{i-k}(\Pi_1, \Pi_2)$ and $f_{i-j}(\Pi_1, \Pi_2)$ are calculated with Equation 5.19.

With a corner partial blending developed, the correction factor $g(\Pi_1, \Pi_2)$ is defined to estimate $u^*_{\mathrm{c}}/\widehat{u^*_{\mathrm{c}_{i-j-k}}}^{+}$ that represents 2-D blending of $\widehat{u^*_c}(\Pi_1, \Pi_2)$. $g(\Pi_1, \Pi_2)$ is asymptotically 1 at R_i R_k R_j, and $\widehat{u^*_{\mathrm{c}_l}}/(\widehat{u^*_{\mathrm{c}_{i-j-k}}}^{+})_l$ at the opposite R_l, where $(\widehat{u^*_{\mathrm{c}_{i-j-k}}}^{+})_l$ is the asymptotic behavior of the corner partial blending in R_l. The 2-D blending of $g(\Pi_1, \Pi_2)$ could not be obtained with corner partial blending directly which can only satisfy three asymptotic regimes.

When the asymptotic in R_l is large, $g_l(\Pi_1, \Pi_2) \geq 1$, a systematic approach to 2-D blending of $g(\Pi_1, \Pi_2)$ that is used in this paper is:

$$g(\Pi_1, \Pi_2) = 1 + \widehat{\mathcal{G}}_l^{+}(\Pi_1, \Pi_2) \tag{5.21}$$

where $\widehat{\mathcal{G}}_l^{+}(\Pi_1, \Pi_2)$ is a corner partial blending based on the opposite R_l. If the asymptotic in R_l is small, $(g)_l(\Pi_1, \Pi_2) < 1$, 2-D blending of $g(\Pi_1, \Pi_2)$ can be transformed to 2-D blending of the reciprocal $1/g(\Pi_1, \Pi_2)$ that is larger than one.

In Equation 5.21, $\mathcal{G}_l(\Pi_1, \Pi_2)$ is an auxiliary function constructed as:

$$\mathcal{G}_l(\Pi_1, \Pi_2) = \frac{u_c^*(\Pi_1, \Pi_2)}{\widehat{u}_{c_{i-j-k}}^{*+}(\Pi_1, \Pi_2)} - 1 \tag{5.22}$$

which tends to zero at R_i R_k R_j, and $(g)_l - 1$ at the opposite R_l. If the asymptotic behaviors of $g(\Pi_1, \Pi_2)$ change with one variable along side R_{k-l} and R_{j-l}, blending of $\mathcal{G}_l(\Pi_1, \Pi_2)$ can be achieved with corner partial blending based on R_l similar to Equation 5.20:

$$\widehat{\mathcal{G}}_l^{+}(\Pi_1, \Pi_2) = \widehat{\mathcal{G}}_l(\Pi_1, \Pi_2) \cdot \mathcal{I}(\Pi_1, \Pi_2) \tag{5.23}$$

where $\widehat{\mathcal{G}}_l(\Pi_1, \Pi_2)$ is the asymptotic expression of $\mathcal{G}_l$ (Equation 5.22) at the base R_l is:

$$\widehat{\mathcal{G}}_l(\Pi_1, \Pi_2) = \frac{\widehat{u}_{c_l}^*(\Pi_1, \Pi_2)}{\left(\widehat{u}_{c_{i-j-k}}^{*+}\right)_l(\Pi_1, \Pi_2)} - 1 \tag{5.24}$$

and $\mathcal{I}(\Pi_1, \Pi_2)$ is an unit correction factor for corner partial blending:

$$\mathcal{I}(\Pi_1, \Pi_2) = \left[1 + \left(a_1 \Pi_1^{b_1}\right)^{n_1}\right]^{1/n_1} \left[1 + \left(a_2 \Pi_2^{b_2}\right)^{n_2}\right]^{1/n_2} \tag{5.25}$$

where a_1, b_1, n_1, a_2, b_2, n_2 are arbitrary blending parameters. Equation 5.25 is one at R_l, $a_1 \Pi_1^{b_1}$ at R_j and $a_2 \Pi_2^{b_2}$ at R_k that tends to zero.

The 2-D blending of the characteristic value u_c^* is formulated on one asymptotic regime, R_i for example, as:

$$\widehat{u}_c^{*+}(\Pi_1, \Pi_2) = \widehat{u}_{c_i}^* \cdot f_{i-k} \cdot f_{i-j} \cdot g \tag{5.26}$$

where $f_{i-k}(\Pi_1, \Pi_2)$ and $f_{i-j}(\Pi_1, \Pi_2)$ are obtained through side partial blending Equation 5.19 and $g(\Pi_1, \Pi_2)$ is obtained through Equation 5.21.

5.6 Asymptotic analysis of isotherm half-width $y_{\max}$

The asymptotic analysis of Equation 5.5 for isotherm half-width $y_{\max}$ and its location $x^*_{\max}$ in Regime III and Regime IV where surface heat losses are negligible yields simple expressions:

$$\widehat{y}^*_{\max_{\mathrm{III}}} = \sqrt{\frac{\pi}{2\mathrm{e}}}\mathrm{Ro} \qquad \text{for Regime III} \qquad (5.27)$$

$$\widehat{x}^*_{\max_{\mathrm{III}}} = -\frac{\pi}{2\mathrm{e}}\mathrm{Ro}^2 \qquad \text{for Regime III} \qquad (5.28)$$

$$\widehat{y}^*_{\max_{\mathrm{IV}}} = 2\exp\left(-\gamma - \frac{1}{\mathrm{Ro}}\right) \qquad \text{for Regime IV} \qquad (5.29)$$

$$\widehat{x}^*_{\max_{\mathrm{IV}}} = -\frac{4}{\mathrm{Ro}}\exp\left(-2\gamma - \frac{2}{\mathrm{Ro}}\right) \qquad \text{for Regime IV} \qquad (5.30)$$

where $\gamma = 0.5772\ldots$ is the Euler-Mascheroni constant. Equations 5.27 and 5.29 are consistent with asymptotic analysis in [130] for fast heat sources and low surface heat losses, and equations 5.28 and 5.28 are consistent with [128]. The asymptotic behaviour is a power law in Regime III (fast) and an exponential dependence, not a power law, in Regime IV (slow); the modified 1D blending is used to obtain global approximation [130].

The asymptotic analysis when surface heat losses are intense is detailed in Appendix. In Regime IIIa, for large values of Ro and h^*, the asymptotic behavior of $y^*_{\max}$ is obtained according to Equation 5.94 and $x^*_{\max}$ is obtained according to Equation 5.93:

$$\widehat{y}^*_{\max_{\mathrm{IIIa}}} = \frac{1}{2}\sqrt{\frac{1}{h^*}}W\left(\pi\mathrm{Ro}^2\right) \qquad \text{for Regime IIIa} \qquad (5.31)$$

$$\widehat{x}^*_{\max_{\mathrm{IIIa}}} = -\frac{W\left(\pi\mathrm{Ro}^2\right)}{2h^*} \qquad \text{for Regime IIIa} \qquad (5.32)$$

where $W(x)$ is Lambert W function, which is the solution to $x = W(x)\,\mathrm{e}^{W(x)}$ [41]. Regime IIIa also captures characteristic values for the case of a fin with an instant amount of heat deposited at the root. The value $\widehat{y}^*_{\max_{\mathrm{IIIa}}}$ represents the maximum reach of a particular temperature along the length of the fin, while the value $\widehat{x}^*_{\max_{\mathrm{IIIa}}}$,

corresponds to time $\widehat{t}_{\max_{\mathrm{IIIa}}} = \widehat{x}_{\max_{\mathrm{IIIa}}}/U$, and indicates the time it takes for the temperature of interest to reach its maximum reach along the length of the fin.

In Regime IVa, for small values of Ro and large values of h^*, the asymptotic behavior of $y^*_{\max}$ is obtained according to Equation 5.81 and $x^*_{\max}$ is obtained according to Equation 5.80:

$$\widehat{y}^*_{\max_{\mathrm{IVa}}} = \frac{2}{\sqrt{h^*}} \exp\left(-\frac{1}{\mathrm{Ro}} - \gamma\right) \qquad \text{for Regime IVa} \tag{5.33}$$

$$\widehat{x}^*_{\max_{\mathrm{IVa}}} = -\frac{4}{\mathrm{Ro}\ h^*} \exp\left(-\frac{2}{\mathrm{Ro}} - 2\gamma\right) \qquad \text{for Regime IVa} \tag{5.34}$$

5.7 Blending of isotherm half-width $y_{\max}$

With the asymptotic behaviours of isotherm half-width in asymptotic regimes, equations 5.27, 5.29, 5.31 and 5.33, side partial blending results are developed firstly along four side regimes, and then 2-D blending of isotherm half-width for the full domain is achieved based on Regime III.

5.7.1 Side partial blending

In asymptotic side Regime III – IV, for small values of h^*, the predictive scaling law has been proposed in previous work neglecting surface heat convection [128]:

$$\widehat{y}^{*+}_{\max_{\mathrm{III-IV}}} = 2\mathrm{e}^{-\frac{1}{\mathrm{Ro}}-\gamma} \left\{1 + \left[\sqrt{\tfrac{8\mathrm{e}}{\pi}} \frac{\exp\left(-\gamma\right)}{\mathrm{Ro}}\right]^{-n}\right\}^{1/n} \tag{5.35}$$

where the blending parameters $n = 1.407$ and the maximum relative error is 6.8% for all values of Ro and $h^* = 0$ [130].

In asymptotic side Regime IIIa – IVa, for large values of h^*, partial blending is obtained with 1-D blending on Ro:

$$\widehat{y}^{*+}_{\max_{\mathrm{IIIa-IVa}}} = \frac{\exp\left(-\frac{1}{\mathrm{Ro}}\right)}{\sqrt{h^*}} \left\{\left(2\mathrm{e}^{-\gamma}\right)^n + \left[\frac{W\left(\pi \mathrm{Ro}^2\right)}{2}\right]^n\right\}^{\frac{1}{n}} \tag{5.36}$$

where the blending parameter $n = 2.205$ and the maximum relative error 2.4%.

In asymptotic side III – IIIa, for large values of Ro, side partial blending can not be obtained through 1-D blending as the asymptotic behaviors of isotherm half-width change with both h^* and Ro. The partial blending results is derived through the asymptotic analysis under $\mathrm{Ro} \to 0$ according to Equation 5.90:

$$\widehat{y}^*_{\max_{\mathrm{III-IIIa}}} = \frac{\omega}{2\sqrt{h^*}}\sqrt{1+\frac{2}{(1+h^*)\omega}} \tag{5.37}$$

where ω is a blending function of Lambert W function:

$$\omega \approx \left\{ \left[\frac{\pi h^* \mathrm{Ro}^2}{\exp\left(\frac{1}{1+h^*}\right)(1+h^*)}\right]^{-1} + \ln\left[\frac{\pi h^* \mathrm{Ro}^2}{\exp\left(\frac{1}{1+h^*}\right)(1+h^*)} + c\right]^{-1} + a\left[\frac{\pi h^* \mathrm{Ro}^2}{\exp\left(\frac{1}{1+h^*}\right)(1+h^*)}\right]^{b} \right\}^{-1} \tag{5.38}$$

where $a = 0.08568$, $b = -0.1028$, $c = 2.586$ to be consistent with [128].

In asymptotic side Regime IV – IVa, for small values of Ro, the partial blending for isotherm half-width is obtained with 1-D blending on h^*:

$$\widehat{y}^{*+}_{\max_{\mathrm{IV-IVa}}} = 2\exp\left(-\frac{1}{\mathrm{Ro}} - \gamma\right)\left[\left(\frac{1}{\sqrt{h^*}}\right)^n + 1\right]^{1/n} \tag{5.39}$$

where $n = -2$, which is derived according to Equation 5.77 rather than from optimization.

5.7.2 2-D blending

With asymptotic and side partial blending expressions proposed, 2-D blending of isotherm half-width for any values of Ro or h^* for isotherm half-width $y^*_{\max}$ is formulated based on Regime III (Equation 5.27) multiplying three correction factors:

$$\widehat{y}^{*+}_{\max} = \sqrt{\frac{\pi}{2\mathrm{e}}}\mathrm{Ro}\cdot f_{\text{III-IV}}\left(\mathrm{Ro}\right)\cdot f_{\text{III-IIIa}}\left(\mathrm{Ro}, h^*\right)\cdot g\left(\mathrm{Ro}, h^*\right) \tag{5.40}$$

where the correction factor $f_{\text{III-IV}}(\mathrm{Ro})$ is for asymptotic side III – IV according to Equation 5.35:

$$f_{\text{III-IV}}\left(\mathrm{Ro}\right) = \exp\left(-\frac{1}{\mathrm{Ro}}\right)\left\{1+\left[\sqrt{\frac{8\mathrm{e}}{\pi}}\frac{\exp\left(-\gamma\right)}{\mathrm{Ro}}\right]^n\right\}^{\frac{1}{n}} \tag{5.41}$$

where $n = 1.407$ to be consistent with [130]. The correction factor $f_{\text{III-IIIa}}\left(\text{Ro}, h^*\right)$, according to side partial blending along asymptotic side Regime III – IIIa Equation 5.37, is:

$$f_{\text{III-IIIa}}\left(\text{Ro}, h^*\right) = \sqrt{\frac{\text{e}}{2\pi h^*}} \frac{\omega}{\text{Ro}} \sqrt{1 + \frac{2}{\omega(1+h^*)}} \tag{5.42}$$

where ω is a function of Ro and h^* calculated with Equation 5.38. The correction factor $g(\text{Ro}, h^*)$ is:

$$g\left(\text{Ro}, h^*\right) = 1 + \widehat{\mathcal{G}_{\text{IVa}}}\left(\text{Ro}, h^*\right) \cdot \mathcal{I}\left(\text{Ro}, h^*\right) \tag{5.43}$$

where the asymptotic expression of $y^*_{\max} \big/ \left(\widehat{y}^*_{\max_{\text{III}}} \cdot f_{\text{III-IV}} \cdot f_{\text{III-IIIa}}\right) - 1$ at Regime IVa is $\widehat{\mathcal{G}_{\text{IVa}}}(\text{Ro}, h^*)$ and corner blending correction factors is $\mathcal{I}(\text{Ro}, h^*)$:

$$\widehat{\mathcal{G}_{\text{IVa}}}(\text{Ro}, h^*) = \sqrt{\frac{2}{\pi \text{e} \text{Ro}^2 + 2\text{e}/(1+h^*)}} \tag{5.44}$$

$$\mathcal{I}(\text{Ro}, h^*) = \left(1 + a_1 \text{Ro}^{b_1}\right)^{n_1} \left(1 + a_2 h^{*b_2}\right)^{n_2} \tag{5.45}$$

The optimal blending parameters are $a_1 = 16.09,\ b_1 = 1.438,\ n_1 = -0.2508,\ a_2 = 0.05885,\ b_2 = -0.3583,\ n_2 = -24.44$. The maximum relative error is 9.6 %.

5.7.3 Engineering expression

The engineering expression with units of isotherm half-width is obtained from Equation 5.40:

$$\widehat{y}^+_{\max} = \frac{1}{\sqrt{2\pi \text{e}}} \frac{q\alpha}{Ukd\left(T_c - T_0\right)} \cdot f_{\text{III - IV}}\left(\text{Ro}\right) \cdot f_{\text{III - IIIa}}\left(\text{Ro}, h^*\right) \cdot g\left(\text{Ro}, h^*\right) \tag{5.46}$$

where the correction factor $f_{\text{III - IV}}\left(\text{Ro}\right)$ is Equation 5.41, $f_{\text{III-IIIa}}\left(\text{Ro}, h^*\right)$ is Equation 5.42 and $g\left(\text{Ro}, h^*\right)$ is Equation 5.43.

5.8 Blending of isotherm half-width location $x^*_{\max}$

Similar to the 2-D blending of isotherm half-width, with the asymptotic behaviours of isotherm half-width location $x^*_{\max}$ in asymptotic regimes, side partial blending results are developed along four side regimes first, and then 2-D blending for the full domain is achieved based on Regime III in this section.

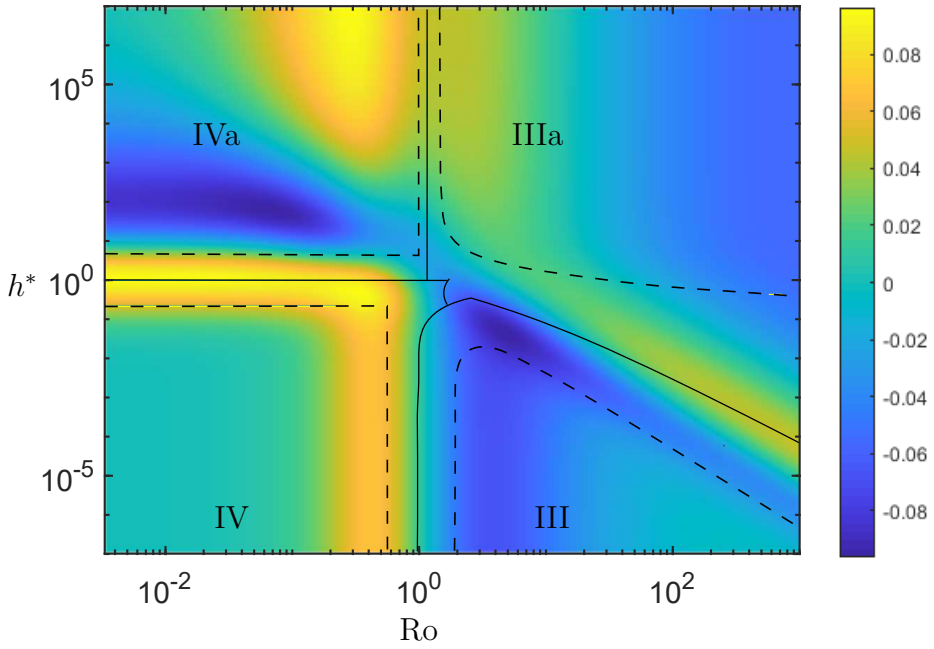

Figure 5.4: The error map of isotherm half-width $y^*_{\max}$ for Equation 5.40.

5.8.1 Partial blending

In asymptotic side Regime III – IV, for small values of h^*, the predictive scaling law has been proposed in previous work ignoring surface heat convection [128]:

$$\widehat{x}^{*+}_{\max_{\mathrm{III-IV}}} = -\exp\left(-\tfrac{2}{\mathrm{Ro}}\right)\left[\tfrac{\pi}{2\mathrm{e}}\mathrm{Ro}^2 + \tfrac{4}{\exp(2\gamma)\mathrm{Ro}} + a\mathrm{Ro}^b\right] \tag{5.47}$$

where the blending parameters are $a = 1.427, b = 1.077$. The maximum error is 6.3% when $h^* = 0$ [128].

In asymptotic side Regime IIIa – IVa, for large values of h^* with intense surface heat loss, the behavior of isotherm half-width location changes with Ro as:

$$\widehat{x}^{*+}_{\max_{\mathrm{IIIa-IVa}}} = -\tfrac{\exp\left(-\frac{2}{\mathrm{Ro}}\right)}{h^*}\left\{\left[\tfrac{W\left(\pi\mathrm{Ro}^2\right)}{2}\right]^n + \left[\tfrac{4}{\mathrm{Ro}\exp(-2\gamma)}\right]^n\right\}^{1/n} \tag{5.48}$$

where the blending parameter $n = 1.112$ and the maximum error is 9.9%.

In asymptotic side Regime IIIa – IIIa, for large values of Ro, the asymptotic behavior of isotherm half-width location changes with both Ro and h^* and can only be achieved by asymptotic analysis. According to Equation 5.89, the side partial

blending of $x^*_{\max}$ is:

$$\widehat{x}^*_{\max_{\text{III}-\text{IIIa}}} = -\frac{1}{2h^*} W\left[\frac{\pi h^* \text{Ro}^2}{\exp\left(\frac{1}{1+h^*}\right)(1+h^*)}\right] \tag{5.49}$$

In asymptotic side Regime IV – IVa, for small values of Ro, the asymptotic behavior changes with h^* and the side partial blending of $x^*_{\max}$ is:

$$\widehat{x}^{*+}_{\max_{\text{IV}-\text{IVa}}} = -\frac{4}{\text{Ro}} \exp\left(-\frac{2}{\text{Ro}} - 2\gamma\right)\left[1 + \left(\frac{1}{h^*}\right)^n\right]^{1/n} \tag{5.50}$$

where $n = -1$ is derived by asymptotic analysis according to Equation 5.76 rather than optimization.

5.8.2 2-D blending

Similar to 2-D blending of $y^*_{\max}$ in Equation 5.40, isotherm half-width location $x^*_{\max}$ is formulated with 2-D blending as asymptotic of Regime III and three correction factors:

$$\widehat{x}^{*+}_{\max} = -\frac{\pi}{2\text{e}}\text{Ro}^2 \cdot f_{\text{III-IV}}(\text{Ro}) \cdot f_{\text{III-IIIa}}(\text{Ro}, h^*) \cdot g(\text{Ro}, h^*) \tag{5.51}$$

The correction factor $f_{\text{III-IV}}(\text{Ro})$ between Regime III – IV is according to Equation 5.47:

$$f_{\text{III-IV}}(\text{Ro}) = \exp\left(-\frac{2}{\text{Ro}}\right)\left[1 + \tfrac{8\text{e}}{\pi \exp(2\gamma)}\text{Ro}^{-3} + \tfrac{2a\text{e}}{\pi}\text{Ro}^{b-2}\right] \tag{5.52}$$

where $a = 1.427,\ b = 1.077$ to be consistent with [128].

The correction factor between Regime III – IIIa $f_{\text{III-IIIa}}(\text{Ro}, h^*)$ according to Equation 5.49 is:

$$f_{\text{III-IIIa}}(\text{Ro}, h^*) = \frac{\text{e}\omega}{\pi \text{Ro}^2 h^*} \tag{5.53}$$

where ω is a function of Ro and h^* calculated with Equation 5.38.

The correction factor from the opposite corner $g(\text{Ro}, h^*)$ is:

$$g(\text{Ro}, h^*) = \left[1 + \widehat{\mathcal{G}_{\text{IVa}}}(\text{Ro}, h^*) \cdot \mathcal{I}(\text{Ro}, h^*)\right]^{-1} \tag{5.54}$$

where $\widehat{\mathcal{G}}\left(\mathrm{Ro}, h^*\right)$ is a function constructed as: $\frac{\widehat{x}^*_{\max_{\mathrm{III}}} \cdot f_{\text{III-IV}} \cdot f_{\text{III-IIIa}}}{x^*_{\max}} - 1 = \frac{\mathrm{e}\omega}{\pi \mathrm{Ro}^2} - 1$. At Regime IVa, the asymptotic behavior of $\widehat{\mathcal{G}_{\mathrm{IVa}}}(\mathrm{Ro}, h^*)$ for small Ro and large h^* is:

$$\widehat{\mathcal{G}_{\mathrm{IVa}}}(\mathrm{Ro}, h^*) = \mathrm{e} - 1 \tag{5.55}$$

and the corner blending correction factors $\mathcal{I}(\mathrm{Ro}, h^*)$ is:

$$\mathcal{I}\left(\mathrm{Ro}, h^*\right) = \left(1 + a_1 \mathrm{Ro}^{b_1}\right)^{n_1} \left(1 + a_2 h^{*b_2}\right)^{n_2} \tag{5.56}$$

where $a_1 = 3.143$, $b_1 = 0.8608$, $n_1 = -0.5360$, $a_2 = 0.3143$, $b_2 = -0.7133$, $n_2 = -2.645$. The maximum relative error is 12 %.

5.8.3 Engineering expression

The engineering expression with units of isotherm half-width location is written based on Regime III:

$$\widehat{x}^+_{\max} = -\frac{\alpha q^2}{4\mathrm{e}\pi U d^2 k^2 \left(T_{\mathrm{c}} - T_0\right)^2} \cdot f_{\text{III - IV}}\left(\mathrm{Ro}\right) \cdot f_{\text{III - IIIa}}\left(\mathrm{Ro}, h^*\right) \cdot g\left(\mathrm{Ro}, h^*\right) \tag{5.57}$$

where the correction factor $f_{\text{III - IV}}\left(\mathrm{Ro}\right)$ is Equation 5.52, $f_{\text{III-IIIa}}\left(\mathrm{Ro}, h^*\right)$ is Equation 5.53 and $g\left(\mathrm{Ro}, h^*\right)$ is Equation 5.54.

5.9 Criterion to neglect surface heat loss

For the cases with negligible surface heat loss effects ($h^* = 0$), previous investigations have reported explicit predictive expressions for isotherm half-width $y^*_{\max}$ [130] and its location $x^*_{\max}$ [128]. The expressions are obtained with modified 1-D blending method of one dimensionless group (Ro number), and they are used as partial blending results in asymptotic side Regime III – IV in this paper (Equation 5.39 for $y^*_{\max}$ and Equation 5.47 for $x^*_{\max}$ respectively). Consistent with the previous predictive expressions, the correction factors for the effect of surface heat losses, $f_{\text{III-IIIa}}(\mathrm{Ro}, h^*)$ and $g(\mathrm{Ro}, h^*)$ in 2-D blending (Equation 5.42, 5.43 for $y^*_{\max}$ and Equation 5.53, 5.54 for $x^*_{\max}$), approach one pointwisely when h^* tends to 0.

For an acceptable relative error of 10 %, for example, the effect of surface heat losses can be neglect under a critical value of h_{c}^{*}. The critical value h_{c}^{*} depends on the Ro number, as illustrated in Figure 5.5. The criterion to disregard correction factors of surface heat loss is suggested for the isotherm half-width $y_{\max}^{*}$ within a relative error of 10 % in [130]:

$$\widehat{h}_{\mathrm{c},y_{\max}^{*}}^{*} = 0.2\left[1+\left(\frac{\pi}{2\mathrm{e}}\mathrm{Ro}^{2}\right)^{n}\right]^{-1/n} \tag{5.58}$$

where $n = 0.9405$; the criterion for the location of isotherm $x_{\max}^{*}$ can be estimated by the blending equation:

$$\widehat{h}_{\mathrm{c},x_{\max}^{*}}^{*} = 0.1\left[1+\left(\frac{\mathrm{e}}{\pi\mathrm{Ro}^{2}}\right)^{n}\right]^{1/n} \tag{5.59}$$

where $n = -1.296$. Blending results of the critical surface heat losses, $\widehat{h}_{\mathrm{c},y_{\max}^{*}}^{*}$ and $\widehat{h}_{\mathrm{c},x_{\max}^{*}}^{*}$, are shown in Figure 5.5.

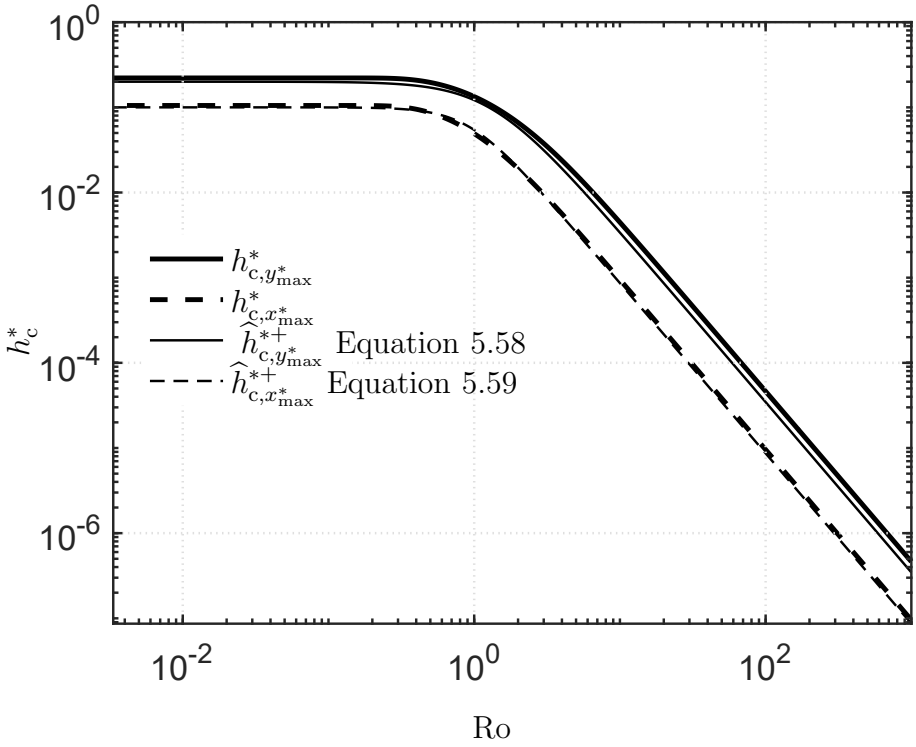

Figure 5.5: Critical values of surface heat losses h_{c}^{*} and its blending approximation $\widehat{h}_{\mathrm{c}}^{*+}$ for isotherm width $y_{\max}^{*}$ and its location $x_{\max}^{*}$ under an acceptable error of 10 %.

For a typical welding processes on steel, thermal diffusivity $\alpha = 10^{-5}\,\mathrm{m}^{2}/\mathrm{s}$, thermal

conductivity $k = 50\,\mathrm{W/mK}$, the velocity $U = 10\,\mathrm{mm/s}$, the heat input $q = 3000\,\mathrm{W}$, the thermal efficiency $\eta = 0.85$, the plate thickness $d = 1\,\mathrm{mm}$, the room temperature $T_0 = 20\,^{\circ}\mathrm{C}$. In consideration of the critical temperature of thermal residual stress $T_\mathrm{c} = 100\,^{\circ}\mathrm{C}$, the Rosenthal number is Ro = 101; the critical to neglect the effect of surface heat loss is $h_\mathrm{c}^* = 3.36 \times 10^{-5}$ and the corresponding coefficient of surface heat loss is $0.42\,\mathrm{W/m^2K}$ that is much smaller than the order of natural convection in air, $10\,\mathrm{W/m^2K}$, and the effect of surface heat loss is therefore significant.

The critical values of the proposed surface heat loss correction factors, h_c^* (equations 5.58 for isotherm half-width and equations 5.59 for isotherm width location), suggest that more significant effects will be necessary for the higher Rosenthal numbers (i.e. lower temperature ranges). The temperature range for the plastic zone associated with residual stress has been previously shown to be approximately an order of magnitude lower than the fusion zone [76] and will therefore be more influenced by surface heat losses.

5.10 Validation

The explicit engineering expressions for isotherm width are validated with data collected from published papers and simulation results of thermal residual stress neglecting and considering the correction factors for surface heat losses, as shown in Figure 5.6 and 5.7. The experimental values were normalized using Equation 5.9, and compared against the partial blending expression (equations 5.40 and 5.41) in Figure 5.7 and 2-D blending expressions with correction factors for surface heat losses (equations 5.40 to 5.43) in Figure 5.7. With the lower temperature range relevant for residual stress, limited literature data is available for measurement of isotherm widths, so additional numerical validation was performed using the computational weld mechanics software package Simufact Welding.

5.10.1 Published data

Measurements were collected for processes like Gas Tungsten Arc Welding (GTAW) [11, 123], Laser Beam Welding (LBW) [100], Underwater Cutting [201], Friction Stir Welding (FSW) [168] for materials including titanium alloys (Ti-6Al-4V [123],Ti [100]), steel (St37 [11],Q235 [201]), stainless steel [11, 168].

In addition to the properties listed in the published papers, the thermal properties of base materials (thermal conductivity and diffusivity) are obtained from material property textbook [143] or software JMatPro (v11), and the effective values are calculated with the method presented in previous work [129, 130]. The thermal efficiency is assumed 0.9 in [11, 168]. The effective surface heat loss coefficient is estimated for validation. The heat loss coefficient is assumed 300 W/m^2K in [11, 100] for processes in atmosphere, and is assumed 500 W/m^2K in [123, 168] accounting for clamping and backing, which are in the order of magnitude $10^{\ 2}$ W/m^2K. For underwater cutting, the effective surface heat loss coefficient is assumed 100,000 W/m^2K in [201]. In [11], only the points away from the centerline in 4× the plate thickness is included, satisfying the criterion for two-dimensional heat flow [130].

5.10.2 Simulation results

A large thin flat plate substrate is considered with a thickness in the z direction of $d = 3$ mm, a length in the x direction of 2400 mm and a half-width in the y direction of 1000 mm. The substrate material was chosen as A36 structural steel with temperature-dependent material properties obtained from the computational material software JMatPro (v11). The heat source was modelled as a cylinder with a depth equal to the plate thickness and a radius of 5 mm.

The substrate mesh consists of 8-node isoparametric bricks with a maximum element size of 40 mm at the plate edge, which decreases to a minimum element size of 2.5 mm at the weld axis. A single layer of elements in the plate thickness direction is adequate to capture the 2-D temperature field associated with the full-penetration

heat source. The mesh size at the weld line is equal to half of the heat source radius, which represents a balance between computational efficiency and limiting instabilities associated with the heat source "jumping" between nodes on the weld line.

The heat transfer coefficient for the bottom plate surface is held constant at $h' = 0$ W/m^{2}K. Three levels are studied for the heat loss coefficient of the top plate surface: $h = 10$ W/m^{2}K (free convection), $h = 20$ W/m^{2}K and $h = 100$ W/m^{2}K (forced convection). The edges of the plate are assumed to be perfectly insulated.

All simulations consider a net power of $q = 1920$ W and a travel speed of $U = 8$ mm/s for an effective welding heat input of $Q' = 240$ J/mm. A xz symmetry plane is applied at the weld axis resulting in a thermal condition equivalent to a centre weld between two plates, and therefore a shape correction to the heat source power used to calculate the 2D Rosenthal temperature field is not necessary.

The isotherm widths are reported for temperatures of $\Delta T = 50 - 350$°C, measured on the top surface of the substrate at the mid-plane. The reported value is obtained by linear interpolation between the maximum temperature recorded for the nodes adjacent to the mid-plane section. The minimum isotherm size corresponding to $\Delta T = 300$°C and $h = 100$ W/m^{2}K was $y_{\max} = 12$ mm which is more than 4× the plate thickness, thereby satisfying the criterion necessary to apply the 2D point heat source model [130].

5.11 Discussion

Similar to the study of the effects of surface heat losses to cooling rate [129], the 2-D blending of isotherm half-width, equations 5.40 to 5.43 for $y^*_{\max}$, and its location, equations 5.51 to 5.54 for $x^*_{\max}$, depends on two dimensionless groups: the Rosenthal number (Equation 5.11) and h^* (Equation 5.7). The Rosenthal number was first proposed by Fuerschbach and Eisler to match experimental results [62]. Ro represents an isotherm in the temperature field of moving heat source problems that is consistent with [128–130]. The h^* is a dimensionless group to illustrate the significance of the

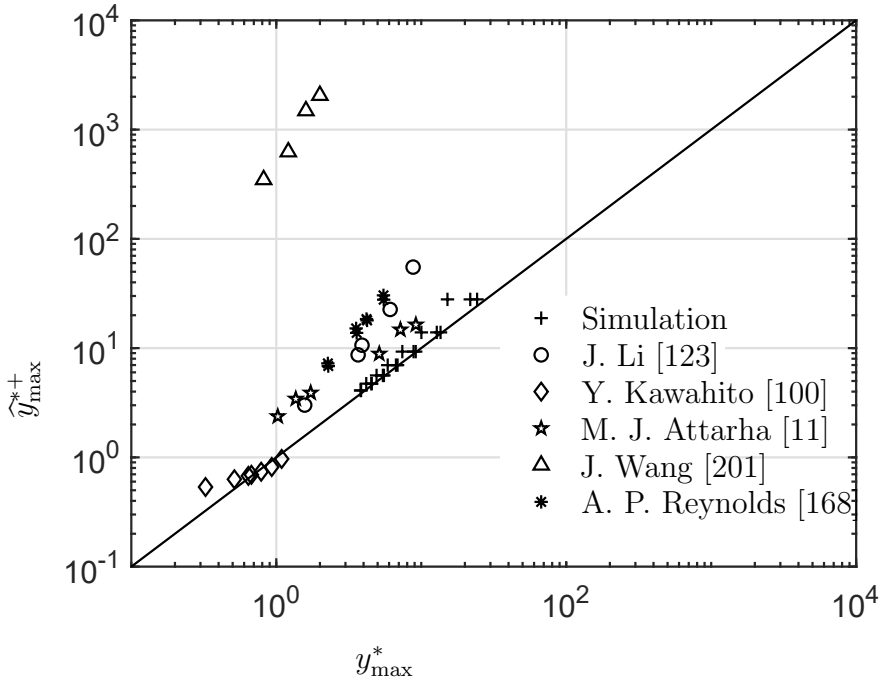

Figure 5.6: Validation of engineering expression for isotherm half-width neglecting correction factors for surface heat loss (Equation 5.40 to 5.41).

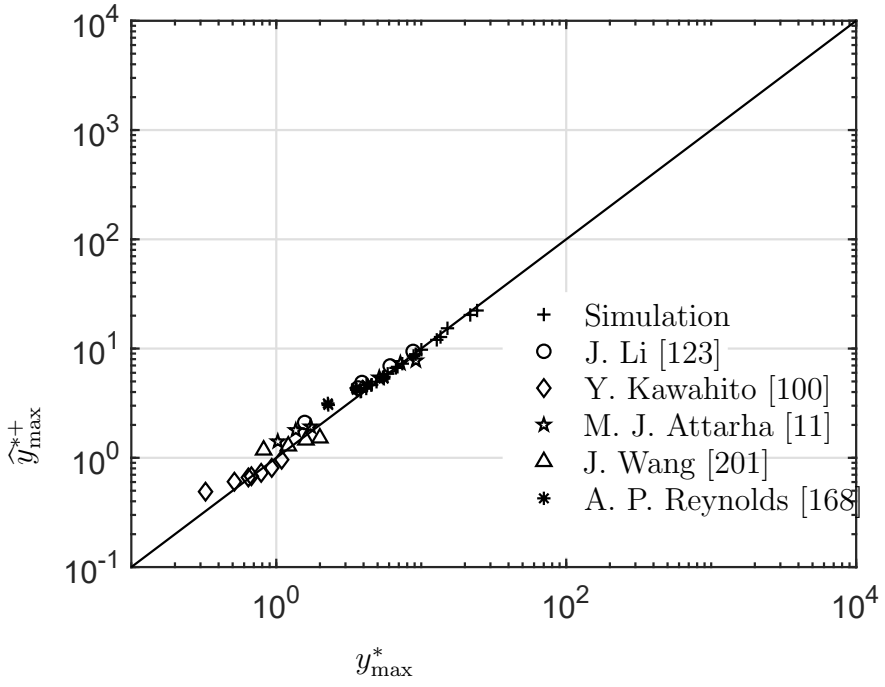

Figure 5.7: Validation of engineering expression for isotherm half-width considering correction factors for surface heat loss (Equation 5.40 to 5.43).

effects of surface heat losses. The surface heat loss (h_{tot}) is total effect of convection (h_{conv}), radiation (h_{rad}) and contact resistance (h_{cond}), $h_{\text{tot}} = h_{\text{tot}} + h_{\text{rad}} + h_{\text{cont}}$. The surface heat losses are in different orders of magnitudes for different cases as discussed in [129]. For cases in air, the surface heat loss is in order of 10 $\text{W/m}^2\text{K}$ without forced convection and in order of 10^2 $\text{W/m}^2\text{K}$ with forced convection. For cases underwater, the surface heat loss is in order of $50-10^3$ $\text{W/m}^2\text{K}$ without forced convection, in order of $10^2-2\times10^4$ $\text{W/m}^2\text{K}$ with forced convection, and in order of $2.5\times10^3-10^5$ $\text{W/m}^2\text{K}$ with phase transformations [92].

To achieve global approximations of $x^*_{\max}$ and $y^*_{\max}$ over the full domain of Ro and h^*, a systematic approach is proposed to obtain 2-D blending results for a characteristic depending on two variables, as introduced in Equation 5.26. The full domain of 2-D blending could be divided into four asymptotic regimes (III, IIIa, IV and IVa in this paper), in terms of extreme values of the two dimensionless groups (0 or ∞ of Ro and h^*). Based on asymptotic expressions in the four regimes, side partial blending can be obtained with either 1-D blending or asymptotic analysis along asymptotic sides between asymptotic regimes next to each other. Then, corner partial blending is obtained by combining partial blending sharing the base regime Equation 5.20. The 2-D blending is finally formulated systematically with corner partial blending on one regime (Regime III in this paper) and blending based on the opposite regime (Regime IVa in this paper), as shown in Equation 5.26. The systematic 2-D blending approach extends the scope of blending methodology from characteristics depending on one dimensionless group [34, 128, 130, 140, 207] to characteristics depending on two dimensionless groups for the first time. Different from 1-D blending that has one correction factor, 2-D blending usually involves three correction factors from the base regime to the other three regimes. However, when $\widehat{\mathcal{G}}_l\left(\Pi_1, \Pi_2\right)$ in Equation 5.24 is zero, 2-D blending is simplified to two correction factors, such as trailing length and centerline cooling rate for a 2-D moving point heat source in [129]. The proposed 2-D blending approach does not engage with the cases with more than four asymptotic

regimes.

The novel 2-D blended expressions presented here offer immense value to industrial practitioners. Since these expressions are explicit and closed-form, they can readily be implemented in procedure development problems or codes and standards. The generality of these equations makes them particularly suitable to broad design problems where empirical methods are neither feasible nor cost-effective. However, the analytical method and associated understanding may also be leveraged in combination with experimental and numerical techniques. For example, consider a time-intensive numerical simulation that has been previously performed with an assumed value for the surface loss coefficient h. The correction factors in this work might be readily applied to answer questions such as how the width of the weld pool and HAZ be expected to change if this coefficient was doubled. It also creates the possibility to perform fewer simulations with parameters optimizing for computational efficiency.

The same is true for empirical investigations. For example, consider a small-scale experiment with forced surface-convection via flowing water, which is conducted for a given material, substrate thickness and flow rate. The blended equations in this work enable previously inaccessible insight as to whether these results will remain valid or need adjustment if applied to field conditions that do not precisely match those which were tested. This methodology is inherent in consideration of essential variables for modern welding procedure design. The theory presented here, for the first time, provides a fundamental basis to extend that philosophy to include the effects of surface heat losses.

5.12 Conclusions

This work presents for the first time practical and rigorous expressions for correction factor for the effects of surface heat losses of an isotherm half-width ($y_{\max}$, Equation 5.46) and its location ($x_{\max}$, Equation 5.57). Examples of processes, where these expressions apply, include underwater processes, in-service welding, welding on a thin

plate, and the calculation of residual stresses associated with moving heat sources.

The isotherm half-width and its location depends on two dimensionless groups: the Rosenthal number and h^*; all cases are therefore divided into four asymptotic regimes: Regime III and Regime IV without convection, Regime IIIa and Regime IVa under intense convection. The proposed expressions have the form of an asymptotic expression (in Regime III) multiplied by three correction factors.

A novel systematic approach is developed for the blending of two variables (Equation 5.26), which develops engineering expressions based on theoretical analysis rather than empirical fitting. The 2-D blending of isotherm width and its location yields global approximation within 9.6 % and 12 % of the exact numerical solution, respectively.

The critical thickness to neglect effects of surface heat losses in the predictions (error below 10 %) of width depends on the temperature considered. For a typical welding process on steel with a convection coefficient of the order of 100 W/m^2K, surface heat losses are negligible for thickness above 0.07 mm for the width of melt (with typical values of Ro $\approx$ 1). Also, for steel, if a temperature of 630°C is considered as representative of the 800 °C to 500 °C, the critical thickness is 2.4 mm. (with typical Ro $\approx$ 10). For the calculations of residual stresses in steel, in which the characteristic temperatures are of the order of 100 °C, the critical thickness is 23 mm (with typical Ro $\approx$ 100).

Validation against published experimental results and simulations shows a close agreement with the predictive equations (Figure 5.7).

Acknowledgments

The authors wish to acknowledge support from the Natural Sciences and Engineering Research Council of Canada (NSERC RGPIN-2019-05981). Student scholarships from the AWS and the CWB were also gratefully received.

References

[4] A. Acrivos, "A rapid method for estimating the shear stress and the separation point in laminar incompressible boundary-layer flows," *Journal of the Aero/Space Sciences*, vol. 27, no. 4, pp. 314–315, 1960.

[11] M. Attarha and I. Sattari-Far, "Study on welding temperature distribution in thin welded plates through experimental measurements and finite element simulation," *Journal of Materials Processing Technology*, vol. 211, no. 4, pp. 688 –694, 2011.

[22] W. A. Bruce and M. A. Boring, "Comparison of methods for predicting safe parameters for welding onto in-service pipelines," in *2006 International Pipeline Conference*, American Society of Mechanical Engineers Digital Collection, 2006, pp. 283–296.

[34] S. W. Churchill and R. Usagi, "A general expression for the correlation of rates of transfer and other phenomena," *AIChE Journal*, vol. 18, no. 6, pp. 1121–1128, 1972.

[38] S. W. Churchill and R. Usagi, "A standardized procedure for the production of correlations in the form of a common empirical equation," *Industrial & Engineering Chemistry Fundamentals*, vol. 13, no. 1, pp. 39–44, 1974.

[41] R. M. Corless, G. H. Gonnet, D. E. G. Hare, D. J. Jeffrey, and D. E. Knuth, "On the Lambert W function," *Advances in Computational Mathematics*, vol. 5, no. 1, pp. 329–359, 1996.

[62] P. W. Fuerschbach and G. R. Eisler, "Determination of material properties for welding models by means of arc weld experiments," in *Trends in Welding Research, Proceedings of the 6th International Conference*, Callaway Gardens Resort, Phoenix, Arizona: ASM International, 2002.

[66] E. Gariboldi and B. Previtali, "High tolerance plasma arc cutting of commercially pure titanium," *Journal of Materials Processing Technology*, vol. 160, no. 1, pp. 77–89, 2005.

[67] P. Ghadimi, H. Ghassemi, M. Ghassabzadeh, and Z. Kiaei, "Three-dimensional simulation of underwater welding and investigation of effective parameters," *Welding journal*, vol. 92, no. 8, pp. 239–249, 2013.

[70] W. H. Giedt and L. N. Tallerico, "Prediction of electron beam depth of penetration," *Welding Research Supplement*, vol. 67, no. 12, 299s–305s, 1988.

[73] J. Gockel, N. Klingbeil, and S. Bontha, "A closed-form solution for the effect of free edges on melt pool geometry and solidification microstructure in additive manufacturing of thin-wall geometries," *Metallurgical and Materials Transactions B*, vol. 47, no. 2, pp. 1400–1408, 2016.

[76] M. R. Grams and P. F. Mendez, "Scaling analysis of the thermal stress field produced by a moving point heat source in a thin plate," *Journal of Applied Mechanics*, pp. 1–34, Sep. 2020.

[77] M. R. Grams and P. F. Mendez, "A general expression for the welding tendon force," *ASME J. Manuf. Sci. Eng.* (under review), 2021.

[84] K. Heller, S. Kessler, F. Dorsch, P. Berger, and T. Graf, "Analytical description of the surface temperature for the characterization of laser welding processes," *International Journal of Heat and Mass Transfer*, vol. 106, pp. 958–969, 2017.

[85] H. Hemmer and Ø. Grong, "Prediction of penetration depths during electron beam welding," *Science and technology of welding and joining*, vol. 4, no. 4, pp. 219–225, 1999.

[88] C. Y. Ho, "Asymptotic analysis for penetration depth during laser welding," *Procedia Engineering*, vol. 15, pp. 5212–5216, 2011.

[92] F. P. Incropera, D. P. DeWitt, T. L. Bergman, and A. S. Lavine, *Fundamentals of heat and mass transfer*. John Wiley & Sons, 2007.

[96] C. L. Jenney and A. O'Brien, Eds., *Welding science and technology*, Ninth. American Welding Society (AWS), 2001, vol. 1, ISBN: 978-0-87171-657-6.

[100] Y. Kawahito, T. Ohnishi, and S. Katayama, "In-process monitoring and feedback control for stable production of full-penetration weld in continuous wave fibre laser welding," *Journal of Physics D: Applied Physics*, vol. 42, no. 8, p. 085 501, 2009.

[123] J. Li, Q. Guan, Y. W. Shi, and D. L. Guo, "Stress and distortion mitigation technique for welding titanium alloy thin sheet," *Science and Technology of Welding and Joining*, vol. 9, no. 5, pp. 451–458, 2004.

[128] Y. Lu and P. F. Mendez, "Characteristic values of the temperature field induced by a moving line heat source," *International Journal of Heat and Mass Transfer*, p. 120 671, 2020.

[129] Y. Lu and P. F. Mendez, "The effect of surface heat losses on isotherm trailing length and cooling rate," 2021.

[130] Y. Lu, Y. Wang, and P. F. Mendez, "Width of thermal features induced by a 2-D moving heat source," *International Journal of Heat and Mass Transfer*, vol. 156, p. 119 793, 2020.

[134] P. F. Mendez, "Synthesis and generalisation of welding fundamentals to design new welding technologies: Status challenges and a promising approach," *Science and Technology of Welding and Joining*, vol. 16, no. 4, pp. 348–356, 2011.

[137] P. F. Mendez, K. E. Tello, and S. S. Gajapathi, "Generalization and communication of welding simulations and experiments using scaling analysis design rules in welding design rules in engineering : Calibrated minimal representation approach," in *Trends in Welding Research, Proceedings of the 9th International Conference*, ASM International, 2012, pp. 249–258.

[140] P. F. Mendez, Y. Lu, and Y. Wang, "Scaling analysis of a moving point heat source in steady- state on a semi-infinite solid," *Journal of Heat Transfer*, vol. 140, no. 8, p. 081 301, 2018.

[141] P. F. Mendez, K. E. Tello, and T. J. Lienert, "Scaling of coupled heat transfer and plastic deformation around the pin in friction stir welding," *Acta Materialia*, vol. 58, no. 18, pp. 6012–6026, 2010.

[143] K. C. Mills, *Recommended values of thermophysical properties for selected commercial alloys*. Woodhead Publishing Limited, 2002.

[144] Y. S. Muzychka and M. M. Yovanovich, "Thermal resistance models for non-circular moving heat sources on a half space," *Journal of Heat Transfer*, vol. 123, no. 4, pp. 624–632, 2001.

[145] P. S. Myers, O. A. Uyehara, and G. L. Borman, "Fundamentals of heat flow in welding," *Welding Research Council Bulletin*, vol. 123, pp. 1–46, 1967.

[149] V. Nemchinsky, "Temperature created by a moving heat source that heats and melts the metal plate (plasma arc cutting)," *Journal of Heat Transfer*, vol. 138, no. 12, p. 122 301, 2016.

[160] V. Pavelic, R. Tanbakuchi, O. A. Uyehara, and P. S. Myers, "Experimental and computed temperature histories in gas tungsten-arc welding of thin plates," *Welding Research Supplement*, vol. 48, pp. 295–305, 1969.

[167] J. A. Ramos-Grez and M. Sen, *Analytical, quasi-stationary wilson-rosenthal solution for moving heat sources*, 2019.

[168] A. P. Reynolds, W. Tang, T. Gnaupel-Herold, and H Prask, "Structure, properties, and residual stress of 304l stainless steel friction stir welds," *Scripta materialia*, vol. 48, no. 9, pp. 1289–1294, 2003.

[171] O. F. T. Roberts, "The theoretical scattering of smoke in a turbulent atmosphere," in *Proceedings of the Royal Society of London*, ser. Series A, Containing Papers of a Mathematical and Physical Character, vol. 104, Royal Society, 1923, pp. 640–654.

[176] D. Rosenthal and R. Schmerber, "Thermal study of arc welding," *Welding journal*, vol. 17, no. 4, pp. 2–8, 1938.

[190] D. T. Swift-Hook and A. E. F. Gick, "Penetration welding with lasers," *Welding Research Supplement*, vol. 52, no. 11, 492s–499s, 1973.

[201] J. Wang, J. Shi, J. Wang, W. Li, C. Liu, G. Xu, S. Y. Maksimov, and Q. Zhu, "Numerical study on the temperature field of underwater flux-cored wire arc cutting process," *The International Journal of Advanced Manufacturing Technology*, vol. 91, no. 5-8, pp. 2777–2786, 2017.

[207] Y. Wang, Y. Lu, and P. F. Mendez, "Scaling expressions of characteristic values for a moving point heat source in steady state on a semi-infinite solid," *International Journal of Heat and Mass Transfer*, vol. 135, pp. 1118–1129, 2019.

[213] A. A. Wells, "Heat flow in welding," *Welding Research Supplement*, vol. 31, no. 5, 263s–267s, 1952.

[214] J. B. Will, N. P. Kruyt, and C. H. Venner, "An experimental study of forced convective heat transfer from smooth, solid spheres," *International Journal of Heat and Mass Transfer*, vol. 109, pp. 1059–1067, 2017.

[218] G. Wood, S. A. Islam, and P. F. Mendez, "Calibrated expressions for welding and their application to isotherm width in a thick plate," *Soldagem & Inspeção*, vol. 19, no. 3, pp. 212–220, 2014.

[219] G. Wood and P. F. Mendez, "First order prediction of bead width and height in coaxial laser cladding," in *Proceedings of Numerical Analysis of Weldability*, Graz, Austria, 2015.

[222] B. Xu, F. Jiang, S. Chen, M. Tanaka, S. Tashiro, and N. Van Anh, "Numerical analysis of plasma arc physical characteristics under additional constraint of keyhole," *Chinese Physics B*, vol. 27, no. 3, p. 034 701, 2018.

[227] G. Yu, R. J. Anderson, T. Maekawa, and N. M. Patrikalakis, "Efficient simulation of shell forming by line heating," *International Journal of Mechanical Sciences*, vol. 43, no. 10, pp. 2349–2370, 2001.

Appendix 5.A Asymptotic analysis in asymptotic side Regime IV – IVa

The isotherm half-width $y^*_{\max}$ and its location $x^*_{\max}$ are expressed implicitly relating to a given temperature T_c:

$$T^*_c = \exp\left(-x^*_{\max}\right) K_0\left(r^*_{\max}\sqrt{1+h^*}\right) \tag{5.60}$$

$$\left.\frac{\partial T^*}{\partial x^*}\right|_{x^*_{\max}, y^*_{\max}} = 0 \tag{5.61}$$

where $r^*_{\max} = \sqrt{x^{*2}_{\max} + y^{*2}_{\max}}$. Equations 5.60 and 5.61 can be transformed to the Rosenthal number, zeroth and first order modified Bessel function of the second kind:

$$\exp\left(-x^*_{\max}\right) K_0\left(r^*_{\max}\sqrt{1+h^*}\right) = \frac{1}{\mathrm{Ro}} \tag{5.62}$$

$$1 + \frac{x^*_{\max}\sqrt{1+h^*}}{r^*_{\max}} \frac{K_1\left(r^*_{\max}\sqrt{1+h^*}\right)}{K_0\left(r^*_{\max}\sqrt{1+h^*}\right)} = 0 \tag{5.63}$$

According to Equation 5.63 and the denotation $R = r^*_{\max}\sqrt{1+h^*}$, the isotherm half-width $y^*_{\max}$ and its location $x^*_{\max}$ can be expressed as:

$$x^*_{\max} = -\frac{r^*_{\max} K_0\left(r^*_{\max}\sqrt{1+h^*}\right)}{\sqrt{1+h^*} K_1\left(r^*_{\max}\sqrt{1+h^*}\right)} = -\frac{R}{1+h^*}\frac{K_0(R)}{K_1(R)} \tag{5.64}$$

$$y^*_{\max} = r^*_{\max}\sqrt{1 - \frac{K_0^2\left(r^*_{\max}\sqrt{1+h^*}\right)}{(1+h^*) K_1^2\left(r^*_{\max}\sqrt{1+h^*}\right)}} \tag{5.65}$$

$$= \frac{R}{\sqrt{1+h^*}}\sqrt{1 - \frac{K_0\left(R\right)^2}{(1+h^*) K_1\left(R\right)^2}} \tag{5.66}$$

In asymptotic side Regime IV – IVa, where $\mathrm{Ro} \to 0$ considering the isotherms close to the heat source, the isotherm half-width $y^*_{\max_{\mathrm{IV-IVa}}} \ll 1$, its location $x^*_{\max_{\mathrm{IV-IVa}}} \ll 1$, $r^*_{\max_{\mathrm{IV-IVa}}} \ll 1$ and $R_{\mathrm{IV-IVa}} \ll 1$. By replacing $x^*_{\max_{\mathrm{IV-IVa}}}$ with Equation 5.64, asymptotic analysis of Equation 5.62 in asymptotic side Regime IV – IVa produces:

$$\frac{1}{\mathrm{Ro}} = -\gamma + \ln(2) - \ln\left(R_{\mathrm{IV-IVa}}\right) + O\left(R_{\mathrm{IV-IVa}}\right) \tag{5.67}$$

Writing the R in asymptotic side Regime IV – IVa as:

$$R_{\mathrm{IV-IVa}} = 2\exp\left(-1/\mathrm{Ro} - \gamma\right)(1+\epsilon) \tag{5.68}$$

Solving $R_{\mathrm{IV-IVa}}$ in Equation 5.67 is identical to finding the root of ϵ. To obtain asymptotic expressions in asymptotic side Regime IV – IVa, asymptotic analysis is performed assuming $\epsilon \to 0$. If the solution to ϵ assures the assumption, asymptotic expression to $\widehat{R}$ is obtained; asymptotic expressions to $\widehat{y}^*_{\max}$ and $\widehat{x}^*_{\max}$ are then derived. Bringing the denotation Equation 5.68 into Equation 5.67 yields:

$$O\left[\exp\left(-\frac{1}{\mathrm{Ro}}\right)\right] = \ln\left(1+\epsilon\right) \tag{5.69}$$

Therefore, as $\mathrm{Ro} \to 0$ in asymptotic side Regime IV – IVa, the solution to Equation 5.67 is:

$$\epsilon = -1 + \exp\left\{O\left[\exp\left(-\tfrac{1}{\mathrm{Ro}}\right)\right]\right\} = O\left[\exp\left(-\tfrac{1}{\mathrm{Ro}}\right)\right] \tag{5.70}$$

$$R_{\mathrm{IV-IVa}} = 2\exp\left(-\tfrac{1}{\mathrm{Ro}} - \gamma\right)\left\{1 + O\left[\exp\left(-\tfrac{1}{\mathrm{Ro}}\right)\right]\right\} \tag{5.71}$$

Substituting Equation 5.71 into Equation 5.64 and Equation 5.66, the solutions to isotherm half-width $y^*_{\max_{\mathrm{IV-IVa}}}$ and its location $x^*_{\max_{\mathrm{IV-IVa}}}$ are:

$$x^*_{\max_{\mathrm{IV-IVa}}} = \frac{R^2_{\mathrm{IV-IVa}}}{1+h^*}\left[\gamma + \ln\left(\frac{1}{2}R_{\mathrm{IV-IVa}}\right)\right] + O\left(R^3_{\mathrm{IV-IVa}}\right) \tag{5.72}$$

$$= -\frac{4\exp\left(-2\gamma - \frac{2}{\mathrm{Ro}}\right)}{\left(1+h^*\right)\mathrm{Ro}} + O\left[\frac{1}{\mathrm{Ro}}\exp\left(-\frac{3}{\mathrm{Ro}}\right)\right] \tag{5.73}$$

$$y^*_{\max_{\mathrm{IV-IVa}}} = \frac{R_{\mathrm{IV-IVa}}}{\sqrt{1+h^*}} + O\left(R^2_{\mathrm{IV-IVa}}\right) \tag{5.74}$$

$$= \frac{2\exp\left(-\gamma - \frac{1}{\mathrm{Ro}}\right)}{\sqrt{1+h^*}} + O\left[\exp\left(-\frac{2}{\mathrm{Ro}}\right)\right] \tag{5.75}$$

In asymptotic side Regime IV – IVa, the partial blending of isotherm half-width and its location are:

$$\widehat{x}^*_{\max_{\mathrm{IV-IVa}}} = -\frac{4\exp\left(-2\gamma - \frac{2}{\mathrm{Ro}}\right)}{\left(1+h^*\right)\mathrm{Ro}} \tag{5.76}$$

$$\widehat{y}^*_{\max_{\mathrm{IV-IVa}}} = \frac{2\exp\left(-\gamma - \frac{1}{\mathrm{Ro}}\right)}{\sqrt{1+h^*}} \tag{5.77}$$

In Regime IV as $h^* \to 0$, the asymptotic expressions for isotherm half-width and

its location are

$$\widehat{x}^*_{\max_{\mathrm{IV}}} = -\frac{4}{\mathrm{Ro}} \exp\left(-2\gamma - \frac{2}{\mathrm{Ro}}\right) \tag{5.78}$$

$$\widehat{y}^*_{\max_{\mathrm{IV}}} = 2 \exp\left(-\frac{1}{\mathrm{Ro}} - \gamma\right) \tag{5.79}$$

In Regime IVa as $h^* \to \infty$, the asymptotic expressions for isotherm half-width and its location are

$$\widehat{x}^*_{\max_{\mathrm{IVa}}} = -\frac{4}{h^*\mathrm{Ro}} \exp\left(-2\gamma - \frac{2}{\mathrm{Ro}}\right) \tag{5.80}$$

$$\widehat{y}^*_{\max_{\mathrm{IVa}}} = \frac{2}{\sqrt{h^*}} \exp\left(-\frac{1}{\mathrm{Ro}} - \gamma\right) \tag{5.81}$$

Appendix 5.B Asymptotic analysis in asymptotic side Regime III – IIIa

In asymptotic side Regime III – IIIa, where $\mathrm{Ro} \to \infty$ considering isotherms away from the heat source, $R_{\text{III - IIIa}} \to \infty$. By replacing $x^*_{\max_{\text{III}-\text{IIIa}}}$ with Equation 5.64, asymptotic analysis of Equation 5.62 in asymptotic side Regime III – IIIa produces:

$$\frac{1}{\mathrm{Ro}} = \exp\left(-\frac{h^*\ R_{\text{III - IIIa}}}{1+h^*} - \frac{1}{2+2h^*}\right) \cdot \left[\sqrt{\frac{\pi}{2R_{\text{III - IIIa}}}} + O\left(\frac{1}{R_{\text{III - IIIa}}}\right)\right] \tag{5.82}$$

Denote ω as:

$$\omega = W\left[\frac{\pi h^* \mathrm{Ro}^2}{\exp\left(\frac{1}{h^*+1}\right)(h^*+1)}\right] \tag{5.83}$$

Write the R in the asymptotic side Regime III – IIIa as:

$$R_{\text{III - IIIa}} = \frac{h^*+1}{2h^*}\omega(1+\epsilon) \tag{5.84}$$

Equation 5.82 is can be written as:

$$1 = \exp\left(-\frac{\epsilon\omega}{2}\right) \frac{1}{\sqrt{1+\epsilon}} \left[1 + O\left(\frac{1}{\sqrt{R_{\text{III - IIIa}}}}\right)\right] \tag{5.85}$$

$$0 \approx -\frac{\epsilon\omega}{2} - \frac{1}{2}\epsilon + O\left(\frac{1}{\sqrt{R_{\text{III - IIIa}}}}\right) \tag{5.86}$$

The solution to ϵ is:

$$\epsilon = O\left[\frac{1}{1+\omega}\frac{\sqrt{2h^*}}{\sqrt{(h^*+1)\omega}}\right] = O\left[\sqrt{\frac{h^*}{(h^*+1)\omega}}\right] \tag{5.87}$$

In asymptotic side Regime III – IIIa, partial blending results of isotherm half-width and its location are:

$$\widehat{R}_{\text{III - IIIa}} = \frac{h^*+1}{2h^*}\omega \tag{5.88}$$

$$\widehat{x}^*_{\max_{\text{III-IIIa}}} = -\frac{1}{2h^*}\omega \tag{5.89}$$

$$\widehat{y}^*_{\max_{\text{III-IIIa}}} = \frac{\omega}{2\sqrt{h^*}}\sqrt{1+\frac{2}{(1+h^*)\,\omega}} \tag{5.90}$$

In Regime III as $h^* \to 0$, the asymptotic expressions for isotherm half-width and its location are:

$$\widehat{x}^*_{\max_{\text{III}}} = -\frac{\pi}{2\text{e}}\text{Ro}^2 \tag{5.91}$$

$$\widehat{y}^*_{\max_{\text{III}}} = 2\exp\left(-\frac{1}{\text{Ro}} - \gamma\right) \tag{5.92}$$

In Regime IIIa as $h^* \to \infty$, the asymptotic expressions for isotherm half-width and its location are:

$$\widehat{x}^*_{\max_{\text{IIIa}}} = -\frac{1}{2h^*}W\left(\pi\text{Ro}^2\right) \tag{5.93}$$

$$\widehat{y}^*_{\max_{\text{IIIa}}} = \frac{1}{2\sqrt{h^*}}W\left(\pi\text{Ro}^2\right) \tag{5.94}$$

Chapter 6

Isotherm half-width of Gaussian moving heat sources on a thick substrate

Abstract

This paper presents a systematic analysis of the maximum isotherm half-width under a Gaussian distributed heat source on a semi-infinite solid. Dimensionless isotherm half-width $y^*_{\max}$ depends on two dimensionless groups: the Ry number representing velocities of heat source, and normalized standard deviation of Gaussian distribution σ^* representing sizes of heat source. A new phenomenon is identified for the first time: the presence of two local width maxima in an isotherm under some parameter combinations. Correction factors for maximum isotherm half-width are determined in closed-form for the first time over a wide range of σ^* and Ry. The methodology employed consists of dimensional analysis, asymptotic analysis, and blending techniques. The maximum error of the proposed equations is within 6.1 % from the analytical solution for Ry $\leq$ 1000 and $\sigma^*/\widehat{\sigma}^{*+}_{\max}(\mathrm{Ry}) \leq 0.9$, where $\widehat{\sigma}^{*+}_{\max}(\mathrm{Ry})$ is the maximum heat source size for certain Ry. The expressions obtained can be calculated using a calculator or a basic spreadsheet and are useful for engineers. Comparisons of the proposed equations are conducted with measurements from literatures.

Table 6.1: Variables used in the paper with the units and description

Variable	Unit	Description
I_m	1	Constant $I_m = 1.280$
k	$\mathrm{W\,m^{-1}\,K^{-1}}$	Thermal conductivity of the substrate
q	W	Power absorbed by substrate
Ry	1	Rykalin number
T	K	Temperature
T_0	K	Initial temperature or preheat
T_c	K	Temperature of interest
$T_{\mathrm{max,c}}$	K	Maximum temperature at centerline
U	$\mathrm{m\,s^{-1}}$	Travel speed of the moving heat source
x, y, z	m	Cartesian coordinates
$x_{\mathrm{max,c}}$	m	Location of maximum temperature at centerline
$x_{\max}$	m	Location of maximum isotherm half-width
$y_{\max}$	m	Maximum isotherm half-width
Greek symbols		
α	$\mathrm{m^2\,s^{-1}}$	Thermal diffusivity of the substrate
χ	1	$\chi = x^* - \sigma^{*2}$
ρ	1	$\rho = \sqrt{(x^* - \sigma^{*2})^2 + y^{*2}}$
σ	m	Standard deviation of a Gaussian function
$\sigma_{\max}$	m	Maximum heat source distribution parameter
Superscripts		
*		Dimensionless value
$\widehat{\ }$		Asymptotic behavior
$^+$		Improvement over asymptotic approximation

Continued on next page

Table 6.1 – continued from previous page

Variable	Unit	Description
Subscripts		
I		Regime I (concentrated and fast heat sources)
II		Regime II (concentrated and slow heat sources)
V		RegVme V (wide and fast heat sources)
VI		Regime VI (wide and slow heat sources)

6.1 Introduction

The maximum isotherm half-width at a temperature of interest is one of the most critical dimension characteristics in investigations of moving heat source problems. For example, maximum isotherm half-widths of melting temperature determine the size of the melt pool and melting efficiencies for fusion welding processes. Maximum isotherm half-widths of phase transformation temperatures, such as Ac_1 for carbon steel, determines sizes of the heat-affected zone or area of surface hardening.

Prediction of the maximum isotherm half-width based on the classic point heat source model has been proposed in previous investigations for thick plates [140, 207] and thin plates [130], which is a reasonable assumption in considering isotherms away from the heat source. However, for isotherms near the heat source, the distribution and size of heat source can not be neglected, that drives development of moving distributed heat source models [39, 74, 150, 212]. The moving Gaussian heat source is one of the most widely applied models [39, 53], that a good representation of heat sources like electronic arcs [113], laser beam [65]. It describes a Gaussian distributed heat source moving on the surface of the workpiece, avoiding the problem of singularity for the temperature field induced by a point heat source. It has been proved that a moving Gaussian source can predict important thermal characteristics such as

isotherm shape, cooling rate and peak temperature with high accuracy [39, 196, 209].

There have been many studies of the maximum isotherm half-width with varying emphases on experiments, numerical simulations and analytical modelling. Based on Rosenthal's thick plate solution, an approximation of fusion zone width was obtained by regression of experimental data for bead-on-plate welds with a limited applicable range [155]. Empirical equations for HAZ width or fusion width have been proposed as a function of interactive processing variables by multiple linear regression [5, 18, 98]. Despite the simplicity, empirical equations are valid for a limited range of parameters and can hardly be extrapolated to conditions beyond which they were developed.

Temperature field in a two-dimensional plate was solved using a finite difference method, and the isotherm width at the melting temperature was correlated to the process variables [160]. Thermal history and shape of isotherms under a double ellipsoid model have been calculated by the finite element method for thick workpieces [74]. A computer model for three-dimensional heat flow under a Gaussian surface source was developed using the finite element method to predict the configuration of the fusion zone and the resultant grain structure [110]. Sophisticated numerical models can take complicated geometry and multiple physics such as latent heat into account. However, the requirement of specialized software and computational skills restricts the applicability of simulations in industrial practice. Furthermore, simulation results can seldom be generalized as explicit and intuitively understood design rules amenable to use by practitioners.

A simple estimation of fusion line width was reported by Wells for single-run butt welds on thin plates [213], but it is only valid under very limited conditions. Asymptotes of fusion width for large Peclet and small Peclet numbers have been derived from Rosenthal's 2D solution [190] but failed to obtain an explicit solution valid for intermediate Peclet numbers. The analytical temperature field of a distributed heat source typically involves improper integrals or summations that require a careful computational implementation to extract a solution for the maximum isotherm width [39,

53, 216].

The objective of this paper is to present a general and easily applicable solution that would predict with high accuracy the maximum isotherm width at a temperature of interest when given operational parameters and thermal properties of the substrate based on previous work on moving point heat source model [140]. A moving Gaussian source model was used as the theoretical basis. A correction factor for the heat distribution parameter was obtained using the 2D blending technique to improve predictions derived from Rosenthal's solutions. The obtained explicit equation for the maximum isotherm width is compared against the Rosenthal calculations and experimental measurements from the literature.

6.2 Moving Gaussian heat source

The moving Gaussian heat source model refers to a constant heat source obeying Gaussian distribution moving at a constant speed on a plate that is thick and wide enough to ignore edge effects. The temperature distribution after a given time interval is solved by Eagar and Tsai using Green's function with average substrate's thermal properties [53]:

$$T = T_0 + \frac{q\alpha^{\frac{1}{2}}}{2k\pi^{\frac{3}{2}}} \int_0^{t_0} \frac{\tau^{-\frac{1}{2}}}{2\alpha\tau + \sigma^2} \exp\left(-\frac{x^2 + 2x\tau U + U^2\tau^2 + y^2}{4\alpha\tau + 2\sigma^2} - \frac{z^2}{4\alpha\tau}\right) \mathrm{d}\tau \qquad (6.1)$$

where x, y, z are coordinates relative to the center of the heat source, T is the temperature field and T_0 is the initial temperature, q and U are the rate and velocity of the heat source, α and k are thermal diffusivity and conductivity of the substrate, σ is the standard deviation of Gaussian distribution, t_0 is the time interval of the heat source motion. As t_0 increases to infinity, the term of time is omitted and the temperature field approach pseudo-steady state.

Normalization reduces the Equation 6.1 to dimensionless form, independent of

specific operating parameters and material properties, with:

$$T^* = \frac{4\pi k\alpha\,(T - T_0)}{qU} \tag{6.2}$$

$$x^* = \frac{Ux}{2\alpha} \tag{6.3}$$

$$y^* = \frac{Uy}{2\alpha} \tag{6.4}$$

$$z^* = \frac{Uz}{2\alpha} \tag{6.5}$$

$$\sigma^* = \frac{U\sigma}{2\alpha} \tag{6.6}$$

where $*$ indicates dimensionless numbers.

The dimensionless pseudo-steady temperature field on the top-surface ($z^* = 0$) is written with Equation 6.2 to 6.6 as:

$$T^* = \frac{1}{\sqrt{2\pi}} \int_0^\infty \frac{\tau^{-\frac{1}{2}}}{\tau + \sigma^{*2}} \exp\left(-\frac{x^{*2} + 2\tau^* x^* + \tau^{*2} + y^{*2}}{2\tau + 2\sigma^{*2}}\right) d\tau \tag{6.7}$$

With variable substitution

$$t = \arctan\left(\frac{\sqrt{\tau}}{\sigma^*}\right) \tag{6.8}$$

the improper bounds of the integral in the normalized temperature field, Equation 6.7, can be avoided:

$$T^* = \frac{2}{\sqrt{2\pi}\sigma^*} \int_0^{\frac{\pi}{2}} \exp\left\{-\frac{\sigma^{*2}}{2}\left[\left(\frac{x^*}{\sigma^{*2}} - 1\right)\cos t + \sec t\right]^2 - \frac{y^{*2}\cos^2 t}{2\sigma^{*2}}\right\} \mathrm{d}t \tag{6.9}$$

The integrand has one peak value located at:

$$t = \arccos\left[\frac{\sigma^*}{\sqrt[4]{\left(\sigma^{*2} - x^*\right)^2 + y^{*2}}}\right] \tag{6.10}$$

By defining variable $\chi = x^* - \sigma^{*2}$, $\rho = \sqrt{\left(\sigma^{*2} - x^*\right)^2 + y^{*2}}$, the temperature field can be reduced to:

$$T^* = \exp(-\chi - \rho)\frac{\int_0^{\frac{\pi}{2}} \exp\left[-\frac{1}{2}\left(\frac{\cos t}{\sigma^*}\rho - \frac{\sigma^*}{\cos t}\right)^2\right] dt}{\sqrt{\pi/2}\,\sigma^*} \tag{6.11}$$

The temperature field is analogous to the temperature field of moving point heat source (the term $\exp(-\chi - \rho)$) as discussed in [140, 207].

Equations 6.11 and 6.7 contain four degrees of freedom. With the normalized temperature field function and the constraints for maximum width, $\partial T^*/\partial x^* = 0$, the investigation of isotherm half-width leaves two degrees-of-freedom. One is captured by Ry number that has been discussed in detail in [140, 207]:

$$\mathrm{Ry} = \frac{qU}{4\pi k\alpha(T_\mathrm{c} - T_0)} \tag{6.12}$$

The remaining degree-of-freedom is σ^* (Equation 6.6) to represent the diameter of Gaussian heat sources, categorizing the heat sources into concentrated and wide cases. The judgement of concentrated or wide heat source depends not only on the value of σ^*, but also on the temperature of interest, i.e., Ry number. The maximum heat source size $\sigma^*_{\max}$ for a given Ry has been studied in [208]. A variable $\sigma^*/\sigma^*_{\max}$ is defined to address the moving Gaussian heat source problems in a better way.

The Ry number ranges from zero to infinity, and the values of σ^* ranges from zero to one. Four asymptotic regimes can be defined for combinations of Ry and σ^* describing four types of heat sources, which are: Regime I for $\mathrm{Ry} \to \infty$, $\sigma^*/\sigma^*_{\max} \to 0$ (fast and concentrated), Regime II for $\mathrm{Ry} \to 0$, $\sigma^*/\sigma^*_{\max} \to 0$ (slow and concentrated), Regime V for $\mathrm{Ry} \to \infty$, $\sigma^*/\sigma^*_{\max} \to 1$ (fast and wide), Regime VI for $\mathrm{Ry} \to 0$, $\sigma^*/\sigma^*_{\max} \to 1$ (slow and wide). The regimes are illustrated in Figure 6.4.

To deal with characteristic values depending on two variables, a systematic 2-D blending method is proposed in previous research in the investigations of two-dimensional heat flow under intense heat losses [127, 129]. The whole domain for 2-D blending involves four asymptotic regimes, where both variables tend to their bounds, and four asymptotic side regimes between neighbor asymptotic regimes, where one of the variables tends to its bounds. When all asymptotic side regimes converges to dependence on one variable and side partial blending can be achieved either with 1-D blending or asymptotic analysis directly, the proposed 2-D blending method produces

global approximations covering the whole domain of two dimensionless groups. In this paper, side partial blending results can be obtained in asymptotic side regimes I – II ($\sigma^*/\sigma^*_{\max} \to 0$), II – VI (Ry $\to 0$), V – VI ($\sigma^*/\sigma^*_{\max} \to 1$). However, in the asymptotic side Regime I – V (Ry $\to \infty$), isotherms with two peaks might occur and this paper did not manage to find corresponding side partial blending. The problem can be treated by considering part of whole domain. For example, the blending result of isotherm half-width is researched for Ry ≤ 1000 in this work.

In the following sections, the cases of isotherms with two local maximum width are studied and the corresponding region in process map is illustrated; the asymptotic expressions for four asymptotic regimes are derived; the side partial blending results are obtained with 1-D blending; the 2-D blending results is formulated and the engineering expressions for isotherm half-width are developed.

6.3 Isotherms with two local width maxima

Study about the moving point heat source model on thick plate [140] has shown that the normalized width of isotherm $y^*_{\max}$ depends only on one dimensionless group Ry number, i.e. the value of $y^*_{\max}$ can be determined solely for any given Ry number. However, isotherms with two peaks, referring to the cases of two local maximum half-widths $y^*_{\max}$ for one isotherm, can be found for some Ry and σ^* numbers. An example of the isotherm with two peaks is the isotherm of Ry = 110 under Gaussian heat source of normalized distribution parameter $\sigma^* = 4$ as illustrated in Figure 6.1.

The special situations of two-peak isotherms can be explained by alternating dominant mechanisms in different regions. In Regime I, in which the heat source moves fast and the distribution parameter of the heat source could be neglected ($\sigma^*/\sigma^*_{\max} \to 0$, Ry $\to \infty$), the heat advection due to the relative motion between the heat source and substrate dominates where the isotherms are far away from the heat source. In Regime II, in which the heat source moves slowly and the distribution parameter of the heat source is neglected ($\sigma^*/\sigma^*_{\max} \to 0$, Ry $\to 0$), the heat conduction in the near

field of heat source is the dominant phenomenon. In regimes V and VI, where the distribution parameter of heat source is the critical factor to the temperature field around the maximum centerline temperature ($\sigma^*/\sigma^*_{\max} \to 1$), the distribution heat source deposited on the substrate is the primary phenomenon. Between regime I and V, when the heat source is large and moves fast (Ry $\to \infty$ and $\sigma^* \to \infty$), the isotherms with two peaks can be found. These isotherms can be interpreted with caution that one isotherm peak is in the near field of heat source and is dominated by direct energy depositions from the Gaussian heat source; the other isotherm peak locates at far field of heat source and is dominated by heat advection.

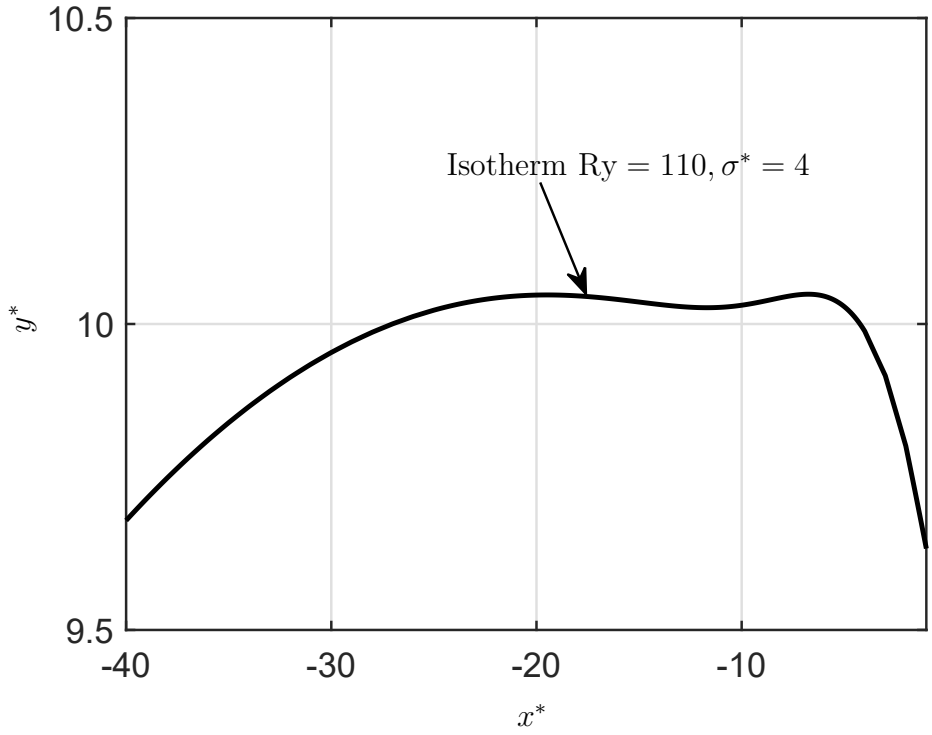

Figure 6.1: Example of the isotherm with two peaks for Ry = 110 and $\sigma^* = 4$.

By substituting Equation 6.35 into Equation 6.11, $\rho_{\max}$ can be solved for maxima and minima of isotherms. For a given normalized Gaussian parameter σ^*, $\rho_{\max}$ is a function of Ry; the isotherm half-width $y^*_{\max}$ and its location $x^*_{\max}$ can be calculated by the value of $\rho_{\max}$ with equation 6.38 and 6.36 (the isotherm minima is also calculated as width $y^*_{\max}$ in this method). For a σ^* where all isotherms have only one peak, the

$y^*_{\max}$ increase with $\rho_{\max}$; for a σ^* where the isotherms with two peaks exist, there is a range of $\rho_{\max}$ in which $y^*_{\max}$ decreasing with $\rho_{\max}$. The criterion can, therefore, be expressed for the existence of isotherms with two peaks:

$$\text{For a given } \sigma^*, \exists\, \rho_{\max},\ \frac{\partial y^*_{\max}}{\partial \rho_{\max}} < 0 \tag{6.13}$$

Because of the definition of $\rho_{\max} = \sqrt{y^{*2}_{\max} + \chi^2_{\max}}$, the criterion, Equation 6.13, can be rewritten as:

$$\frac{\partial y^*_{\max}}{\partial \rho_{\max}} = \frac{\partial \sqrt{\rho^2_{\max} - \chi^2_{\max}}}{\partial \rho_{\max}} = \frac{2\rho_{\max} - 2\chi_{\max}(\frac{\partial \chi_{\max}}{\partial \rho_{\max}})}{2\sqrt{\rho^2_{\max} - \chi^2_{\max}}} < 0 \tag{6.14}$$

Thus, the criterion is that for a σ^*, a $\rho_{\max}$ exist such that:

$$\frac{\partial(\chi^2_{\max})}{\partial(\rho^2_{\max})} > 1 \tag{6.15}$$

A function is constructed to further formulate the criterion (Equation 6.15), and derivatives with respect to $\rho^2_{\max}$:

$$\mathcal{I}(n) = \int_0^{\frac{\pi}{2}} \cos^n t \cdot \exp\left\{-\frac{1}{2}\left[\left(\frac{\cos t}{\sigma^*}\right)^2 \rho^2_{\max} + \left(\frac{\sigma^*}{\cos t}\right)^2\right]\right\} dt \tag{6.16}$$

A recursive relationship is established on the derivatives of function $\mathcal{I}(n)$ with respect to $\rho^2_{\max}$:

$$\frac{\partial \mathcal{I}\,(n)}{\partial\,(\rho^2_{\max})} = \int_0^{\frac{\pi}{2}} \frac{\cos^{n+2} t}{2\sigma^{*2}} \cdot \exp\left[-\frac{1}{2}\left(\frac{\rho^2_{\max}\cos^2 t}{\sigma^{*2}} + \frac{\sigma^{*2}}{\cos^2 t}\right)\right] dt = \frac{\mathcal{I}\,(n+2)}{2\sigma^{*2}} \tag{6.17}$$

Equation 6.35 can be written based on the constructed functions $\mathcal{I}(n)$:

$$\chi_{\max} = -\sigma^{*2}\frac{\mathcal{I}(0)}{\mathcal{I}(2)} \tag{6.18}$$

The derivatives of $\chi^2_{\max}$ with respect to $\rho^2_{\max}$ in the criterion, Equation 6.15, can be formulated according to equations 6.17 and 6.18:

$$\frac{\partial(\chi^2_{\max})}{\partial(\rho^2_{\max})} = 2\chi_{\max}\frac{\partial \chi_{\max}}{\partial(\rho^2_{\max})} = \sigma^{*2}\mathcal{I}(0) \cdot \frac{\mathcal{I}(4)\mathcal{I}(0) - \mathcal{I}(2)^2}{\mathcal{I}(2)^3} \tag{6.19}$$

$\partial(\chi^2_{\max})/\partial(\rho^2_{\max})$ is calculated with Equation 6.19 for some σ^* from 1 to 10, as illustrated in Figure 6.2.

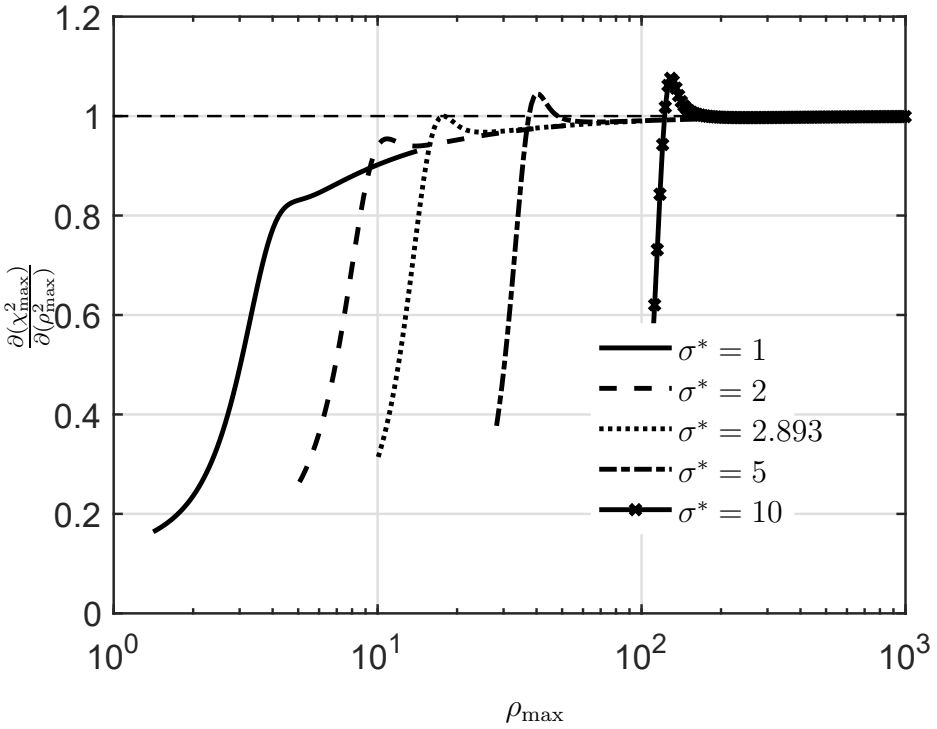

Figure 6.2: The criterion function $\partial(\chi^2_{\max})/\partial(\rho^2_{\max})$ changes with $\rho_{\max}$ for $\sigma^* = 1 \sim 10$. The critical value of normalized Gaussian standard deviation satisfying criterion Equation 6.15 is $\sigma^* = 2.893$.

The criterion for the existence of isotherms with two peak, Equation 6.15, can be rewritten for a given σ^*:

$$\max_{\rho_{\max}} \left[\sigma^{*2} \mathcal{I}(0) \frac{\mathcal{I}(4)\mathcal{I}(0) - \mathcal{I}(2)^2}{\mathcal{I}(2)^3} \right] > 1 \tag{6.20}$$

As shown in Figure 6.2, the critical value of σ^* is 2.893, larger than which isotherms with two peaks exist, and the corresponding critical value of Ry number is 58.20, larger than which there are some values of σ^* induce an isotherm Ry having two peaks. The combinations of Ry and $\sigma^*/\sigma^*_{\max}$ standing for isotherms with two maxima are illustrated in the shaded region in Figure 6.3. For any Ry and $\sigma^*/\sigma^*_{\max}$ in the shaded region, two values of isotherm half-width can be calculated, and the larger value is used in 2-D blending of $y^*_{\max}$.

For example, a heat source of 4000W moves at a velocity $U = 40\,\text{mm/s}$ on Ti-

6Al-4V, assuming thermal conductivity is $k \approx 13\,\mathrm{W/mK}$ and thermal diffusivity $\alpha \approx 5 \times 10^{-6}\,\mathrm{m^2/s}$. The initial temperature is 25 °C. In considering the isotherm of 1000 °C relating to the heat affected zone, the corresponding Ry number is 402 and the normalized maximum heat source size $\sigma^*_{\max}$ is 55. The range of $\sigma^*/\sigma^*_{\max}$ results in two-peak isotherms is 0.11 - 0.14, where the minimum value of heat source size is $\sigma^* = 6.2$ and $\sigma = 1.6$ mm; the maximum critical heat source size is $\sigma^* = 8.1$ and $\sigma = 2.0$ mm. In considering the isotherm of 200 °C relating to thermal residual stress, the corresponding Ry number is 2239 and the normalized maximum heat source size $\sigma^*_{\max}$ is 173. The range of $\sigma^*/\sigma^*_{\max}$ results in two-peak isotherms is 0.057 - 0.11, where the minimum value of heat source size is $\sigma^* = 9.9$ and $\sigma = 2.5$ mm; the maximum critical heat source size is $\sigma^* = 19$ and $\sigma = 4.8$ mm. On the other hand, for a moving heat source of size $\sigma = 2$ mm corresponding to $\sigma^* = 8$, the isotherms involves two peaks for Ry numbers ranging from 396 to 952, or for temperature ranging from 436 °C to 1014 °C.

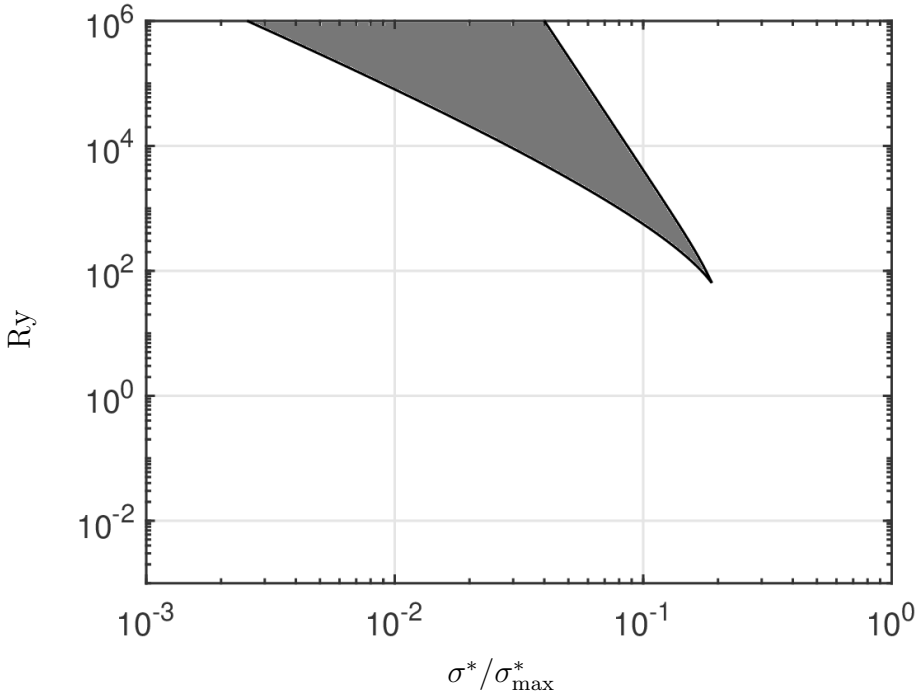

Figure 6.3: Process map for combinations of Ry and $\sigma^*/\sigma^*_{\max}$. In the shaded region, the isotherms have two peaks.

6.4 Asymptotic analysis of isotherm half-width

The asymptotic analysis of the normalized temperature field gives asymptotic expressions in four asymptotic regimes.

In regimes I and II, where $\sigma^*/\sigma^*_{\max} \to 0$ and the Gaussian heat source can be treated as point heat source, the asymptotic expressions are obtained in previous work [140]:

$$\widehat{y}^*_{\max,\mathrm{I}} = \sqrt{\frac{2}{\mathrm{e}}\mathrm{Ry}} \tag{6.21}$$

$$\widehat{y}^*_{\max,\mathrm{II}} = \mathrm{Ry} \tag{6.22}$$

In Regime V, where $\mathrm{Ry} \to \infty$ and $\sigma^*/\sigma^*_{\max} \to 1$ the isotherms are close to the heat source, the asymptotic analysis around the centerline maximum temperature is derived in Appendix Equation 6.61 as:

$$\widehat{y}^*_{\max,\mathrm{V}} = \sqrt{3}\left(\sqrt{\frac{2}{\pi}}I_m\right)^{\frac{2}{3}} \mathrm{Ry}^{\frac{2}{3}} \left(\frac{\sigma^*}{\sigma^*_{\max}}\right) \sqrt{\ln\left(\frac{\sigma^*_{\max}}{\sigma^*}\right)} \tag{6.23}$$

In Regime VI, where $\mathrm{Ry} \to 0$ and $\sigma^*/\sigma^*_{\max} \to 1$ the isotherms are close to the heat source, the asymptotic analysis around the centerline maximum temperature is derived in Appendix Equation 6.48 as:

$$\widehat{y}^*_{\max,\mathrm{VI}} = \sqrt{2\pi}\mathrm{Ry}\left(\frac{\sigma^*}{\sigma^*_{\max}}\right) \sqrt{\ln\left(\frac{\sigma^*_{\max}}{\sigma^*}\right)} \tag{6.24}$$

6.5 Blending of isotherm half-width $y^*_{\max}$

6.5.1 Partial blending

Based on the asymptotic expressions for isotherm half-with, equations 6.21 to 6.24, side partial blending results are obtained along the side regimes I – II, II – VI, V – VI with 1-D blending. In the side Regime I –V, the larger asymptotic value is chosen to predict the isotherm half-width.

In side Regime I – II, where $\sigma^*/\sigma^*_{\max}$ tends to zero and the heat source can be treated as point heat source, the isotherm half-width $y^*_{\max}$ is independent on σ^*. Side partial blending side Regime I – II have been proposed in [140]:

$$\widehat{y}^{*+}_{\max,\mathrm{I-II}} = \mathrm{Ry}\left[1+\left(\sqrt{\frac{2}{\mathrm{eRy}}}\right)^n\right]^{1/n} \tag{6.25}$$

where the optimal blending parameter is $n=-1.731$ with maximum error 0.72 %.

In side Regime II – VI, where Ry tends to zero considering the isotherms around the heat source, the asymptotic behavior of isotherm half-width $y^*_{\max}$ changes with $\sigma^*/\sigma^*_{\max}$. Side partial blending along the side Regime II – VI can be derived by 1-D blending on $\sigma^*/\sigma^*_{\max}$ between asymptotic Equation 6.22 (multiplied by $\exp\left[a\left(\sigma^*/\sigma^*_{\max}\right)^b\right]$ to force crossing as discussed in [128]) and Equation 6.24:

$$\frac{\widehat{y}^{*+}_{\max,\mathrm{II-VI}}}{\mathrm{Ry}} = \left\{\exp\left[a\left(\frac{\sigma^*}{\sigma^*_{\max}}\right)^b\right]^n + \left[\sqrt{2\pi}\frac{\sigma^*}{\sigma^*_{\max}}\sqrt{\ln\left(\frac{\sigma^*_{\max}}{\sigma^*}\right)}\right]^n\right\}^{1/n} \tag{6.26}$$

where $a=-1.560$, $b=4.463$, $n=4.112$ with maximum error of 0.27 %.

In side Regime V – VI, where $\sigma^*/\sigma^*_{\max}\to 1$ considering isotherms under the heat source, the asymptotic behavior of $y^*_{\max}$ changes with Ry. Side partial blending along the side Regime V – VI can be derived by 1-D blending on Ry number between asymptotic Equation 6.23 and Equation 6.24:

$$\frac{\widehat{y}^{*+}_{\max,\mathrm{V-VI}}}{\frac{\sigma^*}{\sigma^*_{\max}}\sqrt{\ln\left(\frac{\sigma^*_{\max}}{\sigma^*}\right)}} = \left\{\left[\sqrt{3}\left(\sqrt{\frac{2}{\pi}}I_m\mathrm{Ry}\right)^{\frac{2}{3}}\right]^n + \left(\sqrt{2\pi}\mathrm{Ry}\right)^n\right\}^{1/n} \tag{6.27}$$

where $n=-3.055$ resulting in a maximum error within 0.38 %.

In side Regime I – V, where Ry tends to infinity, the isotherms with two peaks occur. The isotherm half-widths in this side regime do not converge to a 1-D problem. This paper did not obtain partial blending on side Regime I – V, which results in 2-D blending has an upper bound for Ry ($\mathrm{Ry}\le 1000$ herein).

6.5.2 2-D blending

The asymptotics in four asymptotic regimes and side partial blending in side regimes are proposed from Equation 6.21 to Equation 6.27. The expressions coincide with

exact solutions calculated from the analytical model (Equation 6.7) in their corresponding regimes, but there is a lack of equation covering the whole domain. The formulae for the full domain is carried out with the 2-D blending proposed in [127] by combining the asymptotics and partial blending results. The parameters of partial blending results in Equation 6.25 to 6.27 are adjusted to improve the accuracy of the full domain of 2-D blending.

The 2-D blending of isotherm half-width, $y^*_{\max}$, can be developed based on Regime II with three correction factors for $\mathrm{Ry} \leq 1000$ and $\sigma^*/\widehat{\sigma}^{*+}_{\max} \leq 0.9$

$$\widehat{y}^*_{\max} = \mathrm{Ry} \cdot f_{\mathrm{II-I}} \cdot f_{\mathrm{II-VI}} \cdot g \tag{6.28}$$

The blending equation for maximum heat source size to reach the given temperature $T^*_{\mathrm{c}} = 1/\mathrm{Ry}$ is studied in [208] as:

$$\widehat{\sigma}^*_{\max} = \left[\left(1.014\mathrm{Ry}^{2/3}\right)^n + \left(\sqrt{\pi/2}\mathrm{Ry}\right)^n\right]^{1/n} \tag{6.29}$$

where $n = -2.644$.

The correction factor, $f_{\mathrm{II-I}}$, is for side Regime I – II, depending only on Ry:

$$f_{\mathrm{II-I}} = \left[1 + \left(\sqrt{\frac{2}{\mathrm{eRy}}}\right)^n\right]^{1/n} \tag{6.30}$$

where $n = -1.791$.

The correction factor, $f_{\mathrm{II-VI}}$, is for side Regime II – VI, depending only on $\sigma^*/\widehat{\sigma}^{*+}_{\max}$:

$$f_{\mathrm{II-VI}} = \left\{\exp\left[a\, n\, \left(\frac{\sigma^*}{\widehat{\sigma}^{*+}_{\max}}\right)^b\right] + \left[\sqrt{2\pi}\left(\frac{\sigma^*}{\widehat{\sigma}^{*+}_{\max}}\right)\sqrt{\ln\left(\frac{\widehat{\sigma}^{*+}_{\max}}{\sigma^*}\right)}\right]^n\right\}^{1/n} \tag{6.31}$$

where $n = 4.533$, $a = -3.603$, $b = 13.09$.

The correction factor, g, is for the opposite corner, depending on both Ry and $\sigma^*/\widehat{\sigma}^{*+}_{\max}$:

$$g = 1 + \left(0.8170\,\mathrm{Ry}^{\frac{1}{6}} - 1\right)\left(1 + a_1\mathrm{Ry}^{b_1}\right)^{n_1}\left[1 + a_2\left(\frac{\sigma^*}{\widehat{\sigma}^{*+}_{\max}}\right)^{b_2}\right]^{n_2} \tag{6.32}$$

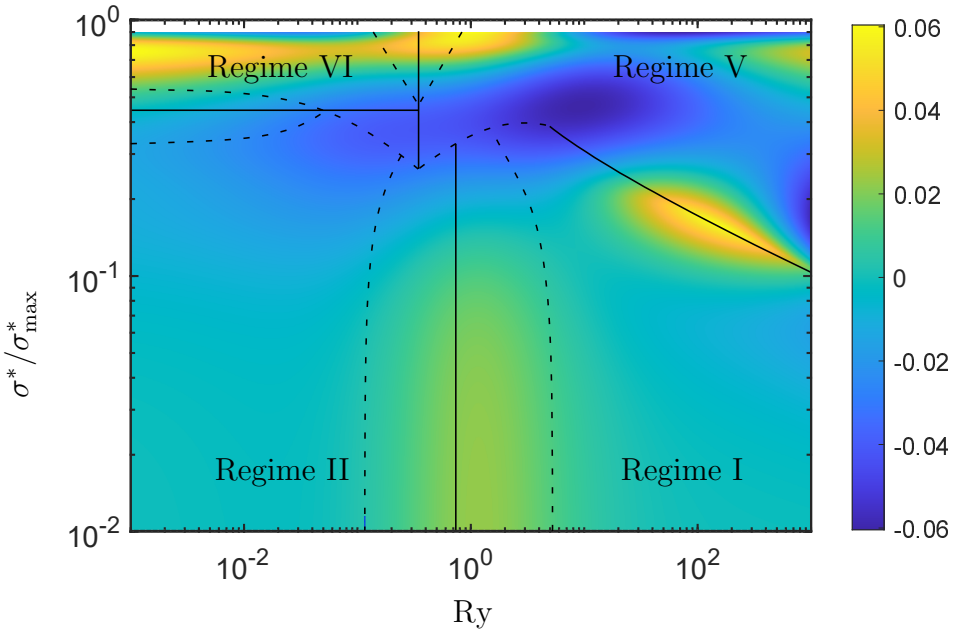

Figure 6.4: The map of 2-D blending errors (equations 6.28 to 6.32) and asymptotic regimes for isotherm half-width $y^*_{\max}$ for Ry ≤ 1000 and $\sigma^*/\widehat{\sigma}^{*+}_{\max} \leq 0.9$. The four asymptotic regimes can be sliced according to a given relative error (dash lines indicate 10 % of error for asymptotic expressions) or the matching of the two asymptotic expressions in side regimes (side regime asymptotics equal on side lines).

where the constant $\sqrt{3}(\sqrt{2/\pi}I_m)^{2/3}/(2\sqrt{\pi/\mathrm{e}}) \approx 0.8170$, and the blending parameters are where $a_1 = 3.859$, $b_1 = -0.5737$, $n_1 = -0.8034$, $a_2 = 0.01703$, $b_2 = -2.202$, $n_2 = -2.226$. The maximum error is 6.1 %, as illustrated in Figure 6.4.

The engineering expressions for isotherm half-width $y^*_{\max}$ can be delivered in dimensional form:

$$\widehat{y}_{\max} = \frac{1}{2\pi}\frac{q}{k(T_\mathrm{c} - T_0)} \cdot f_{\mathrm{II-I}} \cdot f_{\mathrm{II-VI}} \cdot g \tag{6.33}$$

The correction factors $f_{\mathrm{II-I}}$, $f_{\mathrm{II-VI}}$, g, are equations 6.30 to 6.32. The engineering expressions result in a maximum error of 6.1 % for Ry ≤ 1000 and $\sigma^*/\widehat{\sigma}^{*+}_{\max} \leq 0.9$.

6.6 Validation

Prediction of the maximum isotherm half-width calculated by equations 6.28 to 6.32 is validated with experimental measurements collected from the literature for various

materials, including 4145MOD steel, Ti6Al4V, alumina-based refractory, and 316L stainless steel [123, 220, 221, 225].

Although the expressions proposed for isotherm half-widths applies to general moving heat source problems, laser processing of materials is the primary data used for validation because reliable measurements or reasonable estimation of laser beam radius are readily to access. The collected measurements were normalized using equations 6.2 to 6.6 into a dimensionless form such that data of different processes can be plotted and compared in a single graph. The characteristic temperature, T_c in Equation 6.12 corresponds to the melting point of the substrate [123, 220, 221] or the temperature of the heat affected zone [220, 225]. The preheat temperature T_0 were provided in [220, 225] and estimated as 20°C for [123, 221].

Thermal properties are listed in the original papers in all cases, except for [221], where an effective thermal conductivity was obtained using temperature-dependent data from software JMatPro v11. Values of laser absorptivity are provided in the original papers, except for [123] where an estimation of 0.6 was taken to represent the absorption of alumina-based refractory of CO_2 laser radiation according to literature [119].

Measured isotherm half-width is compared with the point heat source prediction (Equations 6.28 and 6.30 without Equation 6.31 and 6.32) in Figure 6.5 and the Gaussian heat source prediction (Equations 6.28 to 6.32) in Figure 6.6. It is obvious that the Gaussian source prediction has a much better agreement with collected experimental data, and there is no obvious bias. The correction factors for the heat distribution parameter can significantly improve the underestimation by point source solution. Despite the large simplifications in the moving Gaussian surface source model, the obtained expression can still predict the maximum isotherm half-width using parameters known before experiments with high accuracy, at least as accurate as measurements.

Secondary phenomena neglected in the model, such as surface heat loss, latent heat

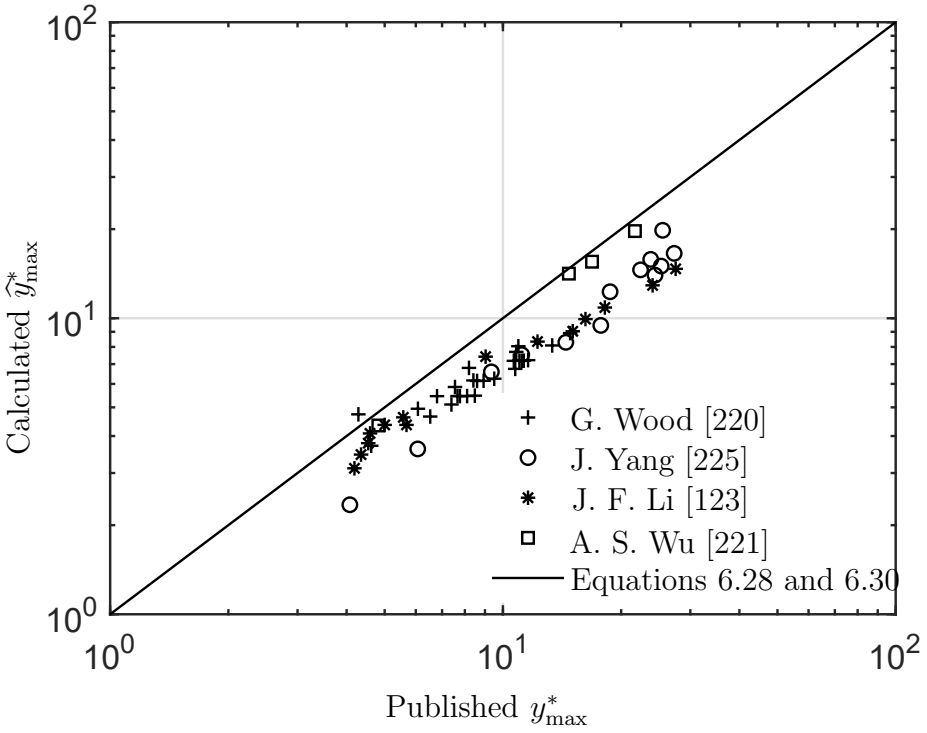

Figure 6.5: Validation of Equations 6.28 and 6.30 with collected published data, neglecting correction factors for size of heat source, equations 6.31 and 6.32.

associated with phase transformations, and fluid flow in the molten pool, contribute to the scatter in the comparisons. Other sources of error include uncertainties in the laser absorptivity and constants used for thermal properties and errors in the measurements.

6.7 Example of application

The laser cladding test performed by Wood [220] is used here as an example of application. The power source was a 3980 W laser in TEM_{00} mode. The distribution parameter of the laser beam was estimated as 1.62 mm. The test was performed on a 20.3 mm-thick 4145-MOD steel substrate. Travel speed and preheat temperature were measured as 38.18 mm/s and 267 °C, respectively. A laser absorptivity of 0.3 was taken from literature [180]. Effective thermophysical properties are provided as: $k = 32.52\text{W/mK}$ and $\alpha = 5.73 \times 10^{-6}\text{m}^2/\text{s}$ [220]. The measured melt width was 1.23

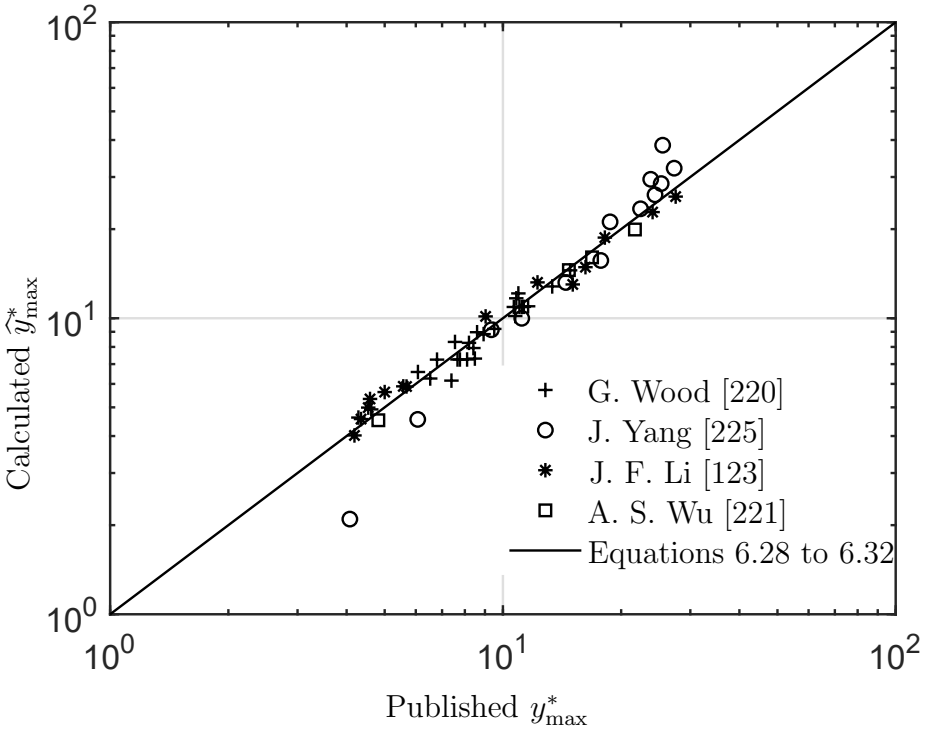

Figure 6.6: Validation of Equations 6.28 and 6.32 with collected published data, taking account correction factors for size of heat source.

mm.

For the case considered, Ry = 16.9 (Equation 6.12), dimensionless heat distribution parameter is $\sigma^* = 5.40$ (Equation 6.6), the dimensionless maximum feasible heat distribution parameter is $\widehat{\sigma}^{*+}_{\max} = 6.56$ (Equation 6.29), yielding a ratio of $\sigma^*/\widehat{\sigma}^{*+}_{\max} = 0.822$. Predicted melt half-width by the point source solution is $\widehat{y}^{+}_{\max,\text{point}} = 1.02$ mm, indicating a relative error of the estimation of -19 % compared to the measured half-width. As Ry ≤ 1000 and $\sigma^*/\widehat{\sigma}^{*+}_{\max} \leq 0.9$, Equation 6.31 and 6.32 can be applied to obtain correction factors for the heat distribution parameter: $f_{\text{II-VI}}(\text{Ry}, \sigma^*) = 0.988$ and $g(\text{Ry}, \sigma^*) = 1.18$. Prediction by the Gaussian model is given by $\widehat{y}^{+}_{\max,\text{Gaussian}} = \widehat{y}^{+}_{\max,\text{point}} \cdot f_{\text{II-VI}}(\text{Ry}, \sigma^*) \cdot g(\text{Ry}, \sigma^*) = 1.19$ mm, and it has an error of 3.3 % compared to the measurement. This is case of calculation, and the accuracy should not be expected for all problems.

6.8 Discussion

Novel expressions in closed-form for maximum isotherm half-width, $y_{\max}$, are obtained under moving Gaussian heat source using a systematic method of asymptotic analysis and blending, based on previous investigation on point heat source problems [140]. Correction factors for the size of heat sources are obtained for the first time to improve the prediction of half-width for isotherms close to heat source. With an introduction of heat distribution size parameter σ (the standard deviation of Gaussian function), the singularity in temperature field caused by point heat source assumption is avoided, and the prediction of isotherm half-width is significantly improved without much complexity, as indicated in Figure 6.5 and 6.6. The correction factors of the heat distribution are presented to extend the usefulness of the point heat source solution to a Gaussian distributed heat source. When σ tends to zero, the correction factors, Equation 6.31 and 6.32, tend to one and the engineering expressions coincide with the point heat source solution in [140].

Division of Regime I, II and Regime V, VI reflects the dominance of two heat transfer mechanisms: heat directly absorbed from the Gaussian surface heat source and heat conduction and advection in the substrate. For a fixed heat source power, the maximum isotherm half-width has different dependence on the heat distribution parameter depending on the distance between the location of interest to the heat source. In the near-field region where the heat absorbed directly from the Gaussian source dominates (Regime V and VI), the maximum isotherm half-width $y_{\max}$ increases with heat distribution parameter σ to a maximum at $\sigma \approx 0.5 \sim 0.6\sigma_{\max}$ and then decreases to zero until $\sigma = \sigma_{\max}$. In the far-field region where conduction and advection dominate (Regime I and II), the maximum isotherm half-width always increases with heat source size parameter. The balance between the heat from the Gaussian source and conduction in the solid can also explain the isotherms with two peaks, which occurs in the transition region from Regime I (far-field) to Regime V

(near-field). Heat absorbed directly from the Gaussian source generates the first peak in the isotherm half-width, while the heat transferred by conduction in the substrate yields the second peak.

The convectional 1-D blending technique has been extended to a 2-D domain in a way consistent with previous publication [127]. The obtained expression maintains the asymptotic behaviours in all regimes, and it can provide accurate prediction in the intermediate regimes with optimized blending constants. When partial blending results can be obtained in side regimes, the 2-D blending is valid in the whole domain. However, because half-width does not converge to dependence on one parameter in side Regime I – V as for Ry $\rightarrow \infty$, partial blending can not be derived and the 2-D blending result fails to cover the whole domain, which is valid only for Ry $\leq$ 1000. In side Regime V – VI, the asymptotics, Equation 6.23 and 6.24, involves a logarithm term $\ln(\sigma^*_{\max}/\sigma^*)$, where a small error in $\sigma^*_{\max}$ could result in a huge error in approximation. In this paper, $\sigma^*_{\max}$ is estimated by Equation 6.29, which will generate a large error when $\sigma^*/\sigma^*_{\max} \rightarrow 1$. The 2-D blending is valid only for $\sigma^*/\widehat{\sigma}^{*+}_{\max} \leq 0.9$.

6.9 Conclusions

The paper presents practical, accurate expressions in closed-form to predict the maximum isotherm half-width under a moving Gaussian surface heat source. The dimensionless form of maximum isotherm half-width, $y^*_{\max}$, depends on two dimensionless groups: Rykalin number (Ry) and $\sigma^*/\sigma^*_{\max}$(Ry), where $\sigma^*_{\max}$(Ry) is a function of Ry calculating the maximum heat source size to reach the temperature of interest $T^*_{\mathrm{c}} = 1/\mathrm{Ry}$. The full domain is divided into four regimes: Regime I (large Ry and $\sigma^*/\sigma^*_{\max} \rightarrow 0$), Regime II (small Ry and $\sigma^*/\sigma^*_{\max} \rightarrow 0$), Regime V (large Ry and $\sigma^*/\sigma^*_{\max} \rightarrow 1$), and Regime VI (small Ry and $\sigma^*/\sigma^*_{\max} \rightarrow 1$).

The expressions to estimate the maximum isotherm half-width are presented in from of a simple formula multiplied by three correction factors written as scaling laws (Equation 6.28 to 6.32), and dimensional engineering expressions (Equation 6.33).

The correction factors consists of the correction factor for moving point heat source, Equation 6.30, and correction factors for the size of heat source (Equation 6.31 and 6.32). The correction factors are obtained with a systematic methodology of dimensional analysis, asymptotic analysis and 2-D blending.

The engineering expressions, derived from 2-D blending, matches the asymptotic behaviours in all four regimes exactly. The maximum error at intermediate regimes compared to the analytical model is smaller than 6.1 % for Ry ≤ 1000, and $\sigma^*/\widehat{\sigma}^{*+}_{\max} \leq 0.9$. Although the blending result, Equation 6.28 to 6.32, inherits all limitations of the moving Gaussian heat source model, it still can reasonably predict the maximum isotherm half-width over a wide range of processes and materials, as indicated in the validation Figure 6.6.

Derived from fundamental principles of heat transfer, the expressions proposed can be applied to manufacturing processes other than laser processing. The expressions in closed-form can be easily calculated by a calculator or a single spreadsheet or embedded into larger metamodels.

References

[5] D. K. Adak, M. Mukherjee, and T. K. Pal, "Development of a direct correlation of bead geometry, grain size and haz width with the gmaw process parameters on bead-on-plate welds of mild steel," *Transactions of the Indian Institute of Metals*, vol. 68, no. 5, pp. 839–849, 2015.

[18] K. Y. Benyounis, A. G. Olabi, and M. S. J. Hashmi, "Optimizing the laser-welded butt joints of medium carbon steel using RSM," *Journal of Materials Processing Technology*, vol. 164-165, pp. 986–989, 2005.

[39] H. E. Cline and T. R. Anthony, "Heat treating and melting material with a scanning laser or electron beam," *Journal of Applied Physics*, vol. 48, no. 9, pp. 3895–3900, 1977.

[53] T. W. Eagar and N. S. Tsai, "Temperature fields produced by traveling distributed heat sources," *Welding Journal*, vol. 62, no. 12, pp. 346–355, 1983.

[65] Z. Gan, G. Yu, X. He, and S. Li, "Numerical simulation of thermal behavior and multicomponent mass transfer in direct laser deposition of co-base alloy on steel," *International Journal of Heat and Mass Transfer*, vol. 104, pp. 28–38, 2017, ISSN: 0017-9310.

[74] J. Goldak, A. Chakravarti, and M. Bibby, "A new finite element model for welding heat sources," *Metallurgical Transactions B*, vol. 15, no. 2, pp. 299–305, 1984.

[98] X. Jia, J. Xu, Z. Liu, S. Huang, Y. Fan, and Z. Sun, "A new method to estimate heat source parameters in gas metal arc welding simulation process," *Fusion Engineering and Design*, vol. 89, no. 1, pp. 40–48, 2014.

[110] S. Kou and Y. Le, "Three-dimensional heat flow and solidification during the autogeneous GTA welding of aluminum plates," *Metallurgical Transactions A*, vol. 14, no. 11, pp. 2245–2253, 1983.

[113] S. Kou, *Welding metallurgy*, Second Edi. Hoboken, New Jersey: John Wiley & Sons, Inc., 2003, 234–235 t85, ISBN: 0471434914.

[119] J. Lawrence and L. Li, "Determination of the absorption length of CO2 and high power diode laser radiation for a high volume alumina-based refractory material," *Applied surface science*, vol. 168, no. 1-4, pp. 71–74, 2000.

[123] J. Li, Q. Guan, Y. W. Shi, and D. L. Guo, "Stress and distortion mitigation technique for welding titanium alloy thin sheet," *Science and Technology of Welding and Joining*, vol. 9, no. 5, pp. 451–458, 2004.

[127] Y. Lu, M. R. Grams, and P. F. Mendez, "Width of thermal features induced by a moving heat source on a thin plate with surface heat losses," 2021.

[128] Y. Lu and P. F. Mendez, "Characteristic values of the temperature field induced by a moving line heat source," *International Journal of Heat and Mass Transfer*, p. 120 671, 2020.

[129] Y. Lu and P. F. Mendez, "The effect of surface heat losses on isotherm trailing length and cooling rate," 2021.

[130] Y. Lu, Y. Wang, and P. F. Mendez, "Width of thermal features induced by a 2-D moving heat source," *International Journal of Heat and Mass Transfer*, vol. 156, p. 119 793, 2020.

[140] P. F. Mendez, Y. Lu, and Y. Wang, "Scaling analysis of a moving point heat source in steady- state on a semi-infinite solid," *Journal of Heat Transfer*, vol. 140, no. 8, p. 081 301, 2018.

[150] N. T. Nguyen, A. Ohta, K. Matsuoka, N. Suzuki, and Y. Maeda, "Analytical solutions for transient temperature of semi-infinite body subjected to 3-D moving heat sources," *Welding Research Supplement*, vol. 78, no. August, 265s–274s, 1999.

[155] N. Okui, D. Ketron, F. Bordelon, Y. Hirata, and G. Clark, "A methodology for prediction of fusion zone shape," *Welding Research Supplement*, vol. 86, no. 2, pp. 35–43, 2007.

[160] V. Pavelic, R. Tanbakuchi, O. A. Uyehara, and P. S. Myers, "Experimental and computed temperature histories in gas tungsten-arc welding of thin plates," *Welding Research Supplement*, vol. 48, pp. 295–305, 1969.

[180] M. F. Schneider and M. F. Schneider, "Laser cladding with powder," PhD thesis, University of Twente, 1998.

[190] D. T. Swift-Hook and A. E. F. Gick, "Penetration welding with lasers," *Welding Research Supplement*, vol. 52, no. 11, 492s–499s, 1973.

[196] N. Tsai, "Heat distribution and weld bead geometry in arc welding," PhD thesis, Massachusetts Institute of Technology, 1983.

[207] Y. Wang, Y. Lu, and P. F. Mendez, "Scaling expressions of characteristic values for a moving point heat source in steady state on a semi-infinite solid," *International Journal of Heat and Mass Transfer*, vol. 135, pp. 1118–1129, 2019.

[208] Y. Wang, Y. Lu, and P. F. Mendez, "Prediction of peak temperature under a moving gaussian surface heat source," 2021.

[209] Y. Wang and P. F. Mendez, "Prediction of maximum isotherm depth under a moving gaussian surface heat source."

[212] P. S. Wei and W. H. Giedt, "Surface tension gradient-driven flow around an electron beam welding cavity," *Welding Journal*, vol. 64, no. 9, 251s–259s, 1985.

[213] A. A. Wells, "Heat flow in welding," *Welding Research Supplement*, vol. 31, no. 5, 263s–267s, 1952.

[216] J. Winczek, "Analytical solution to transient temperature field in a half-infinite body caused by moving volumetric heat source," *International Journal of Heat and Mass Transfer*, vol. 53, no. 25-26, pp. 5774–5781, 2010.

[220] G. D. Wood, "Heat and mass transfer aspects of coaxial laser cladding and its application to nickel-tungsten carbide alloys," PhD thesis, University of Alberta, 2017.

[221] A. S. Wu, D. W. Brown, M. Kumar, G. F. Gallegos, and W. E. King, "An experimental investigation into additive manufacturing-induced residual stresses in 316l stainless steel," *Metallurgical and Materials Transactions A*, vol. 45, no. 13, pp. 6260–6270, 2014.

[225] J. Yang, S. Sun, M. Brandt, and W. Yan, "Experimental investigation and 3D finite element prediction of the heat affected zone during laser assisted machining of Ti6Al4V alloy," *Journal of Materials Processing Technology*, vol. 210, no. 15, pp. 2215–2222, 2010, ISSN: 0924-0136.

Appendix 6.A Expressions for isotherm half-width and its location

According to the definition of isotherm half-width,

$$\left.\frac{\partial T^*}{\partial x^*}\right|_{x^*_{\max},y^*_{\max}} = \frac{2\exp\left(-\chi_{\max}-\rho_{\max}\right)}{\sqrt{2\pi}\sigma^{*3}}.$$

$$\int_0^{\frac{\pi}{2}} \left[-\sigma^{*2}+\left(\sigma^{*2}-\chi_{\max}\right)\cos^2 t\right]\exp\left[-\frac{1}{2}\left(\frac{\cos t}{\sigma^*}\rho_{\max}-\frac{\sigma^*}{\cos t}\right)^2\right]dt = 0 \tag{6.34}$$

Thus, $\chi_{\max}$ depends only on $\rho_{\max}$:

$$\chi_{\max} = \frac{-\sigma^{*2}\int_0^{\frac{\pi}{2}}\exp\left[-\frac{1}{2}\left(\frac{\cos t}{\sigma^*}\rho_{\max}-\frac{\sigma^*}{\cos t}\right)^2\right]dt}{\int_0^{\frac{\pi}{2}}\cos^2 t\exp\left[-\frac{1}{2}\left(\frac{\cos t}{\sigma^*}\rho_{\max}-\frac{\sigma^*}{\cos t}\right)^2\right]dt} \tag{6.35}$$

The isotherm half-width $y^*_{\max}$ and its location $x^*_{\max}$ can be calculated:

$$x^*_{\max} = \sigma^{*2} - \frac{\sigma^{*2}\int_0^{\frac{\pi}{2}}\exp\left[-\frac{1}{2}\left(\frac{\cos t}{\sigma^*}\rho_{\max}-\frac{\sigma^*}{\cos t}\right)^2\right]dt}{\int_0^{\frac{\pi}{2}}\cos^2 t\exp\left[-\frac{1}{2}\left(\frac{\cos t}{\sigma^*}\rho_{\max}-\frac{\sigma^*}{\cos t}\right)^2\right]dt} \tag{6.36}$$

$$y^*_{\max} = \sqrt{\rho^2_{\max}-\chi^2_{\max}} \tag{6.37}$$

$$= \sqrt{\rho^2_{\max} - \left\{\frac{\sigma^{*2}\int_0^{\frac{\pi}{2}}\exp\left[-\frac{1}{2}\left(\frac{\cos t}{\sigma^*}\rho_{\max}-\frac{\sigma^*}{\cos t}\right)^2\right]dt}{\int_0^{\frac{\pi}{2}}\cos^2 t\exp\left[-\frac{1}{2}\left(\frac{\cos t}{\sigma^*}\rho_{\max}-\frac{\sigma^*}{\cos t}\right)^2\right]dt}\right\}^2} \tag{6.38}$$

Appendix 6.B Regime VI, $\sigma^* \to \sigma^*_{\max} \to 0$, $\mathrm{Ry} \to 0$

For cases σ^* tending to $\sigma^*_{\max}$, the isotherm of the given temperature T^*_{c} surrounds the maximum temperature $T^*_{\max,\mathrm{c}}$ locating $x^*_{\max,\mathrm{c}}$ at centerline. The maximum temperature and its location are studied in previous work [208].

At the isotherm half-width $y^*_{\max} = 0 + \mathrm{d}y^*$, and its location $x^*_{\max} = x^*_{\max,\mathrm{c}} - \mathrm{d}x^*$, where $\mathrm{d}x^*, \mathrm{d}y^* \to 0$, the temperature gradient along x-direction equals zero. In first order Taylor expansion, the thermal gradient $\partial T^*/\partial x^* = T^*_{x^*}\left(x^*_{\max}, y^*_{\max}\right)$ is written as:

$$T^*_{x^*}\left(x^*_{\max}, y^*_{\max}\right) = 0 \tag{6.39}$$

$$\approx T^*_{x^*}\left(x^*_{\max,\mathrm{c}}, 0\right) + T^*_{x^*x^*}\left(x^*_{\max,\mathrm{c}}, 0\right)\mathrm{d}x^* + T^*_{x^*y^*}\left(x^*_{\max,\mathrm{c}}, 0\right)\mathrm{d}y^* \tag{6.40}$$

where $T^*_{x^*}\left(x^*_{\max,c}, 0\right) = 0$ according to definition of maximum temperature, and $T^*_{x^*y^*}\left(x^*_{\max,c}, 0\right) = 0$ because the temperature function only involves the term of the second order (y^{*2}). Therefore, the increment of isotherm half-width location $\mathrm{d}x^* \approx 0$, and the location of isotherm half-width can be assumed as the location of centerline temperature

$$x^*_{\max} \approx x^*_{\max,c} \tag{6.41}$$

For $\sigma^*_{\max} \to 0$, the maximum temperature at Regime VI is $T^*_{\max,c} = \sqrt{\frac{\pi}{2}}\ \sigma^{*-1}$ and the location is $x^*_{\max,c} = -\sigma^{*2}$ [208]. The location of isotherm half-width $x^*_{\max} = x^*_{\max,c} = -\sigma^{*2}$ according to Equation 6.41. The temperature near the centerline maximum temperature is expanded in taylor series:

$$\begin{aligned}
&T^*(x^*_{\max}, y^*_{\max}) \approx T^*(x^*_{\max,c}, 0) + T^*_{y^*}(x^*_{\max,c}, 0)\mathrm{d}y^* + \frac{1}{2}T^*_{y^*y^*}(x^*_{\max,c}, 0)\mathrm{d}y^{*2} \\
&= \frac{2}{\sqrt{2\pi}\sigma^*}\int_0^{\frac{\pi}{2}} \exp\left\{-\frac{\sigma^{*2}}{2}\left[\left(\frac{x^*_{\max,c}}{\sigma^{*2}} - 1\right)\cos t + \sec t\right]^2\right\}\mathrm{d}t \\
&\quad - \frac{2}{\sqrt{2\pi}\sigma^*}\int_0^{\frac{\pi}{2}} \exp\left\{-\frac{\sigma^{*2}}{2}\left[\left(\frac{x^*_{\max,c}}{\sigma^{*2}} - 1\right)\cos t + \sec t\right]^2\right\}\frac{\cos^2 t}{2\sigma^{*2}}\mathrm{d}y^{*2}\mathrm{d}t \\
&= \frac{\pi}{\sqrt{2\pi}\sigma^*} - \frac{\mathrm{d}y^{*2}}{\sqrt{2\pi}\sigma^{*3}}\int_0^{\frac{\pi}{2}} \exp\left[-\frac{\sigma^{*2}}{2}\left(-2\cos t + \sec t\right)^2\right]\cos^2 t\,\mathrm{d}t \qquad (6.42) \\
&\approx \frac{\pi}{\sqrt{2\pi}\sigma^*} - \frac{\mathrm{d}y^{*2}}{\sqrt{2\pi}\sigma^{*3}}\int_0^{\frac{\pi}{2}} 1\cdot\cos^2 t\,\mathrm{d}t \qquad (6.43) \\
&\approx \frac{\pi}{\sqrt{2\pi}\sigma^*} - \frac{\mathrm{d}y^{*2}}{\sqrt{2\pi}\sigma^{*3}}\frac{\pi}{4} \qquad (6.44) \\
&= T^*_{\max,c}\cdot\left(1 - \frac{\mathrm{d}y^{*2}}{4\sigma^{*2}}\right) \qquad (6.45)
\end{aligned}$$

Therefore, the isotherm half-width at Regime VI can be solved with Equation 6.45:

$$\widehat{y}^*_{\max,\mathrm{VI}} \approx \mathrm{d}y^* = 2\sigma^*\sqrt{1 - \frac{T^*}{T^*_{\max,c}}} \tag{6.46}$$

Because of the relationship between maximum temperature and heat source diameters at Regime VI [208], $T^*_{\max,c} = \sqrt{\frac{\pi}{2}}\ \sigma^{*-1}$, the asymptotic Equation 6.46 can be

written as function of Ry and $\sigma^*/\sigma^*_{\max}$:

$$\widehat{y}^*_{\max,\mathrm{VI}} = 2\sigma^*\sqrt{\ln\left(\frac{\sigma^*_{\max}}{\sigma^*}\right)} \tag{6.47}$$

$$= \sqrt{2\pi}\mathrm{Ry}\left(\frac{\sigma^*}{\sigma^*_{\max}}\right)\sqrt{\ln\left(\frac{\sigma^*_{\max}}{\sigma^*}\right)} \tag{6.48}$$

Appendix 6.C Regime V: $\sigma^* \to \sigma^*_{\max} \to \infty$, $\mathrm{Ry} \to \infty$

In Regime V, when $\sigma^* \to \sigma^*_{\max}$ and $\sigma^*_{\max} \to \infty$, the maximum temperature is $T^*_{\max,\mathrm{c}} = \sqrt{\frac{2}{\pi}} I_m \, \sigma^{*-1.5}$ and its location $x^*_{\max,\mathrm{c}} = -0.7650\sigma^*$ [208], where $I_m = 1.280$. The location of isotherm half-width, according to Equation 6.41, is $x^*_{\max} = x^*_{\max,\mathrm{c}} - 0.7650\sigma^*$. The temperature around the maximum temperature is expanded in taylor series:

$$\begin{aligned} T^*(x^*_{\max}, y^*_{\max}) &\approx T^*(x^*_{\max,\mathrm{c}}, 0) + T^*_{y^*}(x^*_{\max,\mathrm{c}}, 0)\mathrm{d}y^* + \frac{1}{2}T^*_{y^*y^*}(x^*_{\max,\mathrm{c}}, 0)\mathrm{d}y^{*2} \\ &= \frac{2}{\sqrt{2\pi}\sigma^*}\int_0^{\frac{\pi}{2}} \exp\left\{-\frac{\sigma^{*2}}{2}\left[\left(\frac{x^*_{\max,\mathrm{c}}}{\sigma^{*2}} - 1\right)\cos t + \sec t\right]^2\right\}\mathrm{d}t \\ &\quad - \frac{2}{\sqrt{2\pi}\sigma^*}\int_0^{\frac{\pi}{2}} \exp\left\{-\frac{\sigma^{*2}}{2}\left[\left(\frac{x^*_{\max,\mathrm{c}}}{\sigma^{*2}} - 1\right)\cos t + \sec t\right]^2\right\}\frac{\cos^2 t}{2\sigma^{*2}}\mathrm{d}y^{*2}\mathrm{d}t \end{aligned}$$

In Regime V, as $\sigma^* \to \infty$, the integrand is non-zero around $t \approx 0$, according to Equation 6.10:

$$t = \arccos\left\{\frac{\sigma^*}{\left[\left(\sigma^{*2} - x^*_{\max,\mathrm{c}}\right)^2 + y^{*2}\right]^{\frac{1}{4}}}\right\} \tag{6.49}$$

$$\approx \arccos\left\{\frac{\sigma^*}{\left[\left(\sigma^{*2} + 0.7650\sigma^*\right)^2 + y^{*2}\right]^{\frac{1}{4}}}\right\} \tag{6.50}$$

$$\approx \arccos\left\{\frac{\sigma^*}{\left[\left(\sigma^{*2}\right)^2\right]^{\frac{1}{4}}}\right\} \approx 0 \tag{6.51}$$

$$T^*(x^*_{\max}, y^*_{\max}) = \frac{2}{\sqrt{2\pi}\sigma^*}\int_0^{\frac{\pi}{2}} \exp\left\{-\frac{\sigma^{*2}}{2}\left[\left(\frac{x^*_{\max,c}}{\sigma^{*2}}-1\right)\cos t + \sec t\right]^2\right\}\mathrm{d}t$$

$$-\frac{2}{\sqrt{2\pi}\sigma^*}\int_0^{\frac{\pi}{2}} \exp\left\{-\frac{\sigma^{*2}}{2}\left[\left(\frac{x^*_{\max,c}}{\sigma^{*2}}-1\right)\cos t + \sec t\right]^2\right\}\frac{\mathrm{d}y^{*2}}{2\sigma^{*2}}\mathrm{d}t \tag{6.52}$$

$$=\frac{2}{\sqrt{2\pi}\sigma^*}\int_0^{\frac{\pi}{2}} \exp\left\{-\frac{\sigma^{*2}}{2}\left[\left(\frac{x^*_{\max,c}}{\sigma^{*2}}-1\right)\cos t + \sec t\right]^2\right\}\mathrm{d}t\cdot\left(1-\frac{\mathrm{d}y^{*2}}{2\sigma^{*2}}\right) \tag{6.53}$$

$$\approx\frac{2}{\sqrt{2\pi}\sigma^*}\int_0^{\frac{\pi}{2}} \exp\left\{-\frac{1}{2}\left[\frac{x^*_{\max,c}}{\sigma^*}+\sigma^*(\sec t-\cos t)\right]^2\right\}\mathrm{d}t\cdot\left(1-\frac{\mathrm{d}y^{*2}}{2\sigma^{*2}}\right) \tag{6.54}$$

$$\tag{6.55}$$

$$\approx\frac{2}{\sqrt{2\pi}\sigma^*}\int_0^{\frac{\pi}{2}} \exp\left[-\frac{1}{2}\left(-0.7650+\sigma^* t^2\right)^2\right]\mathrm{d}t\cdot\left(1-\frac{\mathrm{d}y^{*2}}{2\sigma^{*2}}\right) \tag{6.56}$$

$$=T^*_{\max,c}\cdot\left(1-\frac{\mathrm{d}y^{*2}}{2\sigma^{*2}}\right) \tag{6.57}$$

Thus, the asymptotic for isotherm half-width at Regime V can be solved:

$$\widehat{y}^*_{\max,V}\approx 0+\mathrm{d}y^*=\sqrt{2}\sigma^*=\sqrt{1-\frac{T^*}{T^*_{\max,c}}} \tag{6.58}$$

Similarly, because $\frac{T^*}{T^*_{\max,c}}\to 1$ in Regime V,

$$\widehat{y}^*_{\max,V}=\sqrt{2}\sigma^*\sqrt{\ln\left(\frac{T^*_{\max}}{T^*}\right)} \tag{6.59}$$

In Regime V, with the relationship $\widehat{T^*}_{\max,c}=\sqrt{\frac{2}{\pi}}I_m\ \sigma^{*-1.5}$ [208]:

$$\widehat{y}^*_{\max,V}=\sqrt{3}\left(\sqrt{\frac{2}{\pi}}I_m\mathrm{Ry}\right)^{\frac{2}{3}}\left(\frac{\sigma^*}{\sigma^*_{\max}}\right)\sqrt{\ln\left(\frac{\sigma^*_{\max}}{\sigma^*}\right)} \tag{6.60}$$

$$=\sqrt{3}\left(\sqrt{\frac{2}{\pi}}I_m\right)^{\frac{2}{3}}\mathrm{Ry}^{\frac{2}{3}}\left(\frac{\sigma^*}{\sigma^*_{\max}}\right)\sqrt{\ln\left(\frac{\sigma^*_{\max}}{\sigma^*}\right)} \tag{6.61}$$

Chapter 7

Conclusions and future work

7.1 Conclusions

This thesis presented systematic methodologies to obtain engineering expressions in closed-form with broad generalities, high accuracies and practical simplicities, for thermal features of temperature field under moving line or Gaussian heat sources. The proposed engineering expressions are based on theoretical analysis and not empirical. They are valid for all materials, heat source sizes, and surface heat losses that match the framework of the problem.

The engineering expressions are written in the form of a simple solution for the dominant factor and correction factors for secondary phenomena, by dimensional analysis, asymptotic analysis and blending. Normalization and dimensional analysis ensures the generality of the proposed expressions that do not depend on specific processes, operating parameters or material properties; asymptotic analysis yields simple solutions in extreme regimes for dominant factor; blending generates correction factors in the intermediate regimes. The blending of functions with only one dependence is developed based on the modification of the Churchill-Usagi blending equation. The modified 1-D blending method is extended to consider non-power-law, non-crossing asymptotic expressions (Equation 2.25). The modified 1-D blending method also improves the behaviour at the intermediate regime by introducing an additional term, especially when the exact solution is asymmetric (Equation 3.112).

The modified blending technique approach is novel, and it overcomes the limitation of previous studies which was incapable of capturing the behaviour of slow heat sources (e.g. [213]) properly. Beyond modifying and improving the 1-D blending formula, a two-dimensional blending technique is proposed for the first time herein to extend the blending technique applicable to functions of two independent variables (Equation 5.26).

This thesis presents for the first time practical and rigorous expressions for calculating 13 isotherm features of 2-D temperature field under moving line heat source. The isotherm thermal features include: isotherm half-width ($y_{\max}$, Equation 2.29 and Equation 2.30), location of isotherm half-width ($x_{\max}$, Equation 3.13 and Equation 3.14), trailing length of an isotherm (x_{b}, Equation 3.20 and Equation 3.21), cooling rate at a given temperature in the center line ($\dot{T}_{\mathrm{b}}$, Equation 3.30 and Equation 3.31), leading length of an isotherm (x_{f}, Equation 3.37 and Equation 3.38), heating rate at a given temperature in the center line ($\dot{T}_{\mathrm{f}}$, Equation 3.44 and Equation 3.45), maximum temperature at a point away from the center line ($T_{\max}$, Equation 3.52 and Equation 3.53), lateral gradient of maximum temperature ($\mathrm{d}T_{\max}/\mathrm{d}y$, Equation 3.60 and Equation 3.61), aspect ratio of an isotherm ($\mathit{Æ}$, Equation 3.68 and Equation 3.69), melting efficiency (η_{m}, Equation 3.73 and Equation 3.74), cooling time from 800 °C to 500 °C ($t_{8/5}$, Equation 3.79 and Equation 3.80), solidification time (t_{sl}, Equation 3.87 and Equation 3.88) and heat affected zone thickness (Δy_{HAZ}, Equation 3.92 and Equation 3.93). These expressions associated with thermal features of moving line heat source are listed in Table 3.2.

These engineering expressions are developed with the modified 1-D blending method based on Rosenthal's model of moving line heat source. The expressions depend only on the Rosenthal number, Ro, a metric of the intensity of heat source. The Rosenthal number divides all possible solutions into two asymptotic regimes: Regime III corresponding to high Ro (large intensity) and low Ro (small intensity). Because Ro depends on a chosen temperature, the heat sources cannot be deemed intrinsically

high or low intensity until a temperature of interest is selected. The expressions coincide with the exact solution of Rosenthal's model in the extremes, and the blending expression for the intermediate regime, exhibiting a discrepancy within 8 % of the exact solution, except for heating rate within 16 %. A modification of the heat intensity can be made to extend the scope of predictions to dissimilar thicknesses and alternative joint configurations, by replacing the intensity of the heat source $q' = q/d$ with q'_{eff} according to Equation 3.97.

The equations in Table 3.2 can not be applied in processes subject to intense surface losses, such as underwater processes, welding on extreme thin plates, thin-wall additive manufacturing, and the calculation of thermal residual-stresses associated with moving heat sources. A dimensionless number h^* is defined to capture the relative intensity of surface heat losses, and a systematic 2-D blending approach is proposed to capture all combinations of Ro and h^* for the first time. Practical engineering expressions are derived from fundamental analysis for the trailing length (x_{b}, equations 4.19 to 4.22), cooling rate ($\dot{T}_{\text{b}}$, equations 4.35 to 4.37), isotherm half-width ($y_{\max}$, equation 5.40 to 5.43) and its location ($x_{\max}$, equation 5.51 to 5.54). All cases are divided into four asymptotic regimes: Regime III and Regime IV without convection, Regime IIIa and Regime IVa under intense convection. The proposed expressions are in the form of an asymptotic expression (in Regime III) multiplied by two or three correction factors, yielding global approximation within 7.1 % for trailing length, 7.6 % for cooling rate, 9.6 % for isotherm width and 12 % for its location. The consideration of surface heat losses enables the extension of the moving heat source analysis to complex but technologically relevant problems such as underwater wet welding, in-service welding, additive manufacturing of thin walls, and combinations of thickness and low target temperatures where natural convection in the atmosphere becomes relevant (e.g. analysis of residual stresses).

Critical value of dimensionless heat transfer coefficient, h_c^*, is proposed for an acceptable error of 10 % depending on the value of temperature of interest, less than

which the correction factors for surface heat losses can be neglected. The critical h^* for trailing length is Equations 4.39, for cooling rate is Equation 4.40, for isotherm half-width is Equation 5.58, and for location of isotherm half-width is Equation 5.59. For $\mathrm{Ro} = O(1)$, the critical value of h^* is around 0.01.

For the temperature field near the heat source, the heat flow typically can not be treated as two-dimensional, and the distribution of the heat source is a crucial factor. Based on Eagar's Gaussian distributed heat source model [53], the correction factors for Gaussian heat source depend on two dimensionless groups, Ry number (an alternative number for Ro in three-dimensional heat transfer) and σ^* (representing the size of heat source). Therefore, all cases are divided into four asymptotic regimes: Regime I and Regime II for the point heat source, Regime V and Regime VI for Gaussian heat source. The correction factors for isotherm half-width, $y_{\max}$, are derived with the proposed 2-D blending approach, similar to correction factors for surface heat losses, as Equation 6.28 to 6.32 with the maximum error 6.1 % for $\mathrm{Ry} \leq 1000$ and $\sigma^*/\widehat{\sigma}^{*+}_{\max}(\mathrm{Ry}) \leq 0.9$, where $\widehat{\sigma}^*_{\max}(\mathrm{Ry})$ is a function of Ry calculating the maximum heat source size to reach the temperature of interest $T^*_{\mathrm{c}} = 1/\mathrm{Ry}$.

A comprehensive survey of published experiments and simulations is conducted to validate the proposed engineering expressions. The thermal features from a wide range of materials, processes, and parameters are collected to compare with the proposed engineering expressions. The validation of isotherm width, $y_{\max}$, is illustrated in Figures 2.7-2.9, the validation for length of isotherm $(x_{\mathrm{f}} - x_{\mathrm{b}})$ is illustrated in Figure 3.4; the validation for centerline cooling rate, T_{b}, is illustrated in Figure 3.3; the validation for maximum temperature, $T_{\max}$, is illustrated in Figure 3.5, the validation for thickness of heat affected zone, Δy_{HAZ}, is illustrated inFigure 3.6, and the validation for isotherm aspect ratio, $\mathcal{AR}$, is illustrated in (Figure 3.7). The correction factors derived from 2-D blending are also validated. The validation for the correction factors of cooling rate for surface heat losses is illustrated in Figure 4.7(a) and Figure 4.7(b). The validation for the correction factors of isotherm half-width

for surface heat losses is illustrated in Figure 5.6 and Figure 5.7. The validation for the correction factors of isotherm half-width for Gaussian distributed heat source is illustrated in Figure 6.5 and Figure 6.6. Validation against published experiments and simulations shows a close agreement with the predictive engineering expressions despite its simplicity. They capture the essence of the complex physics of moving heat source problems.

The engineering expressions must be applied with an understanding of their limitations caused by the assumptions. For example, they can not be applied in edge parts because of the assumption of the infinitely thin plate. They can not be applied in multilayer welding since the temperature gradient in thickness direction usually can not be neglected. They can not be applied in pulse heat input because of the assumption of pseudo-steady state and constant heat input. They can not be applied when the marangoni flow in the melt pool is significant [82]. For the processes where the engineering expressions can not be applied because of a secondary phenomenon, as mentioned above, correction factors for the secondary phenomenon can be derived by 2-D blending, following similar steps in Chapters 4 and 5 for the effect of surface heat losses.

The engineering expressions provide reasonable predictions of the thermal features, but exact matching to the experiments or sophisticated simulations should not be expected for most engineering calculations. Higher accuracy can be achieved with more sophisticated simulation models or well-designed experiments; however, with the cost of more computational resources, convergence problems, more parameters to be determined prior to calculation, equipment and skill training. For example, volumetric heat sources can improve the accuracy of temperature field prediction in regions close to the heat source, with elaborate choices of parameters. However, it comes with two problems. Firstly, the relevant parameters in the heat source models are difficult to measure or estimate. Secondly, it is nearly unachievable to control the parameters of volumetric heat sources in welding processes, making it impractical to

employ the volumetric heat source parameters in designing rules. The idealizations in this dissertation enable for a much desired practical formula. Fortunately, the gains in practicality come at a relatively low cost in terms of accuracy. The application of analytical modelling at the initial design stage can significantly reduce the time and effort spent in trial and error tests and ensure the mathematical and physical exactness of the obtained expression from the fundamental principles of heat transfer. The validation figures indicate that the idealizations are consistent with most practical problems.

The proposed engineering expressions are rigorous, general, explicit, convenient and accurate. The closed-form expressions are amenable to practical calculations, for example, with Excel spreadsheets or calculators. The engineering expressions deliver engineering understanding and judgment, have clear physical relevance, and provide reasonable predictions in the initial stage in designing and developing new technologies, inspiring creativity and filtering infeasible or inferior designing options by evaluating many optional parameters and processes. The engineering expressions are obtained with a systematic methodology consisting of identification of the dominant phenomena, asymptotic analysis to obtain a simple solution to the dominant mechanism, blending technique to achieve approximation over the whole domain, developing correction factors to capture the deviation from simple solution and validating against analytical solutions, experimental measurements or numerical simulations. The methodology can be adopted in broader engineering problems since the engineering expressions in this thesis show that many important aspects of complex problems can be studied with this methodology. The simple formulae and correction factors can be derived either from asymptotic analysis and blending of analytical modelling as in this thesis, or from regressions of numerical or experimental data.

Novelties

Here is a brief summary of the novelties of this dissertation:

- Modified 1-D blending method (Churchill-Usagi equation) to extend its scope of application to consider non-power-law, non-crossing asymptotic expressions;
- Modified 1-D blending method (Churchill-Usagi equation) with a transitional term to improve accuracy in the intermediate region, especially for "asymmetric" solutions;
- Established a set of engineering expressions for 13 thermal features induced by moving line by implementing the modified 1-D blending method and validated the expressions with published data;
- Extended moving line heat source engineering expressions to dissimilar plate thicknesses and various joint configurations;
- Proposed a systematic 2-D blending approach to achieve global approximation covering the full domain of two dimensionless numbers;
- Proposed correction factors of surface heat losses for isotherm trailing length by implementing the proposed 2-D blending method;
- Proposed correction factors of surface heat losses for cooling rate by implementing the proposed 2-D blending method and validated the correction factors with published data;
- Proposed correction factors of surface heat losses for isotherm half-width and its location by implementing the proposed 2-D blending method and validated the correction factors for isotherm half-width with published data;
- Proposed correction factors of size of Gaussian distributed heat source for isotherm half-width by implementing the proposed 2-D blending method and validated the correction factors with published data;

7.2 Future work

Base on the results presented in this thesis, future work can be conducted on the following aspects:

- To investigate other thermal features of moving heat source problems, for example, correction factors for leading length and heating rate of Gaussian heat sources, moving rectangle heat source that is widely used in surface heat treatments, catchment efficiencies, and many other engineering problems.
- To develop a more general 2-D blending method for cases with more than four asymptotic regimes;
- To implement the 2-D blending approach to establish correction factors for practical characteristic values in other disciplines, like correlations between Nusselt number, Reynold number and Prandtl number;
- To conduct the sensitivity analysis of different operating parameters for practical problems;
- To study blending method depending on more than two variables.

Bibliography

[1] M. Zain-ul abdein, D. Nelias, J. F. Jullien, and D. Deloison, "Prediction of laser beam welding-induced distortions and residual stresses by numerical simulation for aeronautic application," *Journal of Materials Processing Technology*, vol. 209, no. 6, pp. 2907–2917, 2009.

[2] M. Zain-ul abdein, D. Nélias, J. F. Jullien, and D. Deloison, "Experimental investigation and finite element simulation of laser beam welding induced residual stresses and distortions in thin sheets of AA 6056-T4," *Materials Science and Engineering A*, vol. 527, no. 12, pp. 3025–3039, 2010.

[3] A. Acrivos, "On the solution of the convection equation in laminar boundary layer flows," *Chemical Engineering Science*, vol. 17, no. 6, pp. 457–465, 1962.

[4] A. Acrivos, "A rapid method for estimating the shear stress and the separation point in laminar incompressible boundary-layer flows," *Journal of the Aero/Space Sciences*, vol. 27, no. 4, pp. 314–315, 1960.

[5] D. K. Adak, M. Mukherjee, and T. K. Pal, "Development of a direct correlation of bead geometry, grain size and haz width with the gmaw process parameters on bead-on-plate welds of mild steel," *Transactions of the Indian Institute of Metals*, vol. 68, no. 5, pp. 839–849, 2015.

[6] M. J. Adams, "High voltage electron-beam welding," *British Welding Journal*, vol. 15, pp. 451–467, 1968.

[7] M. J. Adams, "Low voltage electron-beam welding," *British Welding Journal*, vol. 15, pp. 134–142, 1968.

[8] M. Akbari, S. Saedodin, D. Toghraie, R. Shoja-Razavi, and F. Kowsari, "Experimental and numerical investigation of temperature distribution and melt pool geometry during pulsed laser welding of Ti6Al4V alloy," *Optics & Laser Technology*, vol. 59, pp. 52–59, 2014.

[9] American Welding Society (AWS) D1 Committee, *Structural welding code - steel*, American Welding Society (AWS) D1 Committee, 2015.

[10] A. Anca, A. Cardona, J. Risso, and V. D. Fachinotti, "Finite element modeling of welding processes," *Applied Mathematical Modelling*, vol. 35, no. 2, pp. 688–707, 2011.

[11] M. Attarha and I. Sattari-Far, "Study on welding temperature distribution in thin welded plates through experimental measurements and finite element simulation," *Journal of Materials Processing Technology*, vol. 211, no. 4, pp. 688 –694, 2011.

[12] H. J. Aval, A. Farzadi, S. Serajzadeh, and A. H. Kokabi, "Theoretical and experimental study of microstructures and weld pool geometry during GATW of 304 stainless steel," *International Journal of Advanced Manufacturing Technology*, vol. 42, no. 11-12, pp. 1043–1051, 2009.

[13] A. S. Azar, S. K. Ås, and O. M. Akselsen, "Determination of welding heat source parameters from actual bead shape," *Computational Materials Science*, vol. 54, pp. 176–182, 2012.

[14] S. Bag, A. Trivedi, and A. De, "Development of a finite element based heat transfer model for conduction mode laser spot welding process using an adaptive volumetric heat source," *International Journal of Thermal Sciences*, vol. 48, no. 10, pp. 1923–1931, 2009.

[15] X. Bai, H. Zhang, and G. Wang, "Improving prediction accuracy of thermal analysis for weld-based additive manufacturing by calibrating input parameters using IR imaging," *The International Journal of Advanced Manufacturing Technology*, vol. 69, no. 5-8, pp. 1087–1095, 2013.

[16] S. Bannour, K. Abderrazak, H. Mhiri, and G. Le Palec, "Effects of temperature-dependent material properties and shielding gas on molten pool formation during continuous laser welding of AZ91 magnesium alloy," *Optics & Laser Technology*, vol. 44, no. 8, pp. 2459–2468, 2012.

[17] D. A. Barry, J. Parlange, L. Li, H. Prommer, C. J. Cunningham, and F. Stagnitti, "Analytical approximations for real values of the Lambert W function," *Mathematics and Computers in Simulation*, vol. 53, pp. 95–103, 2000.

[18] K. Y. Benyounis, A. G. Olabi, and M. S. J. Hashmi, "Optimizing the laser-welded butt joints of medium carbon steel using RSM," *Journal of Materials Processing Technology*, vol. 164-165, pp. 986–989, 2005.

[19] T. L. Bergman, F. P. Incropera, D. P. DeWitt, and A. S. Lavine, *Fundamentals of heat and mass transfer*. John Wiley & Sons, 2011.

[20] A. Birnbaum, P. Aggarangsi, and J. Beuth, "Process scaling and transient melt pool size control in laser-based additive manufacturing processes," in *Proceedings - Solid Freeform Fabrication Symposium*, University of Texas, 2003, pp. 328–339.

[21] I. N. Bronshtein, K. A. Semendyayev, G. Musiol, and H. Mühlig, *Handbook of mathematics*, Fifth. Berlin, Heidelberg: Springer-Verlag Berlin Heidelberg, 2007.

[22] W. A. Bruce and M. A. Boring, "Comparison of methods for predicting safe parameters for welding onto in-service pipelines," in *2006 International Pipeline Conference*, American Society of Mechanical Engineers Digital Collection, 2006, pp. 283–296.

[23] B. Buchmayr and J. S. Kirkaldy, "Modeling of the temperature field, transformation behavior, hardness and mechanical response of low alloy steels during cooling from the austenite region," *Journal of heat treating*, vol. 8, no. 2, pp. 127–136, 1990.

[24] E. Buckingham, "On physically similar systems; illustrations of the use of dimensional equations," *Physical Review*, vol. 4, no. 4, pp. 345–376, 1914.

[25] V. H. Bulsara, Y. Ahn, S. Chandrasekar, and T. N. Farris, "Polishing and lapping temperatures," *Journal of Tribology*, vol. 119, no. 1, pp. 163–170, 1997.

[26] P. Burgardt and C. R. Heiple, "Weld penetration sensitivity to welding variables when near full joint penetration," *Welding journal*, vol. 72, no. 9, pp. 341–347, 1992.

[27] H. S. Carslaw and J. C. Jaeger, *Conduction of heat in solids*, Second. Oxford: Clarendon Press, 1959.

[28] S. Chen, G. Guillemot, and C.-A. Gandin, "Three-dimensional cellular automaton-finite element modeling of solidification grain structures for arc-welding processes," *Acta Materialia*, vol. 115, pp. 448–467, 2016.

[29] Y. H. Chen, Y. Wang, and Z. F. Wang, "Numerical simulation of thermal cycle of in-service welding on X70 steel gas pipeline," in *Multi-Functional Materials and Structures II*, ser. Advanced Materials Research, vol. 79, Trans Tech Publications Ltd, Nov. 2009, pp. 1169–1172.

[30] Z. Chen and X. Gao, "Detection of weld pool width using infrared imaging during high-power fiber laser welding of type 304 austenitic stainless steel," *The International Journal of Advanced Manufacturing Technology*, vol. 74, no. 9-12, pp. 1247–1254, 2014.

[31] J. Cheng and A. Kar, "Mathematical model for laser densification of ceramic coating," *Journal of materials science*, vol. 32, no. 23, pp. 6269–6278, 1997.

[32] S. Chowdhury, N. Yadaiah, S. M. Khan, R. Ozah, B. Das, and M. Muralidhar, "A perspective review on experimental investigation and numerical modeling of electron beam welding process," *Materials Today: Proceedings*, vol. 5, no. 2, pp. 4811–4817, 2018.

[33] N. Christensen, V. d. L. Davies, and K. Gjermundsen, "Distribution of temperatures in arc welding," *British Welding Journal*, vol. 12, no. 2, pp. 54–75, 1965.

[34] S. W. Churchill and R. Usagi, "A general expression for the correlation of rates of transfer and other phenomena," *AIChE Journal*, vol. 18, no. 6, pp. 1121–1128, 1972.

[35] S. W. Churchill, "Comprehensive correlating equations for heat, mass and momentum transfer in fully developed flow in smooth tubes," *Industrial & Engineering Chemistry Fundamentals*, vol. 16, no. 1, pp. 109–116, 1977.

[36] S. W. Churchill, "Comprehensive, theoretically based, correlating equations for free convection from isothermal spheres," *Chemical Engineering Communications*, vol. 24, no. 4:6, pp. 339–352, 1983.

[37] S. W. Churchill and H. H. S. Chu, "Correlating equations for laminar and turbulent free convection from a horizontal cylinder," *International Journal of Heat and Mass Transfer*, vol. 18, no. 9, pp. 1049–1053, 1975.

[38] S. W. Churchill and R. Usagi, "A standardized procedure for the production of correlations in the form of a common empirical equation," *Industrial & Engineering Chemistry Fundamentals*, vol. 13, no. 1, pp. 39–44, 1974.

[39] H. E. Cline and T. R. Anthony, "Heat treating and melting material with a scanning laser or electron beam," *Journal of Applied Physics*, vol. 48, no. 9, pp. 3895–3900, 1977.

[40] G. Comini, S. Del Guidice, R. Lewis, and O. Zienkiewicz, "Finite element solution of non-linear heat conduction problems with special reference to phase change," *International Journal for Numerical Methods in Engineering*, vol. 8, no. 3, pp. 613–624, 1974.

[41] R. M. Corless, G. H. Gonnet, D. E. G. Hare, D. J. Jeffrey, and D. E. Knuth, "On the Lambert W function," *Advances in Computational Mathematics*, vol. 5, no. 1, pp. 329–359, 1996.

[42] L. Cretteur, "Welding and joining of advanced high strength steels (AHSS)," in, ser. Woodhead publishing series in welding and other joining technologies 85. Elsevier, 2015, ch. High-power beam welding of advanced high-strength steels (AHSS), pp. 93–119, ISBN: 978-0-85709-858-0.

[43] J. A. Dantzig and C. L. Tucker, *Modeling in materials processing*. Cambridge, England: Cambridge University Press, 2001.

[44] Z.-S. Deng and J. Liu, "Analytical solutions to 3-D bioheat transfer problems with or without phase change," *Heat Transfer Phenomena and Applications*, p. 205, 2012.

[45] J. Ding, P. Colegrove, J. Mehnen, S. Williams, F. Wang, and P. S. Almeida, "A computationally efficient finite element model of wire and arc additive manufacture," *The International Journal of Advanced Manufacturing Technology*, vol. 70, no. 1-4, pp. 227–236, 2014.

[46] R. Ducharme, K. Williams, P. Kapadia, J. Dowden, B. Steen, and M. Glowacki, "The laser welding of thin metal sheets: An integrated keyhole and weld pool model with supporting experiments," *Journal of Physics D: Appllied Physics*, vol. 27, pp. 1619–1627, 1994.

[47] U. Duman, "Modeling of weld penetration in high productivity GTAW," Ph.D. Colorado School of Mines, 2009.

[48] J. N. DuPont and A. R. Marder, "Thermal efficiency of arc welding processes," *Welding Research Supplement*, vol. 74, no. 12, 406s–416s, 1995.

[49] J. DuPont, "Dilution in fusion welding," *ASM handbook*, vol. 6, pp. 115–121, 2011.

[50] F. Durst, S. Ray, B. Ünsal, and O. A. Bayoumi, "The development lengths of laminar pipe and channel flows," *Journal of Fluids Engineering*, vol. 127, no. 6, pp. 1154–1160, 2005.

[51] R. P. Dutt and R. C. Brewer, "On the theoretical determination of the temperature field in orthogonal machining," *International Journal of Production Research*, vol. 4, no. 2, pp. 91–114, 1965.

[52] D. Dye, O. Hunziker, and R. C. Reed, "Numerical analysis of the weldability of superalloys," *Acta Materialia*, vol. 49, no. 4, pp. 683–697, 2001.

[53] T. W. Eagar and N. S. Tsai, "Temperature fields produced by traveling distributed heat sources," *Welding Journal*, vol. 62, no. 12, pp. 346–355, 1983.

[54] J. W. Elmer, W. H. Giedt, and T. W. Eagar, "The transition from shallow to deep penetration during electron beam welding," *Welding Research Supplement*, vol. 69, no. 5, 167s–176s, 1990.

[55] G. V. Ermolaev, O. B. Kovalev, A. M. Orishich, and V. M. Fomin, "Mathematical modelling of striation formation in oxygen laser cutting of mild steel," *Journal of Physics D: Applied Physics*, vol. 39, no. 19, p. 4236, 2006.

[56] V. D. Fachinotti, A. A. Anca, and A. Cardona, "Analytical solutions of the thermal field induced by moving double-ellipsoidal and double-elliptical heat sources in a semi-infinite body," *International Journal for Numerical Methods in Biomedical Engineerin*, vol. 27, pp. 595–607, 2011.

[57] H. G. Fan, H.-L. Tsai, and S.-J. Na, "Heat transfer and fluid flow in a partially or fully penetrated weld pool in gas tungsten arc welding," *International Journal of heat and mass transfer*, vol. 44, no. 2, pp. 417–428, 2001.

[58] P. S. Fedkiw and J. Newman, "Mass-transfer coefficients in packed beds at very low reynolds numbers," *International Journal of Heat and Mass Transfer*, vol. 25, no. 7, pp. 935–943, 1982.

[59] E. Friedman, "Thermomechanical analysis of the welding process using the finite element method," *Journal of Pressure Vessel Technology*, vol. 97, no. 3, pp. 206–213, 1975.

[60] P. W. Fuerschbach, "A dimensionless parameter model for arc welding processes," in *Trends in Welding Research, Proceedings of the 4th International Conference*, ASM International, 1994.

[61] P. W. Fuerschbach and G. A. Knorovsky, "A study of melting efficiency in plasma arc and gas tungsten arc welding," *Welding Research Supplement*, vol. 70, no. 11, pp. 287–297, 1991.

[62] P. W. Fuerschbach and G. R. Eisler, "Determination of material properties for welding models by means of arc weld experiments," in *Trends in Welding Research, Proceedings of the 6th International Conference*, Callaway Gardens Resort, Phoenix, Arizona: ASM International, 2002.

[63] T. Fukuoka and S. Fuku, "Analysis for cooling process of underwater welding–comparison with welding in air," *Bulletin of Marine Engineering Society in Japan*, vol. 22, no. 2, pp. 86–92, 1994.

[64] S. S. Gajapathi, S. K. Mitra, and P. F. Mendez, "Controlling heat transfer in micro electron beam welding using volumetric heating," *International Journal of Heat and Mass Transfer*, vol. 54, no. 25-26, pp. 5545–5553, 2011.

[65] Z. Gan, G. Yu, X. He, and S. Li, "Numerical simulation of thermal behavior and multicomponent mass transfer in direct laser deposition of co-base alloy on steel," *International Journal of Heat and Mass Transfer*, vol. 104, pp. 28–38, 2017, ISSN: 0017-9310.

[66] E. Gariboldi and B. Previtali, "High tolerance plasma arc cutting of commercially pure titanium," *Journal of Materials Processing Technology*, vol. 160, no. 1, pp. 77–89, 2005.

[67] P. Ghadimi, H. Ghassemi, M. Ghassabzadeh, and Z. Kiaei, "Three-dimensional simulation of underwater welding and investigation of effective parameters," *Welding journal*, vol. 92, no. 8, pp. 239–249, 2013.

[68] A. Ghosh and H. Chattopadhyay, "Mathematical modeling of moving heat source shape for submerged arc welding process," *The International Journal of Advanced Manufacturing Technology*, vol. 69, no. 9-12, pp. 2691–2701, 2013.

[69] A. Ghosh, A. Yadav, and A. Kumar, "Modelling and experimental validation of moving tilted volumetric heat source in gas metal arc welding process," *Journal of Materials Processing Technology*, vol. 239, pp. 52–65, 2017.

[70] W. H. Giedt and L. N. Tallerico, "Prediction of electron beam depth of penetration," *Welding Research Supplement*, vol. 67, no. 12, 299s–305s, 1988.

[71] W. H. Giedt, L. N. Tallerico, and P. W. Fuerschbach, "GTA welding efficiency : Calorimetric and temperature field measurements," *Welding Research Supplement*, vol. 68, no. 1, 28s–32s, 1989.

[72] J. Gockel, J. Fox, J. Beuth, and R. Hafley, "Integrated melt pool and microstructure control for Ti-6Al-4V thin wall additive manufacturing," *Materials Science and Technology*, vol. 31, no. 8, pp. 912–916, 2015.

[73] J. Gockel, N. Klingbeil, and S. Bontha, "A closed-form solution for the effect of free edges on melt pool geometry and solidification microstructure in additive manufacturing of thin-wall geometries," *Metallurgical and Materials Transactions B*, vol. 47, no. 2, pp. 1400–1408, 2016.

[74] J. Goldak, A. Chakravarti, and M. Bibby, "A new finite element model for welding heat sources," *Metallurgical Transactions B*, vol. 15, no. 2, pp. 299–305, 1984.

[75] V. K. Goyal, P. K. Ghosh, and J. S. Saini, "Analytical studies on thermal behaviour and geometry of weld pool in pulsed current gas metal arc welding," *Journal of materials processing technology*, vol. 209, no. 3, pp. 1318–1336, 2009.

[76] M. R. Grams and P. F. Mendez, "Scaling analysis of the thermal stress field produced by a moving point heat source in a thin plate," *Journal of Applied Mechanics*, pp. 1–34, Sep. 2020.

[77] M. R. Grams and P. F. Mendez, "A general expression for the welding tendon force," *ASME J. Manuf. Sci. Eng.* (under review), 2021.

[78] Ø. Grong, *Metallurgical modelling of welding*, First. Cambridge, Great Britain: Institute of Materials, 1994.

[79] M. G. Gunn and E. G. King, "Electron-beam fusion zone penetration in 12 mm (1/2 in.) austenitic stainless steel," in *Advances in Welding Processes Conference*, Harrogate, 1970, pp. 183–186.

[80] C. Habchi, "New correlations for Leidenfrost and Nukiyama temperatures with gas pressure-application to liquid film boiling simulation," in *ILASS Europe*, 2010.

[81] M. Haghpanahi, S. Salimi, P. Bahemmat, and S. Sima, "3-D transient analytical solution based on green's function to temperature field in friction stir welding," *Applied Mathematical Modelling*, vol. 37, no. 24, pp. 9865–9884, 2013.

[82] D. Havrylov, "Hydrodynamic regimes in autogenous fusion welding," PhD thesis, University of Alberta, 2020.

[83] J. C. Heigel, P. Michaleris, and E. W. Reutzel, "Thermo-mechanical model development and validation of directed energy deposition additive manufacturing of Ti–6Al–4V," *Additive manufacturing*, vol. 5, pp. 9–19, 2015.

[84] K. Heller, S. Kessler, F. Dorsch, P. Berger, and T. Graf, "Analytical description of the surface temperature for the characterization of laser welding processes," *International Journal of Heat and Mass Transfer*, vol. 106, pp. 958–969, 2017.

[85] H. Hemmer and Ø. Grong, "Prediction of penetration depths during electron beam welding," *Science and technology of welding and joining*, vol. 4, no. 4, pp. 219–225, 1999.

[86] J. W. Hill, M. J. Lee, and I. J. Spalding, "Surface treatments by laser," *Optics & Laser Technology*, vol. 6, no. 6, pp. 276–278, 1974.

[87] A. Hintze Cesaro and P. F. Mendez, "Models to predict hardness in the HAZ," *Weld Magazine*, pp. 42–55, 2019.

[88] C. Y. Ho, "Asymptotic analysis for penetration depth during laser welding," *Procedia Engineering*, vol. 15, pp. 5212–5216, 2011.

[89] Z. B. Hou and R. Komanduri, "General solutions for stationary/moving plane heat source problems in manufacturing and tribology," *International Journal of Heat and Mass Transfer*, vol. 43, no. 10, pp. 1679–1698, 2000.

[90] Y. F. Hsu and B. Rubinsky, "Two-dimensional heat transfer study on the keyhole plasma arc welding process," *International Journal of Heat and Mass Transfer*, vol. 31, no. 7, pp. 1409–1421, 1988.

[91] M. Inagaki, H. Nakamura, and A. Okada, "Studies of cooling processes in the cases of welding with coated electrode and submerged arc welding," *Journal of the Japan Welding Society*, vol. 34, no. 10, pp. 1064–1075, 1965.

[92] F. P. Incropera, D. P. DeWitt, T. L. Bergman, and A. S. Lavine, *Fundamentals of heat and mass transfer*. John Wiley & Sons, 2007.

[93] C. E. Jackson and A. E. Shrubsall, "Energy distribution in electric welding," *Welding Journal*, vol. 29, no. 5, 231s–241s, 1950.

[94] J. C. Jaeger, "Moving sources of heat and the temperature of sliding contacts," in *Proceedings of the royal society of New South Wales*, vol. 76, 1942, pp. 203–224.

[95] S. J. N. Jason Cheon Degala Venkata Kiran, "Cfd based visualization of the finger shaped evolution in the gas metal arc welding process," *International Journal of Heat and Mass Transfer*, 2016.

[96] C. L. Jenney and A. O'Brien, Eds., *Welding science and technology*, Ninth. American Welding Society (AWS), 2001, vol. 1, ISBN: 978-0-87171-657-6.

[97] P. Jhaveri, W. G. Moffatt, and C. M. Adams, "The effect of plate thickness and radiation on heat flow in welding and cutting," *Welding Research Supplement*, vol. 41, no. 1, 12s–16s, 1962.

[98] X. Jia, J. Xu, Z. Liu, S. Huang, Y. Fan, and Z. Sun, "A new method to estimate heat source parameters in gas metal arc welding simulation process," *Fusion Engineering and Design*, vol. 89, no. 1, pp. 40–48, 2014.

[99] T. Kasuya and N. Yurioka, "Prediction of welding thermal history by a comprehensive solution," *Welding Research Supplement*, vol. 72, no. 3, 107s–115s, 1993.

[100] Y. Kawahito, T. Ohnishi, and S. Katayama, "In-process monitoring and feedback control for stable production of full-penetration weld in continuous wave fibre laser welding," *Journal of Physics D: Applied Physics*, vol. 42, no. 8, p. 085 501, 2009.

[101] J. Kidawa-Kukla, "Temperature distribution in a rectangular plate heated by a moving heat source," *International Journal of Heat and Mass Transfer*, vol. 51, pp. 865–872, 2008.

[102] K. Knothe and S. Liebelt, "Determination of temperatures for sliding contact with applications for wheel-rail systems," *Wear*, vol. 189, no. 1-2, pp. 91–99, 1995.

[103] F. Kolonits, "Analysis of the temperature of the rail/wheel contact surface using a half-space model and a moving heat source," *Proceedings of the Institution of Mechanical Engineers Part F: Journal of Rail and Rapid Transit*, vol. 230, no. 2, pp. 502–509, 2016.

[104] R. Komanduri and Z. B. Hou, "Thermal analysis of the arc welding process : Part I . general solutions," *Metallurgical and Materials Transactions B*, vol. 31B, no. 6, pp. 1353–1370, 2000.

[105] R. Komanduri and Z. B. Hou, "Thermal analysis of the arc welding process. Part II: Effect of variation of thermophysical properties with temperature.," *Metallurgical and Materials Transactions B*, vol. 32, no. 3, 2001.

[106] R. Komanduri and Z. B. Hou, "Thermal analysis of the laser surface transformation hardening process," *International Journal of Heat and Mass Transfer*, vol. 44, no. 15, pp. 2845–2862, 2001.

[107] R. Komanduri and Z. B. Hou, "Unified approach and interactive program for thermal analysis of various manufacturing processes with application to machining," *Machining Science and Technology*, vol. 13, no. 2, pp. 143–176, 2009.

[108] P. J. Konkol, P. M. Smith, C. F. Willibrand, and L. P. Connor, "Parameter study of electron-beam welding," *Welding Journal*, vol. 50, pp. 765–776, 1971.

[109] S. Kou, T. Kanevsky, and S. Fyfitch, "Welding thin plates of aluminum alloys–a quantitative heat-flow analysis," *Welding Research Supplement*, vol. 61, no. 6, 175s–181s, 1982.

[110] S. Kou and Y. Le, "Three-dimensional heat flow and solidification during the autogeneous GTA welding of aluminum plates," *Metallurgical Transactions A*, vol. 14, no. 11, pp. 2245–2253, 1983.

[111] S. Kou and Y. Le, "Welding parameters and the grain structure of weld metal – A thermodynamic consideration," *Metallurgical Transactions A*, vol. 19, no. 4, pp. 1075–1082, 1988.

[112] S. Kou, "Simulation of heat flow during the welding of thin plates," *Metallurgical Transactions A*, vol. 12, no. 12, pp. 2025–2030, 1981.

[113] S. Kou, *Welding metallurgy*, Second Edi. Hoboken, New Jersey: John Wiley & Sons, Inc., 2003, 234–235 t85, ISBN: 0471434914.

[114] S. Kou and D. K. Sun, "Fluid Flow and Weld Penetration in Stationary Arc Welds," *Metallurgical Transactions A*, vol. 16, no. 2, pp. 203–213, 1985.

[115] M. Kubiak, W. Piekarska, and S. Stano, "Modelling of laser beam heat source based on experimental research of Yb : YAG laser power distribution," *International Journal of Heat and Mass Transfer*, vol. 83, pp. 679–689, 2015.

[116] P. K. Kundu, I. M. Cohen, and D. R. Dowling, *Fluid mechanics*, Fifth. Waltham, MA: Academic Press, 2012, ISBN: 978-0-12-382100-3.

[117] Y. Kwon and D. C. Weckman, "Analytical thermal model of conduction mode double sided arc welding," *Science and Technology of Welding and Joining*, vol. 13, no. 6, pp. 539–549, 2008.

[118] D. H. Lammlein, D. R. DeLapp, P. A. Fleming, A. M. Strauss, and G. E. Cook, "The application of shoulderless conical tools in friction stir welding: An experimental and theoretical study," *Materials & Design*, vol. 30, no. 10, pp. 4012–4022, 2009.

[119] J. Lawrence and L. Li, "Determination of the absorption length of CO2 and high power diode laser radiation for a high volume alumina-based refractory material," *Applied surface science*, vol. 168, no. 1-4, pp. 71–74, 2000.

[120] V. N. Lazić, A. S. Sedmak, M. M. Živković, S. M. Aleksandrović, R. D. Čukić, R. D. Jovičić, and I. B. Ivanović, "Theoretical-experimental determining of cooling time ($t_8/5$) in hard facing of steels for forging dies," *Thermal Science*, vol. 14, no. 1, pp. 235–246, 2010.

[121] J. Lee, O. B. Ozdoganlar, and Y. Rabin, "An experimental investigation on thermal exposure during bone drilling," *Medical Engineering & Physics*, vol. 34, no. 10, pp. 1510–1520, 2012.

[122] H. Li, D. Liu, Y. Yan, N. Guo, Y. Liu, and J. Feng, "Effects of heat input on arc stability and weld quality in underwater wet flux-cored arc welding of E40 steel," *Journal of Manufacturing Processes*, vol. 31, pp. 833–843, 2018.

[123] J. Li, Q. Guan, Y. W. Shi, and D. L. Guo, "Stress and distortion mitigation technique for welding titanium alloy thin sheet," *Science and Technology of Welding and Joining*, vol. 9, no. 5, pp. 451–458, 2004.

[124] W.-B. Li, K. E. Easterling, and M. F. Ashby, "Laser transformation hardening of steel-II. hypereutectoid steels," *Acta Metallurgica*, vol. 34, no. 8, pp. 1533–1543, 1986.

[125] Y. Li, Y.-h. Feng, X.-x. Zhang, and C.-s. Wu, "An improved simulation of heat transfer and fluid flow in plasma arc welding with modified heat source model," *International Journal of Thermal Sciences*, vol. 64, pp. 93–104, 2013.

[126] E. V. Locke, E. D. Hoag, and R. A. Hella, "Deep penetration welding with high-power CO2 lasers," *IEEE Journal of Quantum Electronics*, vol. 8, no. 2, pp. 132–135, 1972.

[127] Y. Lu, M. R. Grams, and P. F. Mendez, "Width of thermal features induced by a moving heat source on a thin plate with surface heat losses," 2021.

[128] Y. Lu and P. F. Mendez, "Characteristic values of the temperature field induced by a moving line heat source," *International Journal of Heat and Mass Transfer*, p. 120 671, 2020.

[129] Y. Lu and P. F. Mendez, "The effect of surface heat losses on isotherm trailing length and cooling rate," 2021.

[130] Y. Lu, Y. Wang, and P. F. Mendez, "Width of thermal features induced by a 2-D moving heat source," *International Journal of Heat and Mass Transfer*, vol. 156, p. 119 793, 2020.

[131] C. Luo, Y. Cao, Y. Zhao, L. Zhao, and J. Shan, "Fiber laser welding of 1700-MPa, ultrahigh-strength," *Welding Journal*, vol. 97, 214s–228s, 2018.

[132] S. Malkin, "Thermal aspects of grinding: Part 2 – surface temperatures and workpiece burn," *Journal of Engineering for Industry*, vol. 96, no. 4, pp. 1184–1191, 1974.

[133] O. Manca, B. Morrone, and V. Naso, "Quasi-steady-state three-dimensional temperature distribution induced by a moving circular Gaussian heat source in a finite depth solid," *International Journal of Heat and Mass Transfer*, vol. 38, no. 7, pp. 1305–1315, 1995.

[134] P. F. Mendez, "Synthesis and generalisation of welding fundamentals to design new welding technologies: Status challenges and a promising approach," *Science and Technology of Welding and Joining*, vol. 16, no. 4, pp. 348–356, 2011.

[135] P. F. Mendez, "Reduced order models for welding and solidification processes," in *Proceedings of the 15th Modelling of Casting, Welding and Advanced Solidification Processes Conference (MCWASP XV)*, IOP Conference series: Materials Science and Engineering, 2020.

[136] P. F. Mendez and T. W. Eagar, "Penetration and defect formation in high-current arc welding," *Welding Journal*, vol. 82, no. 10, 296S–306S, 2003.

[137] P. F. Mendez, K. E. Tello, and S. S. Gajapathi, "Generalization and communication of welding simulations and experiments using scaling analysis design rules in welding design rules in engineering : Calibrated minimal representation approach," in *Trends in Welding Research, Proceedings of the 9th International Conference*, ASM International, 2012, pp. 249–258.

[138] P. F. Mendez, "Advanced scaling techniques for the modeling of materials processing," in *Industrial Practice*, vol. 7, ASME, 2006, pp. 393–404, ISBN: 978-0-7918-4358-1.

[139] P. F. Mendez, "Characteristic values in the scaling of differential equations in engineering," *Journal of Applied Mechanics*, vol. 77, no. 6, p. 061 017, 2010.

[140] P. F. Mendez, Y. Lu, and Y. Wang, "Scaling analysis of a moving point heat source in steady- state on a semi-infinite solid," *Journal of Heat Transfer*, vol. 140, no. 8, p. 081 301, 2018.

[141] P. F. Mendez, K. E. Tello, and T. J. Lienert, "Scaling of coupled heat transfer and plastic deformation around the pin in friction stir welding," *Acta Materialia*, vol. 58, no. 18, pp. 6012–6026, 2010.

[142] J. L. Meseguer-Valdenebro, J. Serna, A. Portoles, M. Estrems, V. Miguel, and E. Martínez-Conesa, "Experimental validation of a numerical method that predicts the size of the heat affected zone. optimization of the welding parameters by the Taguchi's method," *Transactions of the Indian Institute of Metals*, vol. 69, no. 3, pp. 783–791, 2016.

[143] K. C. Mills, *Recommended values of thermophysical properties for selected commercial alloys*. Woodhead Publishing Limited, 2002.

[144] Y. S. Muzychka and M. M. Yovanovich, "Thermal resistance models for non-circular moving heat sources on a half space," *Journal of Heat Transfer*, vol. 123, no. 4, pp. 624–632, 2001.

[145] P. S. Myers, O. A. Uyehara, and G. L. Borman, "Fundamentals of heat flow in welding," *Welding Research Council Bulletin*, vol. 123, pp. 1–46, 1967.

[146] O. R. Myhr and Ø. Grong, "Dimensionless maps for heat flow analyses in fusion welding," *Acta Metallurgica et Materialia*, vol. 38, no. 3, pp. 449–460, 1990.

[147] A.-K. Nehad, "Enthalpy technique for solution of stefan problems: Application to the keyhole plasma arc welding process involving moving heat source," *International communications in heat and mass transfer*, vol. 22, no. 6, pp. 779–790, 1995.

[148] T. W. Nelson, R. J. Steel, and W. J. Arbegast, "In situthermal studies and post-weld mechanical properties of friction stir welds in age hardenable aluminium alloys," *Science and Technology of Welding and Joining*, vol. 8, no. 4, pp. 283–288, Aug. 2003.

[149] V. Nemchinsky, "Temperature created by a moving heat source that heats and melts the metal plate (plasma arc cutting)," *Journal of Heat Transfer*, vol. 138, no. 12, p. 122 301, 2016.

[150] N. T. Nguyen, A. Ohta, K. Matsuoka, N. Suzuki, and Y. Maeda, "Analytical solutions for transient temperature of semi-infinite body subjected to 3-D moving heat sources," *Welding Research Supplement*, vol. 78, no. August, 265s–274s, 1999.

[151] S. H. Nikam and N. K. Jain, "Finite element simulation of pre-heating effect on melt pool size during micro-plasma transferred arc deposition process," in *IOP Conference Series: Materials Science and Engineering*, ser. IOP Conference Series: IOP Publishing, vol. 389, 2018, p. 012 006.

[152] A. Nisar, M. J. J. Schmidt, M. A. Sheikh, and L. Li, "Three-dimensional transient finite element analysis of the laser enamelling process and moving heat source and phase change considerations," *Proceedings of the Institution of Mechanical Engineers, Part B: Journal of Engineering Manufacture*, vol. 217, no. 6, pp. 753–764, 2003.

[153] A. Odabaşı, N. Ünlü, G. Göller, and M. N. Eruslu, "A Study on Laser Beam Welding (LBW) Technique: Effect of Heat Input on the Microstructural Evolution of Superalloy Inconel 718," *Metallurgical and Materials Transactions A*, vol. 41A, no. 9, pp. 2357–2365, 2010.

[154] K. Ogawa, "Analysis of temperature distribution around moving heat source in thin plate," *Journal of the Marine Engineering Society in Japan*, vol. 22, no. 4, pp. 257–262, 1987.

[155] N. Okui, D. Ketron, F. Bordelon, Y. Hirata, and G. Clark, "A methodology for prediction of fusion zone shape," *Welding Research Supplement*, vol. 86, no. 2, pp. 35–43, 2007.

[156] G. M. Oreper, T. W. Eagar, and J. Szekely, "Convection in arc weld pools," *Welding Journal*, vol. 62, no. 11, pp. 307–312, 1983.

[157] M. N. Özisik, *Heat conduction*, Second. New York;Toronto: A Wiley-Interscience Publication, 1993.

[158] R. Parkitny and J. Winczek, "Analytical solution of temporary temperature field in half-infinite body caused by moving tilted volumetric heat source," *International Journal of Heat and Mass Transfer*, vol. 60, pp. 469–479, 2013.

[159] W. Paulsen, *Asymptotic analysis and perturbation theory*. CRC Press, 2013.

[160] V. Pavelic, R. Tanbakuchi, O. A. Uyehara, and P. S. Myers, "Experimental and computed temperature histories in gas tungsten-arc welding of thin plates," *Welding Research Supplement*, vol. 48, pp. 295–305, 1969.

[161] Q. Peng, "An analytical solution for a transient temperature field during laser heating a finite slab," *Applied Mathematical Modelling*, vol. 40, no. 5-6, pp. 4129–4135, 2016.

[162] H. H. Pennes, "Analysis of tissue and arterial blood temperatures in the resting human forearm," *Journal of applied physiology*, vol. 1, no. 2, pp. 93–122, 1948.

[163] X.-T. Pham, "Two-dimensional Rosenthal moving heat source analysis using the meshless element free Galerkin method," *Numerical Heat Transfer, Part A: Applications*, vol. 63, no. 11, pp. 807–823, 2013.

[164] W. Piekarska and M. Kubiak, "Theoretical investigations into heat transfer in laser-welded steel sheets," *Journal of thermal analysis and calorimetry*, vol. 110, no. 1, pp. 159–166, 2012.

[165] W. D. Pilkey and D. F. Pilkey, *Peterson's stress concentration factors*. John Wiley & Sons, 2008.

[166] K. Poorhaydari, B. M. Patchett, and D. G. Ivey, "Estimation of cooling rate in the welding of plates with intermediate thickness," *Welding Journal*, vol. 84, no. 10, 149s–155s, 2005.

[167] J. A. Ramos-Grez and M. Sen, *Analytical, quasi-stationary wilson-rosenthal solution for moving heat sources*, 2019.

[168] A. P. Reynolds, W. Tang, T. Gnaupel-Herold, and H Prask, "Structure, properties, and residual stress of 304l stainless steel friction stir welds," *Scripta materialia*, vol. 48, no. 9, pp. 1289–1294, 2003.

[169] D. Rivas and S. Ostrach, "Scaling of low-prandtl-number thermocapillary flows," *International Journal of Heat and Mass Transfer*, vol. 35, no. 6, pp. 1469–1479, 1992.

[170] I. A. Roberts, C. J. Wang, R. Esterlein, M. Stanford, and D. J. Mynors, "A three-dimensional finite element analysis of the temperature field during laser melting of metal powders in additive layer manufacturing," *International Journal of Machine Tools and Manufacture*, vol. 49, no. 12-13, pp. 916–923, 2009.

[171] O. F. T. Roberts, "The theoretical scattering of smoke in a turbulent atmosphere," in *Proceedings of the Royal Society of London*, ser. Series A, Containing Papers of a Mathematical and Physical Character, vol. 104, Royal Society, 1923, pp. 640–654.

[172] M. Rohde, C. Markert, and W. Pfleging, "Laser micro-welding of aluminum alloys: Experimental studies and numerical modeling," *The International Journal of Advanced Manufacturing Technology*, vol. 50, no. 1-4, pp. 207–215, 2010.

[173] W. M. Rohsenow, J. P. Hartnett, Y. I. Cho, *et al.*, *Handbook of heat transfer*, Third, W. M. Rohsenow, J. P. Hartnett, and Y. I. Cho, Eds., ser. McGraw-Hill handbooks. New York: McGraw-Hill, 1998.

[174] D. Rosenthal, "Etude théorique du régime thermique pendant la soudure à l'arc," *Congres National des Sciences Comptes Rendus Bruxelles*, vol. 2, pp. 1277–1292, 1935.

[175] D. Rosenthal, "The theory of moving sources of heat and its application to metal treatments," *Transactions of the A.S.M.E.*, vol. 68, pp. 849–866, 1946.

[176] D. Rosenthal and R. Schmerber, "Thermal study of arc welding," *Welding journal*, vol. 17, no. 4, pp. 2–8, 1938.

[177] D. Rosenthal, "Mathematical theory of heat distribution during welding and cutting," *The Welding Journal*, vol. 20, no. 5, pp. 220–234, 1941.

[178] S. Rouquette, J. Guo, and P. Le Masson, "Estimation of the parameters of a Gaussian heat source by the Levenberg–Marquardt method: Application to the electron beam welding," *International Journal of Thermal Sciences*, vol. 46, no. 2, pp. 128–138, 2007.

[179] N. N. Rykalin, *Calculation of heat flow in welding*. Mashgis, Moscow, Russia: Mashgis, 1951.

[180] M. F. Schneider and M. F. Schneider, "Laser cladding with powder," PhD thesis, University of Twente, 1998.

[181] P. Seyffarth, B. Meyer, and A. Scharff, *Grosser atlas schweiss-ztu-schaubilder*, ser. Fachbuchreihe Schweisstechnik. Düsseldorf: Deutscher Verlag für Schweisstechnik, 1992, ISBN: 9783871551277.

[182] A. K. Shah, S. D. Kulkarni, V. Gopinathan, and R. Krishnan, "Weld heat-affected zone in Ti-6AI-4V alloy Part l–computer simulation of the effect of weld variables on the thermal cycles in the HAZ," *Welding Research Supplement*, vol. 74, no. 9, pp. 297–304, 1995.

[183] Y. Sharir, A. Grill, and J. Pelleg, "Computation of temperatures in thin tantalum sheet welding," *Metallurgical and Materials Transactions B*, vol. 11, no. 2, pp. 257–265, 1980.

[184] S. Shen, I. N. A. Oguocha, and S. Yannacopoulos, "Effect of heat input on weld bead geometry of submerged arc welded ASTM A709 Grade 50 steel joints," *Journal of Materials Processing Technology*, vol. 212, no. 1, pp. 286–294, 2012.

[185] A. Squillace, U. Prisco, S. Ciliberto, and A. Astarita, "Effect of welding parameters on morphology and mechanical properties of Ti-6Al-4V laser beam welded butt joints," *Journal of Materials Processing Technology*, vol. 212, no. 2, pp. 427–436, 2012.

[186] W. M. Steen and J. Mazumder, *Laser material processing*, Fourth. London: Springer, 2010.

[187] Stock Drive Products / Sterling Instrument, *Handbook of METRIC drive components D805*. 2010.

[188] J. Sundqvist, A. F. H. Kaplan, L. Shachaf, and C. Kong, "Analytical heat conduction modelling for shaped laser beams," *Journal of Materials Processing Technology*, vol. 247, pp. 48–54, 2017.

[189] L. E. Svensson, B. Gretoft, and H. K. D. H. Bhadeshia, "An analysis of cooling curves from the fusion zone of steel weld deposits," *Scandinavian Journal of Metallurgy*, vol. 15, pp. 97–103, 1986.

[190] D. T. Swift-Hook and A. E. F. Gick, "Penetration welding with lasers," *Welding Research Supplement*, vol. 52, no. 11, 492s–499s, 1973.

[191] M. R. Talaee and A. Kabiri, "Exact analytical solution of bioheat equation subjected to intensive moving heat source," *Journal of Mechanics in Medicine and Biology*, vol. 17, no. 05, p. 1 750 081, 2017.

[192] Technical Committee CEN/TC 121 Welding, *Welding - recommendations for welding of metallic materials - Part 2 : Arc welding of ferritic steels*, Technical Committee CEN/TC 121 Welding, 2001.

[193] P. Tekriwal and J. Mazumder, "Finite element analysis of three-dimensional transient heat transfer in GMA welding," *Welding Research Supplement*, vol. 67, 150s–156s, 1988.

[194] K. Tello, U. Duman, and P. F. Mendez, "Scaling laws for the welding arc, weld penetration and friction stir welding," in *Trends in Welding Research, Proceedings of the 8th International Conference*, The Material Information Society, ASM International, 2009, pp. 172–181, ISBN: 9781615030026.

[195] R Trivedi, S. David, M. Eshelman, J. Vitek, S. Babu, T Hong, and T DebRoy, "In situ observations of weld pool solidification using transparent metal-analog systems," *Journal of applied physics*, vol. 93, no. 8, pp. 4885–4895, 2003.

[196] N. Tsai, "Heat distribution and weld bead geometry in arc welding," PhD thesis, Massachusetts Institute of Technology, 1983.

[197] M. Ushio, T. Ishimura, F. Matsuda, and Y. Arata, "Theoretical calculation on shape of fusion boundary and temperature distribution around moving heat source (Report I)," *Transactions of JWRI*, vol. 6(1), no. 1, p1–p6, 1977.

[198] M. Van Elsen, M. Baelmans, P. Mercelis, and J.-P. Kruth, "Solutions for modelling moving heat sources in a semi-infinite medium and applications to laser material processing," *International Journal of Heat and Mass Transfer*, vol. 50, no. 23-24, pp. 4872–4882, 2007.

[199] V. R. Voller and C. R. Swaminathan, "General source-based method for solidification phase change," *Numerical Heat Transfer*, vol. 19, pp. 175–189, 1991.

[200] C. S. W. and C. H. H.S., "Correlating equations for laminar and turbulent free convection from a vertical plate," *International Journal of Heat and Mass Transfer*, vol. 18, no. 11, 1975.

[201] J. Wang, J. Shi, J. Wang, W. Li, C. Liu, G. Xu, S. Y. Maksimov, and Q. Zhu, "Numerical study on the temperature field of underwater flux-cored wire arc cutting process," *The International Journal of Advanced Manufacturing Technology*, vol. 91, no. 5-8, pp. 2777–2786, 2017.

[202] L. Wang, S. Felicelli, Y. Gooroochurn, P. T. Wang, and M. F. Horstemeyer, "Optimization of the LENS® process for steady molten pool size," *Materials Science and Engineering: A*, vol. 474, no. 1-2, pp. 148–156, 2008.

[203] L. Wang and S. Felicelli, "Analysis of thermal phenomena in LENS^{TM} deposition," *Materials Science and Engineering: A*, vol. 435, pp. 625–631, 2006.

[204] X. Wang and R. Li, "Intelligent modelling of back-side weld bead geometry using weld pool surface characteristic parameters," *Journal of Intelligent Manufacturing*, vol. 25, no. 6, pp. 1301–1313, Jan. 2014.

[205] Y. Wang, P. Fu, Y. Guan, Z. Lu, and Y. Wei, "Research on modeling of heat source for electron beam welding fusion-solidification zone," *Chinese Journal of Aeronautics*, vol. 26, no. 1, pp. 217–223, 2013.

[206] Y. Wang, Y. Lu, M. Grams, A. H. Cesaro, and P. F. Mendez, "Asymptotics and blending in the modeling of welding," in *Numerical Analysis of Weldability*, Graz, Austria, 2018.

[207] Y. Wang, Y. Lu, and P. F. Mendez, "Scaling expressions of characteristic values for a moving point heat source in steady state on a semi-infinite solid," *International Journal of Heat and Mass Transfer*, vol. 135, pp. 1118–1129, 2019.

[208] Y. Wang, Y. Lu, and P. F. Mendez, "Prediction of peak temperature under a moving gaussian surface heat source," 2021.

[209] Y. Wang and P. F. Mendez, "Prediction of maximum isotherm depth under a moving gaussian surface heat source."

[210] T. Washio and H. Motoda, "Extension of dimensional analysis for scale-types and its application to discovery of admissible models of complex processes," in *International Workshop on Similarity Method*, 1999, pp. 129–147.

[211] J. M. Webster, "Welding at high speed with the CO2 laser," *Metal Progress*, vol. 98, pp. 59–61, 1970.

[212] P. S. Wei and W. H. Giedt, "Surface tension gradient-driven flow around an electron beam welding cavity," *Welding Journal*, vol. 64, no. 9, 251s–259s, 1985.

[213] A. A. Wells, "Heat flow in welding," *Welding Research Supplement*, vol. 31, no. 5, 263s–267s, 1952.

[214] J. B. Will, N. P. Kruyt, and C. H. Venner, "An experimental study of forced convective heat transfer from smooth, solid spheres," *International Journal of Heat and Mass Transfer*, vol. 109, pp. 1059–1067, 2017.

[215] H. A. Wilson, "On convection of heat," in *Proceedings of the Cambridge Philosophical Society*, vol. 12, 1904, pp. 406–423.

[216] J. Winczek, "Analytical solution to transient temperature field in a half-infinite body caused by moving volumetric heat source," *International Journal of Heat and Mass Transfer*, vol. 53, no. 25-26, pp. 5774–5781, 2010.

[217] J. Winczek, A. Modrzycka, and E. Gawrońska, "Analytical description of the temperature field induced by laser heat source with any trajectory," *Procedia Engineering*, vol. 149, pp. 553–558, 2016.

[218] G. Wood, S. A. Islam, and P. F. Mendez, "Calibrated expressions for welding and their application to isotherm width in a thick plate," *Soldagem & Inspeção*, vol. 19, no. 3, pp. 212–220, 2014.

[219] G. Wood and P. F. Mendez, "First order prediction of bead width and height in coaxial laser cladding," in *Proceedings of Numerical Analysis of Weldability*, Graz, Austria, 2015.

[220] G. D. Wood, "Heat and mass transfer aspects of coaxial laser cladding and its application to nickel-tungsten carbide alloys," PhD thesis, University of Alberta, 2017.

[221] A. S. Wu, D. W. Brown, M. Kumar, G. F. Gallegos, and W. E. King, "An experimental investigation into additive manufacturing-induced residual stresses in 316l stainless steel," *Metallurgical and Materials Transactions A*, vol. 45, no. 13, pp. 6260–6270, 2014.

[222] B. Xu, F. Jiang, S. Chen, M. Tanaka, S. Tashiro, and N. Van Anh, "Numerical analysis of plasma arc physical characteristics under additional constraint of keyhole," *Chinese Physics B*, vol. 27, no. 3, p. 034 701, 2018.

[223] N. Yadaiah and S. Bag, "Development of egg-configuration heat source model in numerical simulation of autogenous fusion welding process," *International Journal of Thermal Sciences*, vol. 86, pp. 125–138, 2014.

[224] N. Yadaiah and S. Bag, "Effect of heat source parameters in thermal and mechanical analysis of linear GTA welding process," *ISIJ international*, vol. 52, no. 11, pp. 2069–2075, 2012.

[225] J. Yang, S. Sun, M. Brandt, and W. Yan, "Experimental investigation and 3D finite element prediction of the heat affected zone during laser assisted machining of Ti6Al4V alloy," *Journal of Materials Processing Technology*, vol. 210, no. 15, pp. 2215–2222, 2010, ISSN: 0924-0136.

[226] M. M. Yovanovich, "Four decades of research on thermal contact, gap, and joint resistance in microelectronics," *IEEE transactions on components and packaging technologies*, vol. 28, no. 2, pp. 182–206, 2005.

[227] G. Yu, R. J. Anderson, T. Maekawa, and N. M. Patrikalakis, "Efficient simulation of shell forming by line heating," *International Journal of Mechanical Sciences*, vol. 43, no. 10, pp. 2349–2370, 2001.

[228] L. Zhang, B. L. Tai, G. Wang, K. Zhang, S. Sullivan, and A. J. Shih, "Thermal model to investigate the temperature in bone grinding for skull base neurosurgery," *Medical Engineering & Physics*, vol. 35, no. 10, pp. 1391–1398, 2013.

Appendix A: Matlab codes for blending

Listing A.1: General Matlab class for 1D blending and export latex files.

```
classdef Blending_Grid_size
    %BLENDING_GRID_SIZE blending over varying blending grid size

    properties
        Xdef=struct('xsize',[10,20,40,60,80,100,200,400,600,800,1000,],...
            'xmin',[],'xmax',[]);
        BP=struct('pseed',[],'PList',[],'MaxEList',[],'P',[],'MaxE',[],'BResult',[])
        FigCorrectionFactor=struct('cross_cf_val_error_y2',[],'figure_correction_factor',[], ...
            'accept_error_valy_y1',[], 'accept_error_valx_y1',[], 'accept_error_valy_y2',[],...
            'accept_error_valx_y2',[], 'cross_cf_valx',[], 'cross_cf_valy_y1',[], 'cross_cf_valy_y2',[],...
            'cross_cf_val_error_y1',[]);
    end

    properties
        Funyest
        Blending_Equation
        funy1=@(x) nan;
        funy2=@(x) nan;
        funmodify1=@(x) nan;
        funmodify2=@(x) nan;
        funinter=@(x) nan;
    end
    properties
        latexRegimeI='I'      % name of Regime I
        latexRegimeII='II'    % name of Regime II
        latexX                % name of dependent variable
        latexY                % name of dependent variable
```

```
28          latexBlendingEquation % blending equation
29          latexAsyI                 % asymptotic I
30          latexAsyII                % asymptotic II
31          latexCfI                    % correction factor for regime I
32          latexCfII                   % correction factor for regime II
33          latexBps                  % blending parameters
34      end
35      properties
36          Opt=struct('Isminsearch',1,'options_minsearch',optimset('
                MaxFunEvals',1e10),...
37              'Isminunc',1,'options_minunc',optimoptions(@fminunc,'
                    StepTolerance',1e-40),...
38              'Ismincon',1,'options_mincon',optimoptions(@fmincon,'
                    StepTolerance',1e-60),...
39              'Isga',1,'options_ga',optimoptions(@ga,'PopulationSize',
                    1000,...
40              'HybridFcn', { @fminsearch },'Display', 'off',...
41              'PlotFcn', {@gaplotbestf @gaplotscorediversity }));
42          Pplot=struct('x_label','xx','y_label','yy',...
43              'figname','yx',...
44              'plot_yx',{{true}},...
45              'plot_error',{{true,'x_label','x','y_label','error'}},...
46              'plot_error_p',{{true}},...
47              'pvallist',[]); %[;;])
48      end
49
50      methods
51          function obj = Blending_Grid_size(Funyest,Blending_Equation,xmin,
                xmax,pseed)
52              %BLENDING_GRID_SIZE Construct an instance of this class
53              obj.Funyest =Funyest ;
54              obj.Xdef.xmin = xmin;
55              obj.Xdef.xmax = xmax;
56              obj.BP.pseed = pseed;
57              obj.Blending_Equation = Blending_Equation;
58          end
59
60          function obj = Blending(obj)
61              %Blendig: Blending on different grid size of X
62              for i=1:max(size(obj.Xdef.xsize))
63                  X=logspace(log10(obj.Xdef.xmin),log10(obj.Xdef.xmax),obj.
                        Xdef.xsize(i));
64                  Y=obj.Funyest(X);
65                  Fun_Blending=obj.Blending_Equation(X);
```

```
66              [obj.BP.PList{i},obj.BP.MaxEList{i},~] =
                    fun_blending_general_1D(Fun_Blending,X,Y,obj.BP.pseed)
                    ;
67              disp(['n=',num2str(obj.Xdef.xsize(i))]);
68          end
69          figure(1)
70          plot(obj.Xdef.xsize,100*cell2mat(obj.BP.MaxEList),'-k','
                linewidth',2)
71          xlabel('N')
72          ylabel('Err%')
73          figure(2)
74          p=[];
75          for j=1:max(size(obj.BP.PList))
76              p=[p;obj.BP.PList{j}];
77          end
78          plot(obj.Xdef.xsize,p,'k','linewidth',2); hold on
79          legend
80          xlabel('N')
81          ylabel('p')
82      end
83
84      function obj=FBlending(obj,N)
85          X=logspace(log10(obj.Xdef.xmin),log10(obj.Xdef.xmax),N);
86          Y=obj.Funyest(X);
87          Fun_Blending=obj.Blending_Equation(X);
88          Y1=obj.funy1(X);
89          Y2=obj.funy2(X);
90          Y1modify=obj.funmodify1(X);
91          Y2modify=obj.funmodify2(X);
92
93          [obj.BP.P,obj.BP.MaxE,obj.BP.Result]=fun_blending_general_1D(
                Fun_Blending,X,Y,obj.BP.pseed,...
94              'Y1',Y1,...
95              'Y2',Y2,...
96              'Y1modify',Y1modify,...
97              'Y2modify',Y2modify,...
98              'Isminsearch',obj.Opt.Isminsearch,'options_minsearch',obj
                    .Opt.options_minsearch,...
99              'Isminunc',obj.Opt.Isminunc,'options_minunc',obj.Opt.
                    options_minunc,...
100             'Ismincon',obj.Opt.Ismincon,'options_mincon',obj.Opt.
                    options_mincon,...
101             'Isga',obj.Opt.Isga,'options_ga',obj.Opt.options_ga,...
102             'plot_yx',obj.Pplot.plot_yx,...
103             'plot_error',obj.Pplot.plot_error,...
```

```
104             'plot_error_p',obj.Pplot.plot_error_p,...
105             'pvallist',obj.Pplot.pvallist...
106             );
107 
108         if min((size(Y1)==size(Y)).*(size(Y2)==size(Y)))
109             obj.FigCorrectionFactor= fun_plot_correction_factors_1D(X
                    ,obj.BP.Result.estimation,Y1,Y2,...
110                 'ea',0.1,....
111                 'xlabel',obj.Pplot.x_label,'ylabel',obj.Pplot.y_label)
                        ;
112         end
113     end
114 
115     function obj=funWrite(obj,filename)
116         fileID = fopen(filename,'w');
117         fprintf(fileID,['\\section{',obj.latexY,'}\n']);
118         fprintf(fileID,['\\def\\',obj.latexY,obj.latexRegimeI,'{',obj
                .latexAsyI,'} %% asymptotic \n']);
119         fprintf(fileID,['\\def\\',obj.latexY,obj.latexRegimeII,'{',
                obj.latexAsyII,'} %% asymptotic \n']);
120         fprintf(fileID,['\\def\\',obj.latexY,'B','{',obj.
                latexBlendingEquation,'} %% blending equation \n']);
121         fprintf(fileID,['\\def\\',obj.latexY,'cf',obj.latexRegimeI,'{
                ',obj.latexCfI,'} %% correction factor \n']);
122         fprintf(fileID,['\\def\\',obj.latexY,'cf',obj.latexRegimeII,
                '{',obj.latexCfII,'} %% correction factor\n']);
123         fprintf(fileID,['\\def\\',obj.latexY,'Bps','{',obj.latexBps,'
                } %% blending parameters \n']);
124         fprintf(fileID,['\\def\\',obj.latexY,'BME','{',num2str(round(
                obj.BP.MaxE*100,2,'significant')),'\\%%} %% blending error
                 \n']);
125         fprintf(fileID,['\\def\\',obj.latexY,obj.latexX,obj.
                latexRegimeI,'{',num2str(round(obj.FigCorrectionFactor.
                accept_error_valx_y1,4,'significant')),'} %% valx of 10%%
                acceptable error \n']);
126         fprintf(fileID,['\\def\\',obj.latexY,obj.latexX,obj.
                latexRegimeII,'{',num2str(round(obj.FigCorrectionFactor.
                accept_error_valx_y2,4,'significant')),'} %% valx of 10%%
                acceptable error \n']);
127         fprintf(fileID,['\\def\\',obj.latexY,obj.latexX,'c','{',
                num2str(round(obj.FigCorrectionFactor.cross_cf_valx,4,'
                significant')),'} %% valx of the same error \n']);
128         fprintf(fileID,'\n\n\n\\paragraph{Result of blending:}\n');
129         fprintf(fileID,['Blending parameters are:P= ',num2str(round(
                obj.BP.P,4,'significant')),', the maximum error is ',
```

```
            num2str(round(obj.BP.MaxE*100,4,'significant')),'\\%% \\\\
             \n']);
130         fprintf(fileID,'It is grid size independent:\n');
131         for j=1:max(size(obj.BP.PList))
132             fprintf(fileID,['P=',num2str(round(obj.BP.PList{j},4,'
                    significant')),', Error ',num2str(round(obj.BP.
                    MaxEList{j}*100,4,'significant')),'\\%%, N=',num2str(
                    obj.Xdef.xsize(j)),' \\\\ \n']);
133         end
134         fprintf(fileID,'\n\n\n\\paragraph{Result of Correction
                factors:}\n');
135         fprintf(fileID,'\\begin{align}\n');
136         fprintf(fileID,['Ro_{I}=',num2str(round(obj.
                FigCorrectionFactor.accept_error_valx_y1,4,'significant'))
                ,'\\qquad \\mathrm{where \\quad }f1=',num2str(round(obj.
                FigCorrectionFactor.accept_error_valy_y1,4,'significant'))
                ,'\\\\ \n']);
137         fprintf(fileID,['Ro_{II}=',num2str(round(obj.
                FigCorrectionFactor.accept_error_valx_y2,4,'significant'))
                ,'\\qquad \\mathrm{where \\quad }f1=',num2str(round(obj.
                FigCorrectionFactor.accept_error_valy_y2,4,'significant'))
                ,'\\\\ \n']);
138         fprintf(fileID,['Ro_{c}=',num2str(round(obj.
                FigCorrectionFactor.cross_cf_valx,4,'significant')),'\\
                qquad \\mathrm{where \\quad }f1=',num2str(obj.
                FigCorrectionFactor.cross_cf_valy_y1),'\\quad f2=',num2str
                (round(obj.FigCorrectionFactor.cross_cf_valy_y2,4,'
                significant')),' \n']);
139         fprintf(fileID,'\\end{align}');
140         fclose(fileID);
141     end
142
143 end
144
145 methods
146     function value = get.latexAsyI(obj)
147         value=obj.function2str(func2str(obj.funy1));
148     end
149     function value = get.latexAsyII(obj)
150         value=obj.function2str(func2str(obj.funy2));
151     end
152     function value = get.latexBlendingEquation(obj)
153         value=obj.function2str(func2str(obj.Blending_Equation));
154     end
155     function value = get.latexCfI(obj)
```

```
156             value=obj.function2str(['(',func2str(obj.Blending_Equation),'
                    )/(',func2str(obj.funy1),')']);
157         end
158         function value = get.latexCfII(obj)
159             value=obj.function2str(['(',func2str(obj.Blending_Equation),'
                    )/(',func2str(obj.funy2),')']);
160         end
161         function value = get.latexX(obj)
162             value=obj.Pplot.x_label;
163         end
164         function value = get.latexY(obj)
165             value=obj.Pplot.y_label;
166         end
167         function value = get.latexBps(obj)
168             if max(size(obj.BP.P))==1
169                 value=['n=',num2str(obj.BP.P)];
170             else
171                 if max(size(obj.BP.P))==2
172                     value=['a=',num2str(obj.BP.P(1)),', b=',num2str(obj.BP
                            .P(2))];
173                 else
174                     value=['P=',num2str(obj.BP.P)];
175                 end
176             end
177         end
178         function strout=function2str(obj,f)
179             str = regexprep(f, '^@\(.*?\)|@\(.*?\)|@\(.*?\)|@\(.*?\)|@
                    \(.*?\)', '');
180             str = regexprep(str, '\.\*', '*');
181             str = regexprep(str, '\.\^', '^');
182             str = regexprep(str, '\./', '/');
183             str = regexprep(str, 'exp\(1\)', 'e');
184             if max(size(obj.BP.pseed))>1
185                 str =regexprep(str,'p\(1\)','a');
186                 str =regexprep(str,'p\(2\)','b');
187                 str =regexprep(str,'p\(3\)','c');
188             else
189                 str =regexprep(str,'p\(1\)','n');
190             end
191             strsym = feval(symengine, 'hold', str);
192             strout=strrep(latex(strsym),'\,','');
193             strout=strrep(strout,'\','\\');
194         end
195         function strout = sym2latex2print(fs)
196             strout=strrep(latex(fs),'\,','');
```

```
            strout=strrep(strout,'\','\\');
            strout=[strout,'\n'];
        end
    end
end
```

Listing A.2: Matlab function for general 1D blending.

```
function [P,MaxE,ResultStruct] = fun_blending_general_1D(
    Blending_Equation,X,Y,Pseed,varargin)
%FUN_BLENDING_GENERAL_1D
%   GENERAL 1D BLENDING THAT HAVE TO INPUT BLENDING FORMULA
    _BLENDING_EQUATION_
%
% ----------------------------------
% ----- USAGE EXAMPLE ----
% ----------------------------------
%   [P,MaxE,ResultStruct] = fun_blending_general_1D(...
%   Blending_Equation,X,Y,Pseed,...
%   'Y1',   ,...
%   'Y2',   ,...
%   'lsminsearch',1,'options_minsearch',{},...
%   'lsminunc',1,'options_minunc',{},...
%   'lsmincon',1,'options_mincon',{},...
%   'lsga',1,'options_ga',{},...
%   'Y1modify',   ,...
%   'Y2modify',   ,...
%   'plot_yx',{true  ,..},...
%   'plot_error',{true  ,..},...
%   'plot_error_p',{true  ,..},...
%   'pvallist      ',[,,;,;,;,],...
% )

% ----------------------------------------
% ----- INPUT PARAMETERS ----
% ----------------------------------------
%   Blending_Equation: handle of blending function
%   X: vector of independent variable
%   Y: vector of dependent variable
%   Pseed: initial guess for blending parameters
%   'lsminsearch','options_minsearch'{}: settings of "fminsearch"
%   'lsminunc',1,'options_minunc',{}: settings of "fminunc"
%   'lsmincon',1,'options_mincon',{}: settings of "fmincon"
%   'lsga',1,'options_ga',{}: settings of "ga"
%   'Y1': vector of asymptotic in regime I
```

```
%   'Y2': vector of asymptotic in regime II
%   'Y1modify': vector of modified asymptotic in regime I
%   'Y2modify': vector of modified asymptotic in regime II
%   'plot_yx',{true,..}: setting of plotting figure y vs x
%   'plot_error',{true,..}: setting of plotting figure error vs x
%   'plot_error_p',{true,..}: setting of plotting figure maximum error vs P
%   'pvallist',[,,;,,;,,]: different blending parameters for figure maximum
    error vs P

% ------------------------------------------
% ------ SETTING FOR PLOT --------
% ------------------------------------------
%'Y1',y1,'Y2',y2,'xlabel', xlabel,...
%'ylabel', ylabel,'xscale', xscale,'yscale', yscale,...
%'axis_range',[x0,x1,y0,y1],'xtick', xtick,'ytick', ytick

%% Set output
P=[]; MaxE=[]; ResultStruct=[];
%% Checking size
Yseed=Blending_Equation(Pseed);
if size(Yseed)~= size(Y) & size(X) ~=size(Y)
    disp('X and Y have to be of same size');
    return;
end
%% Parse inputs
[default,parse]=SetDefalutParse;
[p,exitflag]=Parse_Input(default,parse,varargin{:});
if ~exitflag
    disp('Error happends in parsing inputs');
    return;
end
%% error / maximum error function
fun_error=@(p) log(Blending_Equation(p)./Y);
fun_max_error=@(p) max(abs(fun_error(p)));
%% search optimal value
if p.Isminsearch
    Methods{1}='Isminsearch';
    [p_optimal{1,2},m_error(1)]=fminsearch(@(p) fun_max_error(p),Pseed,p
        .options_minsearch);
end
if p.Isminunc
    Methods{2}='Isminunc';
    [p_optimal{2,2},m_error(2)]=fminunc(@(p) fun_max_error(p),Pseed,p.
        options_minunc);
end
```

```
78  if p.Ismincon
79      Methods{3}='Ismincon';
80      [p_optimal{3,2},m_error(3)]=fmincon(@(p) fun_max_error(p),Pseed
            ,[],[],[],[],[],[],[],p.options_mincon);
81  end
82  if p.Isga
83      Methods{4}='Isga';
84      p_vars=max(size(Pseed));
85      [p_optimal{4,2},m_error(4)] = ga (fun_max_error,p_vars
            ,[],[],[],[],[],[],[],[],p.options_ga);
86  end
87  %% find the best one among four results
88  MaxE=min(m_error);
89  P=p_optimal{m_error==MaxE,2};
90  E=fun_error(P);
91  Yest=Blending_Equation(P);
92  ResultStruct=struct('maximum_error',MaxE,'optimal_p',P,...
93      'error', E,'estimation',Yest,'ErrFunHandle',fun_error,'
            MaxErrFunHandle',fun_max_error);
94  ResultStruct.results_of_different_fmin.p=p_optimal;
95  ResultStruct.results_of_different_fmin.max_error=m_error;
96  ResultStruct.results_of_different_fmin.methods=Methods;
97  %% Plotting
98  % plot the y vs. x graph
99  if p.plot_yx{1}
100     ResultStruct.handle_of_figure_y_x=fun_plot_yx_1D(X,Y,p.plot_yx{2:end
            });
101     if size(p.Y1) == size(Y)
102         hold on;
103         plot(X,p.Y1,'--k','linewidth',1);
104     end
105     if size(p.Y2) == size(Y)
106         hold on;
107         plot(X,p.Y2,'--k','linewidth',1);
108     end
109     if size(p.Y1modify) == size(Y)
110         hold on;
111         plot(X,p.Y1modify,'-.k','linewidth',1);
112     end
113     if size(p.Y2modify) == size(Y)
114         hold on;
115         plot(X,p.Y2modify,'-.k','linewidth',1);
116     end
117 end
118
```

```
119 % plot the error vs x graph
120 if p.plot_error{1}
121     pY=100*fun_error(P);
122     [ResultStruct.handle_of_figure_error,l]=fun_plot_yx_1D(X,pY,p.
            plot_error{2:end},'yscale','linear');
123     title('error vs x'); hold on
124     set(l{1},{'DisplayName'},{strcat('n=',num2str(P))});
125 
126     if size(p.pvallist,2)==size(Pseed,2)
127         for ipval=1:size(p.pvallist,1)
128             l2=semilogx(X,100*fun_error(p.pvallist(ipval,:))); hold on
129             set(l2,{'DisplayName'},{strcat('p=',num2str(p.pvallist(ipval
                    ,:)))});
130         end
131     end
132     legend show
133     legend('boxoff')
134 end
135 
136 % plot the error vs p graph
137 if p.plot_error_p{1}
138     if max(size(P))==1
139         plist=linspace(P*0.5,P*1.5,31);
140         MElist=arrayfun(@(x) fun_max_error(x),plist);
141         ResultStruct.handle_of_figure_maximum_error_p=fun_plot_yx_1D(
                plist,100*MElist,'xlabel','n','ylabel','maximum error (\%)','
                xscale','linear','yscale','linear',p.plot_error_p{2:end});
142         title('maximum error vs n'); hold on
143         plot([P,P],[0,1000*MaxE],'--k'); hold on
144         text(P,200*MaxE,strcat('n=',num2str(P)),'Interpreter','tex','
                FontSize',14);
145     else
146         if max(size(P))==2
147             av=linspace(0.7*P(1),1.3*P(1),151);
148             bv=linspace(0.7*P(2),1.3*P(2),151);
149             fun_plot_contour_error_ab(av,bv,fun_max_error,'aop',P(1),'bop
                    ',P(2),p.plot_error_p{2:end})
150         else
151             disp('plot maximum error on P only works for one or two
                    blending parameter');
152         end
153     end
154 end
155 
156 end
```

```
157
158 function [default,parse]=SetDefalutParse
159 default.Isminsearch=true;
160 parse.Isminsearch=@(x) islogical(x) || x==0|| x==1;
161 default.Isminunc=true;
162 parse.Isminunc=@(x) islogical(x) || x==0|| x==1;
163 default.Ismincon=false;
164 parse.Ismincon=@(x) islogical(x) || x==0|| x==1;
165 default.Isga=false;
166 parse.Isga=@(x) islogical(x) || x==0|| x==1;
167
168 default.p_lb=[nan,nan];
169 parse.p_lb=@(x) size(x) == [1,2];
170 default.p_ub=[nan,nan];
171 parse.p_ub=@(x) size(x) == [1,2];
172
173 default.options_minsearch=optimset('TolX',1E-20,'TolFun',1E-10,'
       MaxFunEvals',1e10);
174 parse.options_minsearch=@(x) 1;
175 default.options_minunc=optimoptions(@fminunc,'StepTolerance',1e-40);
176 parse.options_minunc=@(x) 1;
177 default.options_mincon=optimoptions(@fmincon,'StepTolerance',1e-60);
178 parse.options_mincon=@(x) 1;
179 default.options_ga=optimoptions(@ga,'PopulationSize', 1000,...
180     'HybridFcn', { @fminsearch [default.options_minsearch] },'Display',
          'off',...
181     'PlotFcn', {@gaplotbestf @gaplotscorediversity });% options =
          optimoptions(options,'PlotFcn', { @gaplotbestf @gaplotscorediversity });
182 parse.options_ga=@(x) 1;
183
184 default.Y1=[];
185 parse.Y1=@(x) 1;
186 default.Y2=[];
187 parse.Y2=@(x) 1;
188
189 default.Y1modify=[];
190 parse.Y1modify=@(x) 1;
191 default.Y2modify=[];
192 parse.Y2modify=@(x) 1;
193
194
195 default.plot_yx={false};
196 parse.plot_yx=@(x) 1;
197 default.plot_error={false};
198 parse.plot_error=@(x) 1;
```

```
default.plot_error_p={false};
parse.plot_error_p=@(x) 1;
parse.pvallist=@(x) 1;
default.pvallist=[0];
end
function [p,exitflag]=Parse_Input(default,parse,varargin)
% 1. parse the inputs, choosing default value if it's not showed in varargin
% 2. check output with function parse.
% Usage
%      [p, exitflag ]=Parse_ Input(default, parse, varargin )
%% if some problems happened, exitflag = 0
exitflag=1;
%% size of varargin
[r_varargin,c_varargin]=size(varargin);
%% if varargin is empty use default
if r_varargin~=0
    % varargin should be a cell of [1x2n]
    if r_varargin~=1
        disp('Inputs must be a line.');
        exitflag=0;
        return;
    end
    if rem(c_varargin,2)==1
        disp('Inputs must be in pairs');
        exitflag=0;
        return
    end
    % transform the [1x2n] cell to a struct of n.
    varargin_field=varargin(1:2:c_varargin);
    varargin_value=varargin(2:2:c_varargin);
    % check the field name of varargin in default struct
    is_in_fields=isfield(default,varargin_field);
    for i=1:size(is_in_fields,2)
        if is_in_fields(i)<eps
            disp(char(strcat('Property name ',{' '}, varargin_field{i},{'
                '}, 'is wrong')));
        else
            % change the value of default
            default.(varargin_field{i})=varargin_value{i};
        end
    end
end
% pass the changed struct to output
p=default;
% check if the output satisfied the parse
```

```
243 for fld = fieldnames(p)'
244     if ~parse.(fld{1})(p.(fld{1}))
245         disp(char(strcat('Error happened in the value of',{' '}, fld{1}))
                );
246         exitflag=0;
247     end
248 end
249 end
250 function [h,l] = fun_plot_yx_1D(X,Y,varargin)
251 %FUN_PLOT_Y_X_1D format plot of 1D graph
252 %Example:
253 % [H,l]=fun_plot_yx_1D(X,Y,'Y1',y1,'Y2',y2,'xlabel', xlabel ,...
254 % 'ylabel', ylabel ,'xscale', xscale ,'yscale', yscale ,...
255 % 'axis_range',[x0,x1,y0,y1],'xtick', xtick ,'ytick', ytick );
256 %
257 % Output:
258 %       H: handle of figure
259 %       l: handle of line
260 % Properties include :[[[ properties : description [type] {default }]]]
261 %                       Y1/Y2: asymptotics [vector] {nan(size(X))}
262 %                       xlabel: name of x [string] {'x'}
263 %                       ylabel: name of y [string] {'y'}
264 %                       xscale: salce of x [log/linear] {'log'}
265 %                       yscale: salce of y [log/linear] {'log'}
266 %                       axis_range: range of figure [4X1] {[xmin,xmax,ymin,ymax
        ]}
267 %                       xtick: tick of x axis [vector] {[]}
268 %                       ytick: tick of x axis [vector] {[]}
269
270 %% GRAPH SETTINGS (DONT CAHNGE IF NOT SURE)
271 default_curve={'-k','linewidth',2};
272 default_label={'FontSize',14};
273 default_gca={'FontSize',14, 'MinorGridLineStyle','none', 'linewidth',1,'
        box','on'};
274 default_curve_asymptotics={'-k','linewidth',1};
275 %% ckeck for X and Y
276 h=[];
277 if ~min(size(X) == size(Y) )
278     disp('Inputs X Y have to be of same size');
279     return;
280 end
281 if isempty(X)
282     disp('X and Y can not be empty');
283     return;
284 end
```

```
285
286 %% parse varargin
287 [default,parse]=SetDefalutParse(X,Y);
288 % parse inputs
289 [p,exitflag]=Parse_Input(default,parse,varargin{:});
290
291 % if error happened in parsing inputs
292 if ~exitflag
293     disp('Error happends in parsing inputs');
294     return;
295 end
296
297
298 if ~isempty(p.xtick)
299     p.xtickmode='manual';
300 end
301 if ~isempty(p.ytick)
302     p.ytickmode='manual';
303 end
304
305 %% plotting
306 h=figure; % creating handle
307 DefaultGca
308 xdata=X; ydata=Y; % passing data
309
310 l{1}=plot(xdata,ydata,default_curve{:}); hold on;
311 if ~min(isnan(p.Y1))
312     l{2}=plot(xdata,p.Y1,default_curve_asymptotics{:}); hold on;
313 end
314 if ~min(isnan(p.Y1))
315     l{3}=plot(xdata,p.Y2,default_curve_asymptotics{:}); hold on;
316 end
317 xlabel(p.xlabel,default_label{:});
318 ylabel(p.ylabel,default_label{:});
319 set(gca,default_gca{:},...
320     'Xscale',p.xscale,'Yscale',p.yscale,...
321     'XTick',p.xtick,'XTickMode',p.xtickmode,...
322     'YTick',p.ytick,'YTickMode',p.ytickmode,...
323     default_gca{:});
324 grid on;box on;
325 axis(p.axis_range);
326 DefaultGca
327 end
328 function DefaultGca
329 box on;
```

```
set(gca,'FontSize',14,'LineWidth',1,...
    'MinorGridLineStyle','none','box','on');
set(gcf,'color',[1,1,1],...
    'Units','pixels',...
    'PaperPosition',[1.33,3.3125,5.83,4.375],...
    'PaperPositionMode','manual',...
    'Render','painters')
grid on
end
```

Listing A.3: Matlab function to plot maximum error changing with two blending paramters for 1D blending.

```
function fun_plot_contour_error_ab(a,b,funerror,varargin)
%FUN_PLOT_CONTOUR_ERROR_AB: Plot error map for optimization of 2
    parameters
%   fun_plot_contour_error_ab(a,b,funerror,'aop',,'bop',,'vectsz',,...
%         'xlabel','','ylabel','')
figure
% default value
default.aop=nan;
parse.aop=@(x) size(x)==[1,1];
default.bop=nan;
parse.bop=@(x) size(x)==[1,1];
default.vectsz=30;
parse.vectsz=@(x) min(size(x))==1;
default.xlabel='a';
parse.xlabel=@(x) 1;
default.ylabel='b';
parse.ylabel=@(x) 1;
default.axis_range=[-inf,inf,-inf,inf];
parse.axis_range=@(x) 1;
% parse inputs
[p,exitflag]=parsevarargin(default,parse,varargin{:});
% if error happened in parsing inputs
if ~exitflag
    disp('Error happends in parsing inputs');
    return;
end

[AL,BL]=meshgrid(a,b);
error=100*arrayfun(@(a,b) funerror([a,b]),AL,BL);
Vector=linspace(min(min(error)),max(max(error)),p.vectsz);
Vector=round(Vector,1);
contour(a,b,error,Vector,'-k','ShowText','on'); hold on
```

```
contour(a,b,error,max(max(error))*[0,1],'-k','ShowText','on'); hold on
plot(p.aop*[1,1],[min(b),max(b)],'-.k'); hold on
plot([min(a),max(a)],p.bop*[1,1],'--k'); hold on
plot(p.aop*[1,1],p.bop*[1,1],'.k','MarkerSize',24); hold on
shading interp
text(p.aop,p.bop,'me')
title('maximum error vs a,b'); hold on
xlabel(p.xlabel)
ylabel(p.ylabel)
axis(p.axis_range)
DefaultGca;
end

function DefaultGca
box on;
set(gca,'FontSize',14,'LineWidth',1,...
    'MinorGridLineStyle','none','box','on');
set(gcf,'color',[1,1,1],...
    'Units','pixels',...
    'PaperPosition',[1.33,3.3125,5.83,4.375],...
    'PaperPositionMode','manual',...
    'Render','painters')
grid on
end

function [p,exitflag]=parsevarargin(default,parse,varargin)
% 1. parse the inputs, choosing default value if it's not showed in varargin
% 2. check output with function parse.
% if some problems happened, exitflag = 0
exitflag=1;
% size of varargin
[r_varargin,c_varargin]=size(varargin);
% if varargin is empty use default
if r_varargin~=0
    % varargin should be a cell of [1x2n]
    if r_varargin~=1
        disp('Inputs must be a line.');
        exitflag=0;
        return;
    end
    if rem(c_varargin,2)==1
        disp('Inputs must be in pairs');
        exitflag=0;
        return
    end
```

```
    % transform the [1x2n] cell to a struct of n.
    varargin_field=varargin(1:2:c_varargin);
    varargin_value=varargin(2:2:c_varargin);
    % check the field name of varargin in default struct
    is_in_fields=isfield(default,varargin_field);
    for i=1:size(is_in_fields,2)
        if is_in_fields(i)<eps
            disp(char(strcat('Property name ',{' '}, varargin_field{i},{'
                '}, 'is wrong')));
        else
            % change the value of default
            default.(varargin_field{i})=varargin_value{i};
        end
    end
end
% pass the changed struct to output
p=default;
% check if the output satisfied the parse
for fld = fieldnames(p)'
    if ~parse.(fld{1})(p.(fld{1}))
        disp(char(strcat('Error happened in the value of',{' '}, fld{1}))
            );
        exitflag=0;
    end
end
end
```

Listing A.4: Matlab function to plot correction factors for 1D blending.

```
function [R] = fun_plot_correction_factors_1D(X,Y,Y1,Y2,varargin)
%FUN_PLOT_CORRECTION_FACTORS_1D plots the correction factors
%
%FUN_PLOT_CORRECTION_FACTOR_1D(X,Y,Y1,Y2,...
%         'ea  ',0.1,....
%         'Y1est ',[ vect ],' Y2est ',[ vect  ],,...
%         ' xlabel ',' X ',' ylabel ',' y ',
%         ' xscale ',,' yscale ',,' axis_range ',,' xtick ',,' ytick  ',,...
%         'cf_table  ',,...
%         'figure_name',)
%
%INPUTS
%  X is the independent variable
%  Y is the dependent varible
%  Y1, Y2 are the asymtotics for y [vector] {can be empty}
%
```

```
%  Properties  include :
%        - ea: error  acceptable , [ scalar ] {0.1}
%        - xlabel : name of x, [ string ] {'x'}
%        - ylabel : name of y, [ string ] {'y'}
%        - xscale :   salce  of x  [log/ linear ] {'log'}
%        - yscale :   salce  of y  [log/ linear ] {'log'}
%        - axis_range: range  of  figure  [4X1] {[-inf, inf,-inf, inf]}
%        - xtick :   tick  of x  axis  [vector] {[]}
%        - ytick :   tick  of x  axis  [vector] {[]}
%
%  OUTPUTS:
%  R is a  cell ,  containing  the handle  of  figure  and the X_1 X_2 X_c etc.

%% GRAPH SETTINGS (DONT CAHNGE IF NOT SURE)
default_curve={'-k','linewidth',2};
default_label={'FontSize',14};
default_gca={'FontSize',14, 'MinorGridLineStyle','none', 'linewidth',1};
default_vertical_dashline={'-.k','linewidth', 1};
default_horizontal_dashline={'--k','linewidth', 1};
%% ckeck X Y
if size(X) ~= size(Y)
    disp('Inputs X Y have to be of same size');
    R=[];
    return;
end
if isempty(X)
    disp('Inputs X Y can not be empty');
    R=[];
    return;
end
%% parse varargin
% figure  range
if  size(Y1)~=size(X)
    min_py1=0.1;
    max_py1=10;
else
    min_py1=min(Y./Y1);
    max_py1=max(Y./Y1);
end
if  size(Y2)~=size(X)
    min_py2=0.1;
    max_py2=10;
else
    min_py2=min(Y./Y2);
    max_py2=max(Y./Y2);
```

```
end
%% default and parse   criterial
default.axis_range=[min(X),max(X),0.1,10];
if min_py1>0.1&& min_py2>0.1
    default.axis_range(3)=0.1;
else
    default.axis_range(3)=min(min_py1,min_py2);
end
if max_py1<10 && max_py2<10
    default.axis_range(4)=10;
else
    default.axis_range(4)=max(max_py1,max_py2);
end
parse.axis_range=@(x) min(size(x)==[1,4]);
default.ea=0.1;
parse.ea=@(x) isscalar(x) && x>0 ;
default.xlabel='x';
parse.xlabel=@(x) ischar(x);
default.ylabel='y';
parse.ylabel=@(x) ischar(x);
default.xscale='log';
parse.xscale=@(x) sum(strcmpi(x,{'log', 'linear'}));
default.yscale='log';
parse.yscale=@(x)sum(strcmpi(x,{'log', 'linear'}));
default.xtick=[];
default.xtickmode='auto';
parse.xtick=@(x) isa(x,'double');
parse.xtickmode=@(x) sum(strcmpi(x,{'auto','manual'}));
default.ytick=[];
default.ytickmode='auto';
parse.ytick=@(x) isa(x,'double');
parse.ytickmode=@(x) sum(strcmpi(x,{'auto','manual'}));
default.Y1est=nan*Y1./Y1;
default.Y2est=nan*Y2./Y2;
parse.Y1est=@(x) size(x)==size(Y1);
parse.Y2est=@(x) size(x)==size(Y2);
default.cf_table='';
parse.cf_table=@(x) 1;
default.figure_name='';
parse.figure_name=@(x) 1;
% parse  inputs
[p,exitflag]=parsevarargin(default,parse,varargin{:});
% if  error  happened in  parsing  inputs
if ~exitflag
    disp('Error happends in parsing inputs');
```

```
107     R=[];
108     return;
109 end
110
111
112 if ~isempty(p.xtick)
113     p.xtickmode='manual';
114 end
115 if ~isempty(p.ytick)
116     p.ytickmode='manual';
117 end
118
119 %% initialization
120 % cf corresponding to acceptable error
121 vapy1=exp(p.ea);  % acceptable cf under acceptable  error >1
122 vapy2=exp(-p.ea); % acceptable cf under acceptable  error <1
123
124 % indicator of plotting vapy1 vapy2
125 indicator_plot_apy=[false,false]; % vector to describle which dash line (apy1 or
        apy2) has been plot, to avoid plotting one line twice
126
127 % labels on figure X_1 X_2 X_c
128 if p.xlabel(end)=='$'
129     sx=find(p.xlabel=='$');
130     x_strI=strcat(p.xlabel(1:sx(end-1)),'{',p.xlabel(sx(end-1)+1:end-1),
            '}','I');
131     x_strII=strcat(p.xlabel(1:sx(end-1)),'{',p.xlabel(sx(end-1)+1:end-1)
            ,'}','II');
132     x_strc=strcat(p.xlabel(1:sx(end-1)),'{',p.xlabel(sx(end-1)+1:end-1),
            '}','c');
133 else
134     x_strI=strcat(p.xlabel,'I');
135     x_strII=strcat(p.xlabel,'II');
136     x_strc=strcat(p.xlabel,'c');
137 end
138
139 % labels on figure f_I f_II
140 ylcf=p.ylabel; ylcf(ylcf=='$')=[];
141 f_strI=strcat('f',ylcf,'I');
142 f_strII=strcat('f',ylcf,'II');
143
144 if isnan(p.axis_range(1))|| isinf(p.axis_range(1))
145     textfyxval(1)=min(X);
146 else
147     textfyxval(1) = p.axis_range(1);
```

```
148 end
149 if isnan(p.axis_range(2))|| isinf(p.axis_range(2))
150     textfyxval(2)=max(X);
151 else
152     textfyxval(2) = p.axis_range(2);
153 end
154
155 % creat  figure
156 R.figure_correction_factor=figure;
157
158 %% correction  factor  for  Y1
159 if ~isempty(Y1)
160     %check size
161     if size(X) ~= size(Y1)
162         disp('Inputs X Y1 have to be of same size');
163         return;
164     end
165
166     pY1=Y./Y1; % creat  correction  factor
167
168     %  characteristics
169     mean_py1=mean(pY1);
170
171     plot(X,pY1,default_curve{:}); hold on;
172
173     % acceptable  error  dash  lines  >1
174     if mean_py1>1
175         % plot  dash  line  if  there  is  none
176         if ~indicator_plot_apy(1)
177             plot(X,vapy1*X./X,default_horizontal_dashline{:}); hold on
178             indicator_plot_apy(1)=true; % apy1 has been plot
179         end
180         % find the  critical  value  coressponding  to  acceptable  error
181         interp_y=pY1(pY1>((vapy1+1)/2)&pY1<1.2*vapy1);
182         interp_x=X(pY1>((vapy1+1)/2)&pY1<1.2*vapy1);
183         vp1=interp1(interp_y,interp_x,vapy1,'linear');
184         R.accept_error_valy_y1=vapy1;
185     end
186     % acceptable  error  dash  lines  <1
187
188     if mean_py1<1
189         % plot  dash  line  if  there  is  none
190         if ~indicator_plot_apy(2)
191             plot(X,vapy2*X./X,default_horizontal_dashline{:}); hold on
192             indicator_plot_apy(2)=true; % apy2 has been plot
```

```
193         end
194         interp_y=pY1(pY1>0.8*vapy2&pY1<(vapy2+1)/2); interp_x=X(pY1>0.8*
                vapy2&pY1<(vapy2+1)/2);
195         vp1=interp1(interp_y,interp_x,vapy2,'linear');
196         R.accept_error_valy_y1=vapy2;
197     end
198
199     % plot vertical dashline
200     plot([vp1,vp1],[p.axis_range(3),R.accept_error_valy_y1],
            default_vertical_dashline{:}); hold on
201     % label X_1
202     %     text_y1=5*p.axis_range(3);
203     text(vp1,1,x_strI,default_label{:});
204     % label f_I
205     if abs(pY1(1)-1)>abs(pY1(end)-1)
206         text(textfyxval(2).^(5/6)*textfyxval(1).^(1/6),2,f_strI,
                default_label{:});
207     else
208         text(textfyxval(2).^(1/6)*textfyxval(1).^(5/6),2,f_strI,
                default_label{:});
209     end
210     % out put
211     % R.correction_factor_y1=pY1;
212     R.accept_error_valx_y1=vp1;
213 else
214     %output
215     % R.correction_factor_y1=[]; % vector of correction factor for Y1
216     R.accept_error_valx_y1=[]; % the x vlaue of acceptable error for Y1
217     R.accept_error_valy_y1=[]; % the correction factor of acceptable error Y1
218 end
219
220 %% correction factor for Y2
221 if ~isempty(Y2)
222     % check size
223     if size(X) ~= size(Y2)
224         disp('Inputs X Y2 have to be of same size');
225         return;
226     end
227     % define correction factor
228     pY2=Y./Y2;
229     % characteristics
230     mean_py2=mean(pY2);
231
232     plot(X,pY2,default_curve{:}); hold on;
233
```

```
234     % plot acceptable error dash lines
235     if mean_py2>1
236         if ~indicator_plot_apy(1)
237             plot(X,vapy1*X./X,default_horizontal_dashline{:}); hold on
238             indicator_plot_apy(1)=1; % apy1 has been plot
239         end
240         interp_y=pY2(pY2>((vapy1+1)/2)&pY2<1.2*vapy1); interp_x=X(pY2>((
                vapy1+1)/2)&pY2<1.2*vapy1);
241         vp2=interp1(interp_y,interp_x,vapy1,'linear');
242         R.accept_error_valy_y2=vapy1; % the correction factor of acceptable
                error Y2
243     end
244
245     if mean_py2<1
246         if ~indicator_plot_apy(2)
247             plot(X,vapy2*X./X,default_horizontal_dashline{:}); hold on
248             indicator_plot_apy(2)=1; % apy2 has been plot
249         end
250         interp_y=pY2(pY2>0.8*vapy2&pY2<((vapy2+1)/2)); interp_x=X(pY2
                >0.8*vapy2&pY2<((vapy2+1)/2));
251         vp2=interp1(interp_y,interp_x,vapy2,'linear');
252         R.accept_error_valy_y2=vapy2; % the correction factor of acceptable
                error Y2
253     end
254     % plot
255     plot([vp2,vp2],[p.axis_range(3),R.accept_error_valy_y2],
            default_vertical_dashline{:}); hold on
256     % label x_II
257     %     text_y2=5*p.axis_range(3);
258     text(vp2,1,x_strII,default_label{:});
259     % label f_II
260     if abs(pY2(1)-1)>abs(pY2(end)-1)
261         text(textfyxval(2).^(5/6)*textfyxval(1).^(1/6),2,f_strII,
                default_label{:});
262     else
263         text(textfyxval(2).^(1/6)*textfyxval(1).^(5/6),2,f_strII,
                default_label{:});
264     end
265     %
266     %R.correction_factor_y2=pY2; % vector of correction factor for Y2
267     R.accept_error_valx_y2=vp2;% the x vlaue of acceptable error for Y2
268
269 else
270     %output
271     % R.correction_factor_y2=[]; % vector of correction factor for Y2
```

```
    R.accept_error_valx_y2=[]; % the x vlaue of acceptable error for Y2
    R.accept_error_valy_y2=[]; % the correction factor of acceptable error Y2
end

%% plot estimated cf
plot(X,p.Y1est,'--k','linewidth',1); hold on;
plot(X,p.Y2est,'--k','linewidth',1); hold on;
%% cross point
if ~isempty(Y1) && ~isempty(Y2)
    % interp value
    Delta_Y=abs(log(pY1))-abs(log(pY2));
    interp_y=Delta_Y(Delta_Y>-0.5&Delta_Y<0.5);
    interp_x=X(Delta_Y>-0.5&Delta_Y<0.5);
    vc_x=interp1(interp_y,interp_x,0,'linear');
    vc_y1=interp1(X,pY1,vc_x,'linear'); vc_y2=interp1(X,pY2,vc_x,'linear
        ');
    %plot vertical dash line
    plot([vc_x,vc_x],[p.axis_range(3),max(vc_y1,vc_y2)],
        default_vertical_dashline{:}); hold on
    % label x_c
    text(vc_x,1,x_strc,default_label{:});
    % output
    R.cross_cf_valx=vc_x; % the x value of cross cf
    R.cross_cf_valy_y1=vc_y1; % the value of cf for y1 at cross point
    R.cross_cf_valy_y2=vc_y2; % the value of cf for y2 at cross point
    R.cross_cf_val_error_y1=log(vc_y1); % the error of Y1 at cross point
    R.cross_cf_val_error_y2=log(vc_y2); % the error if Y2 at cross point
else
    R.cross_cf_valx=[]; % the x value of cross cf
    R.cross_cf_valy_y1=[]; % the value of cf for y1 at cross point
    R.cross_cf_valy_y2=[]; % the value of cf for y2 at cross point
    R.cross_cf_val_error_y1=[]; % the error of Y1 at cross point
    R.cross_cf_val_error_y2=[]; % the error if Y2 at cross point
end

%% label axis
xlabel(p.xlabel,default_label{:});
ylabel(strcat('correction factor for ',p.ylabel),default_label{:});
set(gca,default_gca{:},...
    'Xscale',p.xscale,'Yscale',p.yscale,...
    'XTick',p.xtick,'XTickMode',p.xtickmode,...
    'YTick',p.ytick,'YTickMode',p.ytickmode);
axis([-inf,inf,0.1,10]);
grid on;box on
DefaultGca
```

```
315 %% save files
316 if ~isempty(p.cf_table)
317     writetable(struct2table(R), strcat(p.cf_table,'.txt'))
318 end
319 if ~isempty(p.figure_name)
320     %    saveas(gcf,p.figure_name,'epsc')
321     %    saveas(gcf, strcat(p.figure_name,'.fig'))
322 end
323
324
325 end
326 function DefaultGca
327 box on;
328 set(gca,'FontSize',14,'LineWidth',1,...
329     'MinorGridLineStyle','none','box','on');
330 set(gcf,'color',[1,1,1],...
331     'Units','pixels',...
332     'PaperPosition',[1.33,3.3125,5.83,4.375],...
333     'PaperPositionMode','manual',...
334     'Render','painters')
335 grid on
336 end
337 function [p,exitflag]=parsevarargin(default,parse,varargin)
338 % 1. parse the inputs, choosing default value if it's not showed in varargin
339 % 2. check output with function parse.
340
341 % if some problems happened, exitflag = 0
342 exitflag=1;
343
344 % size of varargin
345 [r_varargin,c_varargin]=size(varargin);
346 % if varargin is empty use default
347 if r_varargin~=0
348     % varargin should be a cell of [1x2n]
349     if r_varargin~=1
350         disp('Inputs must be a line.');
351         exitflag=0;
352         return;
353     end
354     if rem(c_varargin,2)==1
355         disp('Inputs must be in pairs');
356         exitflag=0;
357         return
358     end
359
```

```
360     % transform the [1x2n] cell to a struct of n.
361     varargin_field=varargin(1:2:c_varargin);
362     varargin_value=varargin(2:2:c_varargin);
363     % check the field name of varargin in default struct
364     is_in_fields=isfield(default,varargin_field);
365     for i=1:size(is_in_fields,2)
366         if is_in_fields(i)<eps
367             disp(char(strcat('Property name ',{' '}, varargin_field{i},{'
                    '}, 'is wrong')));
368         else
369             % change the value of default
370             default.(varargin_field{i})=varargin_value{i};
371         end
372     end
373 end
374 % pass the changed struct to output
375 p=default;
376 % check if the output satisfied the parse
377 for fld = fieldnames(p)'
378     if ~parse.(fld{1})(p.(fld{1}))
379         disp(char(strcat('Error happened in the value of',{' '}, fld{1}))
                );
380         exitflag=0;
381     end
382 end
383 end
```

Appendix B: Supplementary materials for the moving line heat source model

B.1 Matlab codes for isotherm width of moving line heat source in Chapter 2

Listing B.1: Matlab code to calculate and blending isotherm width $y^*_{\max}$ of moving line heat source.

```
clear;clc;close all;
ymII=@(Ro) 2*exp(-0.5772)*exp(-Ro.^-1);
ymI=@(Ro) sqrt(pi./(2*exp(1)))*Ro;
Blending_Equation=@(Ro) @(p) exp(-Ro.^-1).*((2*exp(-0.5772)).^p(1)+(sqrt
    (pi./(2*exp(1)))*Ro).^p(1)).^(1/p(1));
%% blending
Bym=Blending_Grid_size(@fun_ymaxcal,Blending_Equation,1e-2,1e5,1);
Bym.Pplot.pvallist=[1.507;1.307];
Bym.Pplot.x_label= 'Ro';
Bym.Pplot.y_label= 'ymax';
Bym.funy1= ymI; Bym.funy2= ymII;
Bym.funmodify1= @(Ro) sqrt(pi./(2*exp(1)))*Ro.*exp(-Ro.^-1);
Bym=Bym.Blending;
Bym=Bym.FBlending(1000);
%% export latex
Bym.latexRegimeI='III'; Bym.latexRegimeII='IV';
Bym=Bym.funWrite('thin_ymax.tex');
%% calculation of ymax
function [ym]= fun_ymaxcal(Ro)
% fun_ymaxcal: calculate numerical result of ymax
funTRmax=@(rmax) exp(rmax.*besselk(0,rmax,1)./besselk(1,rmax,1)-rmax).*
    besselk(0,rmax,1);
options = optimset('TolX',1e-50);
rmax=zeros(size(Ro));
for i=1:max(size(Ro))
```

```
    rmax(i)= fzero(@(rmax) funTRmax(rmax)-1./Ro(i),[1e-50,1e10],options)
        ;
end
ym=rmax.*sqrt(1-(besselk(0,rmax,1)./besselk(1,rmax,1)).^2);
end
```

B.2 Matlab codes for characteristic values of moving line heat source in Chapter 3

Listing B.2: Matlab code to calculate and blending location of isotherm width $x^*_{\max}$ of moving line heat source.

```
clear;clc;close all;
xmI=@(Ro) -4*exp(-2*0.5772)*Ro.^-1.*exp(-2*Ro.^-1);
xmII=@(Ro) -pi./(2*exp(1))*Ro.^2;
Blending_Equation=@(Ro) @(p) -exp(-2*Ro.^-1).*(((pi./(2*exp(1))*Ro.^2))
    +(4*exp(-2*0.5772)*Ro.^-1)+p(1)*Ro.^p(2));
%% blending
Bxmax=Blending_Grid_size(@fun_xmaxcal,Blending_Equation,1e-2,1e4,[1,1]);
Bxmax.Pplot.pvallist=[1.507;1.307];
Bxmax.Pplot.x_label= 'Ro';
Bxmax.Pplot.y_label= 'xmax';
Bxmax.funy1= xmI; Bxmax.funy2= xmII;
Bxmax.funmodify1= @(Ro) -pi./(2*exp(1))*Ro.^2.*exp(-2*Ro.^-1);
Bxmax=Bxmax.Blending;
Bxmax=Bxmax.FBlending(1000);
%% export latex
Bxmax.latexRegimeI='III'; Bxmax.latexRegimeII='IV';
Bxmax=Bxmax.funWrite('thin_xmax.tex');
function [xm]= fun_xmaxcal(Ro)
% fun_ymaxcal: calculate numerical result of xmax
funTRmax=@(rmax) exp(rmax.*besselk(0,rmax,1)./besselk(1,rmax,1)-rmax).*
    besselk(0,rmax,1);
options = optimset('TolX',1e-50);
rmax=zeros(size(Ro));
for i=1:max(size(Ro))
rmax(i)= fzero(@(rmax) funTRmax(rmax)-1./Ro(i),[1e-50,1e10],options);
end
xm=-rmax.*besselk(0,rmax,1)./besselk(1,rmax,1);
end
```

Listing B.3: Matlab code to calculate and blending trailing length x^*_{b} of moving line heat source.

```
clear;clc;close all;
%%
options=optimset('TolX',1e-50,'MaxIter',1e10);
funTh=@(x) besselk(0,-x,1);
funxb=@(Ro)fzero(@(x) funTh(x) -1./Ro,[-1e300,-1e-300],options);
fun_xbcal=@(Ro) arrayfun(@(a) funxb(a),Ro);
gamma=0.5772;
xbI=@(Ro) -pi/2*Ro.^2;
xbII=@(Ro)-2*exp(-1./Ro-gamma);
Blending_Equation= @(Ro) @(p) -exp(-1./Ro).*((pi/2*Ro.^2)+(2*exp(-gamma)
    )+p(1).*Ro.^p(2));
%% blending
Bxb=Blending_Grid_size(fun_xbcal,Blending_Equation,1e-2,1e4,[1,1]);
Bxb.Pplot.x_label= 'Ro';
Bxb.Pplot.y_label= 'xb';
Bxb.funy1= xbI;
Bxb.funy2= xbII;
Bxb.funmodify1= @(Ro) -pi/2*Ro.^2.*exp(-1./Ro);
Bxb=Bxb.Blending;
Bxb=Bxb.FBlending(1000);
%% export latex
Bxb.latexRegimeI='III'; Bxb.latexRegimeII='IV';
 Bxb=Bxb.funWrite('thin_xb.tex');
```

Listing B.4: Matlab code to calculate and blending centerline cooling rate $\dot{T}_{\mathrm{b}}^{*}$ of moving line heat source.

```
clear;clc;close all;
%%
options=optimset('TolX',1e-50,'MaxIter',1e10);
funTh=@(x) besselk(0,-x,1);
funxb=@(Ro)fzero(@(x) funTh(x) -1./Ro,[-1e300,-1e-300],options);
fun_Tbcal=@(Ro) arrayfun(@(Ro) 1./Ro.*(1-besselk(1, -funxb(Ro),1)./
    besselk(0, -funxb(Ro),1)),Ro);

gamma=0.5772;
TbIII=@(Ro) -1./(pi*Ro.^3);
TbIV=@(Ro) -1/2*exp(1./Ro+gamma);
Blending_Equation=@(Ro) @(p) -exp(1./Ro).*((1./(pi*Ro.^3)).^-1+(1/2*exp(
    gamma)).^-1+p(1).*Ro.^p(2)).^-1;
%% blending
BTb=Blending_Grid_size(fun_Tbcal,Blending_Equation,1e-2,1e2,[-1,-5]);
BTb.Pplot.x_label= 'Ro';
BTb.Pplot.y_label= 'Tb';
BTb.Pplot.figname= 'thin_Tb';
```

```
BTb.funy1= TbIII;
BTb.funy2= TbIV;
BTb.funmodify1= @(Ro) -1./(pi*Ro.^3).*exp(1./Ro);
BTb=BTb.Blending;
BTb=BTb.FBlending(1000);
%% export latex
% BTb.latexRegimeI='III';   BTb.latexRegimeII='IV';
% BTb.funWrite('thin_Tb.tex');
```

Listing B.5: Matlab code to calculate and blending leading length x_{f}^{*} of moving line heat source.

```
clear;clc;close all;
%%
options=optimset('TolX',1e-50,'MaxIter',1e10);
T=@(x) exp(-2*x).*besselk(0,x,1);
funxf=@(t) fzero(@(x) T(x)-t,[1e-300,100],options);
fun_xfcal=@(Ro) arrayfun(@(a) funxf(1./a),Ro);
gamma=0.5772;
xfIII=@(Ro) 2*exp(-gamma-Ro.^-1+1.5484*Ro.^1.3878);%'a=1.5484, b=1.3878'
xfIV=@(Ro) 1/4*lambertw(2*pi*Ro.^2);
Blending_Equation=@(Ro) @(p) ((1/4*lambertw(2*pi*Ro.^2)).^-1+(2*exp(-
    gamma-Ro.^-1+p(1)*Ro.^p(2))).^-1).^(-1);
%% blending
Bxf=Blending_Grid_size(fun_xfcal,Blending_Equation,1e-2,1e4,[1,1]);
Bxf.Pplot.x_label= 'Ro';
Bxf.Pplot.y_label= 'xf';
Bxf.funy1= xfIII;
Bxf=Bxf.Blending;
Bxf=Bxf.FBlending(1000);
%% export latex
Bxf.latexRegimeI='III'; Bxf.latexRegimeII='IV';
% Bxf=Bxf.funWrite('thin_xf.tex');
```

Listing B.6: Matlab code to calculate and blending centerline heating rate $\dot{T}_{\mathrm{f}}^{*}$ of moving line heat source.

```
clear;clc;close all;
%%
options=optimset('TolX',1e-50,'MaxIter',1e10);
T=@(x) exp(-2*x).*besselk(0,x,1);
funxf=@(Tc) fzero(@(x) T(x)-Tc,[1e-300,100],options);
fun_Tfcal=@(Ro) arrayfun(@(Ro) 1./Ro.* (1+besselk(1,funxf(1./Ro),1)./
    besselk(0,funxf(1./Ro),1)),Ro);

gamma=0.5772;
```

```
TfIII=@(Ro) 2./Ro;
TfIV=@(Ro) 1/2*exp(gamma+1./Ro);
Blending_Equation=@(Ro) @(p) exp(1./Ro).*((2./Ro).^-1+(1/2*exp(gamma))
    .^-1+p(1)*Ro.^p(2)).^-1 ;
%% blending
BTf=Blending_Grid_size(fun_Tfcal,Blending_Equation,1e-2,1e4,[1,-1]);
BTf.Pplot.x_label= 'Ro';
BTf.Pplot.y_label= 'Tf';
BTf.funy1= TfIII;
BTf.funy2= TfIV;
BTf.funmodify1= @(Ro) 2./Ro.*exp(1./Ro);
BTf=BTf.Blending;
BTf=BTf.FBlending(1000);
%% export latex
BTf.latexRegimeI='III'; BTf.latexRegimeII='IV';
% BTf=BTf.funWrite('thin_ Tf.tex');
```

Listing B.7: Matlab code to calculate and blending maximum temperature $T^*_{\max}$ of moving line heat source.

```
clear;clc;close all;
TmaxIII=@(yc) sqrt(pi/(2*exp(1)))./yc;
TmaxIV=@(yc) log(1./yc+2);
Blending_Equation=@(yc) @(p) ((sqrt(pi/(2*exp(1)))./yc).^p+ log(1./yc+2)
    .^p).^(1./p);
%%
BTmax=Blending_Grid_size(@fun_Tmax,Blending_Equation,1e-5,1e5,[-1]);
BTmax.Pplot.pvallist=[-2.400;-2.7];
BTmax.Pplot.x_label= 'yc';
BTmax.Pplot.y_label= 'Tmax';
BTmax.funy1= TmaxIII;
BTmax.funy2= TmaxIV;
BTmax=BTmax.Blending;
BTmax=BTmax.FBlending(1000);
%% export latex
BTmax.latexRegimeI='III'; BTmax.latexRegimeII='IV';
% BTmax=BTmax.funWrite('thin_ Tmax.tex');

%% calculate Tmax
function [Tmax]= fun_Tmax(yc)
options = optimset('TolX',1e-150);
xmax = arrayfun(@(yc) fzero(@(x) 1+x./sqrt(x.^2+yc.^2).*besselk(1,sqrt(x
    .^2+yc.^2),1)./besselk(0,sqrt(x.^2+yc.^2),1),-yc,options),yc);
Tmax= exp(-xmax-sqrt(xmax.^2+yc.^2)).*besselk(0,sqrt(xmax.^2+yc.^2),1);
end
```

Listing B.8: Matlab code to calculate and blending maximum temperature gradient $\mathrm{d}T^*_{\max}/\mathrm{d}y^*$ of moving line heat source.

```
clear;clc;close all;
gamma=0.5772;
TmaxIII=@(Ro) -sqrt(2*exp(1)./(pi))./Ro.^2;
TmaxIV=@(Ro) -1/2*exp(gamma+1./Ro);
Blending_Equation=@(Ro) @(p) -exp(1./Ro).* ((sqrt(2*exp(1)./(pi))./Ro
    .^2).^-1+(1/2*exp(gamma)).^-1+p(1).*Ro.^p(2)).^-1;
%%
BdTmdy=Blending_Grid_size(@fun_dTmdy,Blending_Equation,1e-2,1e4,[1,1]);
BdTmdy.Pplot.x_label= 'Ro';
BdTmdy.Pplot.y_label= 'dTmdy';
BdTmdy.funy1= TmaxIII;
BdTmdy.funy2= TmaxIV;
BdTmdy.funmodify1= @(Ro) -sqrt(2*exp(1)./(pi))./Ro.^2.*exp(1./Ro);
BdTmdy=BdTmdy.Blending;
BdTmdy=BdTmdy.FBlending(1000);
%% export latex
BdTmdy.latexRegimeI='III'; BdTmdy.latexRegimeII='IV';
BdTmdy=BdTmdy.funWrite('thin_dTmdy.tex');

%% calculate dTmaxdy
function [dTmaxdy]= fun_dTmdy(Ro)
funTRmax=@(rmax) exp(rmax.*besselk(0,rmax,1)./besselk(1,rmax,1)-rmax).*
   besselk(0,rmax,1);
options = optimset('TolX',1e-50);
rmax=zeros(size(Ro));
for i=1:max(size(Ro))
    rmax(i)= fzero(@(rmax) funTRmax(rmax)-1./Ro(i),[1e-50,1e10],options)
       ;
end
ym=rmax.*sqrt(1-(besselk(0,rmax,1)./besselk(1,rmax,1)).^2);
xm=-rmax.*besselk(0,rmax,1)./besselk(1,rmax,1);
dTmaxdy=-exp(-xm-sqrt(xm.^2+ym.^2)).*ym.*besselk(1,sqrt(xm.^2+ym.^2),1)
    ./sqrt(xm.^2+ym.^2);
end
```

Listing B.9: Matlab code to calculate and blending isotherm aspect ratio $\mathcal{AR}$ of moving line heat source.

```
clear;clc;close all;
ARIII=@(Ro) sqrt(pi*exp(1)./8).*Ro;
ARIV=@(Ro) Ro./Ro;
Blending_Equation=@(Ro) @(p) (1+( sqrt(pi*exp(1)./8).*Ro).^p(1)).^(1./p
    (1));
```

```
%% blending
BAR=Blending_Grid_size(@fun_AR,Blending_Equation,1e-2,1e2,1);
BAR.Pplot.pvallist=[1.8;2.1];
BAR.Pplot.x_label= 'Ro';
BAR.Pplot.y_label= 'AR';
BAR.funy1= ARIII;
BAR.funy2= ARIV;
BAR=BAR.Blending;
BAR=BAR.FBlending(1000);
%% export latex
BAR.latexRegimeI='III'; BAR.latexRegimeII='IV';
% BAR=BAR.funWrite('thin_AR.tex');

%% calculate function
function [AR]= fun_AR(Ro)
funTRmax=@(rmax) exp(rmax.*besselk(0,rmax,1)./besselk(1,rmax,1)-rmax).*
   besselk(0,rmax,1);
options = optimset('TolX',1e-50);
rmax=zeros(size(Ro));
for i=1:max(size(Ro))
    rmax(i)= fzero(@(rmax) funTRmax(rmax)-1./Ro(i),[1e-50,1e10],options)
       ;
end
ym=rmax.*sqrt(1-(besselk(0,rmax,1)./besselk(1,rmax,1)).^2);
xm=-rmax.*besselk(0,rmax,1)./besselk(1,rmax,1);
options=optimset('TolX',1e-50,'MaxIter',1e10);
T=@(x) exp(-2*x).*besselk(0,x,1);
funxf=@(t) fzero(@(x) T(x)-t,[1e-300,100],options);
xf= arrayfun(@(a) funxf(1./a),Ro);
funTh=@(x) besselk(0,-x,1);
funxb=@(Ro)fzero(@(x) funTh(x) -1./Ro,[-1e300,-1e-300],options);
xb= arrayfun(@(a) funxb(a),Ro);
AR=(xf-xb)./(2*ym);
end
```

B.3 Supporting figures for blending results in Chapter 3

B.3.1 $x^*_{\max}$

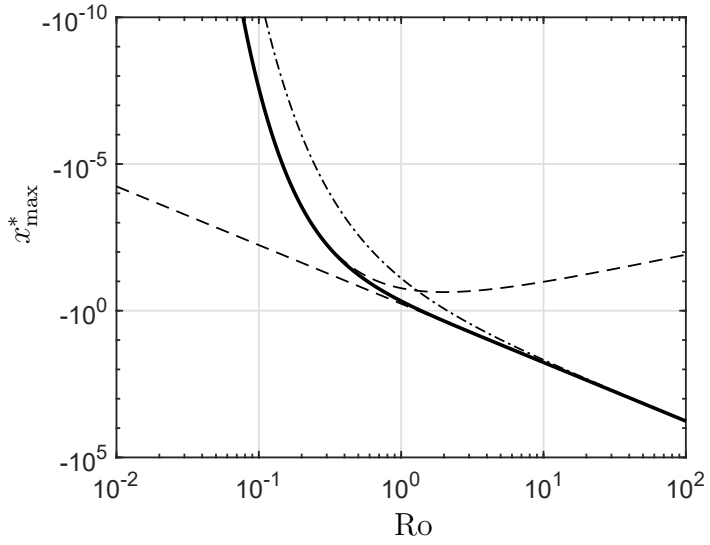

Figure B.1: Location of isotherm width $x^*_{\max}$ changes with Ro number.

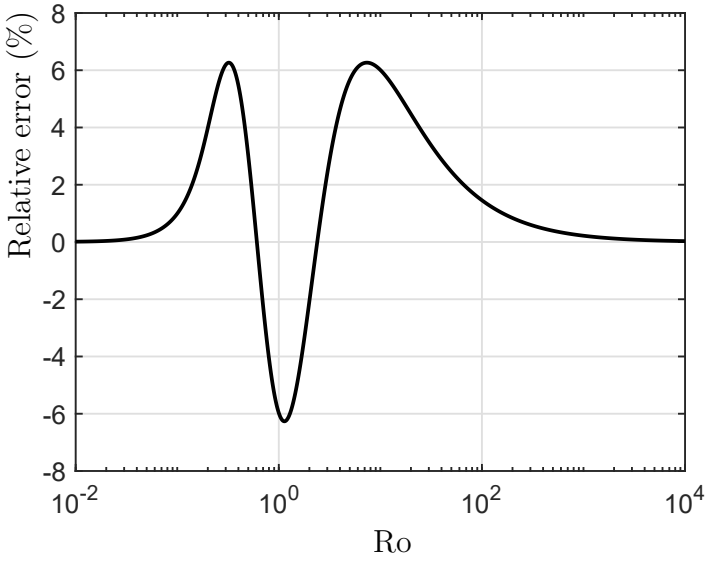

Figure B.2: Relative error changes with Ro for scaling laws of $x^*_{\max}$.

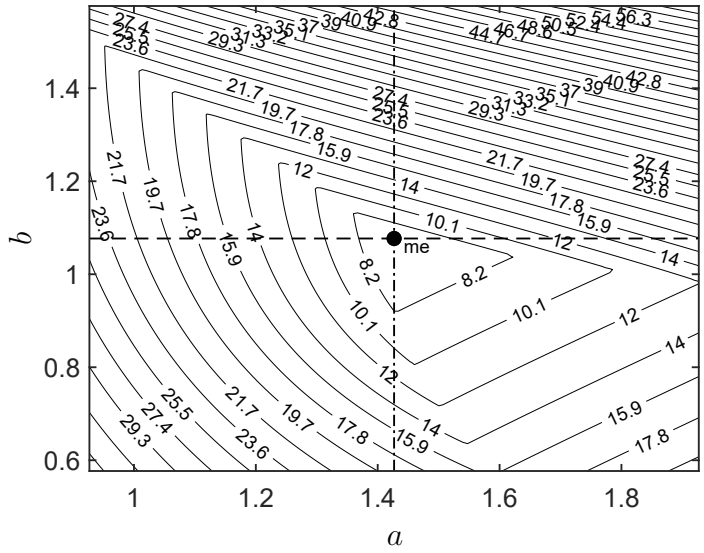

Figure B.3: Optimizing parameters for blending of $x^*_{\max}$.

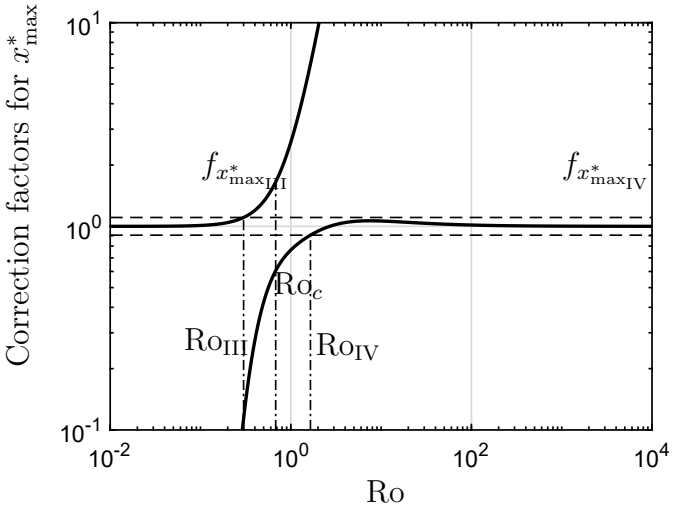

Figure B.4: Correction factors for engineering expressions for $x^*_{\max}$.

B.3.2 x_{f}^{*}

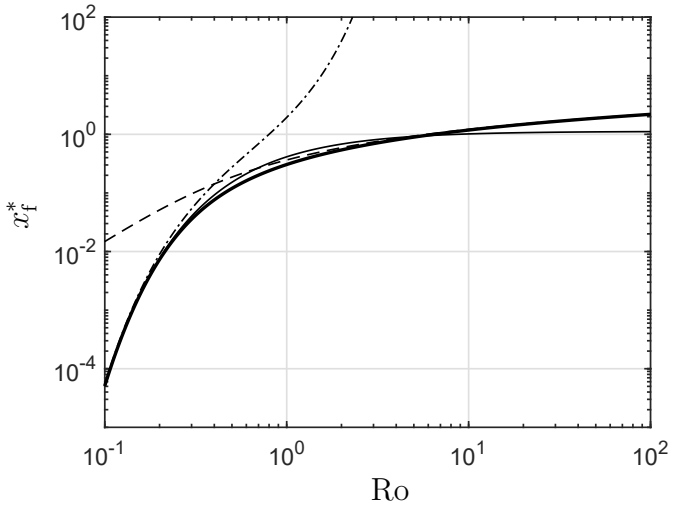

Figure B.5: x_{f}^{*} changes with Ro number.

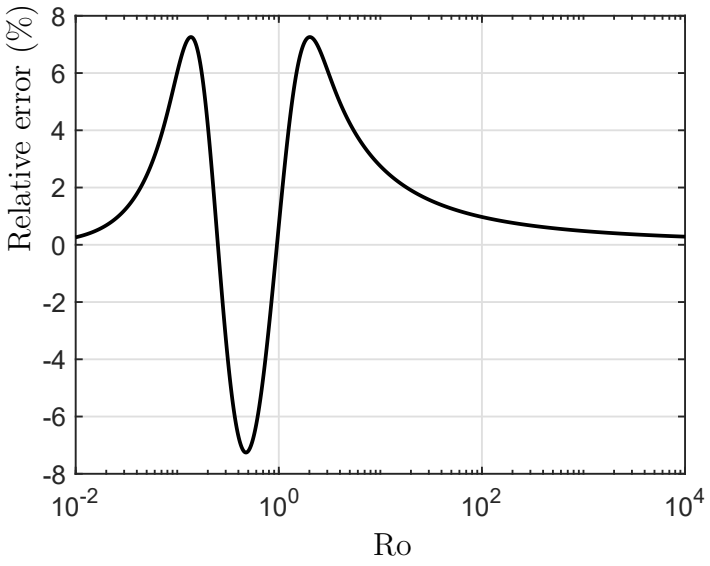

Figure B.6: Relative error changes with Ro for scaling laws of x_{f}^{*}.

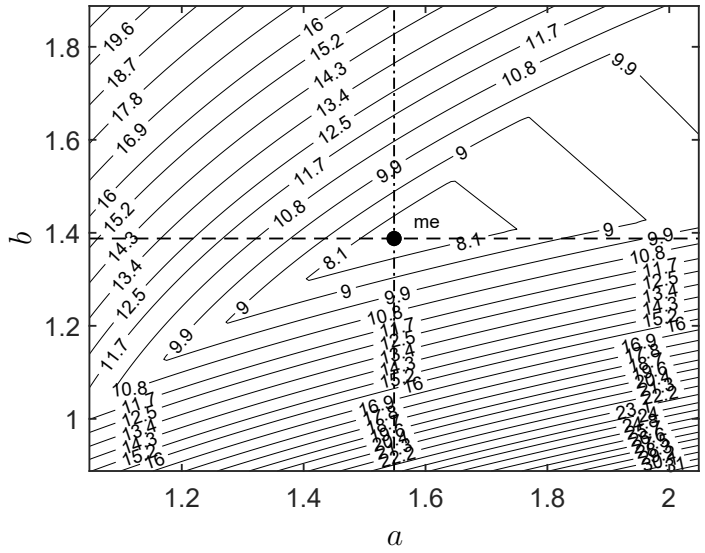

Figure B.7: Optimizing parameters for blending of x_{f}^{*}.

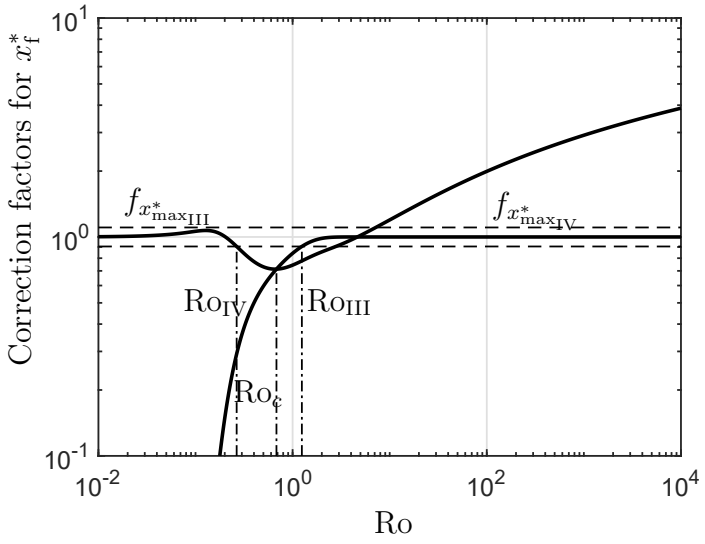

Figure B.8: Correction factors for engineering expressions for x_{f}^{*}.

B.3.3 $\dot{T}_{\mathrm{f}}^{*}$

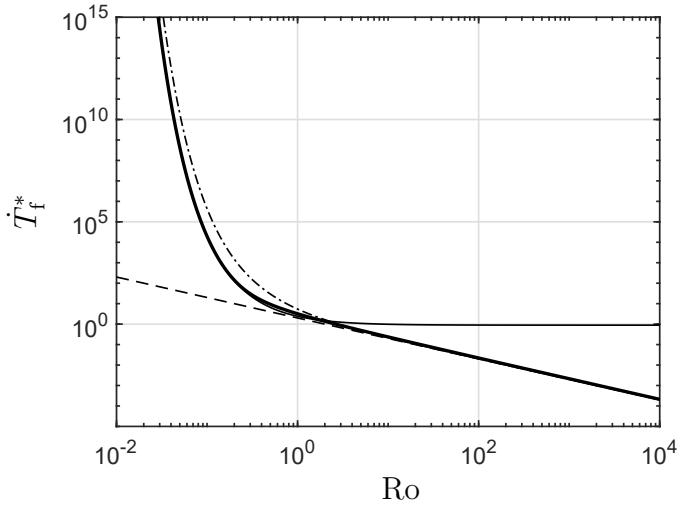

Figure B.9: $\dot{T}_{\mathrm{f}}^{*}$ changes with Ro number.

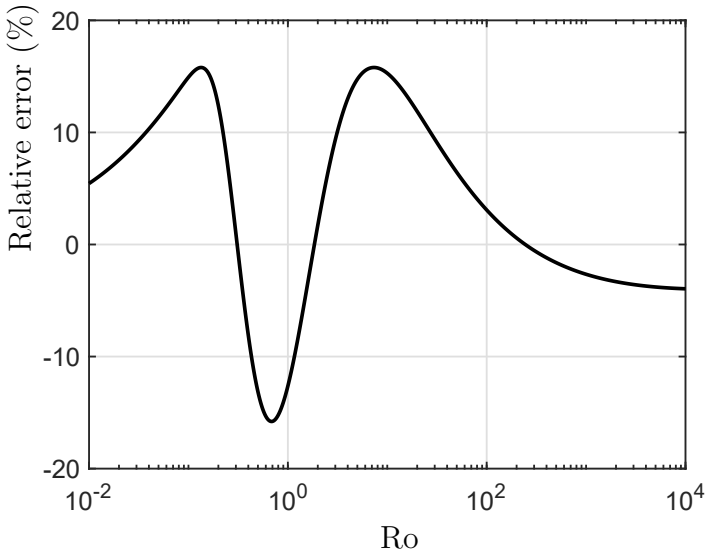

Figure B.10: Relative error changes with Ro for scaling laws of $\dot{T}_{\mathrm{f}}^{*}$.

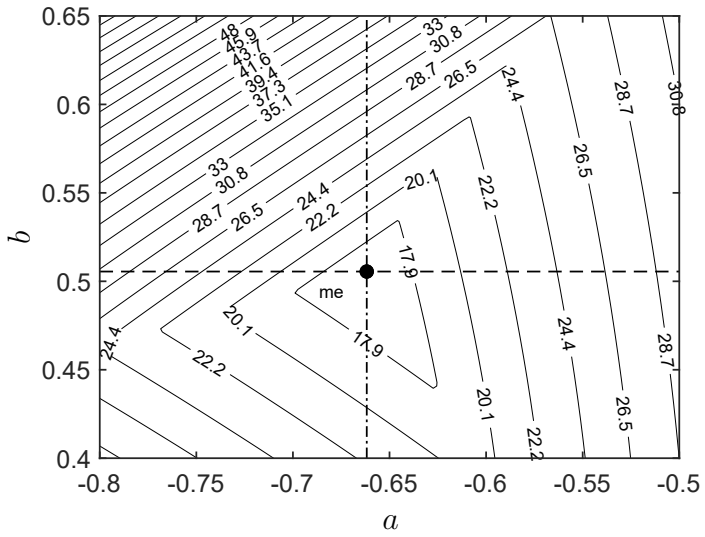

Figure B.11: Optimizing parameters for blending of $\dot{T}_{\mathrm{f}}^{*}$.

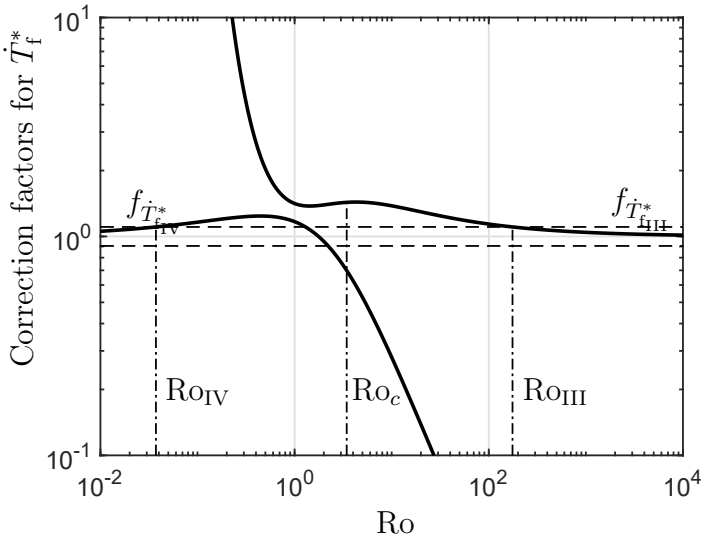

Figure B.12: Correction factors for engineering expressions for $\dot{T}_{\mathrm{f}}^{*}$.

B.3.4 x_{b}^{*}

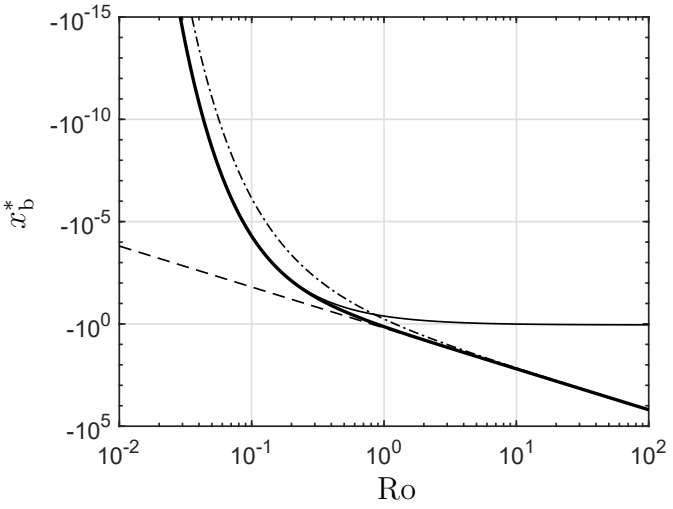

Figure B.13: x_{b}^{*} changes with Ro number.

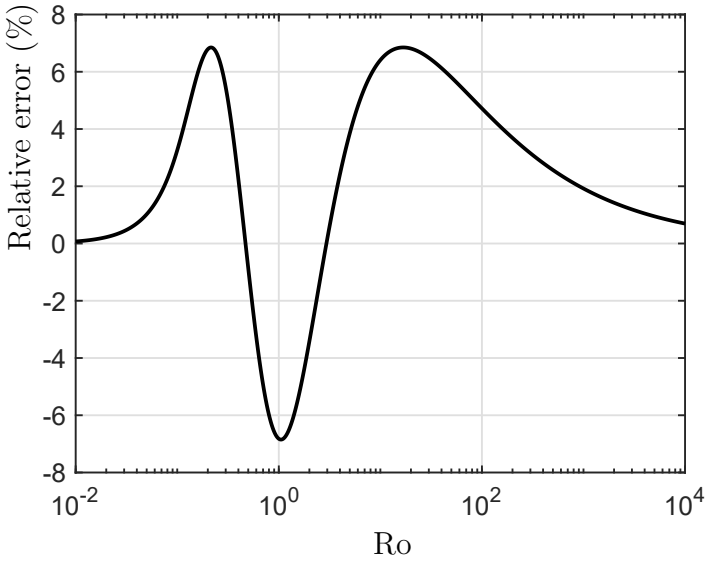

Figure B.14: Relative error changes with Ro for scaling laws of x_{b}^{*}.

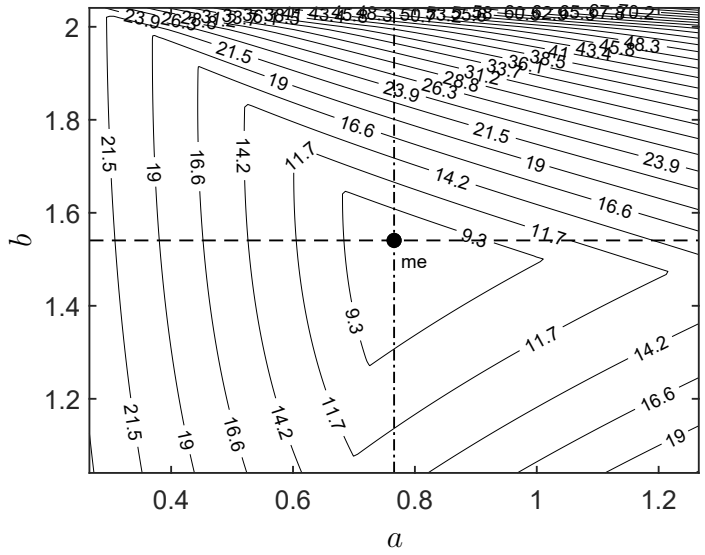

Figure B.15: Optimizing parameters for blending of x_{b}^{*}.

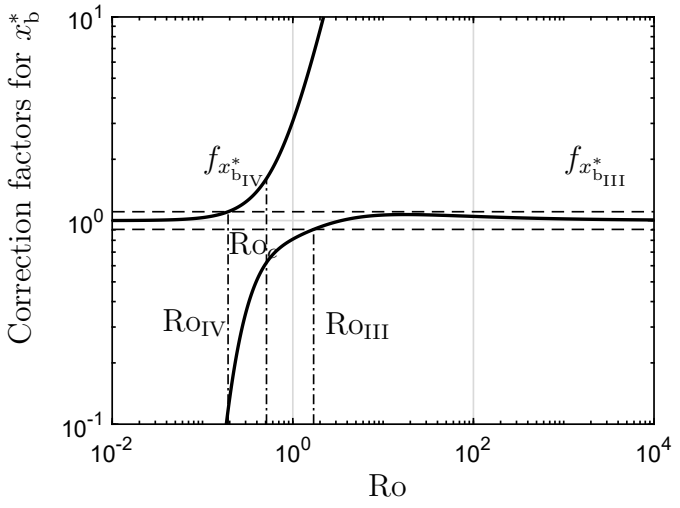

Figure B.16: Correction factors for engineering expressions for x_{b}^{*}.

B.3.5 $\dot{T}_{\mathrm{b}}^{*}$

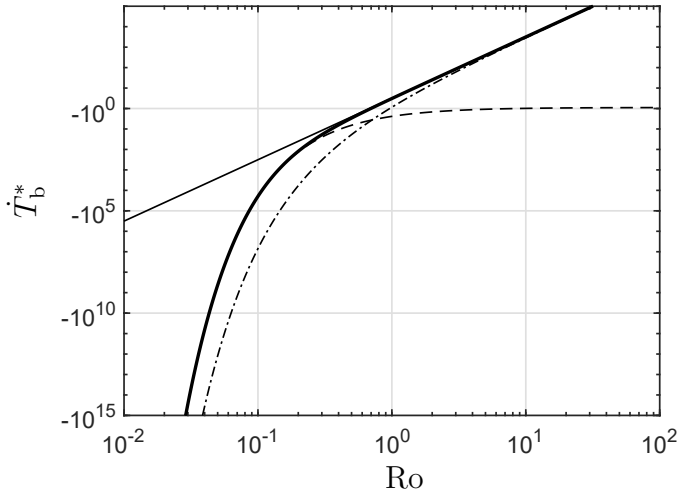

Figure B.17: $\dot{T}_{\mathrm{b}}^{*}$ changes with Ro number.

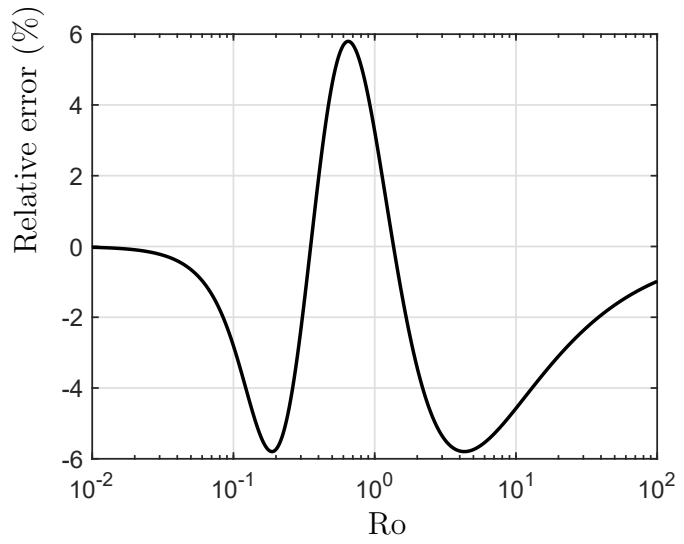

Figure B.18: Relative error changes with Ro for scaling laws of $\dot{T}_{\mathrm{b}}^{*}$.

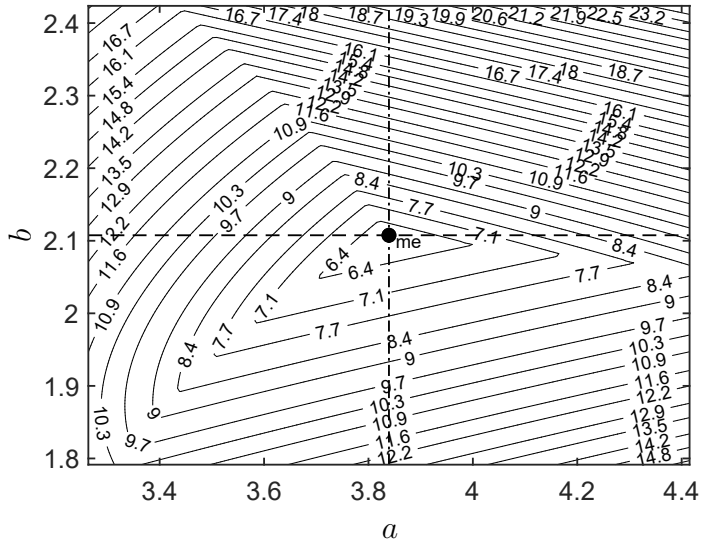

Figure B.19: Optimizing parameters for blending of $\dot{T}_{\mathrm{b}}^{*}$.

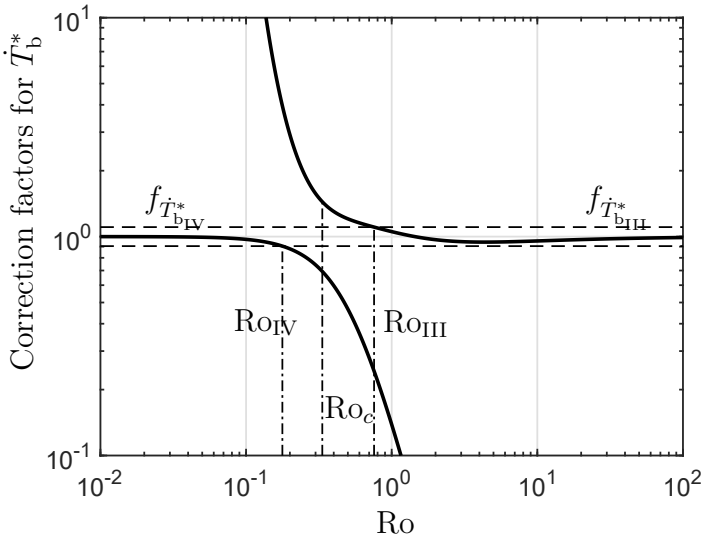

Figure B.20: Correction factors for engineering expressions for $\dot{T}_{\mathrm{b}}^{*}$.

B.3.6 $T^*_{\max}$

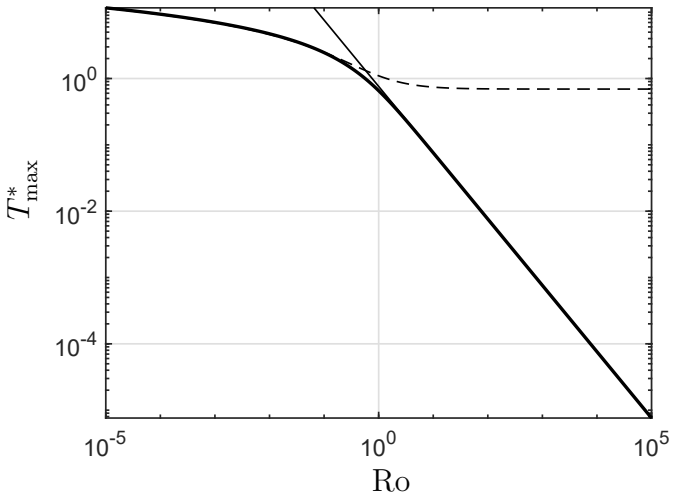

Figure B.21: $T^*_{\max}$ changes with Ro number.

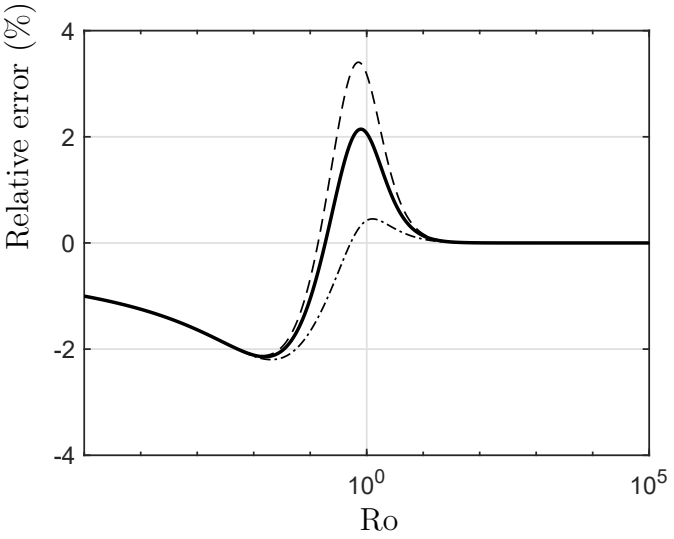

Figure B.22: Relative error changes with Ro for scaling laws of $T^*_{\max}$.

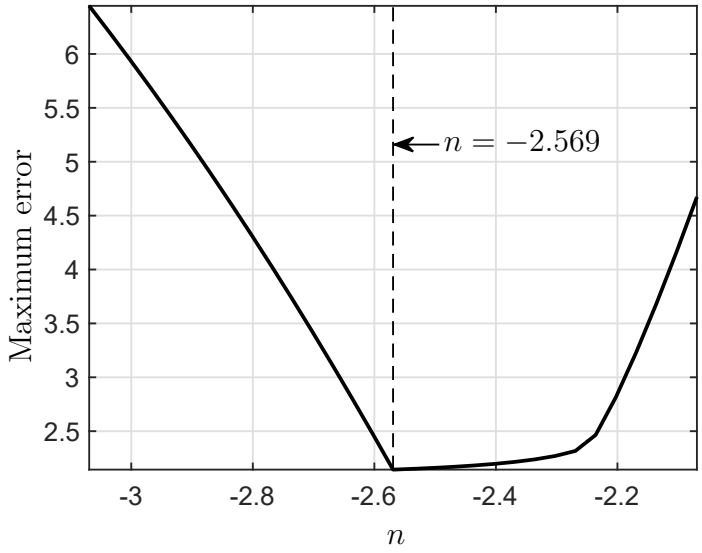

Figure B.23: Optimizing parameters for blending of $T^*_{\max}$.

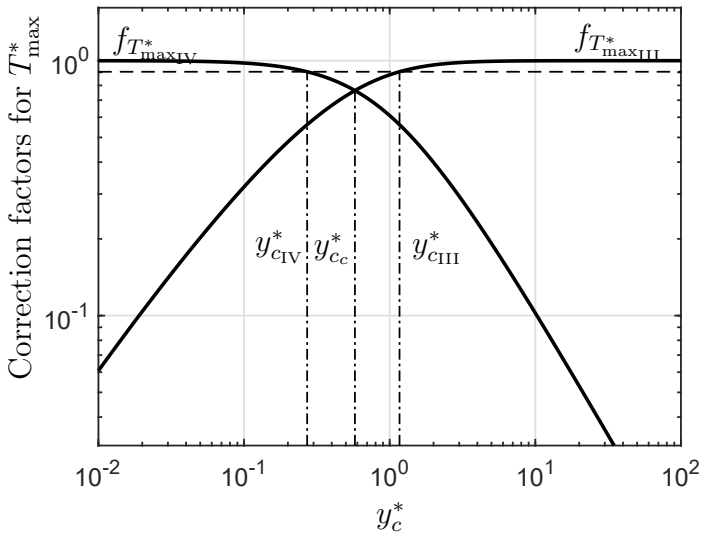

Figure B.24: Correction factors for engineering expressions for $T^*_{\max}$.

B.3.7 dT^*_{m}/dy^*

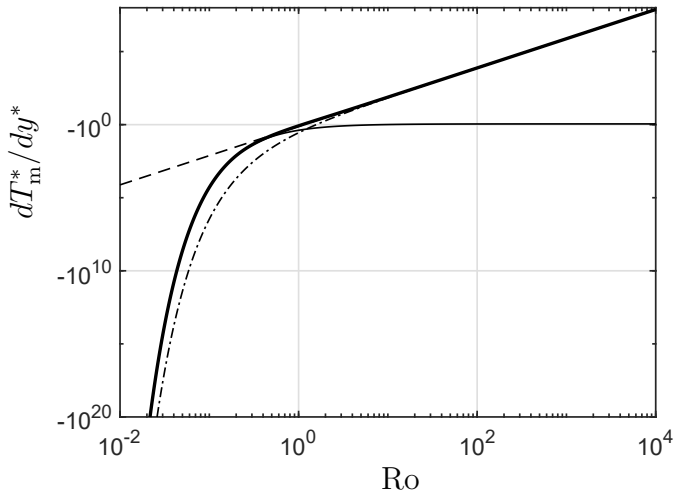

Figure B.25: dT^*_{m}/dy^* changes with Ro number.

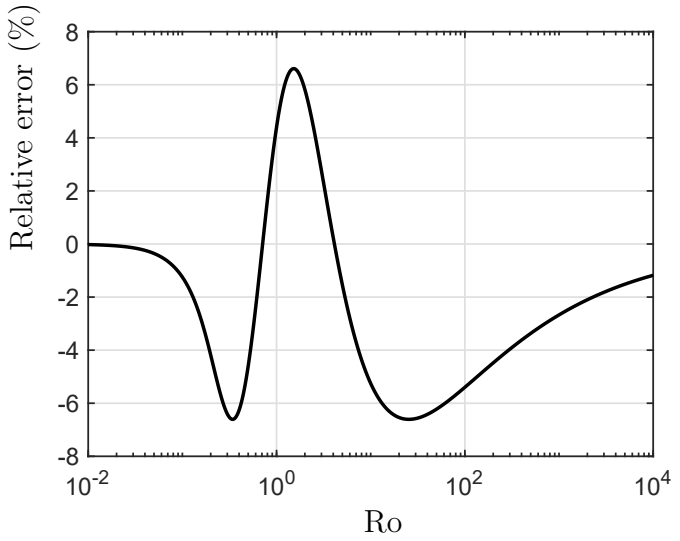

Figure B.26: Relative error changes with Ro for scaling laws of dT^*_{m}/dy^*.

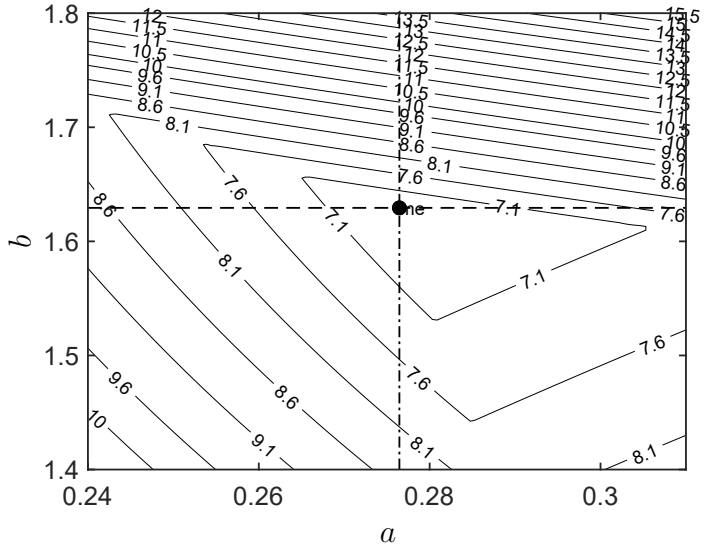

Figure B.27: Optimizing parameters for blending of dT^*_{m}/dy^*.

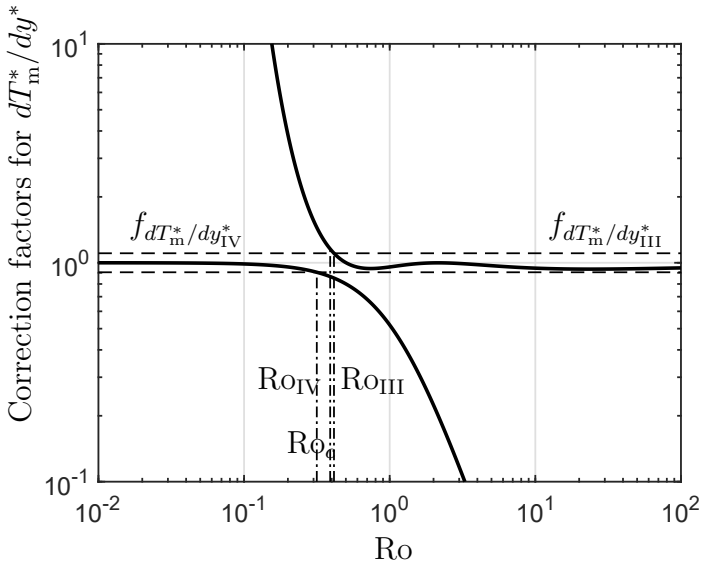

Figure B.28: Correction factors for engineering expressions for dT^*_{m}/dy^*.

B.3.8 $\mathcal{R}$

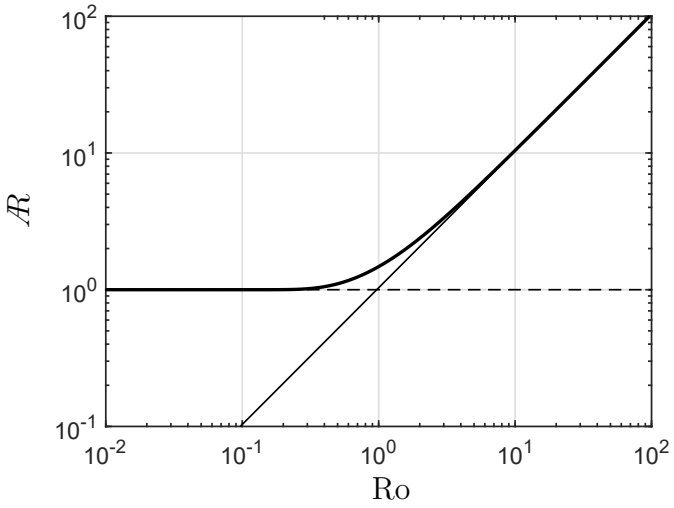

Figure B.29: $\mathcal{R}$ changes with Ro number.

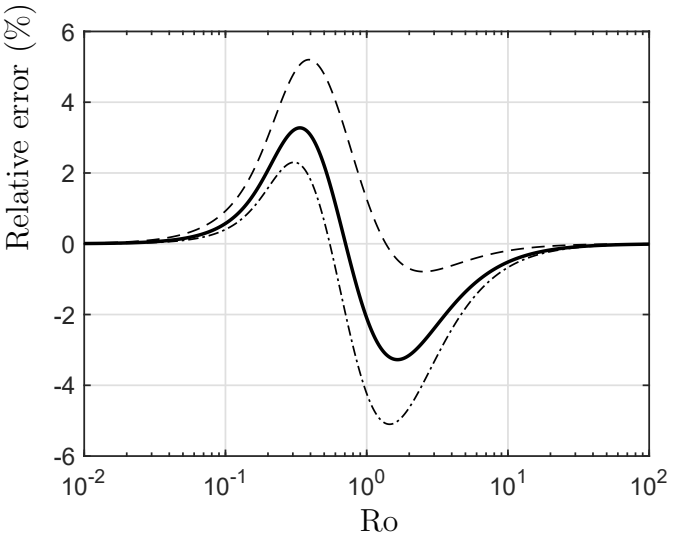

Figure B.30: Relative error changes with Ro for scaling laws of $\mathcal{R}$.

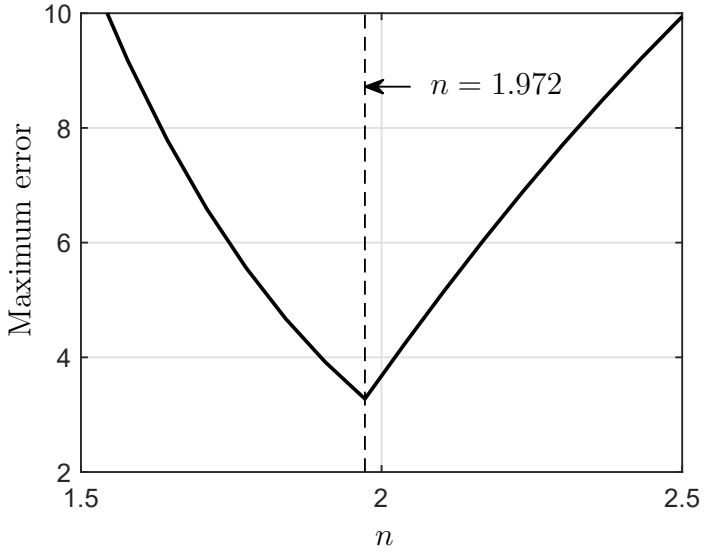

Figure B.31: Optimizing parameters for blending of $\mathit{Æ}$.

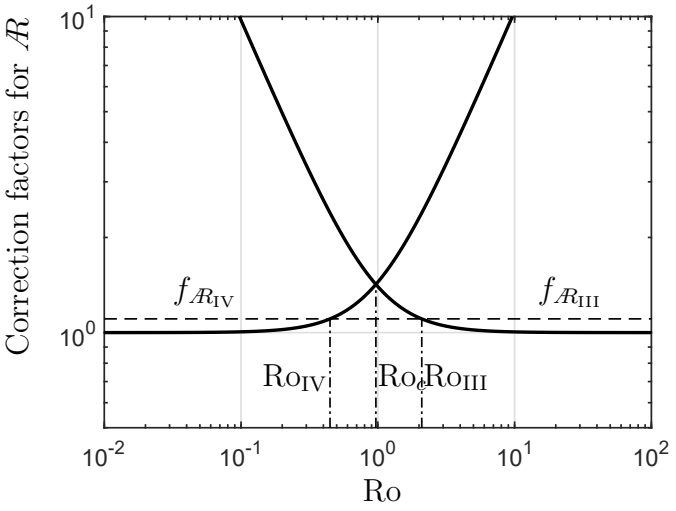

Figure B.32: Correction factors for engineering expressions for $\mathit{Æ}$.

Appendix C: Supplementary materials for the moving line heat source under convection

C.1 Matlab codes for isotherm trailing length and centerline cooling rate of moving heat source under surface heat loss in Chapter 4

C.1.1 Calculation of isotherm trailing length x_{b}^{*} of moving line heat source under surface heat loss

Listing C.1: Calculation of trailing length x_{b}^{*} of moving line heat source under surface heat loss.

```
function main
%%
% Numerical result of xb for Rosenthal model for thin plate with surface
% convection
% The mathematical solution is
% $T^*=\exp(-x^*) K_0 (r^* \sqrt{1+h^*})$
clear;clc;close all;
global PROGRESS_COUNTER PROGRESS_MAX options bar
%% Initialization
vRo=logspace(-5,5,1000);
vh=logspace(-5,5,999);

[mRo,mh]=meshgrid(vRo,vh);

PROGRESS_COUNTER=0;
PROGRESS_MAX = 999*1e3;
options = optimset('TolX',1e-305);
bar = waitbar(0,'Please wait...');

%% Calculation
```

```
xb=arrayfun(@(Ro,h)funxb(Ro,h),mRo,mh)
bar = waitbar(1,'Finished');

%% export solution
save thin2_xb_result.mat vh vRo xb
%%

    function xb=funxb(Ro,h)
        %%
        funT=@(x,h) exp(-x+x*sqrt(1+h)).*besselk(0,-x*sqrt(1+h),1);
        %%
        % determination of the valid range of x for each h
        % calculate form funT=@(x,h) exp(-x+x*sqrt(1+h)).*besselk(0,-x*sqrt(1+
            h),1);
        % -700<x*(sqrt(1+h)-1) % => x>-700/(sqrt(1+h)-1)
        % x*(sqrt(1+h)-1)<700 % => automatically satisfied because x<0 h>0
        % 1e-300<-x*sqrt(1+h)<1e300 % => -1e300/sqrt(1+h)<x<1e-300/sqrt
            (1+h)
        x1=-700./(sqrt(1+h)-1);
        x2= -1e-300;
        Ro1=1./funT(x1,h);
        Ro2=1./funT(x2,h);

        PROGRESS_COUNTER = PROGRESS_COUNTER + 1;
        waitbar(PROGRESS_COUNTER / PROGRESS_MAX,bar);

        if Ro>Ro1 || Ro<Ro2
            xb=nan;
        else
            xb= fzero(@(x) funT(x,h)-1./Ro,[x1,x2],options);
        end
    end

end
```

C.1.2 Blending of isotherm trailing length x_{b}^{*} of moving line heat source under surface heat loss

Listing C.2: Blending of trailing length x_{b}^{*} of moving line heat source under surface heat loss.

```
clear;clc;close all
load('thin2_xb_result.mat')
[Ro,h]=meshgrid(vRo,vh);
```

```
Ro(isnan(xb))=nan;

PI= pi*(1-1./sqrt(1+h)).*Ro.^2;

xbest=@(p) -pi* Ro.^2./(2*sqrt(1+h)).* 1./PI.*( 1./PI+log(PI+p(5)).^-1+p
    (3).*PI.^p(4) ).^-1.*...
    exp(-1./Ro).*(1+4./pi*exp(-0.5772).*Ro.^-2+2*p(1)./pi.*Ro.^(p(2)-2))
        ;

E=@(p) log(xbest(p)./xb);
disp('Original parameters')
pseed=[0.7659 1.541   0.08568  -0.1028   2.586]
max(max(abs(E(pseed))))

disp('2D Optimizing parameters')
[P,fval]=fminsearch(@(p) max(max(abs(E(p)))),pseed)

figure
ErrorXb = E(P)
surf(vRo,vh,ErrorXb);
set(gca,'xscale','log','yscale','log')
shading interp
xlabel('Ro'); ylabel('h')
axis([0.0014527,1e3,1e-5,1e5,-inf,inf])
```

C.1.3 Blending of centerline cooling rate $\dot{T}_{\mathrm{b}}^{*}$ of moving line heat source under surface heat loss

Listing C.3: Blending of centerline cooling rate $\dot{T}_{\mathrm{b}}^{*}$ of moving line heat source under surface heat loss.

```
clear;clc;close all
BlendFourRegimes = false ;
BlendIV_IVh = true;
BlendIIIh_IVh= true;
%%
load('thin2_xb_result.mat')
[Ro,h]=meshgrid(vRo,vh);
Ro(isnan(xb))=nan;
fun_Tb=@(h,Ro,xb) 1./Ro.*(1- sqrt(h+1).*besselk(1,-xb.*sqrt(h+1),1)./
    besselk(0,-xb.*sqrt(h+1),1));
Tb=fun_Tb(h,Ro,xb);
%% four regime blending
if BlendFourRegimes
```

```
    PI= pi*(1-1./sqrt(1+h)).*Ro.^2;
    TbIIIiiih = 1./Ro.*(1-sqrt(1+h)).*(1+1./lambertw(pi*(1-1./sqrt(1+h))
        .*Ro.^2));
    a0=3.839; b0=2.108;
    Tbest=@(p) - sqrt(1+h)./(pi*Ro.^3).* PI.*(1+1./PI+log(PI+p(5)).^-1+p
        (3).*PI.^p(4) ).*exp(1./Ro).*(1+2./pi*exp(-0.5772).*Ro.^-3+p(1)./
        pi.*Ro.^(p(2)-3)).^-1;

    E=@(p) log(Tbest(p)./Tb);
    pseed = [3.839   2.108   0.08568  -0.1028   2.586]

    Xiii = logspace(-5,5,1000);
    EIIIIIIH = @(p) log( (Xiii.*(1+1./Xiii+log(Xiii+p(5)).^-1+p(3).*Xiii
        .^p(4) ))./(Xiii.*(1+1./lambertw(Xiii))));

    ME=@(p) max([max(max(abs(E(p)))),max(max(abs(EIIIIIIH(p))))]);
    [P,fval] = fminsearch(@(p) ME(p),pseed)
    % 3.6524    1.9708    0.0641   -0.1004    6.2523
    PnotBlending= [3.839 2.108 0.08568 -0.1028 2.586];

    ME(PnotBlending)

    figure
    ErrorTb = E(P);
    surf(vRo,vh,ErrorTb);
    set(gca,'xscale','log','yscale','log')
    shading interp
    xlabel('Ro'); ylabel('h');
    axis([0.0014527,1e3,1e-5,1e5,-inf,inf])
end
%% Regime IV IVh
if BlendIV_IVh
    Tbiv= - Tb(:,220)'./(1./2*exp(0.5772+1./vRo(220)));
    funTbivest=@(n) (1+sqrt(vh).^n).^(1./n);
    E=@(n) log(funTbivest(n)./Tbiv);
    [P,fval]=fminsearch(@(p) max(max(abs(E(p)))),1)
end
%% Regime IIIh IVh
if BlendIIIh_IVh
    Tbh= - Tb(end,:)./(sqrt(vh(end)));
    loglog(Tbh,'k'); hold on
    loglog(1./vRo.*exp(1./vRo)); hold on
    loglog(1./2*exp(1./vRo+0.5772)); hold on
    funTbh=@(p) exp(1./vRo)./( 2*exp( - 0.5772) + vRo+p(1).*vRo.^p(2));
    E=@(n) log(funTbh(n)./Tbh);
```

```
    [P,fval]=fminsearch(@(p) max(max(abs(E(p)))),[1,1])
end
```

C.1.4 Critical values of convection coefficients to neglect effects of surface heat loss for trailing length and cooling rate

Listing C.4: Critical values of convection coefficients to neglect effects of surface heat loss.

```
clear;clc;close all
% calculate the negeligible convection area
%% Load data
load('thin2_xb_result.mat')
[mRo,mh]=meshgrid(vRo,vh);
mRo(isnan(xb))=nan;
fun_Tb=@(h,Ro,xb) 1./Ro.*(1- sqrt(h+1).*besselk(1,-xb.*sqrt(h+1),1)./
   besselk(0,-xb.*sqrt(h+1),1));
Tb=fun_Tb(mh,mRo,xb);
%
funTh0=@(x) besselk(0,-x,1);
options = optimset('TolX',1e-100);
funxb0=@(Ro) fzero(@(x) funTh0(x)-1./Ro,[-1e300,-1e-300],options);

xbesth0=nan*vRo;

for j=1:size(vRo,2)
    if vRo(j) > 1e-2
        xbesth0(j)= funxb0(vRo(j));
    end
end

Tbesth0=1./vRo.*(1- besselk(1,-xbesth0,1)./besselk(0,-xbesth0,1));
[xbesth0,~]=meshgrid(xbesth0,vh);
[Tbesth0,~]=meshgrid(Tbesth0,vh);

figure
error_xbesth0=log(xbesth0./xb);
error_Tbesth0=log(Tbesth0./Tb);
contour(vRo,vh,error_xbesth0,[-0.1,0.1],'--k','linewidth',2); hold on
contour(vRo,vh,error_Tbesth0,[-0.1,0.1],'-k','linewidth',2); hold on
set(gca,'xscale','log','yscale','log')

axis([1e-2,1e2,1e-2,1e2])
```

```
xlabel('Ro')
ylabel('h')
DefaultGca


a=0.7659; b=1.541;
AE=0.1;
Rolist=logspace(-2,5,1000);
xbest0= -exp(-1./Rolist) .*(2*exp(-0.5772)+pi/2.*Rolist.^2+a.*Rolist.^b)
    ;

hcrxb=-((2*(besselk(0, -xbest0,1)- besselk(1, -xbest0,1)))./ besselk(1,
    -xbest0,1)).* AE;
hcrtb=-((2*AE*(besselk(0,-xbest0,1) - besselk(1,-xbest0,1)).^2)./(
    xbest0.*besselk(0,-xbest0,1).^2 - besselk(1,-xbest0,1).^2 - xbest0.*
     besselk(1,-xbest0,1).^2));
plot(Rolist,hcrxb,'--k','linewidth',1); hold on
plot(Rolist,hcrtb,'-k','linewidth',1); hold on
legend('hc for xb for\newline 10% accepted error',...
    'hc for Tb for \newline 10% cooling rate',...
    'estimated hc for xb for\newline 10% accepted error',...
    'estimated hc for Tb for\newline 10% accepted error')
```

C.2 Matlab codes for isotherm width and its location of moving line heat source under surface heat losses in Chapter 5

C.2.1 Calculation of isotherm width $y^*_{\max}$ and its location $x^*_{\max}$ of moving line heat source under surface heat loss

Listing C.5: Calculation of $y^*_{\max}$ and $x^*_{\max}$ for moving line heat source under surface heat loss.

```
%% Thin plate with heat  disspation :
clear;clc;close all;
% Calculating  the width and it 's  location
%% Functions used according to  original  equation and dimensional  analysis
fun_T=@(x,r,h) exp(-x-r.*sqrt(1+h)).*besselk(0,r.*sqrt(1+h),1);
fun_xm=@(r,h) -r.*besselk(0,r.*sqrt(1+h),1)./(sqrt(h+1).*besselk(1,r.*
    sqrt(1+h),1));
fun_ym=@(r,h) r.*sqrt(1-(besselk(0,r.*sqrt(1+h),1)./(sqrt(h+1).*besselk
    (1,r.*sqrt(1+h),1))).^2);
fun_Tm=@(r,h) fun_T(fun_xm(r,h),r,h);
```

```
options = optimset('TolX',1e-305);
% Simplify this function: fun_rm=@(T,h,a,b) fzero(@(r) T-fun_Tm(r,h),[a,b],
    options);
fun_rm=@(T,h,a,b) fzero(@(r) T-(exp(r.*(besselk(0,r.*sqrt(1+h),1)./(sqrt
    (h+1).*besselk(1,r.*sqrt(1+h),1))-sqrt(1+h))).*besselk(0,r.*sqrt(1+h
    ),1)),[a,b],options);
%% Setting values
% To make sure @fun_Tm make sense in MATLAB, must be in [1e-308,1e308], and
    must be in[-700,700]
% increase with by plotting
h_val=logspace(-7,7,900);
r0=1e-300*h_val./h_val;r1=arrayfun(@(h) fzero( @(r) -fun_xm(r,h)-r*sqrt
    (1+h) +700,[1e-300,1e300]),h_val);
RANGE_T=[max(fun_Tm(r1,h_val)),min(fun_Tm(r0,h_val))];
T_val=logspace(-3,log10(300),1000);
[T,h]=meshgrid(T_val,h_val); [~,r0]=meshgrid(T_val,r0);[~,r1]=meshgrid(
    T_val,r1);
%% Calculating with disspation
tic
rm=arrayfun(@(T,h,a,b) fun_rm(T,h,a,b),T,h,r0,r1);
toc
xm=fun_xm(rm,h);
ym=fun_ym(rm,h);

rm0= arrayfun(@(T) fun_rm(T,0,1e-300,1e300),T_val);
xm0=fun_xm(rm0,0);
ym0=fun_ym(rm0,0);
save THIN_RES_XM_YM T h T_val h_val xm ym rm xm0 ym0 rm0
```

C.2.2 Blending of isotherm width $y^*_{\max}$ and its location $x^*_{\max}$ of moving line heat source under surface heat loss

Listing C.6: Blending $x^*_{\max}$ for moving line heat source under surface heat loss.

```
clear;clc;close all;
%% load calculation results
path = pwd;
cd ../../
load('THIN_RES_XM_YM.mat'); cd(path)
vRo=1./T_val; Ro=1./T; vh=h_val; e= exp(1);
clear T_val h_val rm rm0 T xm0 ym0
%% Corner III
x_omega = pi*h.*Ro.^2./(exp(1./(1+h)).*(1+h));
```

```
omega = (x_omega.^-1+log(x_omega+2.585).^-1+0.08568*x_omega.^(-0.1028))
    .^-1;
f_III_IV = exp(-2./Ro).*(1+ 8*e/(pi*exp(2*0.5772))*Ro.^-3 +2*1.427*e/pi*
    Ro.^(1.077-2));
f_III_IIIa = e./(pi*Ro.^2.*h).*omega;
xmax_III_IV_IIIA = - pi/(2*exp(1))*Ro.^2.* f_III_IV.*f_III_IIIa;
%% Opposite corner
g = xm./xmax_III_IV_IIIA;
g2 = 1./g ;
G_IVa = e-1 ;
gest =@(p) (1+ G_IVa.*(1 + p(1).*Ro.^p(2)).^(p(3)) .*(1+ p(4).*h.^p(5))
    .^p(6)).^-1 ;
E=@(p) log(gest(p)./g);
options = optimset('MaxFunEvals',1e10);
ME=@(p) max(max(abs(E(p))));
pseed=[3.143   0.8608   -0.5360   0.3143   -0.7133   -2.645];
ME(pseed)
[P,fval] = fminsearch(@(p) ME(p) ,pseed)
%% Plot errormap
EC= E(P);
surf(Ro,h,100*EC)
shading interp
set(gca,'xscale','log','yscale','log')
xlabel('Ro') ; ylabel('h')
```

Listing C.7: Blenidng $y^*_{\max}$ for moving line heat source under surface heat loss.

```
clear;clc;close all;
cd ../../
load('THIN_RES_XM_YM.mat')
cd ./Blending/Blending_ymax
vRo=1./T_val; Ro=1./T; vh=h_val;
e=exp(1);
%% Corner III
x_omega = pi*h.*Ro.^2./(exp(1./(1+h)).*(1+h));
omega = (x_omega.^-1+log(x_omega+2.585).^-1+0.08568*x_omega.^(-0.1028))
    .^-1;

f_III_IV = exp(-1./Ro).*(1+(sqrt(8*exp(1)/pi).*exp(-0.5772)./Ro)
    .^(1.407)).^(1./1.407) ;
f_III_IIIa = sqrt(e./(2*pi*h)).*omega./Ro.*sqrt(1+2./((1+h).*omega));
ymax_III_IV_IIIA = sqrt(pi/(2*exp(1))).*Ro.* f_III_IV.*f_III_IIIa;
%% Opposite corner
g = ym./ymax_III_IV_IIIA;
% G_IVa = Ro./omega.*1./sqrt(e/(2*pi).*(1+(2./((1+h).*omega)))) - 1
```

```
% pseed=[5.929  1.829    −0.5464  0.06783  −0.6749  −19.76];
G_IVa = sqrt(2./(pi*e*Ro.^2+2*e./(1+h))) ;
gest =@(p) (1+ (G_IVa.*(1 +p(1).*Ro.^p(2)).^(p(3)) .*(1+ p(4).*h.^p(5))
    .^p(6))) ;
E=@(p) log(gest(p)./g);
ME=@(p) max(max(abs(E(p))));
set(gca,'xscale','log','yscale','log')
%% Optimization
pseed=[16.09   1.438   -0.2508 0.05885   -0.3583 -24.44];
ME(pseed)
options = optimset('MaxFunEvals',1e5);
[P,fval] = fminsearch(@(p) ME(p) ,pseed,options)
%%
EC =  E(P);
surf(Ro,h,100*EC)
shading interp
set(gca,'xscale','log','yscale','log')
xlabel('Ro') ; ylabel('h')
```

C.2.3 Critical values of convection coefficients to neglect effects of surface heat loss for isotherm width and its location

Listing C.8: Critical values of h_c^* to neglect effects of convection within 10 % relative eror for $y^*_{\max}$ and $x^*_{\max}$.

```
clear;clc;close all;
%%
 load('THIN_RES_XM_YM.mat')
%%
[Mym0,~]= meshgrid(ym0,h_val);
Eym = abs(log(ym./Mym0));
contour(1./T_val,h_val,Eym,[0.1,0.1],'-k','linewidth',2); hold on

[Mxm0,~]= meshgrid(xm0,h_val);
Exm = abs(log(xm./Mxm0));
contour(1./T_val,h_val,Exm,[0.1,0.1],'--k','linewidth',2); hold on

Roval=1./T_val; hcym = 0.2*(1+(pi/(2*exp(1))*Roval.^2).^0.9405)
    .^(-1./0.9405);
plot(Roval,hcym,'-k','linewidth',1); hold on
hcxm =  0.1.*((exp(1)./(Roval.^2*pi)).^(-1.296)+1).^(-1./1.296)
plot(Roval,hcxm ,'--k','linewidth',1); hold on

```

```
set(gca,'xscale','log','yscale','log')
axis([-inf,inf,-inf,1])
xlabel('Ro')
ylabel('hc')
legend('hcym','hcxm','hcymest','hcxmest')
DefaultGca
```

Appendix D: Supplementary materials for moving Gaussian heat source model

D.1 Matlab codes for isotherm width under a moving Gaussian heat source in Chapter 6

D.1.1 Calculation of isotherms with two peaks under a moving Gaussian heat source

Listing D.1: Example of an isotherm with two peaks under a moving Gaussian heat source.

```
clear;clc; close all
xv=[-40:1:-26,-25:0.1:-4,-3:-1]; yv=[9.5:0.01:10.5];
Ry=110;T0 =1./Ry; % 0.009 ;
sigma=4;
funT=@(x,y,s) 1/sqrt(2*pi)*integral(@(t) t.^(-0.5)./(t+s^2).*exp(-((x+t)
    .^2+y^2)./(2*t+2*s^2)),0,inf);
[x,y]=meshgrid(xv,yv);
s=sigma*(x./x);
T2=arrayfun(@(x,y,s) funT(x,y,s),x,y,s);
xlabel('x');
ylabel('y');
text(-15,10.1,'Ry=110,sigma=4'); hold on
contour(xv,yv,T2,T0*[1,1],'k','linewidth',2);
DefaultGca
% savefigures (1,'gaussian_bipeak_example')
```

Listing D.2: Calculation of isotherms with two peaks under a moving Gaussian heat source.

```
clear;clc;close all
% The start value of Ry and sigma, that two peak conditions exist
% If $d (X^2)/d(R^2) = 1$, two peaks exsits
```

```
% *IMPORTANT* , the varable x or r here is modified by X = X-\sigma^2, R = sqrt((x-sigma^2)^2+y^2)
%% calculate the maximum value of $d (X^2)/d(R^2)$ for a given $\sigma$
tola=1e-20; tolb=1e-16;
funTstar=@(x,sigma) 1/sqrt(2*pi)*integral(@(t) t.^(-1/2)./(t+sigma.^2).*exp(-0.5*(x.^2+t.^2+2.*t.*x)./(t+sigma.^2)),0,inf,'RelTol',1e-100,'AbsTol',1e-100);
funxm=@(sigma) fminsearch(@(x) -funTstar(x,sigma),-3,optimset('TolFun',1e-80,'TolX',1e-80,'MaxFunEvals',10000,'MaxIter',5000));
funtm=@(r,sigma) acos(min(sigma/sqrt(r),1));
funp=@(r,n,sigma) integral(@(t) cos(t).^n.*exp(-0.5*(r/sigma*cos(t)-sigma./cos(t)).^2),0,funtm(r,sigma),'RelTol',tola,'AbsTol',tolb)+integral(@(t) cos(t).^n.*exp(-0.5*(r/sigma*cos(t)-sigma./cos(t)).^2),funtm(r,sigma),pi/2,'RelTol',tola,'AbsTol',tolb);
% $d (X^2)/d(R^2)$
fundx2r2=@(r,sigma) sigma^2*funp(r,0,sigma)./funp(r,2,sigma).*(funp(r,0,sigma).*funp(r,4,sigma)./funp(r,2,sigma).^2-1);
% minimal value of R =sqrt((x-sigma^2)^2+y^2), location of center maximum temperature
funrmin = @(sigma) abs(funxm(sigma)-sigma.^2);
%% minimal Ry has two peaks
fun_Rval_dx2dr2_Max=@(sigma) fminsearch(@(r) -fundx2r2(r,sigma),sigma+abs(funxm(sigma)-sigma.^2));
fval_dx2dr2_Max =@(sigma) fundx2r2(fun_Rval_dx2dr2_Max(sigma),sigma);
% find sigma $d (X^2)/d(R^2) = 0 $
[bipeak_min_sigma] = fzero(@(sigma) fval_dx2dr2_Max(sigma) -1,[2,5]);
R_bipeak_min_sigma= fun_Rval_dx2dr2_Max(bipeak_min_sigma);
[Tc_bipeak_min_sigma,xm_bipeak_min_sigma,ym_bipeak_min_sigma] = tm_rm(bipeak_min_sigma,R_bipeak_min_sigma)
Ry_min_bipeak = 1./Tc_bipeak_min_sigma;
%% plot $d (X^2)/d(R^2)$ vs R
sigmalist = [1,2,bipeak_min_sigma,5,10];
for i = 1: max(size(sigmalist))
    sigma = sigmalist(i);
    rlist = abs(funxm(sigma)-sigma.^2)*logspace(0,1,100);
    dx2r2_list =arrayfun(@(r) fundx2r2(r,sigma),rlist);
    semilogx(rlist,dx2r2_list,'k','linewidth',2,'DisplayName',num2str(sigma)); hold on
end
plot([1,1e3],[1,1],'--k','linewidth',1,'HandleVisibility','off')
axis([1,1e3,0,1.2])
xlabel('r')
ylabel('dx2r2')
legend
DefaultGca
```

```
% savefigures (1,'gaussian_bipeak_dX2dR2_R')
% bipeak_min_sigma = 2.8931;
% Ry_min_bipeak = 58.2030;
%% Area of two peak existing
% rmin is the minimal vlaue of $R = sqrt((x-sigma^2)^2+y^2)$ for a given
    $sigma$
% rmax is $R = sqrt((x-sigma^2)^2+y^2)$ for the maximum value of $d (X^2)/d(R
    ^2) = 1$
% r_root_1 and r_root_2 are the two roots of $ d (X^2)/d(R^2) = 1 $ for $sigma$
     larger than bipeak_min_sigma
% Between r_root_1 and r_root_2, ymax decrease with R; and there are two peaks
Sigma = logspace(log10(bipeak_min_sigma),log10(500),1e3); Sigma = Sigma
    (2:end);
Rmax = arrayfun(@(x) fun_Rval_dx2dr2_Max(x) ,Sigma);
Rmin = arrayfun(@(sigma) funrmin(sigma), Sigma) ;
for i=1:max(size(Sigma))
  R_root_1(i)=fzero(@(x) fundx2r2(x,Sigma(i))-1,[Rmin(i), Rmax(i)],
      optimset('TolFun',1e-80,'TolX',1e-80,'MaxFunEvals',10000,'MaxIter'
      ,5000));
  R_root_2(i)=fzero(@(x) fundx2r2(x,Sigma(i))-1,[Rmax(i), 2*Rmax(i)],
      optimset('TolFun',1e-200,'TolX',1e-100,'MaxFunEvals',10000,'MaxIter
      ',5000));
  [Tc_min_bipeak(i),~,~] = tm_rm(Sigma(i),R_root_1(i));
  [Tc_max_bipeak(i),~,~] = tm_rm(Sigma(i),R_root_2(i));
end
figure
funSigmaMax=@(Ry) ((1.0140*Ry.^(2/3)).^-2.3975+(sqrt(pi/2)*Ry).^-2.3975)
    .^(1/-2.3975);
plot(Sigma./funSigmaMax(1./Tc_min_bipeak),1./Tc_min_bipeak); hold on
plot(Sigma./funSigmaMax(1./Tc_max_bipeak),1./Tc_max_bipeak); hold on
axis([1e-3,1e0,1e-3,1e6])
xlabel('sigma/sigmamax')
ylabel('Ry')
set(gca,'xscale','log','yscale','log')
DefaultGca
% savefigures (2,'gaussian_bipeak_area')
%%
save('gaussian_bipeak.mat','R_root_1', 'R_root_2', 'Rmax', 'Rmin', '
    Sigma', 'Tc_max_bipeak', 'Tc_min_bipeak', 'bipeak_min_sigma', '
    Ry_min_bipeak')
```

D.1.2 Calculation of isotherm width $y^*_{\max}$ under a moving Gaussian heat source

Listing D.3: Calculation of $y^*_{\max}$ and $x^*_{\max}$ under a moving Gaussian heat source.

```

clear;clc;close all;

sz1 = 1e3; sz2 = 900;
VRy = logspace(-3,3,sz1);
Vmul = logspace(-3,log10(0.9),sz2);
[MRy,Mmul] = meshgrid(VRy,Vmul);
%% $\sigma_{max}$ and $\sigma$
% Temperature field function
fun_maxintegrand=@(x,y,sigma) acos(min([sigma.*((sigma.^2-x).^2+y.^2)
    .^(-0.25),1]));
fun_T=@(x,y,sigma) 1/sqrt(2*pi)*2./sigma.* (integral(@(z) exp(-0.5*(cos(
    z).^2*(sigma.^2+(x.^2+y.^2)./sigma.^2-2*x)+sigma.^2./(cos(z).^2+1e
    -100)+2.*x-2.*sigma.^2)),0,fun_maxintegrand(x,y,sigma) ,'RelTol',1e
    -6,'AbsTol',1e-21)+ ...
    integral(@(z) exp(-0.5*(cos(z).^2*(sigma.^2+(x.^2+y.^2)./sigma.^2-2*
        x)+sigma.^2./(cos(z).^2+1e-100)+2.*x-2.*sigma.^2)),
        fun_maxintegrand(x,y,sigma),pi/2,'RelTol',1e-6,'AbsTol',1e-21));

% function maximum temperature and its location
fun_xm=@(sigma) fminbnd(@(x) -fun_T(x,0,sigma),5*max(-0.7650*sigma,-
    sigma.^2),0.2*max(-0.7650*sigma,-sigma.^2) ,optimset('MaxFunEvals'
    ,10000,'MaxIter',5000));
fun_Tmaxcenter = @(sigma) fun_T(fun_xm(sigma),0,sigma);

% Rmin = sqrt((xmax_center-sigma^2)^2+0)
fun_rmin = @(sigma) abs(fun_xm(sigma)-sigma.^2);

% maximum sigma for Ry
fun_Sigmamax_blending=@(Ry) ((1.0140*Ry.^(2/3)).^-2.3975+(sqrt(pi/2)*Ry)
    .^-2.3975).^(1/-2.3975);
% fun_Sigmamax = @(Ry) fzero(@(sigma) fun_Tmaxcenter(sigma)-1./Ry,
    fun_Sigmamax_blending(Ry),optimset('MaxFunEvals',1e5,'MaxIter',5000));
Vsigmamax = arrayfun(@(Ry) fun_Sigmamax_blending(Ry),VRy);
[Msigmamax,~] = meshgrid(Vsigmamax,Vmul);
Msigma = Msigmamax.*Mmul;

%% Calculation ymax and xmax
load('gaussian_bipeak.mat')
Mxmax = nan*MRy; Mymax = nan*MRy;
Mxb = nan*MRy; Mxf = nan*MRy;
parfor i=1:sz2
    for j=1:sz1
```

```
34          % location of maximum temperature
35          xmax_center_loop = fun_xm(Msigma(i,j));
36          % leading and trailing length of isotherm
37          [Mxb(i,j),Mxf(i,j)]=fun_xbf(Msigma(i,j),xmax_center_loop,1./MRy(i
                ,j),fun_T);
38          % lower limit of R
39          r0_lim_loop=fun_rmin(Msigma(i,j));
40          % upper limit of R
41          r3_lim_loop = 3*abs(Mxb(i,j)-Msigma(i,j).^2);
42
43          if Msigma(i,j) > bipeak_min_sigma
44              % range of T, two peak exists , for a sigma
45              TmaxBipeak = interp1(Sigma,Tc_max_bipeak,Msigma(i,j),'pchip')
                    ;
46              TminBipeak = interp1(Sigma,Tc_min_bipeak,Msigma(i,j),'pchip')
                    ;
47
48              if (1/MRy(i,j) < TmaxBipeak) && (1/MRy(i,j) > TminBipeak)
49                  % intervals of r for two peak existing
50                  r1_lim_loop=interp1(Sigma,R_root_1,Msigma(i,j),'pchip');
51                  r2_lim_loop=interp1(Sigma,R_root_2,Msigma(i,j),'pchip');
52                  % peak 1
53                  r1_loop=fzero(@(r) tm_rm(Msigma(i,j),r)-1./MRy(i,j),[
                        r0_lim_loop,r1_lim_loop]);
54                  [~,xm1_loop,ym1_loop]=tm_rm(Msigma(i,j),r1_loop);
55                  % peak 2
56                  r2_loop=fzero(@(r) tm_rm(Msigma(i,j),r)-1./MRy(i,j),[
                        r2_lim_loop,r3_lim_loop]);
57                  [~,xm2_loop,ym2_loop]=tm_rm(Msigma(i,j),r2_loop);
58                  % maximum width
59                  Mymax(i,j) = max([ym1_loop,ym2_loop]);
60                  Mxmax(i,j) = sum([xm1_loop,xm2_loop].*([ym1_loop,ym2_loop
                        ]==Mymax(i,j)));
61                  continue;
62              end
63          end
64          % one peak exists
65          r_loop=fzero(@(r) tm_rm(Msigma(i,j),r)-1./MRy(i,j),[r0_lim_loop,
                r3_lim_loop]);
66          [~,Mxmax(i,j),Mymax(i,j)]=tm_rm(Msigma(i,j),r_loop);
67      end
68      i
69  end
70  %%
71  ycal= fun_ymax_Gaussian(MRy,Msigma);
```

```
E= 100*log(ycal./Mymax);
max(max(abs(E)))
save gaussian_ymax



function [xb,xf]=fun_xbf(sigma,xmax_center,Tc,funTstar)
% calculate leading and trailing length xf and xb of isotherm

nmax=300;
% domain sorted :    aa <xb<a<xmax_center<b<xf<bb
aa=xmax_center;
bb=xmax_center;
flaga=0;
flagb=0;
% search the domain contains xf&xb
for i=1:nmax
    if flaga<0.5
        faa=funTstar(aa,0,sigma);
        aa=(10.*aa-1+xmax_center)*(faa>Tc)+(10.*aa-1+xmax_center)*(faa==
            Tc)+aa*(faa<Tc);
        flaga=1*(faa<=Tc);
    end

    if  flagb<0.5
        fbb=funTstar(bb,0,sigma);
        bb=(bb-xmax_center+1)*(fbb>Tc)+(bb-xmax_center+1)*(fbb==Tc)+bb*(
            fbb<Tc);
        flagb=1*(fbb<=Tc);
    end

    if flaga && flagb
        break
    end
end
% bisection xb
if flaga>0.5
    xb=fzero(@(x) funTstar(x,0,sigma)-Tc,[aa,(aa+1-xmax_center)./10],
        optimset('TolFun',1e-18,'TolX',1e-13));
else
    xb= nan;
    fprintf('Fail to find xb\n');
    return;
end
% bisection xf
```

```
if flagb>0.5
    xf=fzero(@(x) funTstar(x,0,sigma)-Tc,[bb-1+xmax_center,bb],optimset(
        'TolFun',1e-18,'TolX',1e-13));
else
    xf = nan;
    fprint('Fail to find xf\n')
    return;
end
end
```

```
function [Tc,xm,ym] = tm_rm(sigma,rm)
%TM_RM Calculate Tm xm ym as a function of Rm
% xm,ym,zm are maximum width $\partial T/\partial x (xm,ym)=0$
% rm= \sqrt((xm-sigma^2)^2+ym^2)

tola=1e-16;tolb=1e-16;
tm=acos(min(sigma/sqrt(rm),1));
p=@(n) integral(@(t) cos(t).^n.*exp(-0.5*(rm/sigma*cos(t)-sigma./cos(t))
    .^2),0,tm,'RelTol',tola,'AbsTol',tolb)...
    +integral(@(t) cos(t).^n.*exp(-0.5*(rm/sigma*cos(t)-sigma./cos(t))
        .^2),tm,pi/2,'RelTol',tola,'AbsTol',tolb);
Xm=-sigma.^2.*p(0)./p(2);
Ym=sqrt(rm.^2-Xm.^2);
Tc=2/(sqrt(2*pi)*sigma)*exp(-Xm-rm).*p(0);
if nargout>1
    xm=Xm+sigma^2;ym=Ym;
end
end
```

D.1.3 Blending of isotherm width under a moving Gaussian heat source

Listing D.4: Partial blending on side Regime II – VI.

```
clear;clc;close all
path = pwd;
cd ../
load('result.mat','Vmul', 'VRy', 'Mmul', 'MRy', 'Mymax', 'Msigma')
cd(path) ;
%% Blending Regime II - VI
X= Vmul;
Y =  Mymax(:,1)./(MRy(:,1)); Y =Y';
fun_f_II_VI = @(mul) interp1(X,Y,mul);
cfII=@(mul) 1.*mul./mul;
```

```
cfVI=@(mul) sqrt(2*pi).*mul .*sqrt(log(1./(mul)));
% method 1
% Blending_Equation=@(mul) @(p) ((1-mul).^p+ (sqrt(2*pi).*mul .*sqrt(log(1./(
    mul)))) .^p) .^(1./p);
% method 2
Blending_Equation=@(mul) @(p) ( (exp(p(2)*mul.^p(3))).^p(1)+ (sqrt(2*pi)
    .*mul.*sqrt(log(1./(mul)))) .^p(1)) .^(1./p(1));
%% blending
Bcf=Blending_Grid_size(fun_f_II_VI,Blending_Equation,1e-3,0.9,[4.1117
    -1.5609 4.4647]);
Bcf.Pplot.x_label= 'mul';
Bcf.Pplot.y_label= 'cf';
Bcf.Pplot.figname= 'gaussian_side_partial_blending_VI_II';
Bcf.funy1= cfII;
Bcf.funy2= cfVI;
Bcf.funmodify1= @(mul) exp( -1.5609*mul.^ 4.4647);
Bcf=Bcf.Blending;
Bcf=Bcf.FBlending(1000);
Bcf.funWrite('gaussian_ymax_cf_partial_blending_II_VI_method2.tex')
%%
figure(4)
plot(logspace(-3,log10(0.9),1e3),Bcf.BP.Result.estimation,'-k','
    linewidth',1)
axis([1e-3,1e0,1e-1,2])
%%
savefigures(1,'gaussian_ymax_cf_partial_blending_II_VI_method2')
```

Listing D.5: Partial blending on side Regime V – VI.

```
clear;clc;close all
path = pwd;
load('gaussian_ymax_s_smax_1.mat','Vmul', 'VRy', 'Mmul', 'MRy', 'Mymax',
     'Msigma')
%% Blending Regime V VI
X= VRy;
i=3;
Y =  Mymax(i,:)./(Vmul(:,i).*sqrt(log(1./Vmul(:,i)))); %Y =Y';
cfV=@(Ry) sqrt(3)*(sqrt(2/pi)*1.280)^(2/3).*Ry.^(2/3);
cfVI=@(Ry) sqrt(2*pi)*Ry;
% loglog(X,Y); hold on
% loglog(X,cfV(X));   hold on
% loglog(X,cfVI(X));   hold on
fun_f_V_VI = @(Ry) interp1(X,Y,Ry);
Blending_Equation=@(Ry) @(p) ((sqrt(3)*(sqrt(2/pi)*1.280)^(2/3).*Ry
    .^(2/3)).^p+ (sqrt(2*pi)*Ry ) .^p) .^(1./p);
```

```
%% blending
Bcf=Blending_Grid_size(fun_f_V_VI,Blending_Equation,1e-3,1e3,-1);
Bcf.Pplot.x_label= 'Ry';
Bcf.Pplot.y_label= 'cf';
Bcf.Pplot.figname= 'gaussian_side_partial_blending_v_vi';
Bcf.funy1= cfV;
Bcf.funy2= cfVI;
% Bcf.funmodify1= @(mul) exp( -1.5609*mul.^ 4.4647);
Bcf=Bcf.Blending;
Bcf=Bcf.FBlending(1000);
Bcf.funWrite('gaussian_ymax_cf_partial_blending_V_VI.tex')
%%
savefigures(1,'gaussian_ymax_cf_partial_blending_V_VI')
```

Listing D.6: 2-D blending of $y^*_{\max}$ under a moving Gaussian heat source.

```
clear;clc;close all
load('gaussian_ymax.mat','Vmul', 'VRy', 'Mmul', 'MRy', 'Mymax', 'Msigma'
    )
% Mymax(MRy>1e3) = nan;
% Vmul =Vmul(1:3:end);
% VRy =VRy(1:3:end);
% Mmul =Mmul(1:3:end,1:3:end);
% MRy =MRy(1:3:end,1:3:end);
% Mymax =Mymax(1:3:end,1:3:end);
% Msigma =Msigma(1:3:end,1:3:end);
n1=-2.398;
sigmax = ((1.014*MRy.^(2/3)).^n1 + (sqrt(pi/2)*MRy).^n1).^( 1/n1);
mul = Msigma ./ sigmax;
%%
format shortG
pseed = [    3.7706    -0.56369    -0.80637    0.016902     -2.1993
   -2.2414     -2.6528     -1.7954      4.5359     -3.5726      13.107 ]
for i = 1:5
error = @(p) log(blending_equation(MRy,Msigma,p)./Mymax);
max_error = @(p) max(max(abs(error(p))));
max_error(pseed)
opts = optimset('MaxFunEvals',1e8);
[pval,eval ] = fminsearch(@(p) max_error(p),pseed,opts)
pseed = pval;
pseed = round(pseed,4,'significant')
end
%%
figure
E=error(pval);
```

```
surf(VRy,Vmul,error(pval));
axis([1e-3,1e3,1e-2,1,-inf,inf])
set(gca,'xscale','log','yscale','log')
shading interp

%%
function y = blending_equation(Ry,sigma,p)
% n1=-2.398;
% n2= -1.731;
% pIIVI= [4.112   -1.560       4.463];
n1 = p(7);
n2 = p(8);
pIIVI = p(9:11);

B = sqrt(3)*(sqrt(2/pi)*1.280).^(2/3)./(2*sqrt(pi/exp(1))) ;

sigmax = ((1.014*Ry.^(2/3)).^n1 + (sqrt(pi/2)*Ry).^n1).^( 1/n1);
mul = sigma ./ sigmax;

y = Ry.*...
    (1+(sqrt(2./(exp(1).*Ry))).^n2 ) .^(1./n2).*...
    ( (exp(pIIVI(2)*mul.^pIIVI(3))).^pIIVI(1)+ (sqrt(2*pi).*mul.*sqrt(
       log(1./(mul)))) .^pIIVI(1)) .^(1./pIIVI(1)) .*...
    (1 + ((B*Ry.^(1/6) -1 ).*(1+p(1).*Ry.^p(2)).^(p(3)).*(1+p(4).*(mul)
       .^p(5)).^(p(6)))) ;
end
```

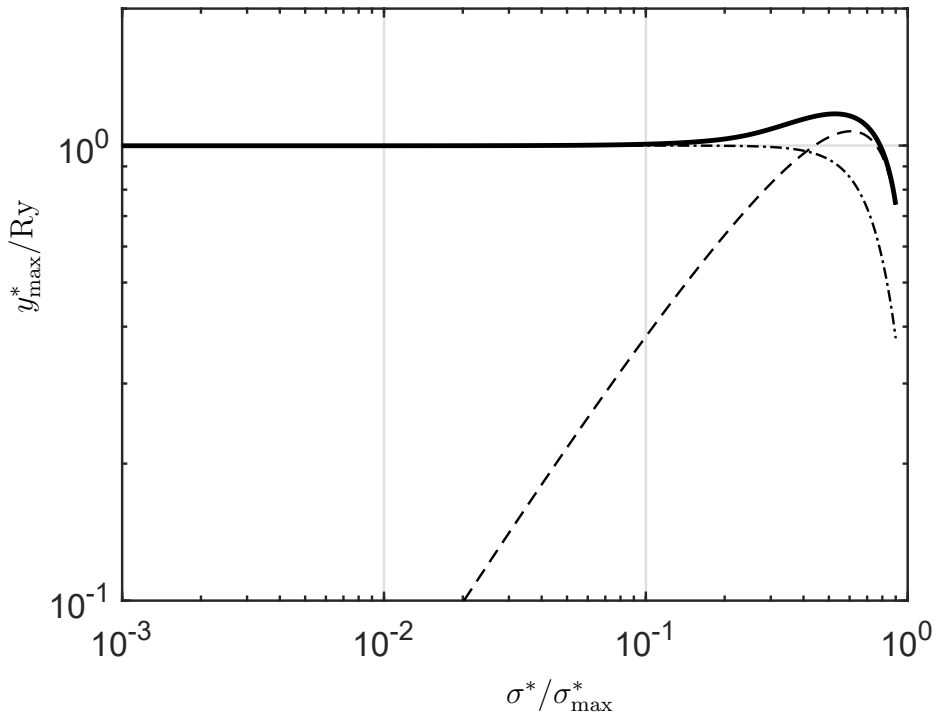

Figure D.1: Partial blending of $y^*_{\max}$ in side Regime II – VI. $y^*_{\max}/\mathrm{Ry}$ changes with $\sigma^*/\sigma^*_{\max}$

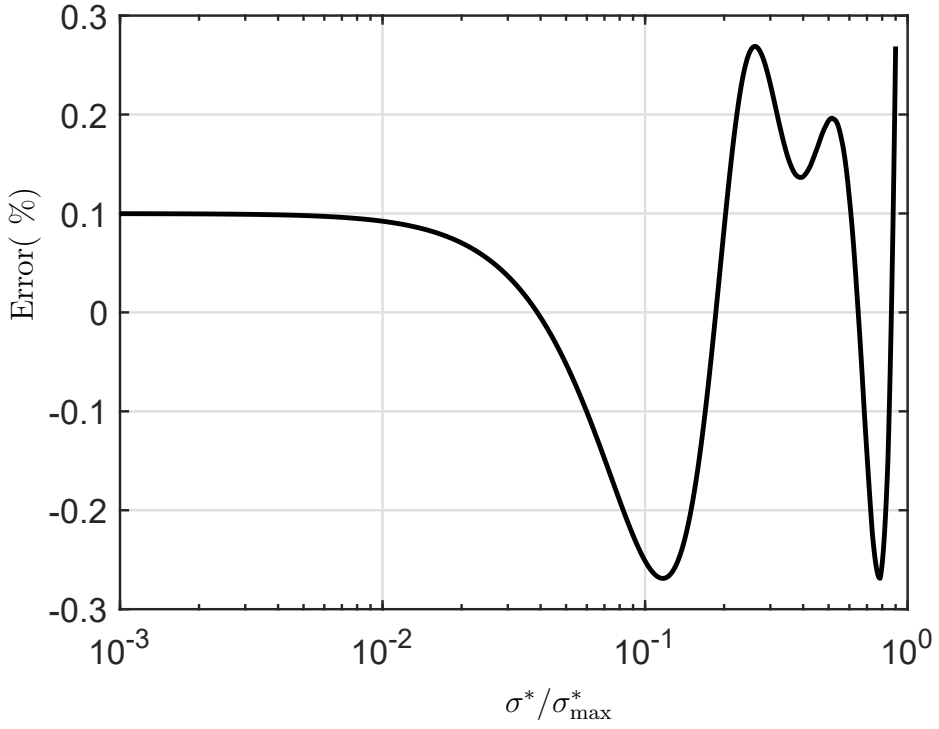

Figure D.2: Error of partial blending in Side Regime II – VI for $y^*_{\max}$ (Equation 6.26) when $a = -1.560$, $b = 4.463$, $n = 4.112$ for $\sigma^*/\sigma^*_{\max} \leq 0.9$.

D.2 Supporting figures for partial blending of $y^*_{\max}$

D.2.1 Supporting figures for partial blending in side Regime II – VI

D.2.2 Supporting figures for partial blending in side Regime V – VI

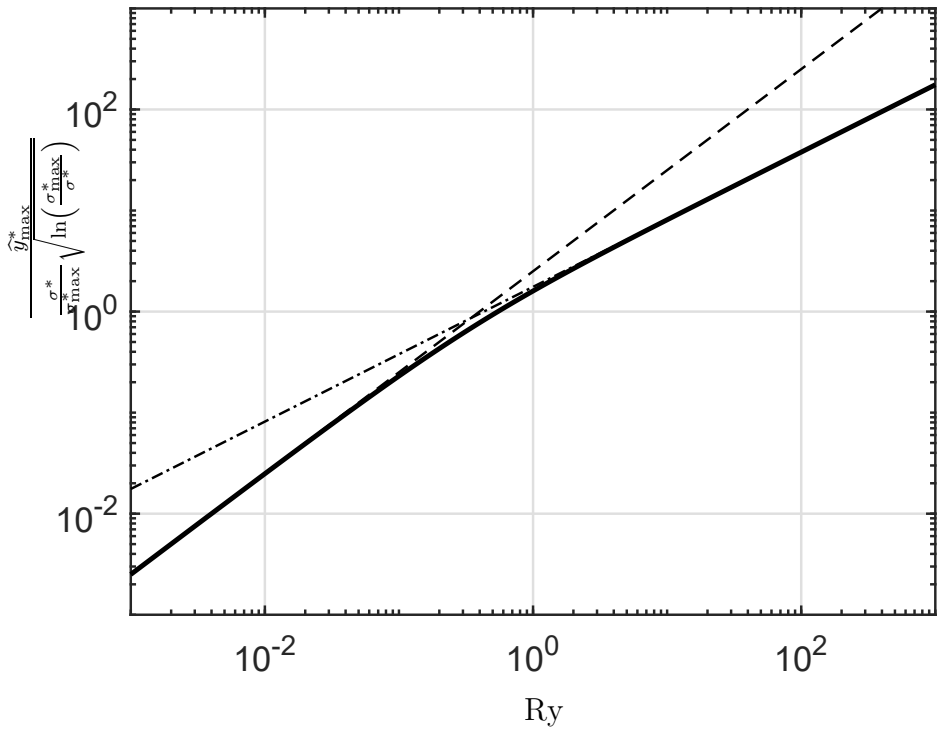

Figure D.3: Partial blending of $y^*_{\max}$ in side Regime V – VI. $\widehat{y}^{*+}_{\max}/\frac{\sigma^*}{\sigma^*_{\max}}\sqrt{\ln\left(\frac{\sigma^*_{\max}}{\sigma^*}\right)}$ changes with Ry.

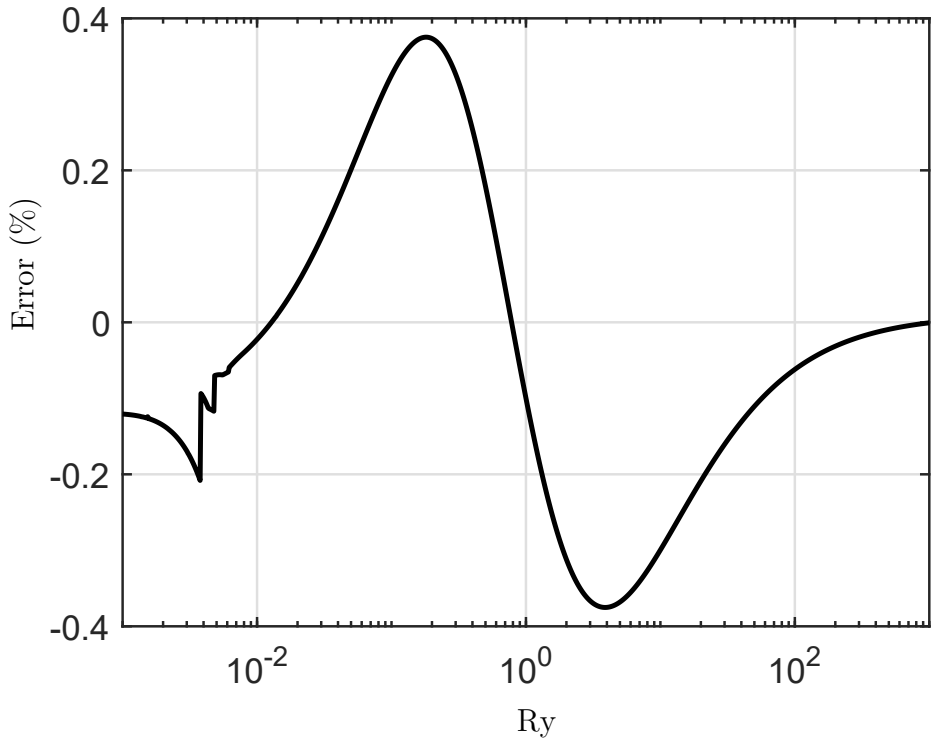

Figure D.4: Error of partial blending of $y^*_{\max}$ in side Regime V – VI (Equation 6.27) when $n = -3.055$.

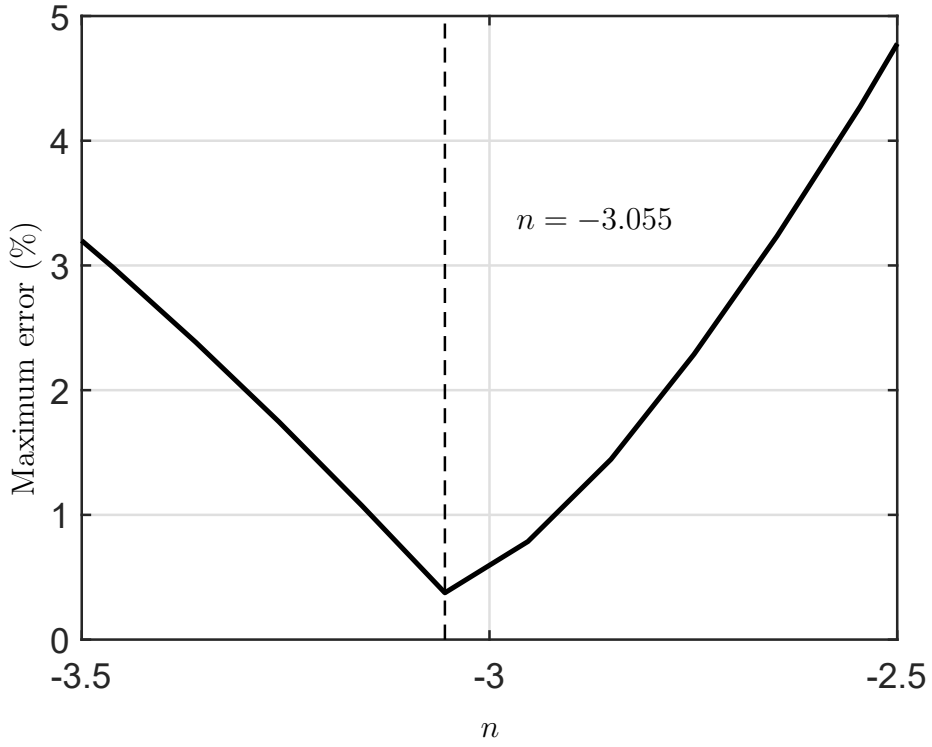

Figure D.5: Maximum error changes with blending parameter n for partial blending of $y^*_{\max}$ in side Regime V – VI.

Appendix E: Catchment efficiency of Gaussian distributed powder cloud under moving Gaussian heat source

E.1 Engineering expression

This appendix illustrated the catchment efficiency of Gaussian distributed powder cloud of diameter σ_p under moving the temperature field σ_h. The temperature field is assumed not affected by powder. Two catchment efficiencies factor are studied in this appendix, the catchment efficiency w_l representing portion of powder deposited in the melt pool, and the catchment efficiency w_s representing the portion of powder deposited ahead of the melt pool.

For an isotherm with thermal features isotherm width $y_{\max}$ (studied in Chapter 6), location of width $x_{\max}$, trailing length x_{b} and leading length x_{f}, the catchment efficiencies can be calculated with

$$w_l = \int_{x_{\mathrm{b}}}^{x_{\mathrm{f}}} dx \int_{-y_i}^{y_i} dy \frac{1}{2\pi\sigma_p^2} \exp\left(-\frac{x^2+y^2}{2\sigma_p^2}\right) \tag{E.1}$$

$$= \sqrt{\frac{\pi}{2}} \frac{1}{\pi\sigma_p} \int_{x_{\mathrm{b}}}^{x_{\mathrm{f}}} dx \exp\left(-\frac{x^2}{2\sigma_p^2}\right) \mathrm{erf}\left(\frac{y_i}{\sqrt{2}\sigma_p}\right) \tag{E.2}$$

and

$$w_s = 2\int_{\infty}^{x_{\max}} dx \int_{y_i}^{y_{\max}} dy \frac{1}{2\pi\sigma_p^2} \exp\left(-\frac{x^2+y^2}{2\sigma_p^2}\right) \tag{E.3}$$

$$= \sqrt{\frac{\pi}{2}} \frac{1}{\pi\sigma_p} \int_{\infty}^{x_{\max}} dx \exp\left(-\frac{x^2}{2\sigma_p^2}\right) \left[\mathrm{erf}\left(\frac{y_{\max}}{\sqrt{2}\sigma_p}\right) - \mathrm{erf}\left(\frac{y_i}{\sqrt{2}\sigma_p}\right)\right] \tag{E.4}$$

Where y_i is a function of x representing the shape of isotherm.

When the distribution size of heat source equals it of powder cloud, the catchment efficiencies can be further investigated. Similar to the analysis of isotherm width in Chapter 6, the catchment efficiencies depend on two dimensionless groups, the Ry number and $\sigma^*/\sigma^*_{\max}$.

This appendix attempts to develop engineering expressions of catchment efficiencies for typical laser cladding processes, not 2-D blending for the whole domain. It generates more practical expressions of more simplicity by curve fitting and does not involve asymptotic analysis. However, it only covers part of the domain for certain

processes, lacking of generality to extend to all possible cases. For typical cases of laser cladding, the Ry is between $5 \sim 100$. For the given range of Ry numbers, the catchment efficiencies are in a band as illustrated in the shadow area of Figure E.1 and E.2. The catchment efficiencies change with $\sigma^*/\sigma^*_{\max}$. The engineering expressions can be achieved by curve fitting. For catchment efficiency of the melt pool w_l, the engineering expression for $5 \leq \text{Ry} \leq 100$ is:

$$\widehat{w_l} = \left[1 + 0.1322\left(1 - \frac{\sigma^*}{\widehat{\sigma}^{*+}_{\max}}\right)^{-6.155}\right]^{-0.1591} \tag{E.5}$$

as illustrated in Figure E.1.

For catchment efficiency of ahead of the melt pool w_s, the engineering expression for $5 \leq \text{Ry} \leq 100$ is:

$$\widehat{w_s} = \left[0.9015\left(\frac{\sigma^*}{\widehat{\sigma}^{*+}_{\max}}\right)^{-0.6428} + 0.3040\left(1 - \frac{\sigma^*}{\widehat{\sigma}^{*+}_{\max}}\right)^{-0.3731}\right]^{-2.824} \tag{E.6}$$

as illustrated in Figure E.2.

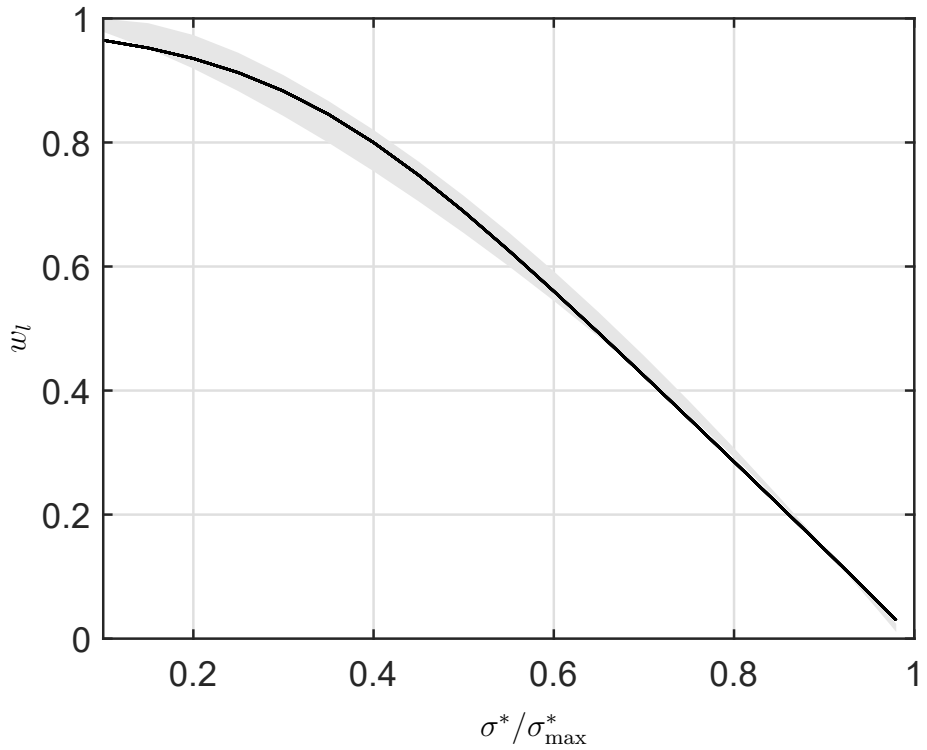

Figure E.1: The catchment efficiency of melt pool w_l change with $\frac{\sigma^*}{\sigma^*_{\max}}$ for $5 \leq \text{Ry} \leq 100$.

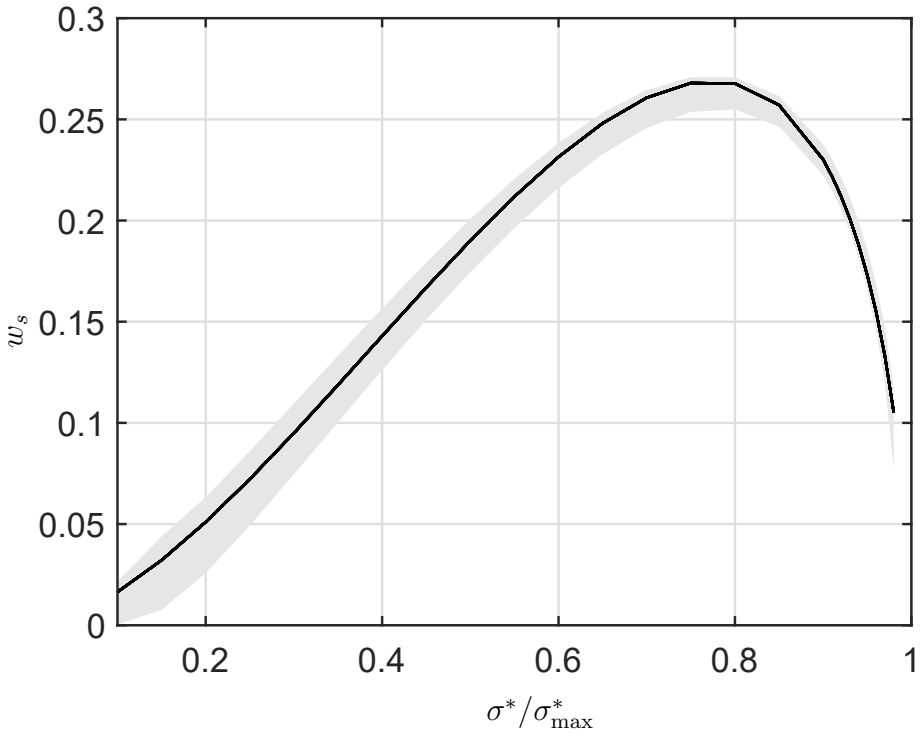

Figure E.2: The catchment efficiency ahead of melt pool w_s change with $\frac{\sigma^*}{\sigma^*_{\max}}$ for $5 \leq \mathrm{Ry} \leq 100$.

E.2 Matlab code

Listing E.1: Calculation of numerical values of catchment efficiencies w_l and w_s.

```
clear;clc;close all
warning off
Ry=[1:1:19,20:10:100]; mul=[0.1:0.05:0.9,0.91:0.01:1];
szmul=max(size(mul));
sigmam= ((((2*1.2798)./(sqrt(2*pi))*Ry).^(2/3)).^(-2.3975)+(sqrt(pi/2)*
    Ry).^(-2.3975)).^(-1./2.3975);
[Ry,~]=meshgrid(Ry,ones(1,szmul-1));
sigma=bsxfun(@times,sigmam,mul(1:end-1)');
[sz1,sz2]=size(Ry);
Ry=reshape(Ry,1,sz1*sz2);
sigma=reshape(sigma,1,sz1*sz2);
wL=Ry*nan;
wS=Ry*nan;
parfor i=1:sz1*sz2
    try
        wL(i) = funEtaDualGaussian(Ry(i),sigma(i),sigma(i));
        wS(i) = funEtaDualGaussianS(Ry(i),sigma(i),sigma(i));
    catch
```

```
    end
    disp(['Loop ',' ',num2str(i)])
end

%%
wL=reshape(wL,sz1,sz2);
wS=reshape(wS,sz1,sz2);
Ry=reshape(Ry,sz1,sz2);
sigma=reshape(sigma,sz1,sz2);
close all
figure
surf(Ry(1,:),mul(1:end-1),wL)
figure
surf(Ry(1,:),sigma,wS)

%%
save res.mat
```

Listing E.2: Function to calculate catchment efficiency w_l.

```
function [eta] = funEtaDualGaussian(Ry,sigmah,sigmap)
%FUNETADUALGAUSSIAN Summary of this function goes here
%   Detailed explanation goes here
[Tmax,xmax] = fun_Tmax_sigma(sigmah);
if 1/Ry>Tmax
    disp('The maximum temperature does not reach required temperature')
    eta=0;
    return
end
[xb,xf]=fun_xbf(sigmah,xmax,1/Ry);
yc =@(x)arrayfun(@(x) fym(sigmah,1/Ry,x,xb,xf),x);
eta=sqrt(pi/2)/(pi*sigmap)*integral(@(x) exp(-x.^2./(2*sigmap.^2)).*erf(
    yc(x)./(sqrt(2)*sigmap)),xb,xf);

end
```

Listing E.3: Function to calculate catchment efficiency w_s.

```
function [eta] = funEtaDualGaussianS(Ry,sigmah,sigmap)
%FUNETADUALGAUSSIAN Catchment effciency for Gaussian cloud on
%Gaussian heat source
[Tmax,xmax] = fun_Tmax_sigma(sigmah);
if 1/Ry>Tmax
    disp('The maximum temperature does not reach required temperature')
    eta=0;
    return
```

```
end
[xb,xf]=fun_xbf(sigmah,xmax,1/Ry);
[ym,Tm,xm] = fun_width(sigmah,Ry);
yc =@(x)arrayfun(@(x) fym(sigmah,1/Ry,x,xb,xf),x);
eta=1/(pi*sigmap.^2)*(integral(@(x) sqrt(pi/2)*sigmap .*exp(-x.^2./(2*
    sigmah.^2)).*(erf(ym./(sqrt(2)*sigmah))-erf(yc(x)./(sqrt(2)*sigmah))
    ),xm,xf)...
    +integral(@(x) sqrt(pi/2)*sigmap .*exp(-x.^2./(2*sigmah.^2)).*(erf(
        ym./(sqrt(2)*sigmah))-erf(0)),xf,inf));

end
```

Listing E.4: Function to calculate maximum centerline temperature and its location.

```
function [Tmax,xm] = fun_Tmax_sigma(sigma)
%FUN_TMAX_SIGMA calculating the maximum temperature for certain sigma
% sigma is the half width of Gaussian distributed heat source
% Tmax is the corresponding maximum temperature
%  xm is the location of maximum temperature

Tstar=@(x,o) 1/sqrt(2*pi)*integral(@(t) t.^(-1/2)./(t+o.^2).*exp(-0.5*(x
    .^2+t.^2+2.*t.*x)./(t+o.^2)),0,inf,'RelTol',1e-100,'AbsTol',1e-100);

xm1=-0.7650*sigma; xm2=-sigma.^2;
seed=[10*min(xm1,xm2),0.1*max(xm1,xm2)];

[xm,Tmax]=fminbnd(@(x) -Tstar(x,sigma),seed(1),seed(2),optimset('TolFun'
    ,1e-80,'TolX',1e-80,'MaxFunEvals',10000,'MaxIter',5000));
Tmax=-Tmax;
end
```

Listing E.5: Function to calculate trailing and leading length.

```
function [xb,xf]=fun_xbf(sigmma,Xm,T)
% calculate xf and xb of pool
% %
    nmax=300;
% domain sorted :   aa <xb<a<xmid<b<xf<bb
    aa=Xm;
    bb=Xm;
    flaga=0;
    flagb=0;
% search the domain contains xf&xb
    for i=1:nmax
        if flaga<0.5
           faa=Tstar(aa,0,sigmma);
```

```
            aa=(10.*aa-1+Xm)*(faa>T)+(10.*aa-1+Xm)*(faa==T)+aa*(faa<T);
            flaga=1*(faa<=T);
         end

        if  flagb<0.5
            fbb=Tstar(bb,0,sigmma);
            bb=(bb-Xm+1)*(fbb>T)+(bb-Xm+1)*(fbb==T)+bb*(fbb<T);
            flagb=1*(fbb<=T); %yaojia
        end

        if flaga && flagb
           break
        end
    end
% bisection xb

    if flaga>0.5
         xb=fzero(@(x) Tstar(x,0,sigmma)-T,[aa,(aa+1-Xm)./10],optimset('
            TolFun',1e-20,'TolX',1e-20));
    else
        fprintf('didnot find interval\n');
        return;
    end
%bisection xf
    if flagb>0.5
        xf=fzero(@(x) Tstar(x,0,sigmma)-T,[bb-1+Xm,bb],optimset('TolFun'
            ,1e-20,'TolX',1e-20));
    else
        fprint('didnot find interval\n')
        return;
    end
end
```

Listing E.6: Function to calculate isotherm width and its location.

```
function [ym,Tm,xm] = fun_width(SIGMA,RY)
%FUN_WIDTH calculating dimensionless value of the half width and maximum
    temperature
% SIGMA and RY are dimensionless
% Half width
TC=1./RY; ym=nan;Tm=nan;xm=nan;
if RY< 0.0172
    disp('If Ry<0.0172, there might be two peaks. TODO on that');
end

```

```
[Tmax_centerline,xmax_centerline]=fun_Tmax_sigma(SIGMA);
r0=abs(xmax_centerline-SIGMA.^2);

list=[0,logspace(-5,50,56)];temp_T=list-list;

for i=1:size(list,2)
    temp_T(i)=tm_rm(SIGMA,r0+list(i));
end
rm_range=r0+[0,list(temp_T==min(temp_T))];
if TC<=min(temp_T)
    disp('the range of rm should be reset')
end
%%
options=optimset('TolX',1e-30);
if Tmax_centerline>=TC
    if temp_T>TC
        disp('pick right range for R')
    else
        rm=fzero(@(r) tm_rm(SIGMA,r)-TC,rm_range,options);
        [t,xm,ym]=tm_rm(SIGMA,rm);
        if ~isreal(ym)
            disp('error in calcuation');
        end
    end
else
    disp('The set maximum temperature is higher than maximum temeprature
        of sigma')
end
Tm=Tmax_centerline;

% max_temperature=preheat+(Tmax_centerline*heat_input*velocity)./(4*pi*
    conductivity* diffusitivity );
% width=2*2* diffusitivity *ym/velocity;
% disp(['Maximum temperature is',num2str(max_temperature)])
% disp(['width  is ', num2str(width)])

end
```

Listing E.7: Curve fitting of catchment efficiency w_l.

```
clear;clc;close all
load('res.mat')
wL=wL(1:end-1,5:28);
wS=wS(:,5:28);
Ry=Ry(:,5:28);
```

```
minwL=min(wL');
maxwL=max(wL');
minwS=min(wS');
maxwS=max(wS');

%%
figure
fill([(mul(1:end-2)),fliplr((mul(1:end-2)))],[minwL,fliplr(maxwL)],[.9
    .9 .9],'linestyle','none'); hold on
XL=[(1-mul(1:17))]; YL=[wL(1:17,16)];
xval = mul(1:end-2)';
xval= xval*ones(1,24);

[xData, yData] = prepareCurveData( xval, wL );

ft = fittype( '(1+a*(1-x).^b).^n', 'independent', 'x', 'dependent', 'y'
    );
opts = fitoptions( 'Method', 'NonlinearLeastSquares' );
opts.Display = 'Off';
opts.StartPoint = [0.0790611899385143 -1 -1];
[fitresult, gof] = fit( xData, yData, ft, opts )

plot(xval,(1+ 0.1322*(1-xval).^ -6.1550).^ -0.1591,'-k','linewidth',1)
xlabel('mul')
ylabel('wL')
axis([0.1,1,0,1])
DefaultGca
```

Listing E.8: Curve fitting of catchment efficiency w_s.

```
clear;clc;close all
load('res.mat')
wL=wL(1:end-1,5:28);
wS=wS(1:end-1,5:28);
Ry=Ry(:,5:28);
minwL=min(wL');
maxwL=max(wL');
minwS=min(wS');
maxwS=max(wS');

%%
figure
fill([(mul(1:end-2)),fliplr((mul(1:end-2)))],[minwS,fliplr(maxwS)],[.9
    .9 .9],'linestyle','none'); hold on

```

```
xval = mul(1:end-2)';
xval= xval*ones(1,24);



[xData, yData] = prepareCurveData( xval, wS );
ft = fittype( '((a1*x.^b1)+(a2*(1-x).^b2)).^(n)', 'independent', 'x', '
    dependent', 'y' );
opts = fitoptions( 'Method', 'NonlinearLeastSquares' );
opts.Display = 'Off';
opts.Lower = [0 0 -inf -Inf -Inf];
opts.StartPoint = [0.5 -0.5 0.5 -0.5 -0.5];
opts.Upper = [Inf Inf 0 0 0];
[fitresult, gof] = fit( xData, yData, ft, opts );
% figure( 'Name', 'untitled fit 1' );
% h = plot( fitresult , xData, yData );
% legend( h, 'wS vs. xval', 'untitled fit 1', 'Location', 'NorthEast', '
    Interpreter', 'none' );
xlabel( 'xval', 'Interpreter', 'none' );
ylabel( 'wS', 'Interpreter', 'none' );
grid on


figure(1)
plot(xval,((0.9015*xval.^-0.6428 )+( 0.304*(1-xval).^-0.3731 ) ).^(
    -2.824 ),'-k')
xlabel('mul')
ylabel('wS')
axis([0.1,1,0,0.3])
DefaultGca
```